RADIOLOGY AND ONCOLOGY

vol.56 no.1
march 2022

RADIOLOGY AND ONCOLOGY

March 2022
Vol. 56 No. 1
Pages 1-128
ISSN 1318-2099
UDC 616-006
CODEN: RONCEM

Publisher
Association of Radiology and Oncology

Aims and Scope
Radiology and Oncology is a multidisciplinary journal devoted to the publishing original and high quality scientific papers and review articles, pertinent to diagnostic and interventional radiology, computerized tomography, magnetic resonance, ultrasound, nuclear medicine, radiotherapy, clinical and experimental oncology, radiobiology, medical physics and radiation protection. Therefore, the scope of the journal is to cover beside radiology the diagnostic and therapeutic aspects in oncology, which distinguishes it from other journals in the field.

Editorial office

Radiology and Oncology
Zaloška cesta 2
P. O. Box 2217
SI-1000 Ljubljana
Slovenia
Phone: +386 1 5879 369
Phone/Fax: +386 1 5879 434
E-mail: gsersa@onko-i.si

Reader for English
Vida Kološa

Secretary
Mira Klemenčič
Zvezdana Vukmirović

Design
Monika Fink-Serša, Samo Rovan, Ivana Ljubanović

Layout
Matjaž Lužar

Printed by
Tiskarna Ozimek, Slovenia

Published quarterly in 400 copies

Beneficiary name: DRUŠTVO RADIOLOGIJE IN ONKOLOGIJE
Zaloška cesta 2
1000 Ljubljana
Slovenia

Beneficiary bank account number: SI56 02010-0090006751
IBAN: SI56 0201 0009 0006 751
Our bank name: Nova Ljubljanska banka, d.d.,
Ljubljana, Trg republike 2,
1520 Ljubljana; Slovenia

SWIFT: LJBASI2X

Subscription fee for institutions EUR 100, individuals EUR 50

The publication of this journal is subsidized by the Slovenian Research Agency.

Indexed and abstracted by:

- *Baidu Scholar*
- *Case*
- *Chemical Abstracts Service (CAS) - CAplus*
- *Chemical Abstracts Service (CAS) - SciFinder*
- *CNKI Scholar (China National Knowledge Infrastructure)*
- *CNPIEC - cnpLINKer*
- *Dimensions*
- *DOAJ (Directory of Open Access Journals)*
- *EBSCO (relevant databases)*
- *EBSCO Discovery Service*
- *Embase*
- *Genamics JournalSeek*
- *Google Scholar*
- *Japan Science and Technology Agency (JST)*
- *J-Gate*
- *Journal Citation Reports/Science Edition*
- *JournalGuide*
- *JournalTOCs*
- *KESLI-NDSL (Korean National Discovery for Science Leaders)*
- *Medline*
- *Meta*
- *Microsoft Academic*
- *Naviga (Softweco)*
- *Primo Central (ExLibris)*
- *ProQuest (relevant databases)*
- *Publons*
- *PubMed*
- *PubMed Central*
- *PubsHub*
- *QOAM (Quality Open Access Market)*
- *ReadCube*
- *Reaxys*
- *SCImago (SJR)*
- *SCOPUS*
- *Sherpa/RoMEO*
- *Summon (Serials Solutions/ProQuest)*
- *TDNet*
- *Ulrich's Periodicals Directory/ulrichsweb*
- *WanFang Data*
- *Web of Science - Current Contents/Clinical Medicine*
- *Web of Science - Science Citation Index Expanded*
- *WorldCat (OCLC)*

This journal is printed on acid- free paper

On the web: ISSN 1581-3207
https://content.sciendo.com/raon
http://www.radioloncol.com

contents

clinical oncology

slovenian abstracts

review

Cancer gene therapy goes viral: viral vector platforms come of age

Urban Bezeljak

COBIK, Ajdovščina, Slovenia

Radiol Oncol 2022; 56(1): 1-13.

Received 25 November 2021
Accepted 4 January 2022

Correspondence to: Urban Bezeljak, Ph.D., COBIK, Mirce 21, 5270 Ajdovščina, Slovenia. E-mail: urban.bezeljak@cobik.si

Disclosure: No potential conflicts of interest were disclosed.

Background. Since the advent of viral vector gene therapy in 1990s, cancer treatment with viral vectors promised to revolutionize the field of oncology. Notably, viral vectors offer a unique combination of efficient gene delivery and engagement of the immune system for anti-tumour response. Despite the early potential, viral vector-based cancer treatments are only recently making a big impact, most prominently as gene delivery devices in approved CAR-T cell therapies, cancer vaccines and targeted oncolytic therapeutics. To reach this broad spectrum of applications, a number of challenges have been overcome – from our understanding of cancer biology to vector design, manufacture and engineering. Here, we take an overview of viral vector usage in cancer therapy and discuss the latest advancements. We also consider production platforms that enable mainstream adoption of viral vectors for cancer gene therapy.

Conclusions. Viral vectors offer numerous opportunities in cancer therapy. Recent advances in vector production platforms open new avenues in safe and efficient viral therapeutic strategies, streamlining the transition from lab bench to bedside. As viral vectors come of age, they could become a standard tool in the cancer treatment arsenal.

Key words: viral vector; gene therapy; oncolytic virus; immunotherapy; bioprocess platform

Introduction

Cancer remains a major public health concern worldwide and is the second leading cause of death in Europe and the United States, with one-in-two to one-in-three chance to develop an invasive cancer during individual's lifetime.[1] In Slovenia, cancer caused over 35 % deaths in males in 2016, which is the highest share in European Union.[2] As a result of positive lifestyle changes and advances in tumour detection and treatment, we can observe a continuous drop in mortality rates in the last 20 years.[3] Despite, current treatments like chemotherapy, surgery and radiation commonly have debilitating side effects. Consequently, new therapeutic options are becoming available to curb the tremendous death toll and increase the quality of life for cancer survivors.[4] In this review we will focus on cancer therapeutics in form of viral gene therapy vectors and oncolytic viruses (OVs).

Viral vectors are an attractive drug delivery option due to their evolved efficiency to transduce human cells. Compared to other delivery methods, viruses are also easier to use in targeted transfer of genetic cargo. That is why modified viruses are used as reliable and safe gene therapy vectors in cancer and hereditary disease treatment.[5] However, early attempts at viral gene therapy came too soon for the budding technology, which lead to controversy and poor public image. For example, the initial trials for severe combined immunodeficiency (SCID) saw only limited improvement and adenovirus vector-associated complications lead to tragic death of Jesse Gelsinger in 1999.[6] The tides turned in later years, when viral vectors were successfully used as *ex vivo* hematopoietic gene delivery de-

vices for severe β-thalassemia, SCID and Wiskott–Aldrich syndrome. In 2003, Gendicine was the first approved adenoviral cancer gene therapeutic in China. It took almost another decade to see the first gene therapy approval in Europe, where the adeno-associated virus (AAV) alipogene tiparvovec (Glybera, uniQure) received authorisation for lipoprotein lipase deficiency (LPLD) treatment in 2012. Since then, many other therapies reached regulatory approval for *in-* or *ex vivo* gene delivery.[7,8] More recently, novel vector-based vaccines are key in battling the coronavirus disease 2019 (COVID-19) pandemic on an unprecedented scale.[9,10] This was made possible by the constant development of viral vector production and purification platforms, which had their roots in viral vector gene therapy. As the technology matures, the rapid turnaround of vector design and scalable particle production capacities hold promise to equally revolutionize cancer gene therapy. Indeed, over two thirds of gene therapy clinical trials are focused on cancer treatment, with many drug candidates in late development stages.[11]

Oncolytic therapy represents another use of viral vectors. It was sparked by serendipitous observations of transient remissions when cancer patients contracted viral infections.[12] This led to experimentation with natural pathogens to help cure tumours, mostly with little success. Although initial attempts of viral oncolytic therapy were ineffective, the genetic engineering revolution enabled development of effective OVs in 1990s.[13,14] Thirty years later, three oncolytic therapeutics are approved for use, with many more entering the clinics. Overall, oncolytic and viral gene delivery vectors have great potential to complement established (immuno)therapy approaches. These advanced nanotherapeutics are armed with a wide variety of genetic elements that take advantage of essential hallmarks of cancer, harnessing the accumulated knowledge in cancer biology, immunology and virology. Examples of therapeutic viral vector platforms, their opportunities and challenges are discussed below.

Viral vectors

At present, over 1000 clinical trials for cancer therapy with viral vectors are underway worldwide (Figure 1).[11] The use of virus particles in cancer treatment can be broadly classified in two groups: as gene delivery vehicles and OVs.[15,16] For gene delivery, lentiviral, adenoviral and AAV vector chassis are used – depending on the specific application and targeting specificity. OVs encompass many viral families and are often additionally armed to eradicate the tumour and induce anti-cancer immune response.[4] The main difference between vectors in gene- and oncolytic therapy is their replicative potential. Gene therapy vectors are specifically engineered to prevent replication. Consequently, they function as nanoparticle drug delivery vehicles and cannot actively infect host cells. In contrast, OVs are less attenuated and can replicate in infected tissues. Each of these vector designs has its own set of advantages and disadvantages, which also depend on the clinical indication. Below, we overview some of the most widely used viral vectors for cancer treatment that were either approved for clinical use or introduce exciting new concepts for future therapies.

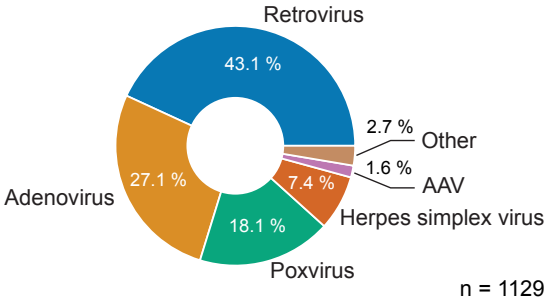

FIGURE 1. Use of viral vectors in clinical trials to treat cancer. Overall, retrovirus viral family vectors are the most widespread. These include lenti- and gammaretroviruses, which are used in adoptive cell therapy. Other popular vectors for cancer treatment are adenovirus, poxvirus like vaccinia, herpes simplex virus (HSV) and adeno-associated virus (AAV). Measles virus, vesicular stomatitis virus (VSV) and poliovirus are some of the other vectors that are not explicitly depicted. Data on all open cancer trials are from Wiley *Journal of Gene Medicine* Gene Therapy Clinical Trials Worldwide database (retrieved October 2021).[11]

Gene delivery

Gene delivery vectors are used to transfer therapeutic genetic material to target tissues. In cancer therapy this includes tumour suppressor genes, tumour-associated antigens (TAAs), pro-inflammatory factors, immune checkpoint inhibitors, anti-angiogenic proteins, small interference RNA (siRNA), cancer stroma-degrading enzymes and cytotoxic convertases.[17] In addition, vector gene delivery is used to reprogramme therapeutic cells *ex vivo* for adoptive cell therapy like chimeric antigen receptor (CAR) T and natural killer (NK) cells.[18,19] Here, we present the most well-known viral vec-

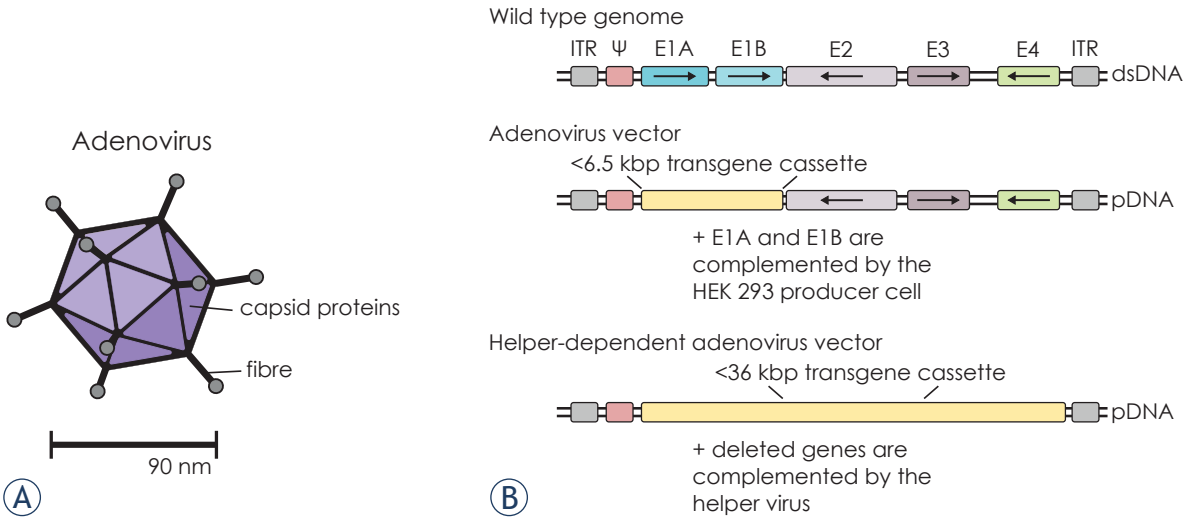

FIGURE 2. Overview of adenovirus vector design. **(A)** Schematic representation of adenovirus structure. Adenoviruses are non-enveloped 90 nm particles with pointing fibre rods. **(B)** Outline of wild type adenovirus genome, the first-generation adenovirus vector plasmid and helper-dependent adenoviral vector plasmid with the transgene expression cassette. The wild type genome highlights key early genes, while other genetic elements are omitted for clarity. The first-generation adenovirus vector particles are assembled in HEK 293 cell line by transgene vector plasmid transfection. Additionally, the helper-dependent vector assembly also requires infection with a helper virus.

ITR = inverted terminal repeat; dsDNA = double-stranded DNA; pDNA = plasmid DNA.

tor platforms: adenovirus, which is used in *in vivo* gene therapy and retroviruses that are used for *ex vivo* gene delivery. In addition, we discuss AAVs, which are currently the most exciting vector platform and will likely set trends in cancer gene therapy in the future.

Adenovirus vectors

Native adenoviruses are 90 nm icosahedral particles (Figure 2A) that commonly cause respiratory, gastrointestinal, urinary and keratoconjunctivitis infections in humans. Their ubiquity results in high proportion of life-long immunity in human population towards the most common serotypes.[20] Adenoviruses have 36 kilobase pair (kbp) linear double-stranded DNA (dsDNA) genome consisting of over 30 genes that are flanked by inverted terminal repeats (ITRs) and a capsid-packing signal sequence ψ. The adenoviral genes are divided into early (E) and late (L) genes, depending on their expression pattern. Early expressed regulatory proteins interact with the host cell and initiate viral genome replication. On the other hand, late genes encode structural proteins that form the virion.[21] Adenoviral vectors were developed by deleting key regulatory genes, which depend on the desired transgene size and application (Figure 2B). Replication-competent adenovirus vectors are used in oncolytic cancer therapy, while non-replicative deletion mutants are gene delivery vehicles. In the first generation of adenovirus vectors, the essential early E1A and E1B genes are replaced by constitutive expression cassette with transgene for gene delivery. Additionally, E2, E3 and E4 genes can also be deleted to accommodate larger therapeutic inserts of 10 kbp and improve performance. For viral vector assembly, the modified adenovirus genome is expressed from plasmid DNA in human embryonic kidney (HEK) 293 cell line that complements for deleted E1, E2 and E4 genes. Lastly, as much as 36 kbp inserts can be accommodated in helper-dependent adenovirus vectors that retain only ITR and genome packaging sequence ψ, rest is filled with one or several transgene expression cassettes. All adenoviral proteins needed for vector replication, packaging and assembly are provided by the replication-competent helper virus, which has its packaging signal flanked by loxP recombination sites. The helper-dependent vector production takes place in cell lines expressing Cre recombinase that specifically excises the loxP-flanked helper ψ sequence. This ensures only the transgene vector retains the ψ packaging signal and is incorporated in the budding viral particles. Remaining helper virus contaminants are eliminated in the following chromatography purification process. Adenoviral vectors have broad tropism and do not integrate

into target cell genome. Instead, the delivered genetic material remains episomal.[15,22]

In gene delivery, acquired and innate immunity towards adenovirus vectors is hindering their application. For example, the most widely used Ad5 serotype has 50% seroprevalence in North America and over 90% in Côte d'Ivoire.[15] Additionally, the adenoviral capsid and nucleic acid stimulates components of the complement system and Toll-like receptors (TLR). This raises safety concerns and efficacy issues for systemic adenoviral gene delivery *in vivo*. However, the intrinsic vector immunogenicity can also be harnessed in local cancer therapy by engaging the immune system and promoting anti-tumour responses.[20]

In 2003, the adenovirus-based Gendicine became the first registered cancer gene therapy treatment. Gendicine is an E1- and E3-deletion Ad5 viral vector, which encodes tumour suppressor p53 under Rous sarcoma virus (RSV) promoter regulation. The loss of p53 protective function is associated with at least half of cancers.[23] Once the Ad5 vector delivers p53 transgene, it resumes anti-tumour function by promoting cancer cell apoptosis and stimulating the immune response. It received approval in China for advanced head and neck cancer treatment.[23,24]

Adenovirus vectors are also used to deliver cancer suicide genes that convert prodrugs to cytotoxic compounds. Examples include 5-fluorouridine (5-FU)-producing cytosine deaminase, purine nucleoside phosphorylase (PNP) that converts fludarabine phosphate (F-ara-AMP) to toxic 2-fluoroadenine, and ganciclovir-converting thymidine kinase (TK).[15] Sitimagene ceradenovec (Cerepro, Ark Therapeutics) is a first-generation Ad5 vector that expresses convertase from herpes virus HSV-TK. In 2005 it entered phase 3 trial for treatment of glioblastoma. In the trial, $1{\cdot}10^{12}$ Ad5 vector particles were applied locally into the resected tumour and ganciclovir was administered intravenously. The study found no effect on survival, while the viral vector treatment improved time to re-intervention or death after resection – the primary trial endpoints.[25] Despite this, the Cerepro marketing application in Europe was withdrawn in 2010.[26]

Similarly, immunostimulatory adenovirus cancer gene therapy was used to promote interferon alpha and beta (IFNα, -β), interleukin 2 (IL-2) and Fms-like tyrosine kinase 3 ligand (Flt3L) expression.[20] A phase 3 trial for bacille Calmette-Guérin (BCG)-unresponsive bladder cancer with nadofaragene firadenovec, a replication deficient vector expressing IFNα, recently reported favourable results.[27] The non-muscle-invasive and BCG-unresponsive bladder cancer currently does not have efficient non-surgical treatments, which are often the only option for many patients. Adenoviral gene therapy is a promising alternative, since local administration led to 60- and 30% complete response rate after 3 and 12 months, respectively.[28] Lastly, the engineered chimpanzee ChAdOx1 vector vaccine platform – also used by the AZD1222 COVID-19 vaccine (Vaxzevria, Oxford-AstraZeneca) – is aimed at prostate cancer treatment in combination with checkpoint inhibitors.[10,29,30] The cancer vaccine treatment consists of ChAdOx1 immunization against 5T4 tumour antigen and a Modified Vaccinia Ankara (MVA) vector boost. The phase 1 trial confirmed vaccine safety and immunogenicity, while phase 1/2 efficacy trial was expected to complete in 2021.[31] Overall, adenoviral gene delivery remains a promising venue for cancer therapy, either alone or in combination with radiotherapy, chemotherapy or checkpoint inhibitors.[32] Also, the ease of industrial scale-up and established Good Manufacturing Practice (GMP) processes will further promote adenoviral platform for *in vivo* patient gene delivery.[33]

Adeno-associated virus vectors

Adeno-associated viruses (AAVs) hold great promise in the gene therapy field. AAVs do not cause any human disease, are non-replicative and have broad tissue tropism. AAVs are 25 nm icosahedral viruses (Figure 3A) with single-stranded DNA (ssDNA) genome, which naturally lacks many key regulatory genes for replication and expression. The missing genes are instead complemented with adenoviral co-infection of the host cell. Alternatively, herpes simplex and baculovirus can also provide the helper function. For gene delivery, the AAV genome is "gutted"—devoid of all viral genes – and replaced with transgene expression cassette (Figure 3B). The major AAV vector downside is its relatively low capacity for transgene inserts – it can accommodate 4.7 kbp of genetic cargo, which can be limiting for many applications.[15,34] The therapeutic AAV particles are commonly produced from three plasmid constructs in transfected HEK 293 cells, which already encode the adenoviral E1 helper gene. The vector plasmids contain the ITR-flanked transgene, AAV rep and cap genes and the adenoviral E2, E4 and VA genes, respectively. A more scalable solution is possible with Sf9 insect cells, which are co-infected with ITR-transgene and AAV cap/rep baculoviruses, respectively.[35]

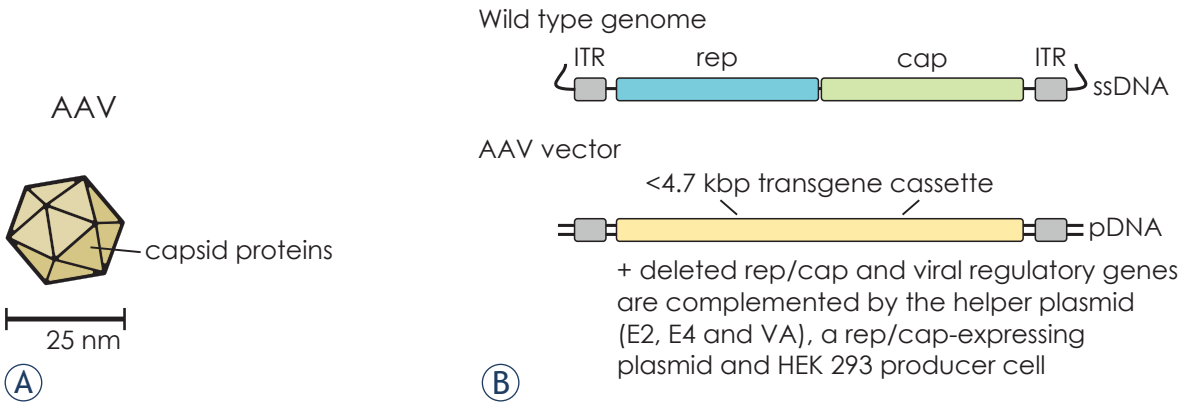

FIGURE 3. Overview of AAV vector design. **(A)** Schematic representation of AAV structure. AAV virions are non-enveloped 25 nm icosahedral particles. **(B)** Outline of wild type AAV genome and AAV vector plasmid with the transgene expression cassette. AAV vector particles are assembled in adenoviral E1-expressing HEK 293 cell line, which is co-transfected with transgene AAV vector plasmid, a helper plasmid and a rep/cap plasmid. Alternatively, AAV vectors can be produced in insect cells, which are co-infected with ITR-flanked transgene and rep/cap recombinant baculoviruses.

ITR = inverted terminal repeat; pDNA = plasmid DNA; ssDNA = single-stranded DNA

Different AAV serotypes display distinct tropism, but they generally require AAV receptor (AAVR) expression, heparin sulphate peptidoglycans, sialic acid or galactose with several co-receptors for cell transduction.[36] Once the vector enters the cell, it travels to nucleus and uncoats the transgene DNA, which persists as concatemerized episomal circle for many years.[35] Currently, AAV vectors are the most successful in treatment of monogenic diseases like spinal muscle atrophy (SMA) with onasemnogene abeparvovec (Zolgensma, Novartis).[37] In contrast, AAV-based cancer therapies are still in early development. However, the modular vector design enables new promising approaches to targeted gene delivery.[38]

For instance, AAVs that cross the blood-brain barrier and are specific for central nervous system could be used for treatment of invasive glioblastoma.[39] To improve cancer specificity, wild-type AAV capsids can also be engineered to target cell surface tumour antigens.[40,41] For example, AAV2 was modified to bind HER2 receptor by inserting designed ankyrin repeat proteins (DARPins) into the AAV capsid.[42] The researches later used these Her2-AAVs to specifically deliver checkpoint inhibitors against programmed cell death protein-1 (PD-1) and HSV-TK suicide gene in a mice xenograft model.[43,44] A single systemic injection of Her2-AAV vector, armed with HSV-TK, lead to considerable tumour mass reduction in combination with ganciclovir.[44] On the other hand, PD-1 inhibition lead to only marginal tumour clearance in combination with chemotherapy.[43] In an *ex vivo* application, an AAV6 vector was used to prepare allogenic CAR-T cells by replacing the endogenous T cell receptor (TCR) with CD19 CAR through targeted cleavage and homologous repair.[45,46] In the future, AAVs could also be used for CAR-T cell generation *in vivo*, replacing the challenging retroviral T cell modification. This concept of "AAV delivering CAR gene therapy" (ACG) was proved on a T-cell leukaemia animal model, where murine immune cells were reprogrammed to express CD4 CAR.[47] Finally, therapeutic AAVs are developed to include CRISPR/Cas gene editing components. This combination of powerful biotechnology platforms promises highly efficient tumour delivery and precise oncogene knock-out or silencing.[48,49] To this end, a sub-4.7 kbp CRISPR/Cas13a that distinguishes between wild type and oncogenic KRAS G12D was constructed and tested in cell culture. A similar AAV vector with oncogene-specific Cas13a could someday induce tumour eradication through mRNA silencing.[50]

Overall, AAV particles are less immunogenic compared to other vector types, although majority of adults have pre-existing neutralizing antibodies that can affect AAV-based gene therapy efficency.[51] Also, AAVs are regarded as very safe due to their non-toxic nature and expected lack of genome integration. However, a recent long-term study of AAV-treated dogs with haemophilia raised concerns as numerous vector integration events were surprisingly discovered in vicinity of cancer-associated genes.[52] Nonetheless, the superior versatility makes AAVs currently the up-and-coming method for gene delivery *in vivo*.[53]

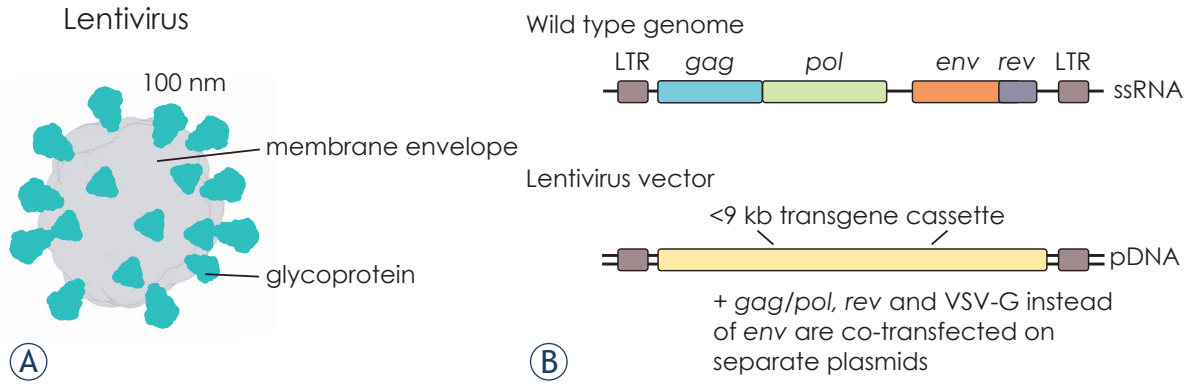

FIGURE 4. Overview of lentivirus vector design. **(A)** Schematic representation of lentivirus structure. Lentiviruses are 100 nm enveloped particles with exposed glycoprotein that defines the virus and vector tropism.[55] **(B)** Outline of wild type lentivirus genome and lentivirus vector plasmid with the transgene expression cassette. Only key genetic elements are highlighted in the genome structure, rest are omitted for clarity. Lentivirus particles are assembled in mammalian cell culture by co-transfection of four plasmids: the transgene plasmid, *gag/pol* and *rev* packaging plasmids and VSV-G expression plasmid.

pDNA = plasmid DNA; ssRNA = single-stranded RNA; LTR= long terminal repeat

Lenti- and gammaretrovirus vectors

While adenovirus and AAV vectors are predominantly used to deliver gene drugs *in vivo*, retrovirus vectors like lenti- and gammaretroviruses are the most common choice for transformation of isolated patient cells *ex vivo*. Another distinction is their structure: retroviruses are enveloped 100 nm particles (Figure 4A), while adenoviruses and AAVs have smaller and more rigid proteinaceous shells. Lentivirus family include human- (HIV-1, HIV-2), simian- (SIV) and feline immunodeficiency viruses (FIV). In fact, the widely used lentiviral vectors are derived from HIV-1 that have been modified not to cause disease and to express vesicular stomatitis virus G glycoprotein (VSV-G) instead of the native envelope (*env*) protein. Pseudotyping the lentivirus particles with VSV-G increased the vector productivity, stability and infectivity, as well as broadened its tropism for different cell types and tissues.[54–56] To guarantee vector safety, the majority of HIV-1 RNA genome is deleted. Only three key structural and regulatory genes remain: *gag, pol* and *rev*. Deletion of viral accessory proteins renders the lentiviral vector harmless. What is more, *gag/pol*, *rev*, VSV-G and the transgene (< 9 kbp) are divided on separate plasmids in the producing cell lines, preventing assembly of replication-competent virus through recombination (Figure 4B).[57] This way only the transgene is included in the lentivirus particles, while other genetic elements remain behind. The produced lentivirus vectors cannot replicate and can transfer the therapeutic gene with high efficiency.[58] The delivered transgene RNA sequence is flanked by modified long terminal repeats (LTR), promoter, packaging and reverse-transcription elements. This expression cassette is integrated into genome of transduced cells, ensuring long-term expression in dividing and non-dividing cells. Alternatively, non-integrating lentiviral vectors (NILVs) were developed that persist as episomal DNA. NILVs circumvent the safety concerns regarding oncogenic potential of integration mutagenesis and offer prolonged transgene expression.[59,60]

In cancer therapy, lentiviral vectors are most used for *ex vivo* modification of T and NK cells. Particularly, CAR-T cells are successful in treating relapsed and refractory non-Hodgkin lymphoma and acute lymphoblastic leukaemia (ALL), resulting in the first FDA-approved therapy tisagenlecleucel (Kymriah, Novartis) in 2017.[61,62] There, the patient T cells are harvested by leukapheresis, activated and transduced with lentivirus vector, which encodes CD19 CAR. The lentivirus is produced under biosafety level 2 (BSL-2) GMP conditions in transfected HEK 293T cells, purified and sterile filtered before T cell transduction.[63,64] A dendritic cell (DC)-specific lentiviral cancer vaccine LV305 was also used to promote expression and immune presentation of New York Esophageal Squamous Cell Carcinoma-1 (NY-ESO-1) cancer antigen. The non-integrating vector is pseudotyped with Sindbis virus envelope glycoprotein that binds CD209 receptor on DC. In the first-in-human phase 1 study, LV305 vaccination induced $CD4^+$ and $CD8^+$ T cell

responses against NY-ESO-1-expressing tumours. Based on these results, further LV305 combination therapies are planned.[65]

Gammaretrovirus vectors, which are derived from murine leukaemia virus (MLV), are another type of retroviral vectors. In contrast to lentivirus, gammaretrovirus vector infects only actively dividing cells and is prone to integrate into gene regulatory regions, raising concerns for insertional oncogenesis.[56] Nevertheless, axicabtagen ciloleucel (Yescarta, Gilead) is a CD19 CAR-T cell therapy for diffuse large B-cell lymphoma, which utilizes gammaretroviral vector for chimeric receptor gene delivery.[66] Another gammaretroviral therapeutic is vocimagene amiretrorepvec (Toca 511), which encodes yeast cytosine deaminase that converts prodrug 5-fluorocytosine to toxic 5-FU in glioma cells.[67] Despite promising results from mouse brain tumour models, a phase 2/3 did not show improved patient survival compared to standard-of-care after Toca 511 injection.[68] Lenti- and gammaretroviral vectors will remain the method of choice for *ex vivo* stable cell transduction. Their use in cancer therapy will focus on next-generation CAR-T and -NK cells with improved potency and solid tumour treatment.[69]

Oncolytic viruses

In contrast to viral vectors for gene therapy, engineered OVs are replication-competent and more closely resemble their natural counterparts. In fact, tumour regressions after natural viral infections have been reported since the end of 19th century.[13] The OV therapy takes advantage of rapidly dividing cancer cells, which often lack antiviral defence mechanisms present in normal cells. For example, misregulation of interferon, Wnt, Ras/MAPK, p53 and pRb signalling pathways leaves cancer vulnerable for viral infection.[70,71] Consequently, OVs preferentially replicate in cancerous cells, resulting in lysis, tumour eradication and immune system engagement. Besides the viral tumour debulking, the immunostimulatory effect is especially important in "cold" tumours with few infiltrating lymphocytes, inhibitory tumour microenvironment (TME) and impaired antigen presentation. There, viral antigens, danger-associated molecular patterns (DAMPs), TAAs and neoantigens are released to TME during infected tumour cell lysis. Released factors are then presented to the innate and adaptive immune system, acting as self-adjuvating *in situ* cancer vaccine. This leads to localized inflammation, recruiting immune cells into TME and mounting response towards distant metastatic lesions.[16,72] The multifaceted oncolytic virotherapy is potentiated with immune checkpoint inhibitors or CAR-T cells, which is reflected in multiple combination therapy approaches.[73–75] Similar to gene delivery vectors, OVs are often armed with transgenes that additionally modulate the TME or the immune system, including matrix-degrading enzymes, cytokines, checkpoint inhibitors, therapeutic anti-/nanobodies and bispecific T cell engagers (BiTEs).[17] The OV therapy can even be custom-made for each individual patient. Personalized therapeutic vectors can be designed by inserting patient-specific antigens directly into viral envelope or by encoding the neoantigen sequences for gene delivery.[76,77] A broad range of oncolytic vectors are used for cancer therapy, representing different viral families. Below we mention some examples, which have been extensively tested and reached late stages of clinical trials.

Replication-competent adenovirus vectors were the first oncolytic viruses to reach clinical trials in 1998 with ONYX-015.[78] This adenoviral vector harbours E1B-55K deletion, which attenuates viral replication in normal cells. While ONYX-015 presented a remarkable safety profile, it conferred only limited responses in combination with chemotherapy for many different cancers.[22] In 2005, a similar vector H101 (Oncorine) became the first approved oncolytic virotherapy for late-stage nasopharyngeal carcinoma treatment in China. The objective response rate of Oncorine in combination with chemotherapy was 76% versus 59% for chemotherapy alone in phase 3 trial.[79] Altogether, hundreds of patients received Oncorine, which was well tolerated and without adverse side effects.[22]

It took 10 years for another OV to be approved by the FDA and EMA in 2015. T-VEC or talimogene laherparepvec (Imlgyc, Amgen) is an oncolytic herpesvirus that expresses immunomodulatory granulocyte macrophage colony-stimulating factor (GM-CSF) for advanced melanoma treatment.[80] Non-modified herpes simplex virus type 1 (HSV-1) is a neurotropic human pathogen with 152 kbp dsDNA genome and about 90 genes. For cancer therapy with T-VEC vector, HSV-1 from a clinical isolate was modified with infected cell protein 34.5 (ICP34.5) deletions, preventing virus replication in neurons and other slowly replicating cells. Conversely, this deletion increases HSV-1 replication specificity for tumour cells, while another deletion in ICP47 increases viral and tumour antigen presentation. Lastly, T-VEC is armed with two copies of GM-CSF to further promote activa-

tion of local antigen-presenting cells.[72,81] The virotherapy proved effective in phase 3 trial where 16% of patients showed durable response compared to 2% for GM-CSF treatment. The overall response rate was 26% for T-VEC and 6% for GM-CSF alone. Furthermore, 64% of injected lesions more than halved in size, together with 34% and 15% of distal uninjected regional and visceral lesions, respectively.[82] A similar antitumour T-VEC activity was recently reported for primary cutaneous B cell lymphoma. Interestingly, this phase 1 study also showed therapeutic virus replication in non-malignant cells and determined that induced immunological responses are more important in cancer eradication than selective viral cell lysis.[83,84] Currently, combination therapy studies with T-VEC are underway for different cancers.[16,85,86] A similar set of HSV-1 attenuations is also present in G47Δ or teserpaturev (Delytact, Daiichi Sankyo), which is derived from a different parental strain. In 2021, it received conditional authorization for malignant glioma therapy in Japan.[87] In contrast to T-VEC, which is armed with GM-CSF, Delytact does not encode any transgenes.[88]

The GM-CSF cytokine sequence is also loaded in oncolytic vaccinia virus pexastimogene devacirepvec (JX-594, Pexa-Vec) to promote *in situ* vaccine activity. Pexa-Vec is a TK-deleted poxvirus that demonstrated specificity for tumour cells, which often have increased TK levels that compensate the OV attenuation. In contrast to T-VEC, Pexa-Vec is administered systemically by intravenous injection for hepatocellular carcinoma (HCC), renal cell cancer and colorectal cancer treatment.[74,89] In early HCC trials, Pexa-Vec replication was detected in cancer and tumour-associated endothelial cells, triggering specific immune response and destruction of tumour blood vessels.[90,91] However, a phase 3 HCC trial with Pexa-Vec and a protein kinase inhibitor sorafenib was prematurely stopped due to lack of interim efficacy.[92] A similar fate faced Prostvac-VF, a vaccinia and fowlpox prime-boost vector combination that delivers prostate cancer-specific antigen PSA and three additional immunostimulatory factors. The dual vector combination prevents antibody neutralization of the replicating viral particles, which resulted in increased survival for prostate cancer patients in phase 2 study. In contrast, a multicentre phase 3 trial did not confirm these findings, ending the study prematurely. Prostvac-VF combination therapies are still evaluated in phase 1 and 2 clinical trials.[93–95]

The complexity of viral vector genomes still poses a potential risk of recombination and acquired pathogenicity during vector production and therapy. Indeed, with an increasing number of effective OVs reaching late clinical trials and regulatory approvals, a particular care is given to biosafety monitoring and interaction of replication-competent vectors with the host and environment. Based on gathered experience, engineered oncolytic viral vectors remain a safe and promising venue for cancer treatment. The most common reported side effects are mild flu-like symptoms, while there was no documented uncontrolled transmission of the oncolytic virus.[14] It is becoming clear that OVs offer unique benefits in tumour immunotherapy, particularly in combination with advanced cell therapies, chemotherapy and checkpoint inhibitors.[96]

Production platforms

Reliable production platforms are key to successful translation of viral vector therapies into clinics. Indeed, the development of robust manufacturing capabilities enabled the widespread adoption of recombinant biotherapeutics like monoclonal antibodies. Compared to proteins, viral vectors are orders of magnitude more complex, where minute changes between serotypes can affect production and purification strategies. What is more, conventional protein purification methods are often not appropriate for shear-sensitive viral particle isolation. Enveloped vectors are easily ruptured during the purification process, which decreases the ratio of functional infectious particles in the final product. Consequently, it is no surprise that viral vector production platforms are continuously being optimized and are yet to reach their full potential on the industrial scale.[6,97] Moreover, viral vectors for gene delivery and oncolysis span several viral families and are further genetically engineered to ensure safety and anti-tumoral potencies, adding to the diversity. This offers exciting opportunities for tailored therapies, but also raises challenges in manufacturing and regulation. Thus, paths to viral vector platform success and adoption are specific for each therapeutic.

In order to support consistent production and reliable scale-up to clinical-grade drug manufacture, an extra care has to be taken in initial selection of viral vector production platforms. Established mammalian cell cultures are most widely used for vector propagation. This makes sense since therapeutic viral vectors originate from natural viruses that co-evolved with vertebrate hosts. The producer cell lines include African green monkey

Vero cells, human HEK 293 and HeLa cells and baby hamster kidney (BHK) line.[98] They are handled under BSL-2 regulations to limit vector dissemination and contamination with adventitious agents.[99] Mammalian cell lines are primarily adherent – growing attached to a solid support. For production, adherent cells are grown on microcarriers in bioreactors, on multilayer tissue plates and roller bottles. However, suspension cell cultures are preferred for easier scale-up. Luckily, many adherent cell lines were successfully adapted for suspension growth in stirred-tank and rocking Wave bioreactors.[97,98,100] For example, the adenovirus-transformed HEK 293 cells are easily adapted for suspension culture and are the most widely used cell line for adenoviral and AAV vector production.

Vector components and helper constructs are delivered to the selected producer cells with transient transfection or infection, which represent a bottleneck and a significant expense in viral vector production for clinical trials.[101] In principle, stable cell lines overcome transfection issues in large scale production. However, assembled vector components are often toxic for the host cell.[5] This is why stable lentiviral production lines rely on inducible vector expression using TetON/OFF system.[102] Alternatively, the cytotoxic VSV-G envelope protein and HIV-1 protease can be swapped with Ampho MLV 4070A glycoprotein and T26S modified protease to generate stable lentiviral vector producers LentiPro26 from HEK 293T cells.[103] Besides mammalian cell cultures, insect cells are also increasingly used for vector assembly. Most commonly, Sf9 or HighFive™ insect cell lines are grown in suspension where therapeutic vector backbones are introduced through infection with recombinant baculoviruses. Insect cell expression system is fast to implement, scalable and has superior safety profile since insects are poor hosts for human pathogens. So far, insect cells are used to produce helper-free AAV vectors for gene therapy.[104,105] Like with mammalian viral vector systems, insect cells are grown in single-use cell culture flasks and bioreactors to ensure reproducibility and sterility during manufacture for clinical use.[101,106]

Viral vector purification platforms encompass purification steps to generate highly pure vector particles that comply with stringent quality, safety and efficacy standards. Historically, purification relied on ultracentrifugation to separate the large viral particles from smaller producer cell contaminants. Nonetheless, this approach is not scalable and does not guarantee elimination of biophysically similar particles.[107] Instead, chromatography-based purification processes are taking the centre stage.[108] Due to diversity of viral vectors – ranging from small 25 nm AAV particles to large enveloped vaccinia vector, which exceeds 300 nm in size – a universal purification process does not exist and has to optimized for each application. Generally, the purification process starts with vector particle harvesting, where secreted vectors like lentiviruses, herpes and poxviruses are separated from cellular debris with centrifugation or filtration, while intracellular adenoviral and AAV particles often require cell lysis for release. Then, the collected harvest is extensively purified over a series of different chromatography columns and tangential-flow filtration (TFF) cassettes to obtain pure therapeutic vector particles. In the end, the purified cancer drug is exchanged to the final formulation solution and sterile filtered through 0.2 μm pores, which can be problematic for some larger vectors. Instead, the entire production can be operated under controlled sterile conditions.[97,108] The final dose of vector particles varies from 10^9 for *ex vivo* gene delivery up to 10^{14}/kg for AAV-based gene therapy.[108,109] However, all purification steps are associated with loss of infectious particles, which increases the cost of manufacture. The complexity of viral vector production and low yields result in exceedingly high price of advanced therapeutics. For example, CAR-T therapies Kymriah and Yescarta cost $373,000, while Zolgensma gene therapy was marketed at $2.125 million at launch in 2019.[15,110] The constant improvements in production technology will make the viral vector therapeutics more accessible to the patients.[111]

With many viral vector therapeutics reaching final clinical stage and regulatory approvals, the attention is focused on vector particle production platforms that support scalable industrial scale production. This is essential to bring down the cost of therapies, which is often prohibitive. New biotechnological solutions like gene editing, bioreactor cultivation and multimodal chromatography are boosting cell-based productivity and improving particle purity. Novel analytical methods are also improving the quality monitoring of the final product. In gene therapy, great emphasis is given to ensuring a high ratio of functional infectious vector particles versus defective and empty capsid contaminants.[112] These exciting developments are enabling the viral vector platforms to produce safe and potent drugs to combat cancer – as monotherapies or in combination with other therapeutic venues.

Conclusions

Viral vectors represent 100% of approved gene therapeutics and over 60% of delivery devices in gene therapy trials, including oncolytic virotherapy.[11] This accumulation of knowledge helps us identify where vector particles can provide the most benefits. Based on recent success and rapid advances in the field, the clinical viral vector use will continue to increase. Particularly, combination therapy with complementary radiotherapy, chemotherapy and immunotherapies like CAR-T and checkpoint inhibitors hold great promise. Due to modular vector genome design, novel biotherapeutics like BiTEs, cytokines and CRISPR/Cas can be encoded in the genetic cargo to expand the repertoire of anti-tumour potency.[113] In addition to new vector development, approved viral drugs like T-VEC are being tested to treat several other solid tumours beyond melanoma. Finally, oncolytic viruses and non-replicative vectors can be used in prime-boost cancer vaccine regimens, covering the full spectrum of the discussed vector platforms.[114]

With obvious benefits to the viral vector oncotherapy, these engineered nanotherapeutics will continue to expand the cancer treatment repertoire. It seems like viral vector platforms are finally living up the high expectations thanks to the advances in biopharmaceutical manufacturing and our understanding of cancer and viral biology. In the future, many more vector particles will enter the clinics. Excitingly, their adaptable design will enable *de novo* engineering and repurposing of existing chassis for novel therapeutic approaches.

Acknowledgments

The author would like to thank A. Smole, R. Hudej and M. Peterka for valuable feedback on the manuscript.

References

1. Siegel RL, Miller KD, Fuchs HE, Jemal A. Cancer statistics, 2021. *CA Cancer J Clin* 2021; **71:** 7-33. doi: 10.3322/caac.21654
2. Eurostat. Cancer statistics - statistics explained. [cited 2021 Nov 18]. Available at: https://ec.europa.eu/eurostat/statistics-explained/index.php?title=Cancer_statistics#Deaths_from_cancer
3. Zadnik V, Zagar T, Lokar K, Tomsic S, Konjevic AD, Zakotnik B. Trends in population-based cancer survival in Slovenia. *Radiol Oncol* 2021; **55**: 42-9. doi: 10.2478/raon-2021-0003
4. Cross D, Burmester JK. Gene therapy for cancer treatment: past, present and future. *Clin Med Res* 2006; **4**: 218-27. doi: 10.3121/cmr.4.3.218
5. Goswami R, Subramanian G, Silayeva L, Newkirk I, Doctor D, Chawla K, et al. Gene therapy leaves a vicious cycle. *Front Oncol* 2019; **9:** 1-25. doi: 10.3389/fonc.2019.00297
6. Sheridan C. Gene therapy finds its niche. *Nat Biotechnol* 2011; **29:** 121-8. doi: 10.1038/nbt.1769
7. Kotterman MA, Chalberg TW, Schaffer DV. Viral vectors for gene therapy: translational and clinical outlook. *Annu Rev Biomed Eng* 2015; **17:** 63-89. doi: 10.1146/annurev-bioeng-071813-104938
8. Daley J. Gene therapy arrives. *Nature* 2019; **576:** S12-3. doi: 10.1038/d41586-019-03716-9
9. Sadoff J, Gray G, Vandebosch A, Cárdenas V, Shukarev G, Grinsztejn B, et al. Safety and efficacy of single-dose Ad26.COV2.S vaccine against Covid-19. *N Engl J Med* 2021; **384**: 2187-201. doi: 10.1056/NEJMoa2101544
10. Voysey M, Clemens SAC, Madhi SA, Weckx LY, Folegatti PM, Aley PK, et al. Safety and efficacy of the ChAdOx1 nCoV-19 vaccine (AZD1222) against SARS-CoV-2: an interim analysis of four randomised controlled trials in Brazil, South Africa, and the UK. *Lancet* 2021; **397:** 99-111. doi: 10.1016/S0140-6736(20)32661-1
11. Ginn SL, Amaya AK, Alexander IE, Edelstein M, Abedi MR. Gene therapy clinical trials worldwide to 2017: an update. *J Gene Med* 2018; **20:** 1-16. doi: 10.1002/jgm.3015
12. Dock G. The influence of compliting disease upon leukaemia. *Am J Med Sci* 1904; **127:** 563-92.
13. Kelly E, Russell SJ. History of oncolytic viruses: genesis to genetic engineering. *Mol Ther* 2007; **15:** 651-9. doi: 10.1038/sj.mt.6300108
14. Miest TS, Cattaneo R. New viruses for cancer therapy: meeting clinical needs. *Nat Rev Microbiol* 2014; **12:** 23-34. doi: 10.1038/nrmicro3140
15. Bulcha JT, Wang Y, Ma H, Tai PWL, Gao G. Viral vector platforms within the gene therapy landscape. *Signal Transduct Target Ther* 2021; **6:** 53. doi: 10.1038/s41392-021-00487-6
16. Saxena M, van der Burg SH, Melief CJM, Bhardwaj N. Therapeutic cancer vaccines. *Nat Rev Cancer* 2021; **21:** 360-78. doi: 10.1038/s41568-021-00346-0
17. Wan PKT, Ryan AJ, Seymour LW. Beyond cancer cells: targeting the tumor microenvironment with gene therapy and armed oncolytic virus. *Mol Ther* 2021; **29:** 1668-82. doi: 10.1016/j.ymthe.2021.04.015
18. Barrett DM, Singh N, Porter DL, Grupp SA, June CH. Chimeric antigen receptor therapy for cancer. *Annu Rev Med* 2014; **65:** 333-47. doi: 10.1146/annurev-med-060512-150254
19. Myers JA, Miller JS. Exploring the NK cell platform for cancer immunotherapy. *Nat Rev Clin Oncol* 2021; **18:** 85-100. doi: 10.1038/s41571-020-0426-7
20. Shaw AR, Suzuki M. Immunology of adenoviral vectors in cancer therapy. *Mol Ther Methods Clin Dev* 2019; **15:** 418-29. doi: 10.1016/j.omtm.2019.11.001
21. McConnell MJ, Imperiale MJ. Biology of adenovirus and its use as a vector for gene therapy. *Hum Gene Ther* 2004; **15:** 1022-33. doi: 10.1089/hum.2004.15.1022
22. Wold WSM, Toth K. Adenovirus vectors for gene therapy, vaccination and cancer gene therapy. *Curr Gene Ther* 2013; **13:** 421-33. doi: 10.2174/15665232132131125095046
23. Peng Z. Current status of gendicine in China: recombinant human Ad-p53 agent for treatment of cancers. *Hum Gene Ther* 2005; **16:** 1016-27. doi: 10.1089/hum.2005.16.1016
24. Wang D, Wang K, Cai Y. An overview of development in gene therapeutics in China. *Gene Ther* 2020; **27:** 338-48. doi: 10.1038/s41434-020-0163-7
25. Westphal M, Ylä-Herttuala S, Martin J, Warnke P, Menei P, Eckland D, et al. Adenovirus-mediated gene therapy with sitimagene ceradenovec followed by intravenous ganciclovir for patients with operable high-grade glioma (ASPECT): a randomised, open-label, phase 3 trial. *Lancet Oncol* 2013; **14:** 823-33. doi: 10.1016/S1470-2045(13)70274-2
26. European Medicines Agency. Ark Therapeutics Ltd withdraws its marketing authorisation application for Cerepro (sitimagene ceradenovec). [cited 2021 Dec 21]. Available at: https://www.ema.europa.eu/en/news/ark-therapeutics-ltd-withdraws-its-marketing-authorisation-application-cerepro-sitimagene

27. Kulkarni GS. Nadofaragene firadenovec: a new gold standard for BCG-unresponsive bladder cancer? *Lancet Oncol* 2021; **22:** 8-9. doi: 10.1016/S1470-2045(20)30586-6

28. Boorjian SA, Alemozaffar M, Konety BR, Shore ND, Gomella LG, Kamat AM, et al. Intravesical nadofaragene firadenovec gene therapy for BCG-unresponsive non-muscle-invasive bladder cancer: a single-arm, open-label, repeat-dose clinical trial. *Lancet Oncol* 2021; **22:** 107-17. doi: 10.1016/S1470-2045(20)30540-4

29. Dicks MD, Spencer AJ, Edwards NJ, Wadell G, Bojang K, Gilbert SC, et al. A novel chimpanzee adenovirus vector with low human seroprevalence: improved systems for vector derivation and comparative immunogenicity. *PLoS One* 2012; **7:** e40385. doi: 10.1371/journal.pone.0040385

30. Mercuri E, Muntoni F, Baranello G, Masson R, Boespflug-Tanguy O, Bruno C, et al. Onasemnogene abeparvovec gene therapy for symptomatic infantile-onset spinal muscular atrophy type 1 (STR1VE-EU): an open-label, single-arm, multicentre, phase 3 trial. *Lancet Neurol* 2021; **20:** 832-41. doi: 10.1016/S1474-4422(21)00251-9

31. Cappuccini F, Bryant R, Pollock E, Carter L, Verrill C, Hollidge J, et al. Safety and immunogenicity of novel 5T4 viral vectored vaccination regimens in early stage prostate cancer: a phase I clinical trial. *J Immunother Cancer* 2020; **8:** 1-13. doi: 10.1136/jitc-2020-000928

32. Sato-Dahlman M, LaRocca CJ, Yanagiba C, Yamamoto M. Adenovirus and immunotherapy: advancing cancer treatment by combination. *Cancers* 2020; **12:** 1295. doi: 10.3390/cancers12051295

33. Lee CS, Bishop ES, Zhang R, Yu X, Farina EM, Yan S, et al. Adenovirus-mediated gene delivery: potential applications for gene and cell-based therapies in the new era of personalized medicine. *Genes Dis* 2017; **4:** 43-63. doi: 10.1016/j.gendis.2017.04.001

34. Xiao X, Li J, Samulski RJ. Production of high-titer recombinant adeno-associated virus vectors in the absence of helper adenovirus. *J Virol* 1998; **72:** 2224-32. doi: 10.1128/JVI.72.3.2224-2232.1998

35. Samulski RJ, Muzyczka N. AAV-mediated gene therapy for research and therapeutic purposes. *Annu Rev Virol* 2014; **1:** 427-51. doi: 10.1146/annurev-virology-031413-085355

36. Srivastava A. In vivo tissue-tropism of adeno-associated viral vectors. *Curr Opin Virol* 2016; **21:** 75-80. doi: 10.1016/j.coviro.2016.08.003

37. Mercuri E, Muntoni F, Baranello G, Masson R, Boespflug-Tanguy O, Bruno C, et al. Onasemnogene abeparvovec gene therapy for symptomatic infantile-onset spinal muscular atrophy type 1 (STR1VE-EU): an open-label, single-arm, multicentre, phase 3 trial. *Lancet Neurol* 2021; **20:** 832-41. doi: 10.1016/S1474-4422(21)00251-9

38. Challis RC, Ravindra Kumar S, Chan KY, Challis C, Beadle K, Jang MJ, et al. Systemic AAV vectors for widespread and targeted gene delivery in rodents. *Nat Protoc* 2019; **14:** 379-414. doi: 10.1038/s41596-018-0097-3

39. Xu X, Chen W, Zhu W, Chen J, Ma B, Ding J, et al. Adeno-associated virus (AAV)-based gene therapy for glioblastoma. *Cancer Cell Int* 2021; **21:** 1-10. doi: 10.1186/s12935-021-01776-4

40. Santiago-Ortiz JL, Schaffer DV. Adeno-associated virus (AAV) vectors in cancer gene therapy. *J Control Release* 2016; **240:** 287-301. doi: 10.1016/j.jconrel.2016.01.001

41. Hacker UT, Bentler M, Kaniowska D, Morgan M, Büning H. Towards clinical implementation of adeno-associated virus (AAV) vectors for cancer gene therapy: current status and future perspectives. *Cancers* 2020; **12:** 1-30. doi: 10.3390/cancers12071889

42. Münch RC, Janicki H, Völker I, Rasbach A, Hallek M, Büning H, et al. Displaying high-affinity ligands on adeno-associated viral vectors enables tumor cell-specific and safe gene transfer. *Mol Ther* 2013; **21:** 109-18. doi: 10.1038/mt.2012.186

43. Reul J, Frisch J, Engeland CE, Thalheimer FB, Hartmann J, Ungerechts G, et al. Tumor-specific delivery of immune checkpoint inhibitors by engineered AAV vectors. *Front Oncol* 2019; **9:** 52. doi: 10.3389/fonc.2019.00052

44. Münch RC, Muth A, Muik A, Friedel T, Schmatz J, Dreier B, et al. Off-target-free gene delivery by affinity-purified receptor-targeted viral vectors. *Nat Commun* 2015; **6:** 6246. doi: 10.1038/ncomms7246

45. MacLeod DT, Antony J, Martin AJ, Moser RJ, Hekele A, Wetzel KJ, et al. Integration of a CD19 CAR into the TCR alpha chain locus streamlines production of allogeneic gene-edited CAR T cells. *Mol Ther* 2017; **25:** 949-61. doi: 10.1016/j.ymthe.2017.02.005

46. Eyquem J, Mansilla-Soto J, Giavridis T, van der Stegen SJC, Hamieh M, Cunanan KM, et al. Targeting a CAR to the TRAC locus with CRISPR/Cas9 enhances tumour rejection. *Nature* 2017; **543:** 113-7. doi: 10.1038/nature21405

47. Nawaz W, Huang B, Xu S, Li Y, Zhu L, Yiqiao H, et al. AAV-mediated in vivo CAR gene therapy for targeting human T-cell leukemia. *Blood Cancer J* 2021; **11:** 119. doi: 10.1038/s41408-021-00508-1

48. Wang D, Zhang F, Gao G. CRISPR-based therapeutic genome editing: strategies and in vivo delivery by AAV vectors. *Cell* 2020; **181:** 136-50. doi: 10.1016/j.cell.2020.03.023

49. Ibraheim R, Tai PWL, Mir A, Javeed N, Wang J, Rodríguez TC, et al. Self-inactivating, all-in-one AAV vectors for precision Cas9 genome editing via homology-directed repair in vivo. *Nat Commun* 2021; **12:** 6267. doi: 10.1038/s41467-021-26518-y

50. Zhao X, Liu L, Lang J, Cheng K, Wang Y, Li X, *et al.* A CRISPR-Cas13a system for efficient and specific therapeutic targeting of mutant KRAS for pancreatic cancer treatment. *Cancer Lett* 2018; **431:** 171-81. doi: 10.1016/j.canlet.2018.05.042

51. Calcedo R, Vandenberghe LH, Gao G, Lin J, Wilson JM. Worldwide epidemiology of neutralizing antibodies to adeno-associated viruses. *J Infect Dis* 2009; **199:** 381-90. doi: 10.1086/595830

52. Venditti CP. Safety questions for AAV gene therapy. *Nat Biotechnol* 2021; **39:** 24-6. doi: 10.1038/s41587-020-00756-9

53. Shirley JL, de Jong YP, Terhorst C, Herzog RW. Immune responses to viral gene therapy vectors. *Mol Ther* 2020; **28:** 709-22. doi: 10.1016/j.ymthe.2020.01.001

54. Naldini L, Blömer U, Gallay P, Ory D, Mulligan R, Gage FH, et al. In vivo gene delivery and stable transduction of nondividing cells by a lentiviral vector. *Science* 1996; **272:** 263-7. doi: 10.1126/science.272.5259.263

55. Cockrell AS, Kafri T. Gene delivery by lentivirus vectors. *Mol Biotechnol* 2007; **36:** 184-204. doi: 10.1007/s12033-007-0010-8

56. Milone MC, O'Doherty U. Clinical use of lentiviral vectors. *Leukemia* 2018; **32:** 1529-41. doi: 10.1038/s41375-018-0106-0

57. Dull T, Zufferey R, Kelly M, Mandel RJ, Nguyen M, Trono D, et al. A third-generation lentivirus vector with a conditional packaging system. *J Virol* 1998; **72:** 8463-71. doi: 10.1128/jvi.72.11.8463-8471.1998

58. Trono D. Lentiviral vectors: turning a deadly foe into a therapeutic agent. *Gene Ther* 2000; **7:** 20-3. doi: 10.1038/sj.gt.3301105

59. Yáñez-Muñoz RJ, Balaggan KS, MacNeil A, Howe SJ, Schmidt M, Smith AJ, et al. Effective gene therapy with nonintegrating lentiviral vectors. *Nat Med* 2006; **12:** 348-53. doi: 10.1038/nm1365

60. Philippe S, Sarkis C, Barkats M, Mammeri H, Ladroue C, Petit C, et al. Lentiviral vectors with a defective integrase allow efficient and sustained transgene expression in vitro and vivo. *Proc Natl Acad Sci U S A* 2006; **103:** 17684-9. doi: 10.1073/pnas.0606197103

61. Brentjens RJ, Davila ML, Riviere I, Park J, Wang X, Cowell LG, et al. CD19-targeted T cells rapidly induce molecular remissions in adults with chemotherapy-refractory acute lymphoblastic leukemia. *Sci Transl Med* 2013; **5:** 177ra38. doi: 10.1126/scitranslmed.3005930

62. Vairy S, Garcia JL, Teira P, Bittencourt H. CTL019 (Tisagenlecleucel): CAR-T therapy for relapsed and refractory B-cell acute lymphoblastic leukemia. *Drug Des Devel Ther* 2018; **12:** 3885-98. doi: 10.2147/DDDT.S138765

63. Levine BL, Miskin J, Wonnacott K, Keir C. Global manufacturing of CAR T cell therapy. *Mol Ther Methods Clin Dev* 2017; **4:** 92-101. doi: 10.1016/j.omtm.2016.12.006

64. Levine BL. Performance-enhancing drugs: design and production of redirected chimeric antigen receptor (CAR) T cells. *Cancer Gene Ther* 2015; **22:** 79-84. doi: 10.1038/cgt.2015.5

65. Somaiah N, Block MS, Kim JW, Shapiro GI, Do KT, Hwu P, et al. First-in-class, first-in-human study evaluating LV305, a dendritic-cell tropic lentiviral vector, in sarcoma and other solid tumors expressing NY-ESO-1. *Clin Cancer Res* 2019; **25:** 5808-17. doi: 10.1158/1078-0432.CCR-19-1025

66. Kochenderfer JN, Feldman SA, Zhao Y, Xu H, Black MA, Morgan RA, et al. Construction and preclinical evaluation of an anti-CD19 chimeric antigen receptor. *J Immunother* 2009; **32:** 689-702. doi: 10.1097/CJI.0b013e3181ac6138

67. Ostertag D, Amundson KK, Lopez Espinoza F, Martin B, Buckley T, Galvão da Silva AP, et al. Brain tumor eradication and prolonged survival from intratumoral conversion of 5-fluorocytosine to 5-fluorouracil using a nonlytic retroviral replicating vector. *Neuro Oncol* 2012; **14:** 145-59. doi: 10.1093/neuonc/nor199

68. Cloughesy TF, Petrecca K, Walbert T, Butowski N, Salacz M, Perry J, et al. Effect of vocimagene amiretrorepvec in combination with Flucytosine vs standard of care on survival following tumor resection in patients with recurrent high-grade glioma: a randomized clinical trial. *JAMA Oncol* 2020; **6:** 1939-46. doi: 10.1001/jamaoncol.2020.3161

69. Albinger N, Hartmann J, Ullrich E. Current status and perspective of CAR-T and CAR-NK cell therapy trials in Germany. *Gene Ther* 2021; **28:** 513-27. doi: 10.1038/s41434-021-00246-w

70. Pikor LA, Bell JC, Diallo JS. Oncolytic viruses: Exploiting cancer's deal with the devil. *Trends in Cancer* 2015; **1:** 266-77. doi: 10.1016/j.trecan.2015.10.004

71. Twumasi-Boateng K, Pettigrew JL, Kwok YYE, Bell JC, Nelson BH. Oncolytic viruses as engineering platforms for combination immunotherapy. *Nat Rev Cancer* 2018; **18:** 419-32. doi: 10.1038/s41568-018-0009-4

72. Russell SJ, Peng KW. Oncolytic virotherapy: a contest between apples and oranges. *Mol Ther* 2017; **25:** 1107-16. doi: 10.1016/j.ymthe.2017.03.026

73. Harrington K, Freeman DJ, Kelly B, Harper J, Soria JC. Optimizing oncolytic virotherapy in cancer treatment. *Nat Rev Drug Discov* 2019; **18:** 689-706. doi: 10.1038/s41573-019-0029-0

74. Lawler SE, Speranza MC, Cho CF, Chiocca EA. Oncolytic viruses in cancer treatment: a review. *JAMA Oncol* 2017; **3:** 841-9. doi: 10.1001/jamaoncol.2016.2064

75. Lichty BD, Breitbach CJ, Stojdl DF, Bell JC. Going viral with cancer immunotherapy. *Nat Rev Cancer* 2014; **14:** 559-67. doi: 10.1038/nrc3770

76. Ylösmäki E, Malorzo C, Capasso C, Honkasalo O, Fusciello M, Martins B, et al. Personalized cancer vaccine platform for clinically relevant oncolytic enveloped viruses. *Mol Ther* 2018; **26:** 2315-25. doi: 10.1016/j.ymthe.2018.06.008

77. Shemesh CS, Hsu JC, Hosseini I, Shen BQ, Rotte A, Twomey P, et al. Personalized cancer vaccines: Clinical landscape, challenges, and opportunities. *Mol Ther* 2021; **29:** 555-70. doi: 10.1016/j.ymthe.2020.09.038

78. Ries S, Korn WM. ONYX-015: mechanisms of action and clinical potential of a replication-selective adenovirus. *Br J Cancer* 2002; **86:** 5-11. doi: 10.1038/sj.bjc.6600006

79. Liang M. Oncorine, the world first oncolytic virus medicine and its update in China. *Curr Cancer Drug Targets* 2018; **18:** 171-6. doi: 10.2174/1568009618666171129221503

80. Zheng M, Huang J, Tong A, Yang H. Oncolytic viruses for cancer therapy: barriers and recent advances. *Mol Ther - Oncolytics* 2019; **15:** 234-47. doi: 10.1016/j.omto.2019.10.007

81. Shen Y, Nemunaitis J. Herpes simplex virus 1 (HSV-1) for cancer treatment. *Cancer Gene Ther* 2006; **13:** 975-92. doi: 10.1038/sj.cgt.7700946

82. Andtbacka RHI, Kaufman HL, Collichio F, Amatruda T, Senzer N, Chesney J, et al. Talimogene laherparepvec improves durable response rate in patients with advanced melanoma. *J Clin Oncol* 2015; **33:** 2780-8. doi: 10.1200/JCO.2014.58.3377

83. Ramelyte E, Tastanova A, Balázs Z, Ignatova D, Turko P, Menzel U, et al. Oncolytic virotherapy-mediated anti-tumor response: a single-cell perspective. *Cancer Cell* 2021; **39:** 394-406.e4. doi: 10.1016/j.ccell.2020.12.022

84. Kaufman HL, Maciorowski D. Advancing oncolytic virus therapy by understanding the biology. *Nat Rev Clin Oncol* 2021; **18:** 197-8. doi: 10.1038/s41571-021-00490-4

85. Haitz K, Khosravi H, Lin JY, Menge T, Nambudiri VE. Review of talimogene laherparepvec: a first-in-class oncolytic viral treatment of advanced melanoma. *J Am Acad Dermatol* 2020; **83:** 189-96. doi: 10.1016/j.jaad.2020.01.039

86. Ribas A, Dummer R, Puzanov I, VanderWalde A, Andtbacka RHI, Michielin O, et al. Oncolytic virotherapy promotes intratumoral T cell infiltration and improves anti-PD-1 immunotherapy. *Cell* 2017; **170:** 1109-1119.e10. doi: 10.1016/j.cell.2017.08.027

87. Jahan N, Ghouse SM, Martuza RL, Rabkin SD. *In situ* cancer vaccination and immunovirotherapy using oncolytic HSV. *Viruses* 2021; **13:** 1-27. doi: 10.3390/v13091740

88. Todo T, Martuza RL, Rabkin SD, Johnson PA. Oncolytic herpes simplex virus vector with enhanced MHC class I presentation and tumor cell killing. *Proc Natl Acad Sci U S A* 2001; **98:** 6396-401. doi: 10.1073/pnas.101136398

89. Parato KA, Breitbach CJ, Le Boeuf F, Wang J, Storbeck C, Ilkow C, et al. The oncolytic poxvirus JX-594 selectively replicates in and destroys cancer cells driven by genetic pathways commonly activated in cancers. *Mol Ther* 2012; **20:** 749-58. doi: 10.1038/mt.2011.276

90. Guo ZS, Lu B, Guo Z, Giehl E, Feist M, Dai E, et al. Vaccinia virus-mediated cancer immunotherapy: Cancer vaccines and oncolytics. *J Immunother Cancer* 2019; **7:** 1-21. doi: 10.1186/s40425-018-0495-7

91. Heo J, Reid T, Ruo L, Breitbach CJ, Rose S, Bloomston M, et al. Randomized dose-finding clinical trial of oncolytic immunotherapeutic vaccinia JX-594 in liver cancer. *Nat Med* 2013; **19:** 329-36. doi: 10.1038/nm.3089

92. Foerster F, Galle PR. The current landscape of clinical trials for systemic treatment of HCC. *Cancers* 2021; **13:** 1962. doi: 10.3390/cancers13081962

93. Gregg JR, Thompson TC. Considering the potential for gene-based therapy in prostate cancer. *Nat Rev Urol* 2021; **18:** 170-84. doi: 10.1038/s41585-021-00431-x

94. Gulley JL, Borre M, Vogelzang NJ, Ng S, Agarwal N, Parker CC, et al. Phase III Trial of PROSTVAC in asymptomatic or minimally symptomatic metastatic castration-resistant prostate cancer. *J Clin Oncol* 2019; **37:** 1051-61. doi: 10.1200/JCO.18.02031

95. Madan RA, Arlen PM, Mohebtash M, Hodge JW, Gulley JL. Prostvac-VF: a vector-based vaccine targeting PSA in prostate cancer. *Expert Opin Investig Drugs* 2009; **18:** 1001-11. doi: 10.1517/13543780902997928

96. Shi T, Song X, Wang Y, Liu F, Wei J. Combining oncolytic viruses with cancer immunotherapy: establishing a new generation of cancer treatment. *Front Immunol* 2020; **11:** 1-13. doi: 10.3389/fimmu.2020.00683

97. Moleirinho MG, Silva RJS, Alves PM, Carrondo MJT, Peixoto C. Current challenges in biotherapeutic particles manufacturing. *Expert Opin Biol Ther* 2019; **20:** 451-65. doi: 10.1080/14712598.2020.1693541

98. Ungerechts G, Bossow S, Leuchs B, Holm PS, Rommelaere J, Coffey M, et al. Moving oncolytic viruses into the clinic: clinical-grade production, purification, and characterization of diverse oncolytic viruses. *Mol Ther - Methods Clin Dev* 2016; **3:** 16018. doi: 10.1038/mtm.2016.18

99. Ghosh S, Brown AM, Jenkins C, Campbell K. Viral vector systems for gene therapy: a comprehensive literature review of progress and biosafety challenges. *Appl Biosaf* 2020; **25:** 7-18. doi: 10.1177/1535676019899502

100. Merten OW, Schweizer M, Chahal P, Kamen AA. Manufacturing of viral vectors for gene therapy: part I. Upstream processing. *Pharm Bioprocess* 2014; **2:** 183-203. doi: 10.4155/pbp.14.16

101. van der Loo JCM, Wright JF. Progress and challenges in viral vector manufacturing. *Hum Mol Genet* 2016; **25:** R42-52. doi: 10.1093/hmg/ddv451

102. Ferreira MV, Cabral ET, Coroadinha AS. Progress and perspectives in the development of lentiviral vector producer cells. *Biotechnol J* 2021; **16**. doi: 10.1002/biot.202000017

103. Tomás HA, Rodrigues AF, Carrondo MJT, Coroadinha AS. LentiPro26: novel stable cell lines for constitutive lentiviral vector production. *Sci Rep* 2018; **8:** 1-11. doi: 10.1038/s41598-018-23593-y

104. Felberbaum RS. The baculovirus expression vector system: a commercial manufacturing platform for viral vaccines and gene therapy vectors. *Biotechnol J* 2015; **10:** 702-14. doi: 10.1002/biot.201400438

105. Kurasawa JH, Park A, Sowers CR, Halpin RA, Tovchigrechko A, Dobson CL, et al. Chemically defined, high-density insect cell-based expression system for scalable AAV vector production. *Mol Ther Methods Clin Dev* 2020; **19:** 330-40. doi: 10.1016/j.omtm.2020.09.018

106. Gupta P, Monge M, Boulais A, Chopra N, Hutchinson N. Single-use process platforms for responsive and cost-effective manufacturing. In: Eibl R, Eibl D, editors. *Single-use technology in biopharmaceutical manufacture*. Hoboken, NY, USA: John Wiley & Sons, Inc 2019. p. 201-10. doi: 10.1002/9781119477891.ch16

107. Minh A, Kamen AA. Critical assessment of purification and analytical technologies for enveloped viral vector and vaccine processing and their current limitations in resolving co-expressed extracellular vesicles. *Vaccines* 2021; **9:** 823. doi: 10.3390/vaccines9080823

108. Merten O-W, Schweizer M, Chahal P, Kamen A. Manufacturing of viral vectors: part II. Downstream processing and safety aspects. *Pharm Bioprocess* 2014; **2:** 237-51. http://www.future-science.com/doi/abs/10.4155/pbp.14.15%0Apapers2://publication/doi/10.4155/pbp.14.15

109. Kaemmerer WF. How will the field of gene therapy survive its success? *Bioeng Transl Med* 2018; **3:** 166-77. doi: 10.1002/btm2.10090

110. Salzman R, Cook F, Hunt T, Malech HL, Reilly P, Foss-Campbell B, et al. Addressing the value of gene therapy and enhancing patient access to transformative treatments. *Mol Ther* 2018; **26:** 2717-26. doi: 10.1016/j.ymthe.2018.10.017

111. Capra E, Godfrey A, Loche A, Smith J. Innovation in viral-vector gene therapy: unlocking the promise. [cited 2021 Dec 24]. Available at https://www.mckinsey.com/industries/life-sciences/our-insights/gene-therapy-innovation-unlocking-the-promise-of-viral-vectors

112. Wolf MW, Reichl U. Downstream processing of cell culture-derived virus particles. *Expert Rev Vaccines* 2011; **10:** 1451-75. doi: 10.1586/erv.11.111

113. Martin NT, Bell JC. Oncolytic virus combination therapy: killing one bird with two stones. *Mol Ther* 2018; **26:** 1414-22. doi: 10.1016/j.ymthe.2018.04.001

114. Bridle BW, Boudreau JE, Lichty BD, Brunellière J, Stephenson K, Koshy S, et al. Vesicular stomatitis virus as a novel cancer vaccine vector to prime antitumor immunity amenable to rapid boosting with adenovirus. *Mol Ther* 2009; **17:** 1814-21. doi: 10.1038/mt.2009.154

review

Ultrasound-guided carpal tunnel injections

Tilen Tumpaj[1], Vesna Potocnik Tumpaj[2], Domenico Albano[3], Ziga Snoj[2,4]

[1] Department of Anaesthesiology and Intensive Care Medicine, University Medical Centre Ljubljana, Slovenia
[2] Institute of Radiology, University Medical Centre Ljubljana, Slovenia
[3] Istituto Ortopedico Galeazzi, IRCCS Milano "Galeazzi", Unit of Diagnostic and Interventional Radiology Milan, Italy
[4] Faculty of Medicine, University of Ljubljana, Ljubljana, Slovenia

Radiol Oncol 2022; 56(1): 14-22.

Received 10 Avgust 2021
Accepted 15 December 2021

Correspondence to: Tilen Tumpaj, M.D., Department of Anaesthesiology and Intensive Care Medicine, University Medical Centre Ljubljana, Zaloška 7, SI-1000 Ljubljana, Slovenia. E-mail: tilen.tumpaj@gmail.com

Disclosure: No potential conflicts of interest were disclosed.

Background. Carpal tunnel syndrome (CTS), one of the most common entrapment neuropathies, can, in fact, be considered as a socio-economic issue that reduces work productivity, increases disability, and requires prolonged rehabilitation. The imaging modality of choice in CTS imaging is the ultrasound (US), as several morphological parameters can be used in CTS diagnosis and follow-up. In recent years, US-guided CTS injection therapy has become an established treatment option for mild to moderate CTS. The authors of this review performed a literature search that revealed several differences in US-guided carpal tunnel injection in an attempt to unify individual stages of CTS injections protocol for future guidance: patient preparation, injection approach, needle positioning, injected medications, and injectate volume. The three approaches to carpal tunnel injections described in the literature, that is, the ulnar, radial, and longitudinal, can be implemented with single or multiple deposits and different injection volumes. Medications used for injections are corticosteroids, local anaesthetics, dextrose, saline, platelet-rich plasma, and progesterone.

Conclusions. Although no consensus has yet been reached as to which protocol should be used, the ulnar approach with a single deposit injected in large volumes should be considered as the first choice, while dextrose should be the first-line medication option. Furthermore, as terminological differences make it difficult to draw a uniform comparison the presented steps for US-guided carpal tunnel injection might serve as a guideline for future studies.

Key words: carpal tunnel syndrome; ultrasound-guided injections; injection approach; needle positioning; corticosteroid; local anaesthetics

Introduction

Carpal tunnel syndrome (CTS), one of the most common entrapment neuropathies, can, in fact, be considered as a socio-economic issue that reduces work productivity, increases disability, and requires prolonged rehabilitation.[1] The diagnostic workup of CTS must include a comprehensive evaluation including clinical findings, nerve conduction studies, and ultrasound imaging (US)[2,3], which represents the modality of choice due to the superficial course of the median nerve (MN).[3,4] Nerve US examination is performed with high-frequency probes that provide a detailed depiction of nerve echotexture and fascicles.[5,6] US-based morphological parameters for detecting CTS are an increased cross-section area (CSA) of the MN at the carpal tunnel inlet or outlet, flattening of the MN, and bowing of the transverse carpal ligament (TCL) at the level of the carpal tunnel outlet.[7-9] Elastography has been proven as a useful adjunct US method in CTS evaluation.[10]

Therapeutic recommendations for CTS depend on disease severity and may include anything from a conservative approach to surgical intervention.[2,3] US-guided injections have become increasingly

important in the treatment of mild and moderate CTS[2,3] and, as landmark-guided injections have been proven to be less effective and cause more complications, US imaging has become the foundation of therapeutic recommendations.[2,3] US-guided carpal tunnel injections are the most effective minimally invasive treatment method with minimum side effects that can remarkably improve the symptoms and functional status.[11] The authors of this review performed a literature search that revealed several differences in US-guided carpal tunnel injections and summarized the differences in an attempt to unify individual stages of CTS injections protocol for future guidance.

Carpal tunnel injections

Literature search

For our narrative review paper, we conducted an Ovid MEDLINE and PubMed search in which we included the papers published from 2002, when the first paper on US-guided injection was published[12], to 2021 with the keywords »carpal tunnel injection« and »ultrasound-guided carpal tunnel injection«. The search results included case-control studies, systematic reviews, and meta-analyses that contained data on US-guided carpal tunnel injections. References in these papers were carefully reviewed and were included in our review if they met our criteria (Figure 1). After we reviewed the papers, we used the differences between them to define the steps of US-guided carpal tunnel injections: patient preparation, approaches, needle positioning, injected medications and injected volumes.

Patient preparation

The patient can be either seated or lying supine.[13] When seated, the elbow is resting on the examination table in a 90° flexion position.[14] When lying supine, the arm is abducted to 90° with the elbow extended.[11,15,16] In both positions the forearm is supinated and the wrist is in a 15–35° dorsiflexion position.[11,15,16] Careful US examination is important for injection planning. The wrist is examined with a linear probe along the carpal tunnel and special attention is given to the MN anatomy (size, position, aberrant variants) and the course of blood vessels.[13,17,18]

Authors reported two different procedures for disinfecting the skin[11,16,17,19]: some clean the puncture area with an alcohol swab and use a sterile ultrasound gel[11], while others perform surgical disinfection and use a sterile probe sleeve.[16,17,19] Even though there is no clear consensus on patient preparation, in recent years some authors (*e.g.* Guo, Green, Chianca, *etc.*) have reported that surgical disinfection of the area can help avoid infections of the puncture site or the deep tissues[16,17,19], which can also be avoided if a sleeve is used for the US probe. A few authors have reportedly used a short-acting local anaesthetic to numb the dermal and subdermal area before performing US-guided carpal tunnel injection[15,20], but in the majority of cases, the local anaesthetic is added to the injected mixture.[21-23] Needles of different sizes (22 to 30 Gauges) have been used in US-guided carpal tunnel injections.[11,14-16,24] Needles with a small diameter cause less pain upon insertion and are less likely to cause nerve damage during the procedure, but are not

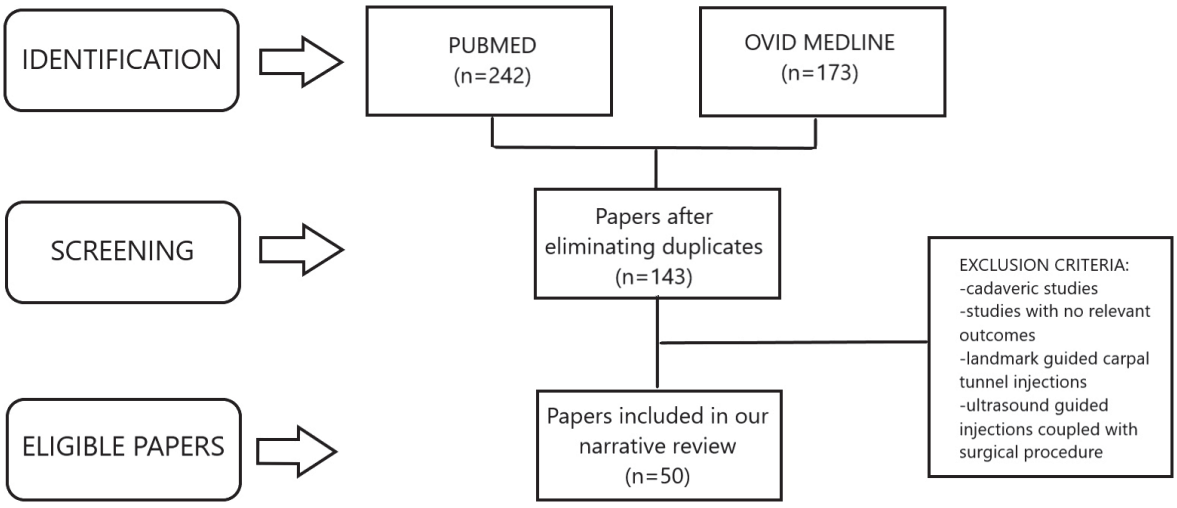

FIGURE 1. Depicting a flowchart of paper search and selection with exclusion criteria.

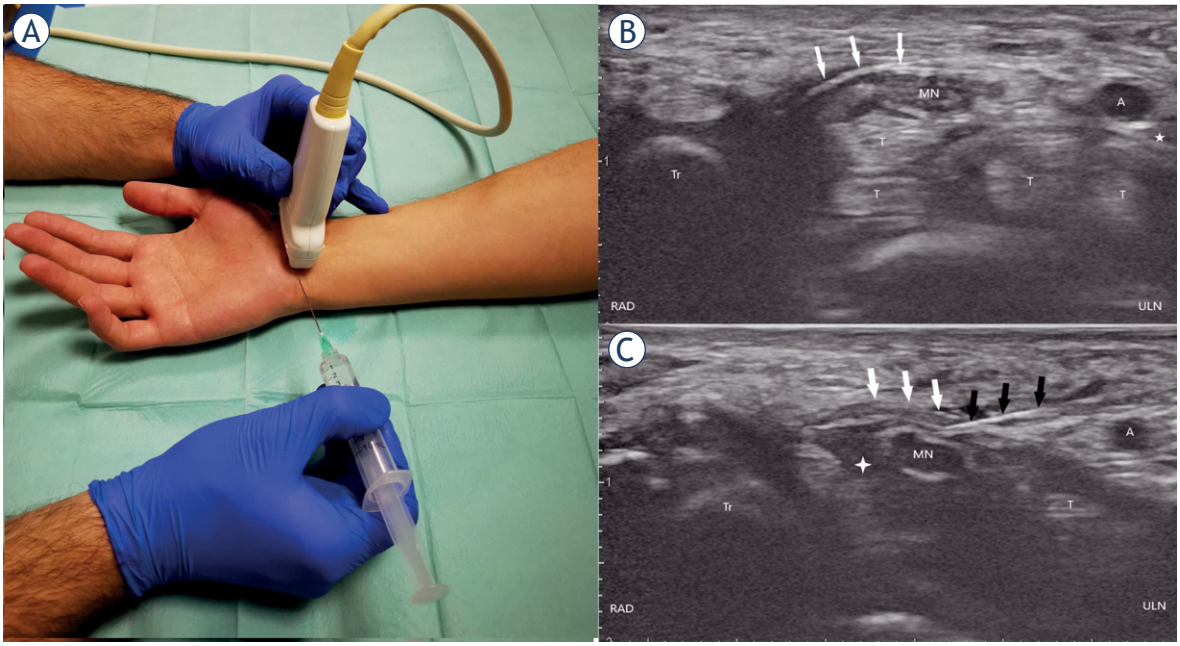

FIGURE 2. (A), **(B)**, and **(C)** showing the ulnar approach. **(A)** wrist and needle positioning for carpal tunnel injection, **(B)** ultrasound anatomy of the carpal tunnel shown in the short axis, **(C)** penetrating transverse carpal ligament positioning the needle tip above the median nerve. Ultrasound of the carpal tunnel after the needle penetrates the transverse carpal ligament. Comparing B and C note the expansion of the perineural space marked with a white cross.

A = ulnar artery; black arrows = needle; MN = median nerve; RAD = radial; T = flexor tendons; Tr = trapezium; ULN = ulnar; white arrows = transverse carpal ligament; white cross = perineural injectate; white star = ulnar nerve

suitable for injecting protein-rich plasma, because they damage the platelets due to the small diameter and platelet size.[11,14-16,24,25]

Approaches

Three approaches to carpal tunnel injections can be found in the literature and all of them are performed with a linear transducer of varying frequencies (5–17 MHz).[11,13,14,26-29]

Ulnar approach

The transducer is positioned at the distal wrist crease perpendicularly to the course of the MN (Figure 2A).[13] The probe is then moved ulnarly keeping the MN in view until the pisiform bone, ulnar nerve, and artery are brought into view. On the ulnar side, the pisiform is seen as a hyperechoic structure and the honeycomb appearance of the ulnar nerve may be differentiated radially to the pulsating ulnar artery (Figure 2B).[13] The needle is introduced in plane in an ulnar to radial direction, then passes the ulnar nerve and ulnar artery superficially, and punctures the TCL so that the needle tip can be advanced adjacently to the MN (Figure 2C).[15,26-28]

Radial approach

In the radial approach, the transducer is positioned at the distal wrist crease perpendicularly to the course of the MN (Figure 3A).[14] The probe is moved radially keeping the MN in view until the scaphoid and flexor carpi radialis tendon are brought into view. On the radial side, the scaphoid is seen as a hyperechoic structure and the flexor carpi radialis tendon lies inferolateral to the MN (Figure 3B). The needle is introduced in plane in a radial to ulnar direction, then proceeds above the flexor carpi radialis tendon, and punctures the TCL so that the needle tip can be advanced adjacently to the MN (Figure 3C).[14]

Longitudinal approach

In the longitudinal approach, the transducer is positioned parallel to the MN at the distal wrist so that the MN is seen along the TCL from the carpal tunnel inlet to the carpal tunnel outlet (Figures 4A,B).

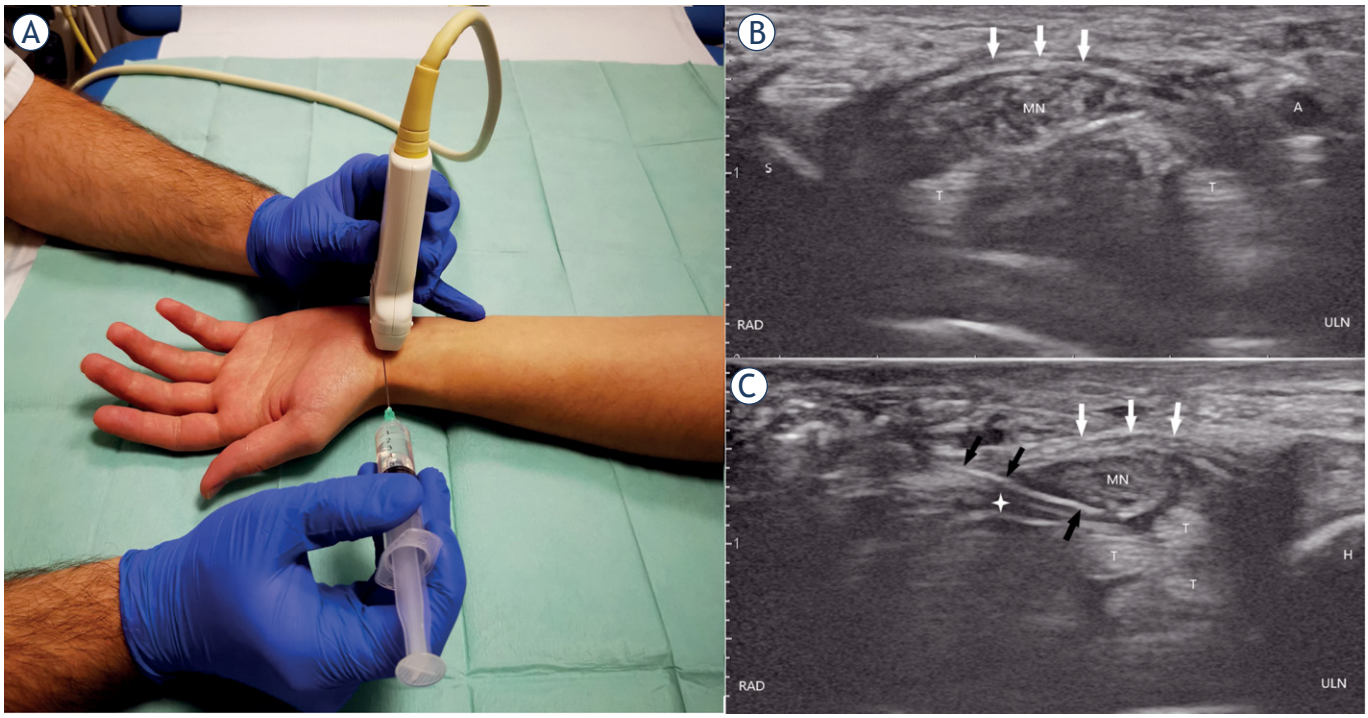

FIGURE 3. (A), **(B)**, and **(C)** showing the radial approach. **(A)** wrist and needle positioning for carpal tunnel injection, **(B)** ultrasound anatomy of the carpal tunnel shown in the short axis, **(C)** penetrating transverse carpal ligament positioning the needle tip below the median nerve. Ultrasound of the carpal tunnel after the needle penetrates the transverse carpal ligament. Comparing figures B and C note the expansion of the perineural space marked with a white cross.

A = ulnar artery; black arrows = needle; H = hamate; RAD = radial; S = scaphoid; MN = median nerve; T = flexor tendons; ULN = ulnar; white arrows = transverse carpal ligament; white cross = perineural injectate

The probe is then moved laterally to the MN approximately 0.5 cm until the nerve disappears.[11] Two modifications can be found in the literature, namely the proximal to the distal and the distal to the proximal.[11,29] In the proximal to distal, the needle is inserted at the distal wrist crease and is advanced distally.[29] In the distal to proximal, the needle is inserted approximately 2 cm distally to the distal wrist crease and is advanced proximally.[11] In both modifications, the needle is introduced in plane and punctures the TCL so that the needle tip can be advanced adjacently to the MN (Figures 4C,D).[11,29]

Needle positioning

The aim of carpal tunnel injection is to position the needle tip adjacent to the MN without inducing nerve or vascular injury. When the needle is positioned perineurally, the injection volume can be injected as a single or multiple deposit. In a single deposit, the injection is deposited at a single location[11,14,29], whereas in a multiple deposit, the needle is repositioned to deposit the injection volume on multiple locations.[16]

Injected medications

Medications used for carpal tunnel injections are corticosteroids[30-35], local anaesthetics (LA)[35], dextrose[36,37], platelet-rich plasma (PRP)[25,38], progesterone[23,39] and saline.[40] The most widely used medications for carpal tunnel injections are corticosteroids[30-35], which ameliorate MN compression due to their anti-inflammatory properties.[3] Particulate (*e.g.* methylprednisolone) or nonparticulate (*e.g.* dexamethasone) corticosteroids can be injected in doses of 40–80 mg.[30-35] The adverse effects of corticosteroids are rare and range from skin discoloration and irritation at the injection site to neurotoxicity and atrophy of thenar muscles.[35] Another medication commonly used in the treatment of CTS are LAs[35], predominantly short-acting LAs (*e.g.* lidocaine 2%) that can be injected as a single compound or in conjunction with corticosteroids.[28,35] These offer immediate pain relief and may give long-lasting

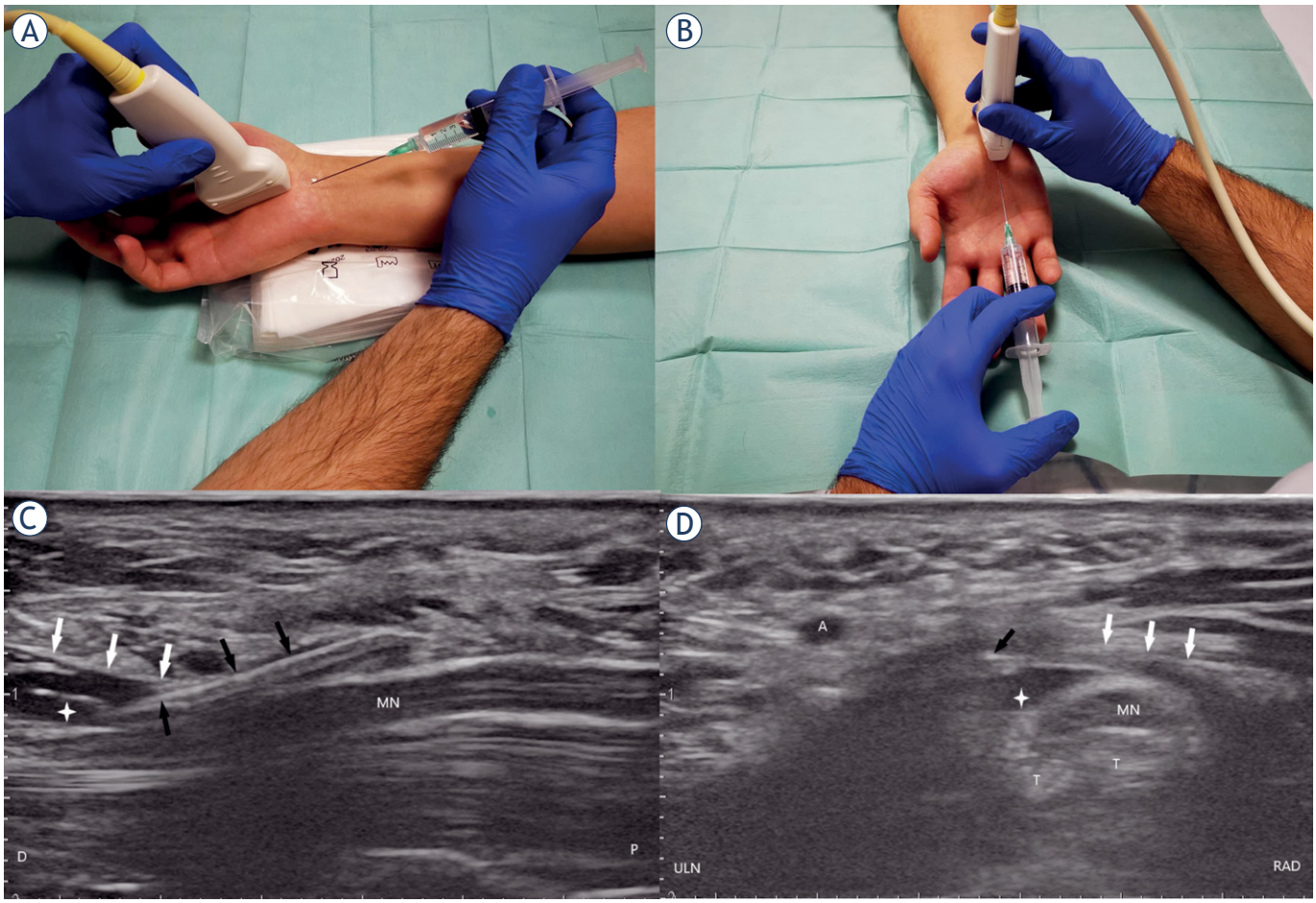

FIGURE 4. (A), (B), (C), and **(D)** showing the longitudinal approach. **(A)** Wrist and needle positioning for carpal tunnel injection for the proximal to distal approach, **(B)** Wrist and needle positioning for carpal tunnel injection for the distal to proximal approach, **(C)** Ultrasound of the carpal tunnel shown in the long axis after the needle penetrates the transverse carpal ligament and positioning the needle tip parallel to the median nerve, **(D)** ultrasound of the carpal tunnel shown in the short axis after the needle penetrates the transverse carpal ligament positioning the needle tip parallel to the median nerve. Note in C and D the expanded perineural space marked with a white cross.

A = ulnar artery; black arrows = needle; D = distal; MN = median nerve; P = proximal; RAD = radial; T = flexor tendons; ULN = ulnar; white arrows = transverse carpal ligament; white cross = perineural injectate

effects, which are speculated to be caused by the blockage of the sympathetic reflex arc, suppression of nociceptive discharge, blockade of sensitization, and anti-inflammatory effects.[35] Adverse effects of LAs are rare and range from common allergic reactions to inadvertent intravascular injection, a very serious complication that can lead to seizures and heart conduction blocks.[35] More recently, dextrose has also been used as a medication.[36,37] The exact mechanism of action of dextrose is not known, but it is thought that it stimulates an anti-inflammatory response through the inhibition of capsaicin, causing sensitive receptors to prevent the release of substance P and calcitonin gene-related peptide, both of which are known to cause swelling of the nerve and induce pain.[37] The main advantage of dextrose is that no serious adverse effects due to biochemical properties were reported.[37] Saline is widely used either as a single compound in hydrodissection or as a diluting substance for corticosteroids or LAs (Figure 5A,B,C).[30-35,40,41] There are no serious adverse effects of saline; however, pain upon injection has been reported when no LA is added.[22,28,30,40] A promising type of injectate is PRP[25,38] that triggers a neuroregenerative response by releasing several hormones and growth factors, such as platelet-derived growth factor, transforming growth factor, epidermal growth factor, vascular endothelial growth factor, and insulin-like growth factor-1. These stimulate healing by reducing the

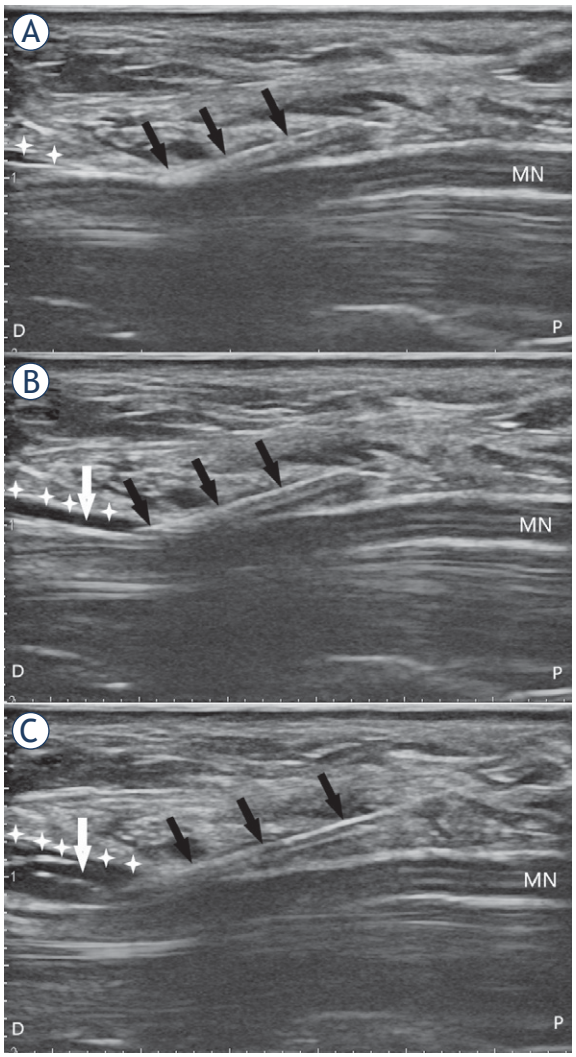

FIGURE 5. (A), **(B)**, and **(C)** showing the carpal tunnel in the long axis. The effect of injectate volume on perineural space expansion and subsequent hydrodissection. Note the expansion of the perineural space (white arrow) around the median nerve before **(A)**, during **(B)** and after injecting 6 ml of the injectate and subsequent hydrodissection **(C)**.

black arrows = needle; D = distal; MN = median nerve; P = proximal; white cross = transverse carpal ligament

inflammatory response.[38] Lastly, progesterone, which has anti-inflammatory and neuroprotective effects on nerves, has also been used recently as an injectate.[23,39]

Injection volume

There is no consensus on the optimal volume injected into the carpal tunnel and injection volumes anywhere between 1 ml to 10 ml can be found in the literature.[30-35,37,40,42-46] The injectate can be a manufactured single-compound solution or a multi-compound preparation. The latter is a mixture of active compounds with either saline or LA or both.[30-35,40,42-46] Corticosteroids are predominantly injected as a multi-compound solution of 1–2 ml corticosteroids with 1–2 ml of LA or 1–2 ml of saline.[28,30-34,45,46] LAs are usually added to multi-compound solutions as an anaesthetic during the injection and are rarely injected as a single compound, but when they are, the volume ranges from 0.5 to 4 ml.[35,47] Saline is mostly used as a mixture substance for other medications as a part of multi-compound solutions.[30-37,40,44-46] In hydrodissection, saline is used as a single-compound solution of 3–10 ml in volume.[40,48] Dextrose is injected as a single-compound solution of 3–10 ml in volume.[37,40,48] PRP is injected as a single-compound solution of 1–3 ml in volume.[25,38] Progesterone is injected as a multi-compound solution, a mixture of 0.5 ml of LA and 0.5 ml of progesterone.[23,39]

Discussion

Even though US-guided injection therapy has become an established treatment option for CTS[2], no consensus has yet been achieved on what steps should be taken to achieve the best results. Carpal tunnel injections may be performed with the landmark-guided approach, but several complications have been noted, such as nerve injury, intravascular application of medication, failure to perforate TCL, *etc.*[18] When the US is used to guide the injections, the risk of these complications is reduced.[18]

Three approaches to carpal tunnel injections can be found in the literature. The ulnar approach is the most frequently used, as it helps better visualize the carpal tunnel content and thus enables accurate perineural injection by avoiding neurovascular structures.[13] This approach is also easier to learn in comparison to the other two approaches and provides good needle control.[13] Reports on radial and longitudinal approaches are scarce.[14,27,29,49] The reviewed authors do not offer any personal perspective on the benefits and difficulties of the radial approach.[14] Jurbala and Burbank have come to the conclusion that the ulnar approach carries a higher risk of inadvertent penetration of the neurovascular structures because the needle is directed toward and not tangential to the MN.[11] It has to be noted that scanning in the long axis can be challenging because it is difficult to differentiate between swollen nerve fascicles, muscles, and inflamed tendons.[11] Only a single study was found

where different approaches – radial and ulnar, to be precise – were compared to one another, but the results showed no difference in patient outcome or measured US parameters.[14] Even so, the ulnar approach should be considered as the first choice because it is backed by the largest amount of evidence and is easier to learn than other approaches.[13]

Only a few papers included a detailed report on needle positioning, making it difficult to discern the benefits of different approaches.[11,16,29] A randomized controlled study on US-guided single-deposit injections of corticosteroids showed no difference in patient outcome, electrodiagnostic, and US findings in terms of deposition between the MN and TCL or deposition between the MN and flexor tendons.[14] The authors emphasized that placing the needle below the MN is technically less demanding and is, therefore, the better option for less experienced practitioners.[14] A study by Nwawka *et al.* where the spread of US-guided injections was observed in different anatomical positions concluded that a single-deposit injection offers circumferential coverage using injection volumes of 2 ml, suggesting that it is unnecessary to place the needle between the MN and TCL at multiple sites along the nerve.[49] These two studies suggest that a single deposit offers circumferential coverage of the MN.[14,49] Further studies are warranted to discern the potential superiority of multiple deposit versus single deposit; however, a single deposit should be considered as the first choice as a multiple deposit is harder to perform and has not yet shown any superior benefits.

Another aspect to be taken into consideration in US-guided CTS injection treatment is the choice of medication. Several medications can be used for carpal tunnel injections, of which the most widely utilized are corticosteroids.[30-35] Although there is no consensus on what type or dose of corticosteroids achieves the best outcome, it is thought that the effect of particulate corticosteroids lasts longer due to the quick uptake of nonparticulate corticosteroids; however, recent studies did not prove the superiority of either type of corticosteroids.[30-35] Salman Roghani *et al.* compared the effects of 40 mg to 80 mg of methylprednisolone for carpal tunnel injections and found no significant differences in patient outcome.[33] Similarly, Karimzadeh *et al.* found no significant differences in patient outcome between 40 mg of methylprednisolone and 80 mg triamcinolone, but on the other hand, Habib *et al.* emphasized that a lower dose could be beneficial due to fewer side effects such as pain upon injection, glucose control after the procedure, and potential neurotoxicity.[31,32] The majority of US-guided carpal tunnel injections are performed with LAs as part of the multi-compound solution, but these can also be used as a single-compound solution. The effects of LAs as a single compound are poorly researched and only a few studies have been published on this topic.[35,47] Karadas *et al.* compared the effects of LAs and corticosteroids in CTS treatment and found no significant difference in patient outcome.[47] In recent years, dextrose and PRP have also been used in the treatment of CTS. The effects of dextrose as a single-compound solution have been widely researched[36,37,43,50], but it is still unclear whether they are caused by the release of anti-inflammatory tissue mediators after the injection or better median nerve gliding due to hydrodissection. Comparison between dextrose, saline, and corticosteroids has shown that dextrose is superior in terms of patient outcome.[37,43] Due to improved patient outcomes, authors have even proposed that dextrose should be a first-line medication option for patients with CTS.[37,43] Injections of PRP have also given promising results in CTS treatment. In a meta-analysis by Lin *et al.* PRP was ranked second to dextrose in the terms of clinical effects.[43] The downside of PRP is the difference in the preparation protocol, which can produce different clinical outcomes due to compositional differences.[43] There are also the issues of higher costs, more complex organization, and limited availability of machines needed to prepare PRP.[43] Progesterone has also been proposed as a possible choice of injectate and its effect has been compared to that of corticosteroids due to their similar molecular structure.[23,39] According to the proposed theory, progesterone receptors are located on the transverse ligament lining cells and wrist synovial tissue.[39] Bahrami *et al.* concluded that progesterone is equal to corticosteroids in patient outcomes, while Raeissadat *et al.* reported that progesterone is equal or even superior to corticosteroids in symptom relief.[23,39] Several medications are used in clinical practice with no clinical consensus on medication of choice; however, the papers with the highest level of evidence suggest that dextrose should be the first-line medication option.[37,43]

Injection volume also remains a question of debate as only a few studies compared the effects of different volumes. In most studies, relatively low volumes of injectate were used (1–3 ml).[42] In the study by Lin *et al.*, the authors compared different injection volumes of dextrose (1, 2, and 4 ml) and concluded that the injection of 4 ml provided the best outcome.[43] However, Schrier *et al.* were unable to prove the superiority of a 5 ml versus 2 ml in-

jection of corticosteroids and LA.[28] It is speculated that larger injected volumes (> 5 ml) yield better results due to the conjoined effect of hydrodissection and better injection distribution.[30,43] With hydrodissection, adhesiolysis can be achieved by separating TCL from the MN and enabling normal tendon gliding.[28,41] A prospective randomized control trial on the effects of hydrodissection showed a significant improvement of the intervention group at a 3-month follow-up in comparison to the control group.[37] In the intervention group, a multideposit injection was performed to detach the MN from the TCL and separate the MN from the flexor tendons, whereas in the control group saline was injected subcutaneously.[37] It has been suggested that a cumulative effect of hydrodissection may be expected if injections are repeated.[37,40] Although only a few studies have been published on this topic, there appears to be a tendency of better outcomes with larger injected volumes.

Some limitations of our review need to be noted. The majority of papers reported a short-term follow-up and only a few reported a follow-up of up to 12 months. Furthermore, all the reviewed papers provided very little information on the optimal protocol of US-guided carpal tunnel injection. Even though we retrieved a large number of papers, only a few of them focused on a specific question related to the proposed steps in US-guided carpal tunnel injection. Further studies are required to fully assess the contribution and efficacy of US-guided injection therapy for CTS, and this paper should serve as a reference to determine which study aims are important.

Conclusions

In recent years, US-guided injection therapy has become an established treatment option in mild to moderate CTS. Although no consensus has yet been reached as to which protocol gives the best results, the ulnar approach with a single deposit should be considered as the first choice and dextrose as the first-line medication option injected in larger volumes. Furthermore, as terminological differences make it difficult to draw a uniform comparison between the reviewed papers, the presented steps of US-guided carpal tunnel injection might serve as a guideline for future studies.

References

1. Petrover D, Richette P. Treatment of carpal tunnel syndrome: from ultrasonography to ultrasound-guided carpal tunnel release. *Joint Bone Spine* 2018; **85:** 545-52. doi: 10.1016/j.jbspin.2017.11.003
2. Padua L, Coraci D, Erra C, Pazzaglia C, Paolasso I, Loreti C, et al. Carpal tunnel syndrome: clinical features, diagnosis, and management. *Lancet Neurol* 2016; **15:** 1273-84. doi: 10.1016/S1474-4422(16)30231-9
3. Sconfienza LM, Adriaensen M, Albano D, Allen G, Aparisi Gómez MP, Bazzocchi A, et al; Ultrasound and Interventional Subcommittees of the European Society of Musculoskeletal Radiology (ESSR). Clinical indications for image-guided interventional procedures in the musculoskeletal system: a Delphi-based consensus paper from the European Society of Musculoskeletal Radiology (ESSR)-part III, nerves of the upper limb. *Eur Radiol* 2020; **30:** 1498-506. doi: 10.1007/s00330-019-06479-z
4. Sconfienza LM, Albano D, Allen G, Bazzocchi A, Bignotti B, Chianca V, et al. Clinical indications for musculoskeletal ultrasound updated in 2017 by European Society of Musculoskeletal Radiology (ESSR) consensus. *Eur Radiol* 2018; **28:** 5338-51. doi: 10.1007/s00330-018-5474-3
5. Albano D, Aringhieri G, Messina C, De Flaviis L, Sconfienza LM. High-frequency and ultra-high frequency ultrasound: musculoskeletal maging up to 70 MHz. *Semin Musculoskelet Radiol* 2020; **24:** 125-34. doi: 10.1055/s-0039-3401042
6. Snoj Ž, Serša I, Matičič U, Cvetko E, Omejec G. Nerve fascicle depiction at MR microscopy and high-frequency US with anatomic verification. *Radiology* 2020; **297:** 672-4. doi: 10.1148/radiol.2020201910
7. Gonzalez-Suarez CB, Fidel BC, Cabrera JTC, Dela Cruz FC, Gesmundo MVT, Regala CFG, et al. Diagnostic accuracy of ultrasound parameters in carpal tunnel syndrome: additional criteria for diagnosis. *J Ultrasound Med* 2019; **38:** 3043-52. doi: 10.1002/jum.15012
8. Mallouhi A, Pülzl P, Trieb T, Piza H, Bodner G. Predictors of carpal tunnel syndrome: accuracy of gray-scale and color Doppler sonography. *AJR Am J Roentgenol* 2006; **186:** 1240-5. doi: 10.2214/AJR.04.1715
9. Peer S, Gruber H, Loizides A. Sonography of carpal tunnel syndrome: why, when and how. *Imag in Med* 2012; **4:** 287-97. doi: 10.2217/iim.12.25
10. Snoj Ž, Wu CH, Taljanovic MS, Dumić-Čule I, Drakonaki EE, Klauser AS. Ultrasound elastography in musculoskeletal radiology: past, present, and future. *Semin Musculoskelet Radiol* 2020; **24:** 156-66. doi: 10.1055/s-0039-3402746
11. Jurbala BM, Burbank TA. A sonographically guided in-plane distal-to-proximal transligamentous approach to carpal tunnel injections. *Hand* 2018; **13:** 522-28. doi: 10.1177/1558944717725375
12. Grassi W, Farina A, Filippucci E, Cervini C. Intralesional therapy in carpal tunnel syndrome: a sonographic-guided approach. *Clin Exp Rheumatol* 2002; **20:** 73-6. PMID:11892715
13. Smith J, Wisniewski SJ, Finnoff JT, Payne JM. Sonographically guided carpal tunnel injections: the ulnar approach. *J Ultrasound Med* 2008; **27:** 1485-90. doi: 10.7863/jum.2008.27.10.1485
14. Babaei-Ghazani A, Forogh B, Raissi GR, Ahadi T, Eftekharsadat B, Yousefi N, et al. Ultrasound-guided corticosteroid injection in carpal tunnel syndrome: comparison between radial and ulnar approaches. *J Pain Res* 2020; **13:** 1569-78. doi: 10.2147/JPR.S248600
15. Guo XY, Xiong MX, Lu M, Cheng XQ, Wu YY, Chen SY, et al. Ultrasound-guided needle release of the transverse carpal ligament with and without corticosteroid injection for the treatment of carpal tunnel syndrome. *J Orthop Surg Res* 2018; **13:** 69. doi: 10.1186/s13018-018-0771-8
16. Guo K, McCool L, Wang H, Guo D, Guo D. The modified ultrasound-guided distal-to-proximal carpal tunnel injection with median nerve hydrodissection: a retrospective safety review of 827 procedures. *Hand* 2021; **16:** 407-9. doi: 10.1177/1558944719861715
17. Green DP, MacKay BJ, Seiler SJ, Fry MT. Accuracy of carpal tunnel injection: a prospective evaluation of 756 patients. *Hand* 2020; **15:** 54-8. doi: 10.1177/1558944718787330
18. Babaei-Ghazani A, Roomizadeh P, Forogh B, Moeini-Taba SM, Abedini A, Kadkhodaie M, et al. Ultrasound-guided versus landmark-guided local corticosteroid injection for carpal tunnel syndrome: a systematic review and meta-analysis of randomized controlled trials. *Arch Phys Med Rehabil* 2018; **99:** 766-75. doi: 10.1016/j.apmr.2017.08.484

19. Chianca V, Orlandi D, Messina C, Albano D, Corazza A, Rapisarda S, et al. Interventional therapeutic procedures to treat degenerative and inflammatory musculoskeletal conditions: state of the art. *Radiol Med* 2019; **124:** 1112-20. doi: 10.1007/s11547-019-01018-8

20. Cartwright MS, White DL, Demar S, Wiesler ER, Sarlikiotis T, Chloros GD, et al. Median nerve changes following steroid injection for carpal tunnel syndrome. *Muscle Nerve* 2011; **44:** 25-9. doi: 10.1002/mus.22067

21. Hsu YC, Yang FC, Hsu HH, Huang GS. Ultrasound-guided corticosteroid injection in patients with carpal tunnel syndrome: efficacy of intra-epineurial injection. *Ultraschall Med* 2018; **39:** 334-42. doi: 10.1055/s-0043-120109

22. Malone DG, Clark TB, Wei N. Ultrasound-guided percutaneous injection, hydrodissection, and fenestration for carpal tunnel syndrome: description of a new technique. *J Appl Res* 2010; **10:** 107-14.

23. Raeissadat SA, Shahraeeni S, Sedighipour L, Vahdatpour B. Randomized controlled trial of local progesterone vs corticosteroid injection for carpal tunnel syndrome. *Acta Neurol Scand* 2017; **136:** 365-71. doi: 10.1111/ane.12739

24. Lam KHS, Hung CY, Chiang YP, Onishi K, Su DCJ, Clark TB, et al. Ultrasound-guided nerve hydrodissection for pain management: rationale, methods, current literature, and theoretical mechanisms. *J Pain Res* 2020; **13:** 1957-68. doi: 10.2147/JPR.S247208

25. Uzun H, Bitik O, Uzun Ö, Ersoy US, Aktaş E. Platelet-rich plasma versus corticosteroid injections for carpal tunnel syndrome. *J Plast Surg Hand Surg* 2017; **51:** 301-5. doi: 10.1080/2000656X.2016.1260025

26. Kim DH, Jang JE, Park BK. Anatomical basis of ulnar approach in carpal tunnel injection. *Pain Physician* 2013; **16:** E191-8. PMID: 23703418

27. Lee JY, Park Y, Park KD, Lee JK, Lim OK. Effectiveness of ultrasound-guided carpal tunnel injection using in-plane ulnar approach: a prospective, randomized, single-blinded study. *Medicine* 2014; **93:** e350. doi: 10.1097/MD.0000000000000350

28. Schrier VJMM, Brault JS, Amadio PC. Ultrasound-guided hydrodissection with corticosteroid injection in the treatment of carpal tunnel syndrome: a pilot study. *J Ultrasound Med* 2020; **39:** 1759-68. doi: 10.1002/jum.15279

29. Ustün N, Tok F, Yagz AE, Kizil N, Korkmaz I, Karazincir S, et al. Ultrasound-guided vs. blind steroid injections in carpal tunnel syndrome: a single-blind randomized prospective study. *Am J Phys Med Rehabil* 2013; **92:** 999-1004. doi: 10.1097/PHM.0b013e31829b4d72

30. DeLea SL, Chavez-Chiang NR, Poole JL, Norton HE, Sibbitt WL Jr, Bankhurst AD. Sonographically guided hydrodissection and corticosteroid injection for scleroderma hand. *Clin Rheumatol* 2011; **30:** 805-13. doi: 10.1007/s10067-010-1653-6

31. Habib GS, Badarny S, Rawashdeh H. A novel approach of local corticosteroid injection for the treatment of carpal tunnel syndrome. *Clin Rheumatol* 2006; **25:** 338-40. doi: 10.1007/s10067-005-0002-7

32. Karimzadeh A, Bagheri S, Raeissadat SA, Bagheri S, Rayegani SM, Rahimi-Dehgolan S, et al. The comparison of the effectiveness between different doses of local methylprednisolone injection versus triamcinolone in carpal tunnel syndrome: a double-blind clinical trial. *J Pain Res* 2019; **12:** 579-84. doi: 10.2147/JPR.S190652

33. Salman Roghani R, Holisaz MT, Tarkashvand M, Delbari A, Gohari F, Boon AJ, et al. Different doses of steroid injection in elderly patients with carpal tunnel syndrome: a triple-blind, randomized, controlled trial. *Clin Interv Aging* 2018; **13:** 117-24. doi: 10.2147/CIA.S151290

34. Stark H, Amirfeyz R. Cochrane corner: local corticosteroid injection for carpal tunnel syndrome. *J Hand Surg Eur* 2013; **38:** 911-4. doi: 10.1177/1753193413490848

35. MacMahon PJ, Eustace SJ, Kavanagh EC. Injectable corticosteroid and local anesthetic preparations: a review for radiologists. *Radiology* 2009; **252:** 647-61. doi: 10.1148/radiol.2523081929

36. Li TY, Chen SR, Shen YP, Chang CY, Su YC, Chen LC, et al. Long-term outcome after perineural injection with 5% dextrose for carpal tunnel syndrome: a retrospective follow-up study. *Rheumatology* 2021; **60:** 881-7. doi: 10.1093/rheumatology/keaa361

37. Wu YT, Ho TY, Chou YC, Ke MJ, Li TY, Tsai CK, et al. Six-month efficacy of perineural dextrose for carpal tunnel syndrome: a prospective, randomized, double-blind, controlled trial. *Mayo Clin Proc* 2017; **92:** 1179-89. doi: 10.1016/j.mayocp.2017.05.025

38. Catapano M, Catapano J, Borschel G, Alavinia SM, Robinson LR, Mittal N. Effectiveness of platelet-rich plasma injections for nonsurgical management of carpal tunnel syndrome: a systematic review and meta-analysis of randomized controlled trials. *Arch Phys Med Rehabil* 2020; **101:** 897-906. doi: 10.1016/j.apmr.2019.10.193

39. Bahrami MH, Shahraeeni S, Raeissadat SA. Comparison between the effects of progesterone versus corticosteroid local injections in mild and moderate carpal tunnel syndrome: a randomized clinical trial. *BMC Musculoskelet Disord* 2015; **16:** 322. doi: 10.1186/s12891-015-0752-6

40. Wu YT, Chen SR, Li TY, Ho TY, Shen YP, Tsai CK, et al. Nerve hydrodissection for carpal tunnel syndrome: a prospective, randomized, double-blind, controlled trial. *Muscle Nerve* 2019; **59:** 174-80. doi: 10.1002/mus.26358

41. Evers S, Thoreson AR, Smith J, Zhao C, Geske JR, Amadio PC. Ultrasound-guided hydrodissection decreases the gliding resistance of the median nerve within the carpal tunnel. *Muscle Nerve* 2018; **57:** 25-32. doi: 10.1002/mus.25723

42. Evers S, Bryan AJ, Sanders TL, Gunderson T, Gelfman R, Amadio PC. Influence of injection volume on rate of subsequent intervention in carpal tunnel syndrome over 1-year follow-up. *J Hand Surg Am* 2018; **43:** 537-44. doi: 10.1016/j.jhsa.2018.02.024

43. Lin MT, Liao CL, Hsiao MY, Hsueh HW, Chao CC, Wu CH. Volume matters in ultrasound-guided perineural dextrose injection for carpal tunnel syndrome: a randomized, double-blinded, three-arm trial. *Front Pharmacol* 2020; **11:** 625830. doi: 10.3389/fphar.2020.625830

44. Armstrong T, Devor W, Borschel L, Contreras R. Intracarpal steroid injection is safe and effective for short-term management of carpal tunnel syndrome. *Muscle Nerve* 2004; **29:** 82-8. doi: 10.1002/mus.10512

45. Atroshi I, Flondell M, Hofer M, Ranstam J. Methylprednisolone injections for the carpal tunnel syndrome: a randomized, placebo-controlled trial. *Ann Intern Med* 2013; **159:** 309-17. doi: 10.7326/0003-4819-159-5-201309030-00004

46. Cass SP. Ultrasound-guided nerve hydrodissection. *Current Sports Medicine Reports* 2016; **15:** 20-2. doi: 10.1249/jsr.0000000000000226

47. Karadaş Ö, Tok F, Akarsu S, Tekin L, Balaban B. Triamcinolone acetonide vs procaine hydrochloride injection in the management of carpal tunnel syndrome: a randomized placebo-controlled study. *J Rehabil Med* 2012; **44:** 601-4. doi: 10.2340/16501977-0990

48. Elawamy A, Hassanien M, Hamed A, Roushdy ASI, Abass NA, Mohammed G, et al. Efficacy of hyalase hydrodissection in the treatment of carpal tunnel syndrome: a randomized, double-blind, controlled, clinical trial. *Pain Physician* 2020; **23:** E175-83. PMID: 32214296

49. Nwawka OK, Miller TT, Jawetz ST, Saboeiro GR. Ultrasound-guided perineural injection for nerve blockade: does a single-sided injection produce circumferential nerve coverage? *J Clin Ultrasound* 2016; **44:** 465-9. doi: 10.1002/jcu.22364

50. Chen LC, Ho TY, Shen YP, Su YC, Li TY, Tsai CK, et al. Perineural dextrose and corticosteroid injections for ulnar neuropathy at the elbow: a randomized double-blind trial. *Arch Phys Med Rehabil* 2020; **101:** 1296-303. doi: 10.1016/j.apmr.2020.03.016

research article

Lack of association between cortical amyloid deposition and glucose metabolism in early stage Alzheimer´s disease patients

Daniela Ehrlich[1], Andreas Dunzinger[2], Gertraud Malsiner-Walli[3], Bettina Grün[4], Raffi Topakian[5], Marina Hodolic[6,7], Elmar Kainz[1], Robert Pichler[2,8,9]

[1] Department of Gerontology, Kepler University Hospital, Neuromed Campus, Linz, Austria
[2] Institute of Nuclear Medicine, Kepler University Hospital, Neuromed Campus, Linz, Austria
[3] Institute for Applied Statistics, Johannes Kepler University, Linz, Austria
[4] Institute for Statistics and Mathematics, WU University of Economics and Business, Vienna, Austria
[5] Department of Neurology, Klinikum Wels-Grieskirchen, Wels, Austria
[6] Nuclear Medicine Research Department, IASON, Graz, Austria
[7] Department of Nuclear Medicine, Faculty of Medicine and Dentistry, Palacky University Olomouc, Olomouc, Czech Republic
[8] Institute of Nuclear Medicine, Steyr Hospital, Steyr, Austria
[9] Department of Radiology, Clinic of Nuclear Medicine, Medical University Graz, Graz, Austria

Radiol Oncol 2022; 56(1): 23-31.

Received 12 October 2021
Accepted 9 November 2021

Correspondence to: Prof. Marina Hodolic, M.D., Ph.D, Nuclear Medicine Research Department, IASON GmbH, Feldkirchner Straße 4, A-8054 Graz Seiersberg, Austria. Phone: + 43 664 830 9492; E-mail: marina.hodolic@gmail.com

Disclosure: No potential conflicts of interest were disclosed.

Background. Beta amyloid (Aβ) causes synaptic dysfunction leading to neuronal death. It is still controversial if the magnitude of Aβ deposition correlates with the degree of cognitive impairment. Diagnostic imaging may lead to a better understanding the role of Aβ in development of cognitive deficits. The aim of the present study was to investigate if Aβ deposition in the corresponding brain region of early stage Alzheimer´s disease (AD) patients, directly correlates to neuronal dysfunction and cognitive impairment indicated by reduced glucose metabolism.

Patients and methods. In 30 patients with a clinical phenotype of AD and amyloid positive brain imaging, 2-[18F] fluoro-2-deoxy-d-glucose (FDG) PET/CT was performed. We extracted the average [18F] flutemetamol (Vizamyl) uptake for each of the 16 regions of interest in both hemispheres and computed the standardized uptake value ratio (SUVR) by dividing the Vimazyl intensities by the mean signal of positive and negative control regions. Data were analysed using the R environment for statistical computing and graphics.

Results. Any negative correlation between Aβ deposition and glucose metabolism in 32 dementia related and corresponding brain regions in AD patients was not found. None of the correlation coefficient values were statistically significant different from zero based on two-sided p- value.

Conclusions. Regional Aβ deposition did not correlate negatively with local glucose metabolism in early stage AD patients. Our findings support the role of Aβ as a valid biomarker, but does not permit to conclude that Aβ is a direct cause for an aberrant brain glucose metabolism and neuronal dysfunction.

Key words: Alzheimer disease, PET, tau, FDG

Introduction

Alzheimer's disease (AD) is the most common cause of dementia in the elderly people. The hallmark pathologies include beta-amyloid (Aβ) depositions in plaques and brain vessels, tau pathology, microglia activation, and inflammation. The causes of AD are unknown; however, Aβ may play an im-

portant role in development of AD. According to the amyloid cascade hypothesis, Aβ causes synaptic dysfunction and neuronal death leading to cognitive impairment.[1,2]

However, several studies suggested only a modest correlation between Aβ pathology and cognition. There is little correlation between amyloid plaques location at autopsy and affected brain regions according to patient's clinical symptoms.[3] A large burden of amyloid plaques is found in subjects without cognitive deficits.[4] Amyloid plaque formation does occur late in hippocampus, although this structure is the first to fail clinically.[5] Indeed, the reduction of plaque load in the brain in therapeutic trials has not yielded to cognitive benefit in AD patients.[6]

In contrast, the burden of neurofibrillary tangles, consisting of hyperphosphorylated tau, correlates with the degree of cognitive impairment in AD.[7] *In vivo* studies using PET tracers for tau replicated these findings showing that more advanced Braak stages are associated with decreased global cognitive status.[8,9] Tau pathology leads to a reduced glucose metabolism correlating with cognitive decline.[10] Thus, tau pathology rather than amyloid accumulation, may contribute to cognitive dysfunction in AD patients.

Imaging may lead to a better understanding the role of Aβ in the development of cognitive deficits. Techniques such as 2-[18F]fluoro-2-deoxy-d-glucose (FDG) Positron Emission Tomography (PET) or amyloid PET are widely used for supporting the diagnosis of dementia. To exclude cerebral pathologies, such as tumors, subdural hematoma or normal pressure hydrocephalus, magnetic resonance imaging (MRI) is used. Morphologically, MRI may detect a hippocampal volume reduction in AD [11]. Amyloid PET allows *in vivo* detection of amyloid plaques indicating the pathophysiologic state of dementia. Several tracers, such as 18[F] florbetapir, 18[F] flutemetamol and 18[F] florteban are approved by the US Food and Drug Administration (FDA). Timing of amyloid accumulation is at a preclinical stage of AD.[12]

However, healthy individuals without cognitive symptoms can have a positive amyloid PET scan. Thus, amyloid imaging may be helpful for differential diagnosis in early onset dementia, particularly to rule out AD dementia. FDG PET is an important tool to detect early neurodegenerative dementia, differentiate neurodegenerative dementia or comorbidity of other neurodegenerative disease. FDG PET is described as a neuronal injury biomarker in AD and neuronal dysfunction is indicated by reduced glucose metabolism.[13] In AD patients, FDG PET demonstrates a glucose metabolic reduction in the parietotemporal association cortices, posterior cingulate and precuneus regions.[14] In the later stages of AD, hypometabolic regions spread to the frontal association cortices.[15] In patients with mild cognitive impairment (MCI), the transitional stage between aging and AD, FDG PET appears to add the greatest prognostic information.[16]

According to the amyloid cascade hypothesis, in brain regions with amyloid deposition, neuronal injury and an altered FDG metabolism may be expected. However, several studies showed controversial findings regarding the correlation of amyloid deposition and glucose metabolism.[17-19] Thus, it is still not clear if amyloid deposition comparably to tau pathology is a leading cause of cognitive impairment.

In this study, we included patients with a clinical phenotype of AD with cognitive dysfunction and amyloid deposition in cortical brain areas as detected by Aβ binding PET tracer.

The aim was to investigate if Aβ deposition in the corresponding brain region directly correlates to neuronal dysfunction indicated by reduced glucose metabolism. Such a correlation should be easy and convenient to recognize when clinically AD is at a relatively early stage and impaired glucose metabolism is still restricted to certain areas and not globalized. Therefore, our cohort consists mostly of patients at the early stage of disease.

Patients and methods

Patients

Ninety patients underwent amyloid PET analysis at the Institute of Nuclear Medicine, Kepler University Hospital, Neuromed Campus, Linz, between January 2016 and November 2017. These patients were assigned from Departments of Gerontology, Neurology or Psychiatry of various hospital institutions located in upper Austria. At least all amyloid positive patients (n = 30) underwent a comprehensive clinical and neuropsychological evaluation. Probable AD was diagnosed clinically and according to the S3 guidelines for dementia by experienced clinicians.[20] For screening, the mini mental state examination (MMSE) according to Folstein was performed.[21] Each subject underwent computed tomography or MRI to rule out any structural abnormalities, such as brain tumours, hematomas, hydrocephalus or ischemia,

as the cause for dementia. Vitamin deficiencies and thyroid abnormalities were excluded by blood analysis. FDG PET, amyloid PET and neuropsychological testing were acquired within 60 days. Brain Aβ deposition was quantified by performing PET scans using the tracer 18[F] flutemetamolm (Vizamyl). In a standardized procedure patients were rated as amyloid positive (n = 30, age 65.0 ± 14.3 years) or amyloid negative (n = 60, age 64.6 ± 8.7 years).

FDG PET was used to evaluate brain glucose metabolism. It was rated in clinical routine by experienced clinicians blinded to clinical symptoms using the Neuro Q, Version 3.5, 2007-analysis system, a schematic summary, comparing the patients scan to the scan of an asymptomatic control group. For our investigation, we selected 32 dementia related brain regions as regions of interest (Table 1). The regions of interest were based on brain areas, which are suggested by the Neuro Q program and include all dementia related brain regions. For each region NeuroQ compares the FDG metabolism to that of a cohort of normal persons, numbers indicate extent of standard deviation in comparison to a normal situation. Negative numbers represent relative hypometabolism.

For correlation, we manually defined cortical areas of representative gyri in dementia related brain regions of amyloid positive PET scans and excluded non cortical areas and sulci to avoid bias. Pons and the cerebellum represent the reference regions for positive and negative control within each brain. Further, we evaluated the Vizamyl uptake value ratio in corresponding brain regions. We extracted the average Vizamyl uptake for each of the 16 regions of interest in both hemispheres and computed the standardized uptake value ratio (SUVR) by dividing the Vimazyl intensities by the mean signal of the individual positive and negative control regions as mentioned above.

TABLE 1. Regions of interest

superior frontal cortex
middle frontal cortex
Inferior frontal cortex
anterior cingulate cortex
posterior cingulate cortex
sensorimotoric cortex
superior lateral temporal cortex
medial anterior temporal cortex
medial posterior temporal cortex
inferior lateral anterior temporal cortex
inferior lateral posterior temporal cortex
superior parietal cortex
inferior parietal cortex
parietotemporal cortex
primary visual cortex
associative visual cortex

Positron emission tomography

All PET scans were obtained with a Philips Gemini GXL PET/CT. For amyloid imaging patients received 185 MBq of 18F-Flutemetamol i.v. The tracer was distributed by GE healthcare Austria. PET/CT images were obtained 60 min after tracer injection.

FDG PET had been scheduled on a different day. Patients fasted for a minimum of 6 h before FDG injection to ensure standardized metabolic conditions. Blood glucose level was measured and had to be < 160 mg % in all patients. 185 MBq of FDG was injected i.v.. PET images were acquired 30 min post injection (3D acquisition). The scanner acquires transaxial planes, simultaneously covering an 18 cm axial field of view. Eliminating the sub-sampling required in conventional techniques, line-of-response (LOR) removes averaging and consequent image degradation. Detector material is gadolinium oxyorthosilicate (GSO) with a crystal size of 4 x 6 x 30 mm. A 6-slice helical CT – Philips brilliance air 6 – was used for attenuation correction. For further evaluation, data were transferred to a Hermes Medical Solutions, Sweden work station (HERMES).

PET interpretation was done visually by two experienced nuclear medicine specialists in knowledge of clinical data of the patient and consensually. The procedure and technical data are described in detail by Pichler *et al*.[22,23]

Statistics

Data were analysed using the R environment for statistical computing and graphics.[24] Scatter plots of the amyloid mean score versus the FDG mean score visualize separately for each region and side the association. To test for association between these two scores, the Pearson correlation coefficient was determined for each region and side. Two-sided p-values were calculated assuming normally distributed data. P-values were for each side corrected for multiple testing using Holm's method.[25]

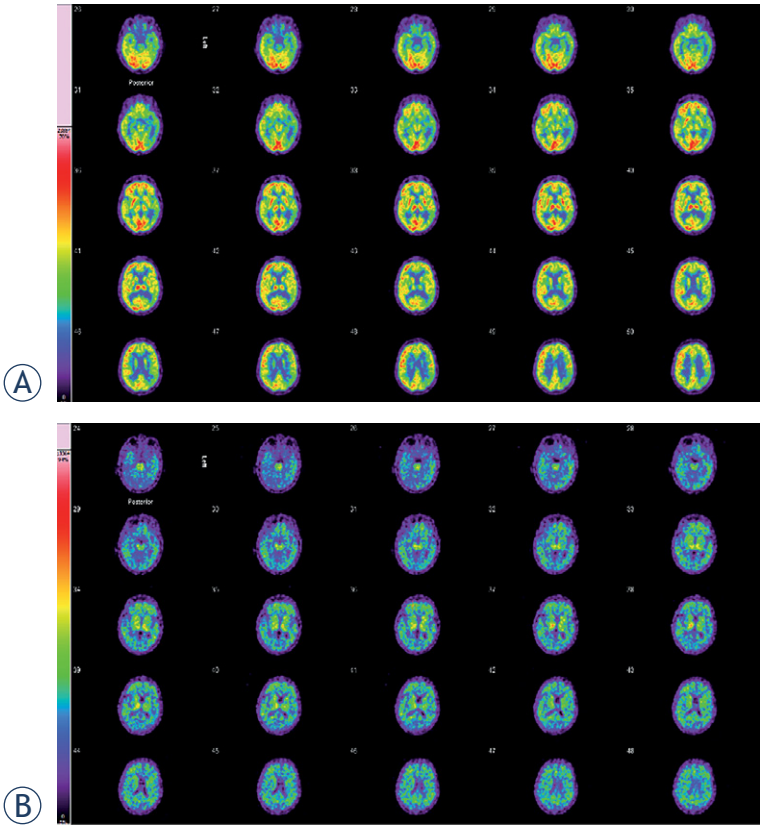

FIGURE 1. 2-[18F] fluoro-2-deoxy-d-glucose (FDG) and amyloid brain PET/CT of 59-year-old woman. **(A)** FDG brain PET/CT of a 59-year-old woman with a history of fluctuating cognitive impairment (mini mental state examination [MMSE] = 14/30). Glucose hypometabolism was demonstrated in the parietal dorsolateral and temporolateral, and occipatal cortical areas. The glucose metabolism in the left temporomesial area is weak. The other cortical structures show a slight attenuation of FDG metabolism. Basal ganglia show more intense uptake compared to the cortical areas. This FDG brain PET study shows the typical picture of abnormal glucose metabolism that occurs in Alzheimer´s disease (AD) and is additionally compatible with pronounced microvascular changes. **(B)** On the amyloid PET a non-specific tracer accumulation from the pons to the basal ganglia is evident. PET images of the white matter demonstrate individual non-specific enrichments. In the frontal and temporal cortices as well as sporadically in the parietal cortical areas, a pathological tracer accumulation occurs. This global cortical tracer uptake is consistent with the neuropathology of AD.

The study was done in accord with ethical standards and in accord with the Helsinki Declaration of 1975.

Results

In clinical routine, 90 amyloid PET scans for diagnosis of dementia were performed. In detail, AD was diagnosed in 30 patients (65.0 ± 14.3 years), 16 male and 14 female. All patients with amyloid positive PET scan underwent also PET scanning with FDG and computed tomography (CT) or MRI, as well as neuropsychological and clinical examination.

In the AD group mean score MMSE was 23 ± 5 (n = 30).

Figures 1 and 2 demonstrate FDG PET and amyloid positive PET images of patients with the clinical suspected diagnosis of AD.

In 43 subjects with amyloid negative PET scans a MMSE was performed. In the non AD group the mean score MMSE was 26 ± 3 (n = 43). Subjects with negative amyloid PET (n = 60, 24 female, 36 male, age 64.6 ± 8.7) received the following diagnosis according to ICD-10: affective disorders (n = 33), Parkinson's disease (n = 3), psychoorganic syndrom (POS, n = 3), Hashimoto's encephalopathy (n = 1), hepatic encephalopathy (n = 1), frontotemporal dementia (FTD, n = 8), vascular dementia (vaD, n = 8) and β-amyloid associated angiopathy (n = 3).

As shown in Figure (3) and Figure (4) we did not find any significant negative correlation between amyloid deposition and glucose metabolism in 32 dementia related and corresponding brain regions in AD patients. The estimated correlation coefficient values differed between 0.48 and -0.32. None of the correlation coefficient values were statistically significant different from zero based on two-sided p- value at significance level 0.05 after correcting for multiple testing for each side using Holm´s method. No statistical evidence was found to confirm a negative correlation between amyloid deposition and glucose metabolism in general or specifically for some brain regions.

Discussion

There is an ongoing debate to which extent amyloid is related to AD pathology. The concept of a direct mechanism leading to clinical manifestation lead to various trials of vaccination therapies. As therapeutic success was disappointing the pathophysiological role of amyloid in AD had to be rediscussed.

In AD pathology, the amyloid cascade hypothesis may play a fundamental role.[2] Plaques in AD brains consist of insoluble Aβ peptides cleaved by different secretases from the amyloid precursor protein (APP).[26] The cleavage results in Aβ-40 with a length of 40 amino acids and Aβ-42 with a length of 42 amino acids, which is the plaque proning form. Distinct plaque subtypes with low (diffuse plaques) and high (cored or neurotic plaques)

proportion of fibrillar components have been identified.[27]

In fact, insoluble Aβ exceeds soluble forms of Aβ by a factor of about 100-fold in AD brain.[28] However, Aβ does not correlate well with clinical symptoms and anti-amyloid pharmaceuticals have failed to improve significantly patient's symptoms[3,6], even when amyloid deposits are efficiently reduced.[29] As a possible exception, the updated analysis of the EMERGE trial showed a significant reduction in decline of global functions for the patients treated with a high dose of aducanumab.[30]

Thus, it is still not clear if Aβ directly leads to neuronal dysfunction. High levels of Aβ may subsequently lead to a downstream of pathological events, including tau pathology, inflammation, oxidative stress, excitotoxicity, loss of synaptic connections, and cell death, causing the clinical symptoms of AD. Levels of prefibrillar Aβ forms, such as soluble oligomers and protofibrils, correlate better than plaques with disease severity.[31] This may indicate that soluble species are the neurotoxic form of Aβ leading to neurodegeneration.[31]

Aβ deposition is a valid biomarker to support AD diagnostic.[32] Available PET radioligands visualizing Aβ bind to insoluble fibrils, such as Aβ plaques. Recently, several 18F-labeled tracers were designed including flobetapir ([18F]AV-45), flutemetamol ([18F]GE067), florbetaben ([18F] BAY94–9172) [28, 33-36]. We used [18F]flutemetamol PET as a surrogate marker for brain amyloid deposition. Several studies suggested a high correlation between [18F]flutemetamol retention and neuropathologic findings.[37-40] However, amyloid specific tracers may not be able to provide an accurate measurement of Aβ. In fact, there is a lack of data of *in vivo* Aβ specificity.[41] Amyloid PET scan is able to rule out an AD diagnosis. Amyloid PET may have an additive, but primarily confirmatory role as a diagnostic marker in patients suspected of early-onset AD. An amyloid-positive PET scan often supports or changes diagnosis into AD.[42] Amyloid pathology is also present in other forms of dementia and interpreted as mixed or copathology and not always the primary cause of the clinical manifestation of dementia.

FDG PET, a neuroimaging tool in AD, plays an important role in discriminating different forms of dementia.[12,34] Decreased glucose metabolism in temporal and parietal cortex indicates synaptic dysfunction and in contrast to amyloid deposition, this occurs mainly in the symptomatic phase of AD.[28] In the present study, we investigated a possible correlation between local amyloid deposition and glucose metabolism in dementia related corresponding brain regions in AD patients. In an early stage of AD impaired glucose metabolism is still restricted to certain areas and not globalized.[43] Our cohort consists mostly of patients at the early stage of disease, which is a result of reasonable referrals. Clinical impact for different diagnosis of dementia in an advanced state of disease is questionable, because all therapeutical strategies are more helpful at an early phase of the disease. The availability of both PET modalities in 30 patients diagnosed for AD in the present study allowed investigating the correlation of amyloid deposition and glucose metabolism, retrospectively.

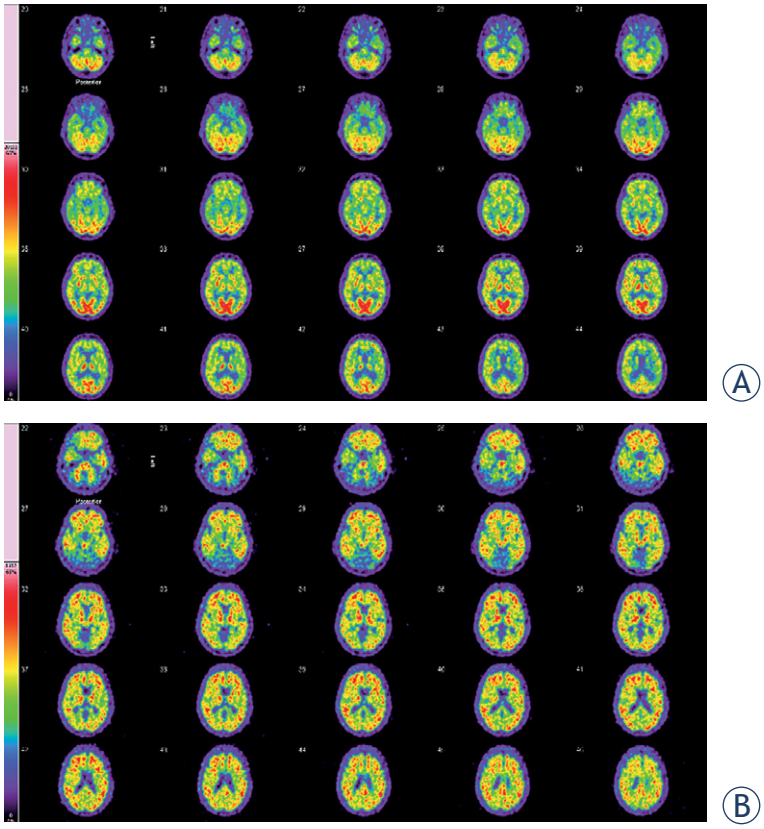

FIGURE 2. FDG and amyloid brain PET/CT of a 70-year-old woman. **(A)** 2-[18F] fluoro-2-deoxy-d-glucose (FDG) brain PET/CT of a 70-year-old woman, who presented with a history of cognitive decline (mini mental state examination [MMSE] = 15/30). The glucose metabolism in the cerebral cortex is inhomogenous and moderately attenuated. In the cerebellum, normal glucose metabolism was demonstrated. This FDG brain PET study does not show the typical picture of abnormal glucose metabolism that occurs in Alzheimer´s disease (AD), but temporomesial and temporolateral some decreased tracer uptake can be observed. Additionally the images are compatible with pronounced microvascular changes. **(B)** Amyloid PET images demonstrate pathologically increased tracer accumulation in the entire brain, more pronounced in the frontal and temporal cortical areas. This is compatible with the diagnosis of AD.

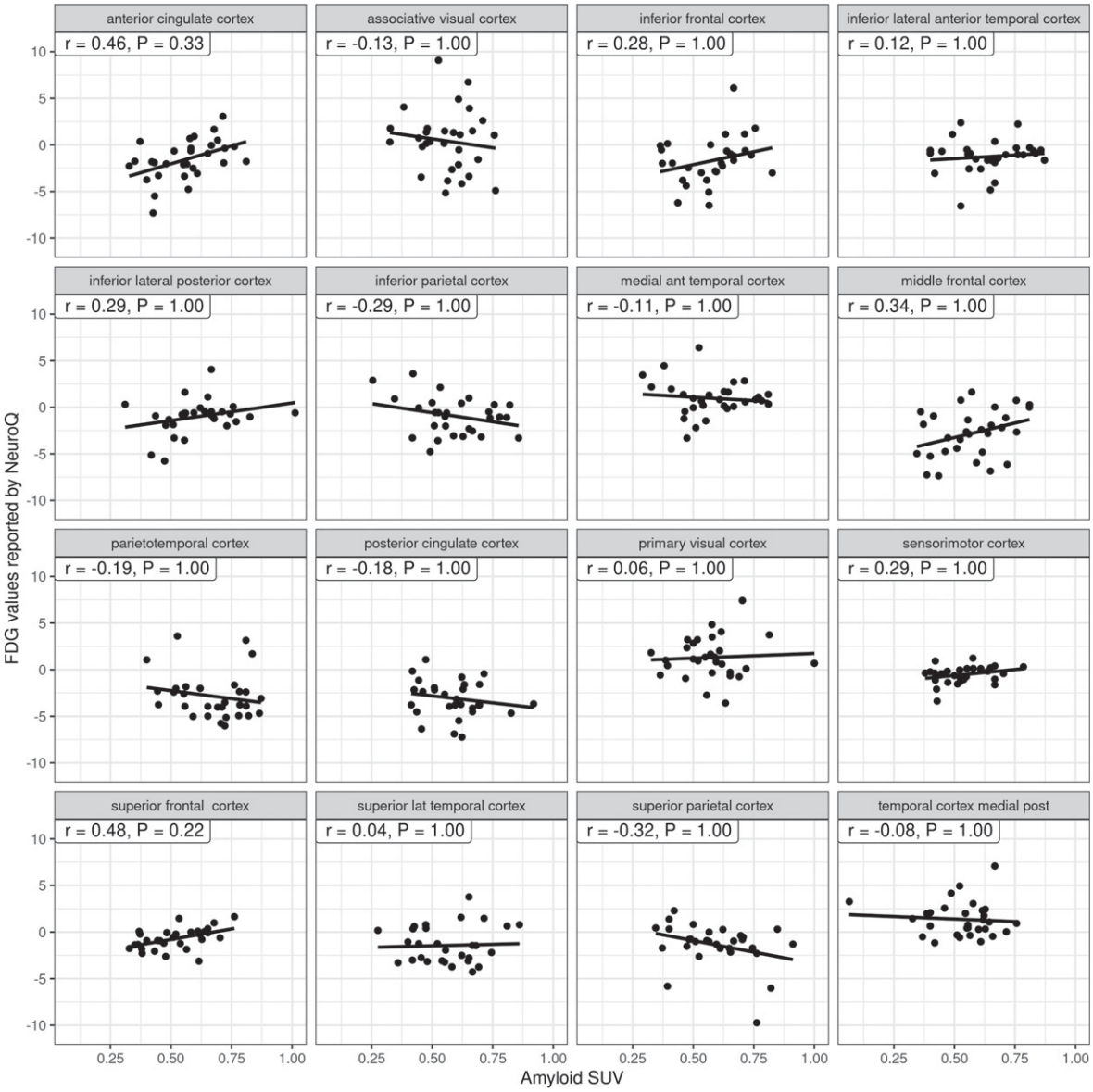

FIGURE 3. Scatter plots of the amyloid standardized uptake value (SUV) (on the x- axis) and the 2-[18F] fluoro-2-deoxy-d-glucose (FDG) values represented by NeuroQ (on the y-axis) for the 30 amyloid positive patient for the left side. Each panel represents a brain regions with the name indicated in the strip. Least-squares regression lines with slope proportional to the Pearson correlation coefficient indicate the association. The Pearson correlation (r) and the associated p-value (P) are shown in the label on the top of each panel.

To avoid bias due to computer assisted measurement we manually designated the cortical areas of dementia related brain regions and evaluated the SUVR of [18F]flutemetamol. Compared to previous investigations[17-19] we included a higher number of AD patients. Engler *et al*. found a negative correlation with metabolism in parietal cortex in 16 AD patients.[17] Another author showed that a higher amyloid tracer uptake correlated with lower regional glucose metabolism in 19 AD patients.[18] We did not find any negative correlation of amyloid tracer uptake and glucose metabolism in corresponding brain areas in 30 AD patients. Our data supports the concept that amyloid depositions may not be the direct cause of dysfunctional metabolism.

One limitation of this study is that measurement of Aβ40, Aβ 42 and phosphorylated tau in the cerebrospinal fluid (CSF) was not performed[44] and thus, the correlation between CSF amyloid levels

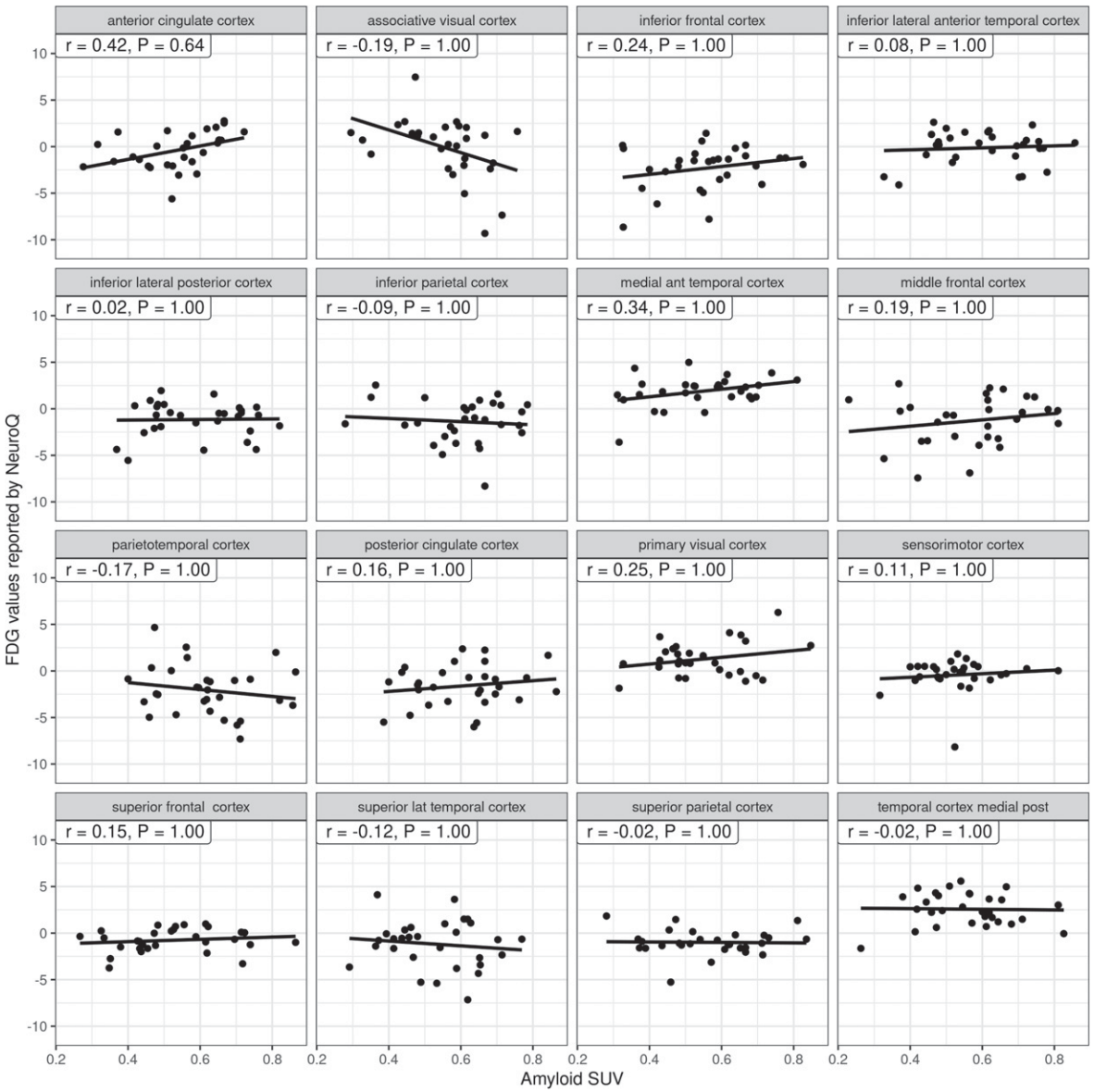

FIGURE 4. Scatter plots of the amyloid standardized uptake value (SUV) (on the x-axis) and the 2-[18F] fluoro-2-deoxy-d-glucose (FDG) values represented by NeuroQ (on the y-axis) for the 30 amyloid positive patient for the right side. Each panel represents a brain regions with the name indicated in the strip. Least-squares regression lines with slope proportional to the Pearson correlation coefficient indicate the association. The Pearson correlation (r) and the associated p-value (P) are shown in the label on the top of each panel.

and amyloid tracer uptake could not be shown. If Aβ deposition plays a role in the development of cognitive deficits in AD, the lack of direct correlations requires other involved mechanisms such as tau pathology.[2,45,46]

The hyperphosphorylation and abnormal aggregation of tau, a microtubule-associated protein essential to neuronal stability and functioning, is a hallmark in AD pathology. Tau imaging revealed that neurofibrillary tangels are mainly located in the hippocampus and associative cortical regions.[47] Tau PET imaging may serve as a valuable and early biomarker for the localization of neuronal injury. In contrast to Aβ accumulation, tau may cause cognitive decline mediated by glucose hypometabolism. Indeed, tau pathology was observed in brain regions related to clinical symptoms and overlapped with areas of hypometabolism.[48,49] Exactly what we were not able to show for the relation of amyloid and glucose metabolism. Aβ may play an indirect

role in AD pathology in the development of NFTs. It is likely, that Aβ indirectly promotes tau phosphorylation through upregulation of kinases such as GSK-3β and CDK5, which phosphorylate tau.[50]

Conclusios

The focus of the study was to investigate the correlation between local amyloid deposition and glucose metabolism *in vivo* at corresponding brain areas. Therefore, we manually designated the areas of interest in an early stage of disease, which in that manner has not been performed before. We showed that regional amyloid deposition did not correlate negatively with local glucose metabolism. Our findings support the role of Aβ as a valid biomarker, but does not permit to conclude that Aβ is a direct cause for an aberrant glucose metabolism and neuronal dysfunction. On the contrary our data added a piece of puzzle to the concept that amyloid does not directly cause AD pathology but has to be considered as a prerequisite only.

Acknowledgements

The authors are grateful to Ms. Silke Kern and Ms. Sieglinde Prechtl and to their whole team of technicians for invaluable support at the Institute of Nuclear Medicine.

Contribution of authors: DE, MH & RP manuscript writing; AD & RP nuclear imaging; GMW & BG statistics; DE, RT & EK clinical part.

References

1. Hardy JA, Higgins GA. Alzheimer's disease: the amyloid cascade hypothesis. *Science* 1992; **256:** 184-5. doi: 10.1126/science.1566067
2. Hardy J, Selkoe DJ. The amyloid hypothesis of Alzheimer's disease: progress and problems on the road to therapeutics. *Science* 2002; **297:** 353-6. doi: 10.1126/science.1072994
3. Murphy MP, LeVine H. Alzheimer's disease and the amyloid-beta peptide. *J Alzheimers Dis* 2010; **19:** 311-23. doi: 10.3233/JAD-2010-1221
4. Jack CR Jr, Wiste HJ, Knopman DS, Vemuri P, Mielke MM, Weigand SD, et al. Rates of beta-amyloid accumulation are independent of hippocampal neurodegeneration. *Neurology* 2014; **82:** 1605-12. doi: 10.1212/WNL.0000000000000386
5. Altmann A, Ng B, Landau SM, Jagust WJ, Greicius MD. Regional brain hypometabolism is unrelated to regional amyloid plaque burden. *Brain* 2015; **138:** 3734-46. doi: 10.1093/brain/awv278
6. Salloway S, Sperling R, Fox NC, Blennow K, Klunk W, Raskind M, et al; Bapineuzumab 301 and 302 Clinical Trial Investigators. Two phase 3 trials of bapineuzumab in mild-to-moderate Alzheimer's disease. *N Engl J Med* 2014; **370:** 322-33. doi: 10.1056/NEJMoa1304839
7. Nelson PT, Alafuzoff I, Bigio EH, Bouras C, Braak H, Cairns NJ, et al. Correlation of Alzheimer disease neuropathologic changes with cognitive status: a review of the literature. *J Neuropathol Exp Neurol* 2012; **71:** 362-81. doi: 10.1097/NEN.0b013e31825018f7
8. Cho H, Choi JY, Hwang MS, Lee JH, Kim YJ, Lee HM, et al. Tau PET in Alzheimer disease and mild cognitive impairment. *Neurology* 2016; **87:** 375-83. doi: 10.1212/WNL.0000000000002892
9. Schöll M, Ossenkoppele R, Strandberg O, Palmqvist S, Jögi J, Ohlsson T, et al. Distinct 18F-AV-1451 tau PET retention patterns in early- and late-onset Alzheimer's disease. *Brain* 2017; **140:** 2286-94. doi: 10.1093/brain/awx171
10. Saint-Aubert L, Almkvist O, Chiotis K, Almeida R, Wall A, Nordberg A. Regional tau deposition measured by [18F]THK5317 positron emission tomography is associated to cognition via glucose metabolism in Alzheimer's disease. *Alzheimers Res Ther* 2016; **8:** 38. doi: 10.1186/s13195-016-0204-z
11. Jack CR Jr, Petersen RC, Xu YC, O'Brien PC, Smith GE, Ivnik RJ, et al. Prediction of AD with MRI-based hippocampal volume in mild cognitive impairment. *Neurology* 1999; **52:** 1397-403.
12. Villemagne VL, Burnham S, Bourgeat P, Brown B, Ellis KA, Salvado O, et al. Australian Imaging Biomarkers and Lifestyle (AIBL) Research Group. Amyloid β deposition, neurodegeneration, and cognitive decline in sporadic Alzheimer's disease: a prospective cohort study. *Lancet Neurol* 2013; **12:** 357-67. doi: 10.1016/S1474-4422(13)70044-9
13. McKhann GM, Knopman DS, Chertkow H, Hyman BT, Jack CR Jr, Kawas CH, et al. The diagnosis of dementia due to Alzheimer's disease: recommendations from the National Institute on Aging-Alzheimer's Association workgroups on diagnostic guidelines for Alzheimer's disease. *Alzheimers Dement* 2011; **7:** 263-9. doi: 10.1016/j.jalz.2011.03.005
14. Shivamurthy VK, Tahari AK, Marcus C, Subramaniam RM. Brain FDG PET and the diagnosis of dementia. *AJR Am J Roentgenol* 2015; **204:** W76-85. doi: 10.2214/AJR.13.12363
15. Ishii K. PET approaches for diagnosis of dementia. *AJNR Am J Neuroradiol* 2014; **35:** 2030-8. doi: 10.3174/ajnr.A3695
16. Shaffer JL, Petrella JR, Sheldon FC, Choudhury KR, Calhoun VD, Coleman RE, et al. Predicting cognitive decline in subjects at risk for Alzheimer disease by using combined. *Radiology* 2013; **266:** 583-91. doi: 10.1148/radiol.12120010
17. Engler H, Forsberg A, Almkvist O, Blomquist G, Larsson E, Savitcheva I, et al. Two-year follow-up of amyloid deposition in patients with Alzheimer's disease. *Brain* 2006; **129:** 2856-66. doi: 10.1093/brain/awl178
18. Edison P, Archer HA, Hinz R, Hammers A, Pavese N, Tai YF, et al. Amyloid, hypometabolism, and cognition in Alzheimer disease: An [11C]PIB and [18F]FDG PET study. *Neurology* 2007; **68:** 501-8. doi: 10.1212/01.wnl.0000244749.20056.d4
19. Cohen AD, Price JC, Weissfeld LA, James J, Rosario BL, Bi W, et al. Basal cerebral metabolism may modulate the cognitive effects of Aβ in mild cognitive impairment: an example of brain reserve. *J Neurosci* 2009; **29:** 14770-8. doi: 10.1523/JNEUROSCI.3669-09.2009
20. Deuschl G, Maier W, et al; Steuerungsgruppe. S3- Guideline dementias. [German]. In: German Society for Neurology, editor. *Guidelines for diagnostics and therapy in neurology.* [German]. 2016. [cited 2021 Sep 12]. Available at: www.dgn.org/leitlinien
21. Folstein MF, Folsten SE, McHugh PR. Mini-mental state: a practical method for grading the cognitive state of patients for the clinician. *J Psychiatr Res* 1975; **12:** 189-98. doi: 10.1016/0022-3956(75)90026-6
22. Pichler R, Dunzinger A, Wurm G, Pichler J, Weis S, Nussbaumer K, et al. Is there a place for FET PET in the initial evaluation of brain lesions with unknown significance? *Eur J Nucl Med Mol Imaging* 2010; **37:** 1521-8. doi: 10.1007/s00259-010-1457-6
23. Hodolic M, Topakian R, Pichler R. ^{18}F-fluorodeoxyglucose and ^{18}F-flumazenil positron emission tomography in patients with refractory epilepsy. *Radiol Oncol* 2016; **50:** 247-53. doi: 10.1515/raon-2016-0032
24. R Core Team. *A language and environment for statistical computing*. Vienna, Austria: R Foundation for Statistical Computing; 2019. [cited 2021 Sep 13]. Available at: http://www.R-project.org/
25. Holm S. A simple sequentially rejective multiple test procedure. *Scand J of Stat* 1979; **6:** 65-70.
26. Murphy MP, LeVine H. Alzheimer's disease and the amyloid-beta peptide. *J Alzheimers Dis* 2010; **19:** 311-23. doi: 10.3233/JAD-2010-1221

27. Dickson TC, Vickers JC. The morphological phenotype of beta-amyloid plaques and associated neuritic changes in Alzheimer's disease. *Neuroscience* 2001; **105:** 99-107. doi: 10.1016/s0306-4522(01)00169-5

28. Vlassenko AG, Benzinger TL, Morris JC. PET amyloid-beta imaging in preclinical Alzheimer's disease. *Biochim Biophys Acta* 12012; **1822:** 370-9. doi: 10.1016/j.bbadis.2011.11.005

29. Lowe SL, Willis BA, Hawdon A, Natanegara F, Chua L, Foster J, et al. Donanemab (LY3002813) dose-escalation study in Alzheimer's disease. *Alzheimers Dement (N Y)* **7:** e12112. doi: 10.1002/trc2.12112

30. Huang LK, Chao SP, Hu CJ. Clinical trials of new drugs for Alzheimer disease. *J Biomed Sci* 2020; **27:** 18. doi: 10.1186/s12929-019-0609-7

31. Tomic JL, Pensalfini A, Head E, Glabe CG. Soluble fibrillar oligomer levels are elevated in Alzheimer's disease brain and correlate with cognitive dysfunction. *Neurobiol Dis* 2009; **35:** 352-8. doi: 10.1016/j.nbd.2009.05.024

32. Weiner MW, Veitch DP, Aisen PS, Beckett LA, Cairns NJ, Cedarbaum J, et al. 2014 Update of the Alzheimer's Disease Neuroimaging Initiative: a review of papers published since its inception. *Alzheimers Dement* 2015; **11:** e1-120. doi: 10.1016/j.jalz.2014.11.001

33. Small GW, Kepe V, Ercoli LM, Siddarth P, Bookheimer SY, Miller KJ, et al. PET of brain amyloid and tau in mild cognitive impairment. *N Engl J Med* 2006; **355:** 2652-63. doi: 10.1056/NEJMoa054625

34. Rowe CC, Ackerman U, Browne W, Mulligan R, Pike KL, O'Keefe G, et al. Imaging of amyloid beta in Alzheimer's disease with 18F-BAY94-9172, a novel PET tracer: proof of mechanism. *Lancet Neurol* 2008; **7:** 129-35. doi: 10.1016/S1474-4422(08)70001-2

35. Koole M, Lewis DM, Buckley C, Nelissen N, Vandenbulcke M, Brooks DJ, et al. Whole-body biodistribution and radiation dosimetry of 18F-GE067: a radioligand for in vivo brain amyloid imaging. *J Nucl Med* 2009; **50:** 818-22. doi: 10.2967/jnumed.108.060756

36. Kung HF, Choi SR, Qu W, Zhang W, Skovronsky D. 18F stilbenes and styrylpyridines for PET imaging of a beta plaques in Alzheimer's disease: a miniperspective. *J Med Chem* 2010; **53:** 933-41. doi: 10.1021/jm901039z

37. Frings L, Hellwig S, Spehl TS, Bormann T, Buchert R, Vach W, et al. Asymmetries of amyloid-β burden and neuronal dysfunction are positively correlated in Alzheimer's disease. *Brain* 2015; **138:** 3089-99. doi: 10.1093/brain/awv229

38. Jack CR Jr, Wiste HJ, Knopman DS, Vemuri P, Mielke MM, Weigand SD, et al. Rates of beta-amyloid accumulation are independent of hippocampal neurodegeneration. *Neurology* 2014; **82:** 1605-12. doi: 10.1212/WNL.0000000000000386

39. Scahill RI, Schott JM, Stevens JM, Rossor MN, Fox NC. Mapping the evolution of regional atrophy in Alzheimer's disease: unbiased analysis of fluid-registered serial MRI. *Proc Natl Acad Sci USA* 2002; **99:** 4703-7. doi: 10.1073/pnas.052587399

40. Pearson RC, Esiri MM, Hiorns RW, Wilcock GK, Powell TP. Anatomical correlates of the distribution of the pathological changes in the neocortex in Alzheimer disease. *Proc Natl Acad Sci USA* 1985; **82:** 4531-4. doi: 10.1073/pnas.82.13.4531

41. Kepe V, Moghbel MC, Långström B, Zaidi H, Vinters HV, Huang SC, et al. Amyloid-β positron emission tomography imaging probes: a critical review. *J Alzheimers Dis* 2013; **36:** 613-31. doi: 10.3233/JAD-130485

42. Zwan MD, Bouwman FH, Konijnenberg E, van der Flier WM, Lammmertma AA, Verhey FR, et al. Diagnostic impact of [18F]flutemetamol PET in early-onset dementia. *Alzheimers Res Ther* 2017; **9:** 2. doi: 10.1186/s13195-016-0228-4

43. Braak H, Braak E. Neuropathological stageing of Alzheimer-related changes. *Acta Neuropathol* 1991; **82:** 239-59. doi: 10.1007/BF00308809

44. Morbelli S, Bauckneht M, Scheltens P. Imaging biomarkers in Alzheimer's Disease: added value in the clinical setting. *Q J Nucl Med Mol Imaging* 2017; **61:** 360-71. doi: 10.23736/S1824-4785.17.03011-4

45. Bennett DA, Schneider JA, Wilson RS, Bienias JL, Arnold SE. Neurofibrillary tangles mediate the association of amyloid load with clinical Alzheimer disease and level of cognitive function. *Arch Neurol* 2004; **61:** 378-84. doi: 10.1001/archneur.61.3.378

46. Shankar GM, Li S, Mehta TH, Garcia-Munoz A, Shepardson NE, Smith I, et al. Amyloid-beta protein dimers isolated directly from Alzheimer's brains impair synaptic plasticity and memory. *Nat Med* 2008; **14:** 837-42. doi: 10.1038/nm1782

47. Braak H, Alafuzoff I, Arzberger T, Kretzschmanr H, Del Tredici K. Staging of Alzheimer disease-associated neurofibrillary pathology using paraffin sections and immunhistochemistry. *Acta Neuropathol* 2006; **112:** 389-404. doi: 10.1007/s00401-006-0127-z

48. Dronse J, Fliessbach K, Bischof GN, Reutern von B, Faber J, Hammes J, et al. In vivo patterns of tau pathology, amyloid-β burden, and neuronal dysfunction in clinical variants of Alzheimer's disease. *J Alzheimers Dis* 2017; **55:** 465-71. doi: 10.3233/JAD-160316

49. Bejanin A, Schonhaut DR, La Joie R, Kramer JH, Baker SL, Sosa N, et al. Tau pathology and neurodegeneration contribute to cognitive impairment in Alzheimer's disease. *Brain* 2017; **140:** 3286-300. doi: 10.1093/brain/awx243

50. Huber CM, Yee C, May T, Dhanala A, Mitchell CS. Cognitive decline in preclinical Alzheimer's disease: amyloid-beta versus tauopathy. *J Alzheimers Dis* 2018; **61:** 265-81. doi: 10.3233/JAD-170490

research article

Reliability of new radiographic measurement techniques for elbow bony impingement

Uros Meglic[1,2], Oskar Zupanc[1,2]

[1] Department of Orthopaedic Surgery, University Medical Centre Ljubljana, Ljubljana, Slovenia
[2] Faculty of Medicine, University of Ljubljana, Ljubljana, Slovenia

Radiol Oncol 2022; 56(1): 32-36.

Received 19 October 2021
Accepted 10 November 2021

Correspondence to: Prof. Oskar Zupanc, M.D., Ph.D, Department of Orthopedic Surgery, University Medical Centre Ljubljana, Slovenia.
E-mail: oskarzupanc@gmail.com

Disclosure: No potential conflicts of interest were disclosed.

Background. Identifying the location and scale of radiographic changes in elbow bony impingement (EBI) is critical in formulating an appropriate diagnosis and treatment plan for such patients. The purpose of present study was to evaluate the intra-rater and inter-rater reliability of the new radiographic parameters, Anterior Impingement angle (AIa) and Posterior Impingement angle (PIa), for EBI. In addition, to determine if there was a relationship between radiographic parameters and clinical evaluation.

Patients and methods. Three raters of different levels of training evaluated the radiographs of 60 patients (30 in EBI group and 30 in normal group) twice, at least 2 weeks apart. Intra-rater and inter-rater reliabilities were calculated by Intraclass Correlation Coefficients (ICC) with 95% confidence intervals. Correlation between radiographic parameters and clinical evaluation was calculated by Pearson correlation coefficient.

Results. In both groups, intra-rater and inter-rater reliabilities were substantial. There were no significant differences in reliability between upper-hand expert surgeons and resident for either measurement. Good correlation was observed between impingement arcs and range of motion values.

Conclusions. Both AIa and PIa measurements demonstrated substantial intra-rater and inter-rater reliability for normal radiographs and in EBI patients. Good reliability, for either expert surgeons or residents in training, and good correlation between radiographic measurements and manual testing, appoints this method may be easily and reliably used in every day practice.

Key words: elbow; osteoarthritis; impingement; classification; reliability

Introduction

Bony impingement of the elbow (EBI) is an early radiographic sign of the elbow degenerative disease.[1] Although being rare in general population, with prevalence up to 2%, it can be noticed with increased prevalence, up to 10%, in professional overhead athletes and manual laborers.[2] As a result of excessive and repetitive motions, bony osteophytes occur in anterior and posterior compartment of the elbow.[3] Changing elbow geometry, it causes flexion and extension deficit of the elbow motion.[4]

Although a flexion-extension range of motion (fROM) between 30 degrees and 130 degrees of flexion is enough to achieve 90% of the daily living activities, in professional athletes or manual laborers even a smaller loss of fROM can be devastating, with huge impact on their quality of life.[5] Thus it has to be recognized early and treated properly.

To date, there is no consensus among orthopedic surgeons as to when in the course of the disease and how much to treat EBI, to provide symptomatic relief for a given patient. One reason for the lack of consensus is an inability to predict success based on preoperative assessment. A paucity of informa-

tion regarding specific radiographic parameters is a significant cause in these cases.

The purpose of present study was, first, to evaluate the intra-rater and inter-rater reliability of the new radiographic parameters for EBI. The second goal was to determine if there was a relationship between radiographic parameters and clinical evaluation.

Patients and methods

Slovenia National Medical Ethics Committee approval (No. 1650513) was obtained for this investigation.

A total 60 subjects were enrolled. Among them 30 subjects with fROM deficit and diagnosed, not yet treated, EBI were recruited as the EBI group. Remaining 30 subjects with other elbow pathologies (epicondylitis, ulnar neuritis etc.), but with a normal fROM and no clinical signs of EBI were recruited as the NORMAL group. A brief clinical history was obtained in order to rule out previous injury or upper extremity abnormality. Focused physical examination was performed with manual fROM testing.

Standard antero-posterior and lateral x-ray views were obtained. Unsatisfactory films were repeated in order to maintain consistency. Digital radiograph images were analyzed using Agfa IMPAX 6 software (Agfa HealthCare, Belgium). Broberg and Morrey (BM) as well as Hasting and Rettig (HR) classifications of elbow osteoarthritis were used to assess elbow joint's degenerative changes.[6,7] Sigmoid notch coverage (SNC) measurement was performed as described by Goldfarb *et al.*, as a line connecting the center of the circle, fitted to sigmoid notch, to both the tip of the olecranon and coronoid (Figure 1C).[8] Measurements of the Anterior Impingement angle (AIa) and Posterior Impingement angle (PIa) were obtained on lateral x-ray images as previously described by Meglic and Zupanc.[9] The angle between the centralized ulnar direction line and the line between the center of rotation (COR) and the tip of the coronoid presents AIa. The angle between the centralized ulnar direction line and the line between the COR and the tip of the olecranon presents PIa (Figure 1A, B).[9] For reliability evaluation, two upper extremity surgeons (OZ, UM) and one resident after radiological training (NK), independently evaluated each radiograph for radiographic measurements of AIa and PIa. Each evaluator re-measured both parameters after an interval of at least 2 weeks, a period used in other reliability studies in upper extremity.[1,10] The examiners were blinded to their previous measurements.

Subjects were excluded from participation if there was evidence of: an upper extremity injury history, a growth or congenital abnormality, moderate or severe grade on BM or HR classification (grade II and III).

Statistical Package for Social Sciences version 21.0 (SPSS Inc, Chicago, IL, USA) was used for all statistical analyses. Student t test was used for group comparisons when normality was accepted, and a Mann-Whitney U test was used if normality was rejected. The Fisher exact test was used for categorical data between groups. Original data from all 3 raters were used to assess reliability of measurements. Inter- and intra-rater reliability were calculated using intraclass correlation coefficients (ICC), ICC 2.1 for inter-rater, ICC 3.1 for intra-rater.[11] Pearson correlation coefficient was used to measure correlation between impingement arcs and fROM. Correlation coefficient values less than 0.5 are indicative of poor reliability, values between 0.5 and 0.74 indicate moderate reliability, values between 0.75 and 0.89 indicate good reliability, and values greater than 0.90 indicate excellent reliability.[11] All tests were 2-tailed, with $p < 0.05$ considered significant. All ICC values were calculated with 95% confidence interval (95% CI).

Results

All patients included in the study were analyzed (60 patients, 100%). There were 20 males (67%), 10 females (33%) in EBI group and 12 males (40%), 18 females (60%) in NORMAL group ($p = 0.07$). The average age was 44 years (range 21–64 years) in EBI group and 33 years (range 18–60 years) in NORMAL group ($p = 0.02$). Pathology was presented on dominant hand in 22 cases (73%) in EBI group and in 26 cases (87%) in NORMAL group ($p = 0.33$). In EBI group in all cases BM and HR classification was graded stage I and in NORMAL group in all cases, no radiographic signs of osteoarthrosis were reported.

Table 1 summarizes manual and radiographic measurements, comparing both groups. In all measurements, the differences between groups were statistically significant.

ICCs for AIa and Pia measurements demonstrated good to excellent intra-rater and inter-rater reliability in both groups. Almost all ICCs were in 0.75–0.89 class, except intra-rater ICC in AIa in

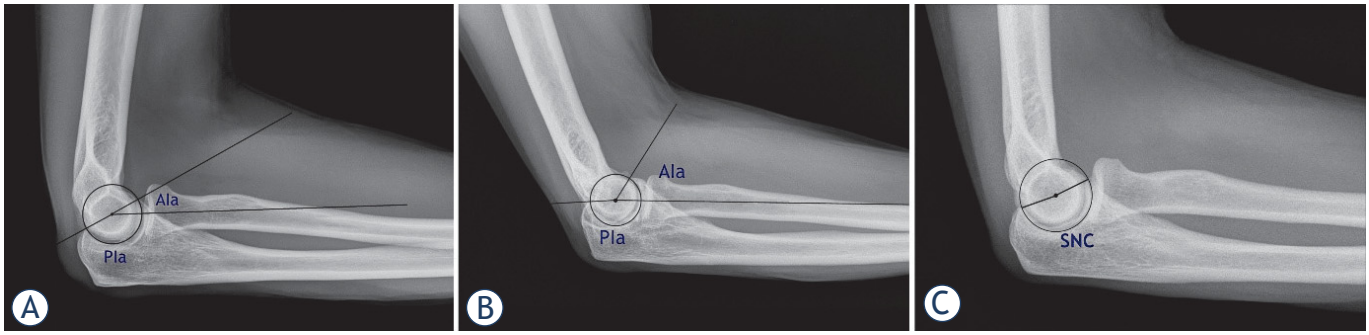

FIGURE 1. Radiographic measurements: **(A)** Anterior Impingement angle (AIa) and Posterior Impingement angle (PIa) in normal group, **(B)** AIa and Pia in EBI group, **(C)** sigmoid notch coverage angle (SNC) in normal group.

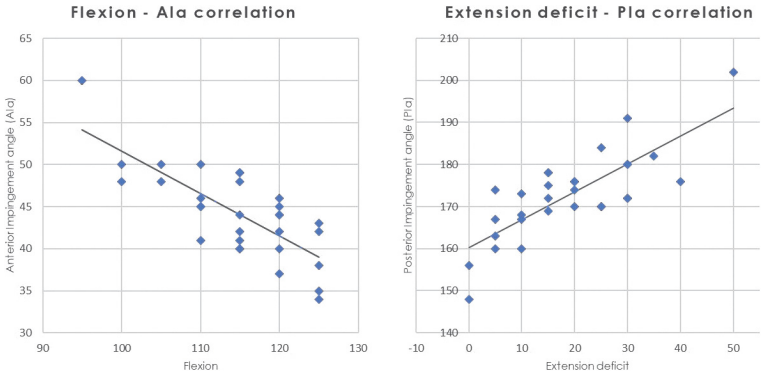

FIGURE 2. Manual flexion-extension range of motion (fROM) and radiographic measurement correlations between **(A)** flexion and Anterior Impingement angle AIa, **(B)** extension deficit and Posterior Impingement angle (Pia).

TABLE 1. Manual and radiographic measurements

	EBI group[a]	NORMAL group[a]	p
Flexion (°)	115 ± 8	139 ± 5	< 0.05
Extension deficit (°)	19 ± 12	0 ± 0	< 0.05
fROM (°)	96 ± 14	139 ± 5	< 0.05
SNC (°)	217 ± 10	170 ± 6	< 0.05
AIa (°)	44 ± 5	20 ± 4	< 0.05
Pia (°)	173 ± 10	150 ± 5	< 0.05

[a] Mean ± SD;

AIa = Anterior Impingement angle; EBI = elbow bony impingement; SNC = sigmoid notch coverage; PIa = Posterior Impingement angle; fROM = flexion-extension range of motion

NORMAL group and inter-rater ICC in AIa between Surgeon 1 and Resident in NORMAL group being in > 0.90 class. AIa measurements ranged from 34° to 60° (average 44°) in EBI group and from 10° to 25° (average 20°) in NORMAL group. PIa measurements ranged from 148° to 202° (average 173°) in EBI group and from 140° to 160° (average 150°) in NORMAL group. Inter-rater reliability and intra-rater reliabilities for all 3 raters are summarized in Table 2.

There were no significant differences in reliability between two upper-hand expert surgeons and one resident for either measurement. Both surgeons and a resident demonstrated a substantial agreement in all measurements. Inter-rater reliabilities between all raters are summarized in Table 3.

Statistically significant correlations were observed between fROM measurements and according Impingement arc. Correlation coefficient showed good negative correlation between flexion and AIa measurements, measured 0.76, (95% CI = 0.86–0.51; p < 0.05) (Figure 2A). A good positive correlation between extension deficit and PIa measurements was observed, measured 0.79, (95% CI = 0.59–0.89; p < 0.05) (Figure 2B).

Discussion

Treating EBI remains a challenging problem. A factor influencing heavily in determining the appropriate treatment choice is a lack of a reliable and accurate measurement technique. Very little information exists describing pathologic radiographic anatomy of EBI, thus making diagnosis and treatment difficult for both clinical and research purposes.

The results of this study revealed substantial intra-rater and inter-rater reliability of both AIa and PIa measurements on EBI and normal elbow radiographs. For selecting and reporting ICC reliability we used Koo *et al*. guidelines.[11] Following Koo's guidelines, we used 3 raters with blinded re-measurements, used ICC 3.1 for intra-rater and ICC 2.1 for inter-rater reliability and reported all

TABLE 2. Inter-rater and intra-rater reliabilities[a]

		Inter-rater reliability[a]	Intra-rater reliability for rater 1[a]	Intra-rater reliability for rater 2[a]	Intra-rater reliability for rater 3[a]
EBI group	AIa	0.85 (0.75–0.94)	0.87 (0.75–0.94)	0.87 (0.74–0.94)	0.87 (0.75–0.95)
	PIa	0.84 (0.69–0.92)	0.83 (0.66–0.91)	0.88 (0.76–0.94)	0.85 (0.75–0.93)
NORMAL group	AIa	0.87 (0.76–0.94)	0.90 (0.81–0.95)	0.87 (0.74–0.94)	0.87 (0.75–0.95)
	PIa	0.85 (0.75–0.93)	0.86 (0.73–0.93)	0.86 (0.73–0.93)	0.86 (0.74–0.94)

[a] ICC value (95% CI);

AIa = Anterior Impingement angle; CI = confidence interval; EBI = elbow bony impingement; ICC = intraclass correlation coefficients; PIa = Posterior Impingement angle

TABLE 3. Inter-rater reliability between two upper-hand expert surgeons and one resident

		Surgeon 1 *vs.* surgeon 2[a]	Surgeon 1 *vs.* resident[a]	Surgeon 2 *vs.* resident[a]
EBI group	AIa	0.85 (0.71–0.93)	0.85 (0.74–0.94)	0.86 (078–0.95)
	PIa	0.84 (0.69–0.92)	0.89 (0.79–0.95)	0.87 (0.74–0.94)
NORMAL group	AIa	0.87 (0.74–0.94)	0.90 (0.80–0.95)	0.88 (0.77–0.94)
	PIa	0.85 (0.71–0.93)	0.89 (0.77–0.94)	0.87 (0.760–0.94)

[a] ICC value (95% CI);

AIa = Anterior Impingement angle; CI = confidence interval; EBI = elbow bony impingement; ICC = intraclass correlation coefficients; PIa = Posterior Impingement angle

results with 95% CI. Therefore, we can conclude that our results, with good to excellent reliability, are valid.

Furthermore, our results suggest that training level does not affect the reliability of both measurement techniques, which is largely substantial for both surgeons and trainees before applying them to practice.

Lastly, correlation of manual testing and radiographic measurements is necessary before routine use of these methods. Our results showed a good correlation of AIa with flexion measurement, and PIa with extension deficit. Thus, these radiographic measurements are valid for diagnosing and clinical evaluation of EBI.

In up to date literature, previous studies focus mainly on normal radiographic anatomy, ossification patterns, gender differences and fracture outcomes.[8,12-14] Most of those described parameters are not usable in EBI evaluations, as it is an early sign of elbow degeneration. For elbow osteoarthrosis HR classification is usually used.[7] Yet, no specific radiographic parameter in HR is described that can be used for EBI classification, only staging of the disease. Without a specific method of measurement, that is objectively verifiable, measurements and conclusions can vary markedly from evaluator to evaluator.

To our knowledge, ours is the first study examining reliability and clinical correlation of Impingement angles for EBI evaluation. Only parameter in the literature being slightly associated with EBI is the SNC described by Goldfarb *et al*..[8] Although, they report SNC being only a moderately reliable parameter, we decided to use it in our measurements for group comparison. SNC was significantly greater in EBI group compared to NORMAL group. We believe this reflects the common characteristics seen in degenerative elbow disease, such as osteophyte formation. However, SNC does not specify the origin and extent of EBI, as impingement can be mainly in anterior or in posterior compartment of the elbow joint. For that reason, we decided not to use it in the reliability measurements.

Our study has a few limitations. It demonstrated substantial reliability that may be partially due to the smaller number of raters, all from a single institution. Also, the strong reliability between upper-hand expert surgeons and a resident may be because the resident-rater was under the tutelage of the surgeon-rater. However, our study was

designed with Koo's ICC guidelines and can be treated as valid.

Another limitation is that radiographic assessment was performed only on plain radiographs. In clinical practice a computer tomography (CT) scan is often used for evaluating EBI in cases to be surgically treated.[15] A 3D CT study by Lim *et al*. showed osteophytes predominating in the humeroulnar compartment, specifically in the anterior coronoid area (in 95%) and posteromedial compartment (in 86%).[16] A CT scan helps visualizing osteophytes and asses their relationship to normal joint surfaces. Nonetheless, given the fact that most clinical assessments are based on plain radiographs and obtaining a CT scan in most cases means a transfer of patient to another department, we feel our techniques are reasonable in a way to be easy accessible.

Lastly, as a study limitation, elbow motion includes pronation and supination, which was not assessed. Clinically, patients with EBI have limited flexion-extension ROM and pain in terminal extension and forced flexion. Characteristically, these patients (grade I on HR) do not have pronation-supination limitations.[7] Pronation-supination limitations are associated with radio-capitellar joint degeneration and subluxation, estimated grade II or III on HR, which was an exclusion parameter in our study.[7]

In summary, the findings in our study support the use of AIa and PIa measurements on plain radiographs of elbow joint in patients with suspected EBI. This may prove helpful in future studies by allowing comparison of function, treatment choice and outcomes according to radiographic measurements.

Conclusions

Identifying the location and scale of radiographic changes in EBI is critical in formulating an appropriate diagnosis and treatment plan for such patients. Both AIa and PIa measurement demonstrated substantial intra-rater and inter-rater reliability. In this study both measurements were reliably applied by expert surgeons and resident, with good correlation to manual testing of the elbow function.

Acknowledgments

The authors thank Nerma Kulasic for the support and contribution in this study.

References

1. Amini MH, Sykes JB, Olson ST, Smith RA, Mauck BM, Azar FM, et al. Reliability testing of two classification systems for osteoarthritis and post-traumatic arthritis of the elbow. *J Shoulder Elbow Surg* 2015; **24:** 353-7. doi: 10.1016/j.jse.2014.10.015
2. Adla DN, Stanley D. Primary elbow osteoarthritis: an updated review. *Shoulder Elbow* 2011; **3:** 41-8. doi: 10.1111/j.1758-5740.2010.00089.x
3. Adams JE, Wolff LH 3rd, Merten SM, Steinmann SP. Osteoarthritis of the elbow: results of arthroscopic osteophyte resection and capsulectomy. *J Shoulder Elbow Surg* 2008; **17:** 126-31. doi: 10.1016/j.jse.2007.04.005
4. Wilson V. Upper extremity injuries in the throwing athlete. *Mo Med* 2011; **108:** 170-2. PMID: 21736074
5. Blonna D, Bellato E, Marini E, Scelsi M, Castoldi F. Arthroscopic treatment of stiff elbow. *ISRN Surg* 2011; **2011:** 378135. doi: 10.5402/2011/378135
6. Broberg MA, Morrey BF. Results of delayed excision of the radial head after fracture. *J Bone Joint Surg Am* 1986; **68:** 669-74. PMID: 3722222
7. Rettig LA, Hastings H 2nd, Feinberg JR. Primary osteoarthritis of the elbow: lack of radiographic evidence for morphologic predisposition, results of operative debridement at intermediate follow-up, and basis for a new radiographic classification system. *J Shoulder Elbow Surg* 2008; **17:** 97-105. doi: 10.1016/j.jse.2007.03.014
8. Goldfarb CA, Patterson JM, Sutter M, Krauss M, Steffen JA, Galatz L. Elbow radiographic anatomy: measurement techniques and normative data. *J Shoulder Elbow Surg* 2012; **21:** 1236-46. doi: 10.1016/j.jse.2011.10.026
9. Meglic U, Zupanc O. Significance of radiographic parameters in the diagnosis and treatment of a bony impingement of the elbow. *Mater Technol* 2019; **53:** 747-50. doi: 10.17222/mit.2018.232
10. Blonna D, Zarkadas PC, Fitzsimmons JS, O'Driscoll SW. Validation of a photography-based goniometry method for measuring joint range of motion. *J Shoulder Elbow Surg* 2012; **21:** 29-35. doi: 10.1016/j.jse.2011.06.018
11. Koo TK, Li MY. A Guideline of selecting and reporting intraclass correlation coefficients for reliability research. *J Chiropr Med* 2016; **15:** 155-63. doi: 10.1016/j.jcm.2016.02.012
12. Cheng JC, Wing-Man K, Shen WY, Yurianto H, Xia G, Lau JT, et al. A new look at the sequential development of elbow-ossification centers in children. *J Pediatr Orthop* 1998; **18:** 161-7. PMID: 9531396
13. Keenan WN, Clegg J. Variation of Baumann's angle with age, sex, and side: implications for its use in radiological monitoring of supracondylar fracture of the humerus in children. *J Pediatr Orthop* 1996; **16:** 97-8. doi: 10.1097/01241398-199601000-00019
14. Zarezadeh A, Mamelson K, Thomas WC, Schoch BS, Wright TW, King JJ. Outcomes of distal humerus fractures: what are we measuring? *Orthop Traumatol Surg Res* 2018; **104:** 1253-1258. doi: 10.1016/j.otsr.2018.08.017
15. Ko CC, Tai MH, Lin CH, Tzeng WS, Chen JH, Shu G, et al. Posteromedial olecranon impingement of the pitching elbow: additional findings provided by CT. *Eur J Radiol* 2016; **85:** 211-217. doi: 10.1016/j.ejrad.2015.11.022
16. Lim YW, van Riet RP, Mittal R, Bain GI. Pattern of osteophyte distribution in primary osteoarthritis of the elbow. *J Shoulder Elbow Surg* 2008; **17:** 963-6. doi: 10.1016/j.jse.2008.03.012

research article

Efficacy of transvaginal ultrasound versus magnetic resonance imaging for preoperative assessment of myometrial invasion in patients with endometrioid endometrial cancer: a prospective comparative study

Anis Cerovac[1,2], Dzenita Ljuca[2], Lejla Arnautalic[3], Dubravko Habek[4], Gordana Bogdanovic[2,5], Jasminka Mustedanagic-Mujanovic[2,6], Gordana Grgic[2,5]

[1] Department of Gynaecology and Obstetrics, General Hospital Tešanj, Tešanj, Bosnia and Herzegovina
[2] School of Medicine, University of Tuzla, Tuzla, Bosnia and Herzegovina
[3] Clinic for Radiology and Nuclear Medicine, University Clinical Centre Tuzla, Tuzla, Bosnia and Herzegovina
[4] University Department of Gynaecology and Obstetrics Clinical Hospital "Sveti Duh", Zagreb, School of Medicine, Catholic University of Croatia, Zagreb, Croatia
[5] Clinic for Gynaecology and Obstetrics, University Clinical Centre Tuzla, Tuzla, Bosnia and Herzegovina
[6] Department for Pathology, Policlinic for Laboratory Diagnostic, University Clinical Center Tuzla, Tuzla, Bosnia and Herzegovina

Radiol Oncol 2022; 56(1): 37-45.

Received 03 09 2021
Accepted 13 12 2021

Correspondence to: Anis Cerovac, M.D., Department of Gynaecology and Obstetrics, General Hospital Tešanj, Tešanj, Bosnia and Herzegovina. E-mail: Cerovac.anis@gmail.com

Disclosure: No potential conflicts of interest were disclosed.

Background. We compared the accuracy of preoperative transvaginal ultrasound (TVUS) *versus* magnetic resonance imaging (MRI) for the assessment of myometrial invasion (MI) in patients with endometrial cancer (EC), while definitive histopathological diagnosis served as a reference method.

Patients and methods. Study performed at a single tertiary centre from 2019 to 2021, included women with a histopathological proven EC, hospitalized for scheduled surgery. TVUS and MRI were performed prior to surgical staging for assessment MI, which was estimated using two objective TVUS methods (Gordon's and Karlsson's) and MRI. Patients were divided into two groups, after surgery and histopathological assessment of MI: superficial (≤ 50%) and deep (> 50%).

Results. Sixty patients were eligible for the study. According to the reference method, there were 34 (56.7%) cases in the study with MI < 50%, and 26 (43.3%) with MI > 50%. Both objective TVUS methods and MRI showed no statistical significant differences in overall diagnostic performance for the preoperative assessment of MI. The concordance coefficient between both TVUS methods, MRI and histopathology was statistically significant ($p < 0.001$). Gordon's method calculating MI reached a positive predictive value (PPV) of 83%, negative predictive value (NPV) of 83%, 77% sensitivity, 88% specificity, and 83% overall accuracy. Karlsson's method reached PPV of 82%, NPV of 79%, 69% sensitivity, 88% specificity, and 80% overall accuracy. Accordingly, MRI calculating MI reached PPV of 83%, NPV of 97%, 97% sensitivity, 85% specificity, and 90% overall accuracy.

Conclusions. We found that objective TVUS assessment of myometrial invasion was performed with a diagnostic accuracy comparable to that of MRI in women with endometrial cancer.

Key words: endometrial neoplasms; radiology; oncology; cancer staging

Introduction

Endometrial cancer (EC) is the most common malignancy in the female genital tract in developed countries and its incidence is increasing.[1-3] Due to the early occurrence of abnormal uterine bleeding, most cases are diagnosed at first stage, when prognosis is very good, with a 5-year survival rate of 90%.[4] The EC prognosis is determined by the FIGO (International Federation of Obstetrics and Gynecology) stage of disease, the histological type and grade of tumour, the depth of myometrial invasion (MI), cervical stromal invasion, and lymph nodes involvement.[1-3] The depth of MI > 50%, which is considered to be one of the most important prognostic factors, highly correlates with lymph node metastases.[1-3] The preoperative assessment of the depth of MI is crucial to determining the most effective therapeutic approach and to decide whether the patient should be referred for hysterectomy with bilateral adnexectomy or pelvic lymphadenectomy is need.[1-3]

The depth of MI can be evaluated by a number of imaging methods. These are magnetic resonance imaging (MRI), computer tomography (CT) and transvaginal ultrasonography (TVUS), among which the best results can be achieved by the MRI.[1,3] TVUS has been used extensively to assess depth of MI by EC.[3] TVUS when carried out by experienced hands has been shown to perform equally well as MRI, in the preoperative staging of EC.[4]

Several studies, systematic review and meta-analyses compared subjective assessment and objective TVUS measurements techniques[2,5,6], TVUS (subjective assessment) and MRI[3,7-11], three-dimensional TVUS and MRI[12], and different MRI techniques.[13-15] However, to the best of our knowledge this is the first study that compared two objective TVUS measurements techniques (Gordon's and Karlsson's method) with MRI on the same set of patients.

The aim of our study was to determine the accuracy of preoperative TVUS *versus* MRI for the assessment of MI depth in EC patients, while definitive histopathological diagnosis served as a reference method.

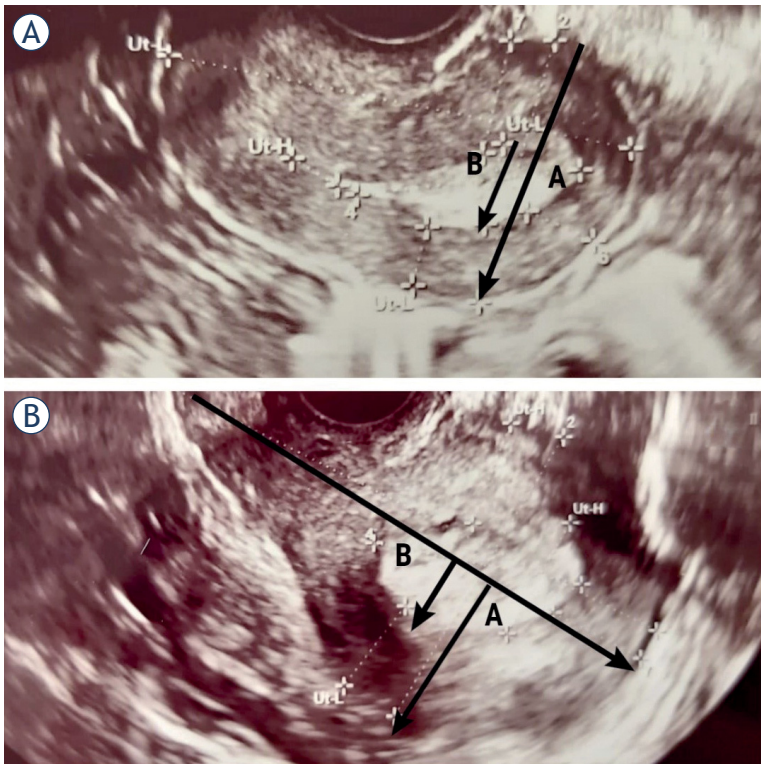

FIGURE 1. Assessment of myometrial invasion in patients with transvaginal ultrasonography (TVUS). Stage IA endometrial cancer in a 61-year-old postmenopausal woman, correctly diagnosed by TVUS and MRI. Karlsson's method indicating infiltration of superficial muscle (29%) **(A)**. Stage IA endometrial cancer in a 53-year-old postmenopausal woman. Gordon's method indicating infiltration of superficial muscle (35%) **(B)**.

Patients and methods

Patients

This prospective cohort study included 60 women with a histopathological proven endometrioid EC by dilatation and curettage, hospitalized for scheduled surgery during the period between July 2019 and April 2021 at the Clinic for Gynaecology and Obstetrics, University Clinical Centre Tuzla. Inclusion criteria were women with a histopathological proven endometrioid EC. Exclusion criteria were women with another malignant disease, who previously have surgery for EC or other malignant disease, who have previously received chemotherapy and/or radiotherapy due to a malignant disease, women with a histopathological proven EC who preoperatively have made pelvic CT, cases that were diagnosed incidentally after hysterectomy. Patients were divided into two groups, after surgery and histopathological assessment of depth of MI: invasion to less or equal and to more than half the thickness of the myometrium. The survey was approved by the Ethics Committee of the University Clinical Centre (No 02-09/2-2/20) Tuzla and signed informed consent of patients was obtained.

Methods

Transvaginal ultrasonography

All TVUS examinations were performed by a single ultrasound examiner (CA), certified for ultrasound diagnostics, on standardized study protocol containing all investigated sonographic parameters defined before the beginning of the study. TVUS was made using a Voluson E8® equipped with a 5–9-MHz two-dimensional transducer, within ten days before surgery, without insight into the MRI finding. We assessed of MI by two TVUS methods, those proposed by Gordon *et al.* and Karlsson *et al.*[2,5] Transvaginally, the whole uterus was observed in sagittal and transversal section.[5]

Depth of MI was measured as the ratio between the maximum AP diameter of the endometrial tumor (B) and the uterine AP diameter (A) in sagittal plane, with B/A > 50% indicating deep MI introduced by Karlsson *et al.* (Figure 1A, Figure 2A).[2,5] In other objective method, investigated by Gordon *et al.*, depth of MI was measured as the ratio of the distance between the maximum tumor depth (B) and the total myometrial thickness (A) in sagittal plane, with B/A > 50% indicating deep MI (Figure 1B, Figure 2B).[2,5]

The selected cut-off limit for the extent of MI (50%) followed FIGO staging classification from 2009.[5]

Static images with all measurements were collected for each patient and examination protocols were noted immediately during image acquisition.

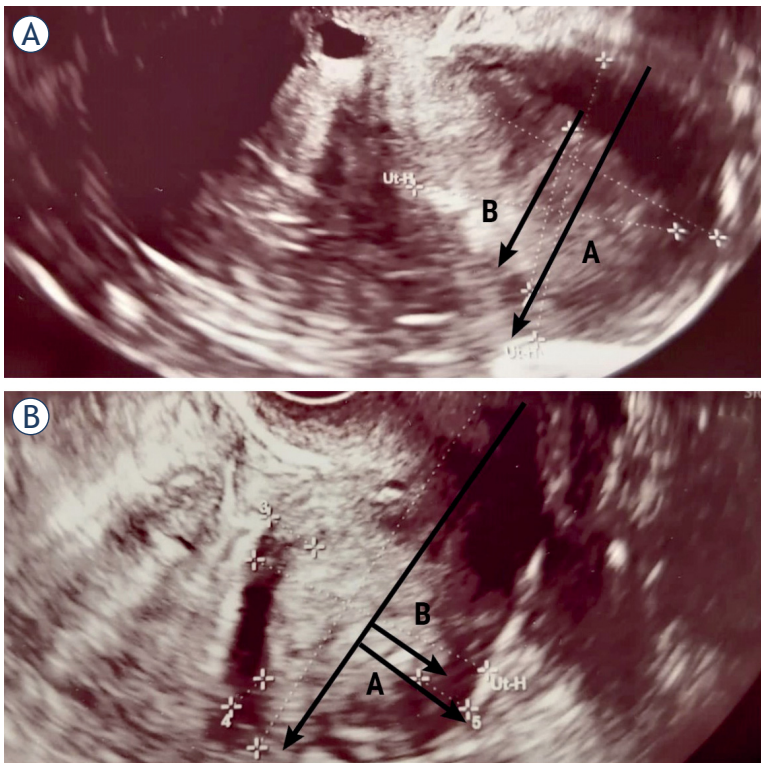

FIGURE 2. Assessment of myometrial invasion in patients with transvaginal ultrasonography (TVUS). Stage IB endometrial cancer in a 78-year-old postmenopausal woman, correctly diagnosed by TVUS and MRI. Karlsson's method indicating infiltration of deep muscle (58%) **(A)**. Stage IB endometrial cancer in an 83-year-old postmenopausal woman. Gordon's method indicating infiltration of deep muscle (73%) **(B)**.

Magnetic resonance imaging

Abdominal and pelvic MRI examination was composed of T2 and T1-weighted images and dynamic contrast-enhanced fat-suppressed images at 1.5 Tesla Avanto Siemens Medical Systems® device, according to the dedicated MRI protocol of the European Society of Uro-Genital Radiologists since 2009 for the diagnosis of EC.[11,16] All study participants underwent abdominal and pelvic MRI examination within 10 days prior to surgery.

MRI protocol for accurate assessment of MI, based on T2-weighted images in three orthogonal planes oriented perpendicular and parallel to the uterine cavity (sagittal, axial, coronal and oblique axial), in axial and sagittal plane in T1-weighted images and T1-weighted contrast-enhanced fat-suppressed images.[14,16] For optimal assessment of MI dynamic contrast-enhanced fat-suppressed MRI was done after intravenous bolus injection of 1 mg/kg of a paramagnetic contrast agent is administered.[14,16]

The criteria for MRI MI diagnosis was disruption and irregularity of the endomyometrial junctional zone.[12] The ratio of the tumor to the endomyometric junctional zone and the depth of MI to the junctional zone were determined. If the signal intensity of the tumour on T2W was greater than half, it was regarded as a deep MI.[12]

In order to measure the depth of MI on MRI, the line must be drawn along the expected inner edge of the myometrium (corresponding to the endomyometric junctional zone) on axial oblique plane obtained perpendicular to the endometrium; then, two measures should be taken: one represents the thickness of the entire myometrium; the second is measuring the maximum range of tumor within the myometrium. The ratio of these measures represents the percentage of MI. The ratio of the thickness of the tumor from the uterine cavity to the outer border and the total thickness of the

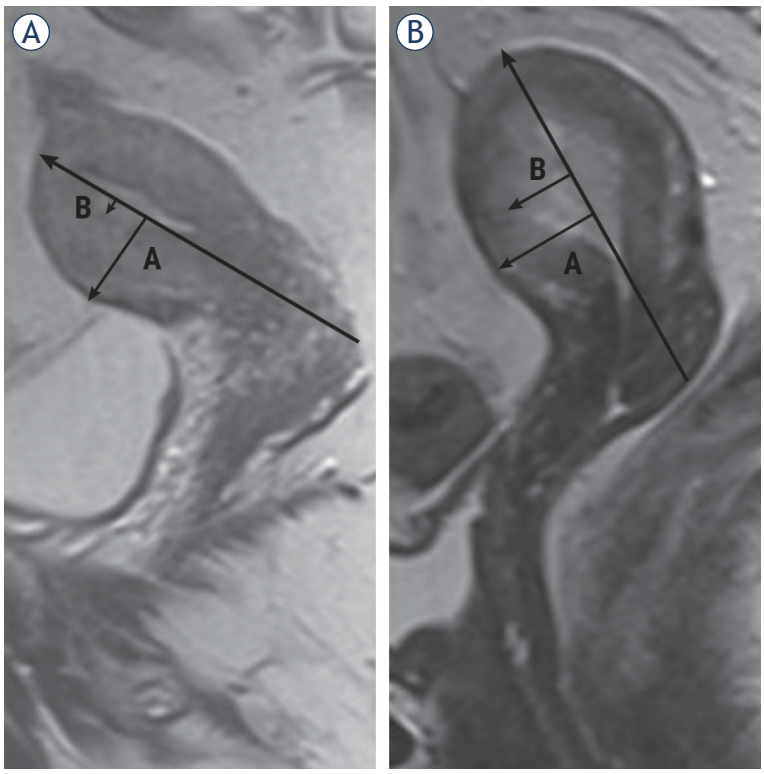

FIGURE 3. Assessment of myometrial invasion in patients with MRI, sagittal T2-weighted. Stage IA endometrial cancer in a 68-year-old postmenopausal woman, correctly diagnosed by TVUS and MRI. Arrow shows blurring of the junctional zone and the infiltration of superficial muscle (20%) **(A)**. Stage IB endometrial cancer in a 58-year-old postmenopausal woman, correctly diagnosed by TVUS and MRI. Arrows refers to deep myometrial infiltration (60%) **(B)**.

TABLE 1. Demographic and clinical characteristics of 60 women with histologically confirmed endometrial cancer

Characteristics	Value (%)
Age (years)	60 (40–83)
Body mass index (kg/m²)	32.05 (21.6–49.2)
Postmenopausal	45 (75)
Myometrial invasion	
Superficial (≤ 50 %)	34 (56.7)
Deep (> 50%)	26 (43.3)
Hystological grade	
Grade 1	18 (30)
Grade 2	35 (58)
Grade 3	7 (12)

Data are given as median (5th percentile; 95th percentile) for continuous variables; *n* (%) for categorical variables.

myometrial wall on the side on which the tumor is located was calculated (Figure 3).

The radiologist was not blinded to the diagnosis of EC but remained unaware of the TVUS results. All analyses have been performed by the same radiologist (LA), with experience in analysing abdominal and pelvic MRI.

Surgical procedure

Primary surgery was performed by an gynaecological oncological surgeon with experience in gynaecologic-oncological surgery in median ten days after MRI, and ten day after TVUS.

Scheduled surgery was indicated based on preoperative histopathological diagnosis with tumour type and grade, TVUS and MRI. The surgeon was not blinded towards the histopathological diagnosis, TVUS and MRI results.[11] Surgery was performed by an open abdominal approach and according to the decision of the gynaecologic-oncological interdisciplinary tumour board. The surgical approach was planned based on the FIGO classification derived from MRI.[11] The depth of MI obtained by TVUS and MRI has been correlated to help shed light on the dilemma of whether classical hysterectomy with bilateral adnexectomy is sufficient or pelvic lymphadenectomy is necessary for oncological treatment to be adequate.

Histopathological diagnosis

Surgical specimens were examined by pathologists with experience in gynaecologic oncology using a predetermined protocol regarding: histological subtype, grade, lymphovascular invasion, tumour size, depth of myometrial invasion, minimal tumour-free myometrium, presence of cervical stromal invasion, presence, location and number of fibroids.[5] The FIGO 2009 criteria were applied for clinical staging. The "gold standard" was based on final histology of the specimen obtained by hysterectomy.[5]

Statistical analysis

Basic tests of descriptive statistics were made, showing the measures of central tendency and dispersion (Table 1). Sensitivity, specificity, positive predictive value (PPV) and negative predictive value (NPV), overall accuracy, likelihood ratio of a positive test, likelihood ratio of a negative test, as well as receiver operating characteristics (ROC)

TABLE 2. Myometrial invasion in endometrial cancer according to histopathology, transvaginal ultrasonography and magnetic resonance imaging

Histopathology	TVUS (Gordon)		TVUS (Karlsson)		MRI		Total N(%)
	≤ 50% N(%)	> 50% N(%)	≤ 50% N(%)	> 50% N(%)	≤ 50% N(%)	> 50% N(%)	
≤ 50% N (%)	30 (88.2)	4 (11.8)	30 (88.2)	4 (11.8)	29 (85.3)	5 (14.7)	34 (100)
> 50% N(%)	6 (23.1)	20 (76.9)	8 (30.8)	18 (69.2)	1 (3.8)	25 (96.2)	26 (100)
Total	36 (60)	24 (40)	38 (63.3)	22 (36.7)	30 (50)	30 (50)	60 (100)

TVUS = transvaginal ultrasound

curves assessing MI were calculated for each staging method (TVUS; Gordon's and Karlsson's method and MRI) in comparison to the final histology. Receiver operating characteristic (ROC) curves were used to evaluate the accuracy of the tests.

Statistical processing was done in the software package SPSS 24.0 (Chicago, IL, USA). All statistical tests were performed with a statistical probability level of 95% ($p < 0.05$).

Results

Of 72 cases diagnosed with endometrioid EC during the study period and who underwent preoperative TVUS and MRI, 60 cases were enrolled in the study, of mean (SD) age 60 (10) in range from 40–83 years. Forty-five (75%) out of the 60 were postmenopausal. Median body mass index was 32.05 kg/m^2 (range 21.6-49.2). The most frequently encountered histological grade was grade 2 (58%, 35/60).

Twelve cases (16.6%) evaluated during the study period were excluded from the database, because of preoperatively made CT (morbid obesity and/or claustrophobia).

The patient demographics and tumour characteristics are summarized in Table 1.

Regarding final surgical procedure, 60 cases (100%) underwent open surgery. Hysterectomy with bilateral adnexectomy was performed in 60 cases (100%). Pelvic lymphadenectomy was performed in 32 cases out of 60 (53.3%). Pelvic lymphadenectomy was performed in eight cases out of 36 (22.2%) with MI ≤ 50%, in 24 cases out of 26 (92.3%) with MI > 50%, that is statistically significant frequently in group with MI > 50% ($z = -5.29$, $p < 0.00001$).

According to the gold standard, histopathological diagnostics, there were 34 (56.7%) cases in the study with MI ≤ 50%, and 26 (43.3%) with MI > 50%.

The depth of MI was correctly assessed by Gordon's method in 50 (83.3 %) cases, overestimated in four (6.6%) and underestimated in six (10%) (Table 2).

The concordance coefficient between TVUS and histopathology was also statistically significant ($p < 0.001$) and kappa was 0.658. These data corresponded to a PPV of 83% and NPV of 83%, 77% sensitivity, 88% specificity, and 83 % overall accuracy (Table 3).

TABLE 3. Diagnostic performance of transvaginal ultrasonography and magnetic resonance imaging in predicting myometrial invasion in endometrial cancer

Diagnostic test measure	TVUS (Gordon)	TVUS (Karlsson)	MRI
	%, (95% CI)	%, (95% CI)	%, (95% CI)
Accuracy	83 (70–92)	80 (67–88)	90 (78–93)
Sensitivity	77 (62–87)	69 (54–79)	97 (83–99)
Specificity	88 (77–96)	88 (77–96)	85 (75–88)
Positive predictive value	83 (67–94)	82 (64–93)	83 (72–87)
Negative predictive value	83 (72–90)	79 (69–86)	97 (85–99)
Likelihood Ratio of a Positive Test	6.54 (2.65–19.00)	5.89 (2.30–18.17)	6.54 (3.31–8.37)
Likelihood Ratio of a Negative Test	0.26 (0.14–0.50)	0.35 (0.22–0.60)	0,05 (0.002–0.23)

The estimates are stated along with the 95% confidence intervals (95% CI); TVUS = transvaginal ultrasound

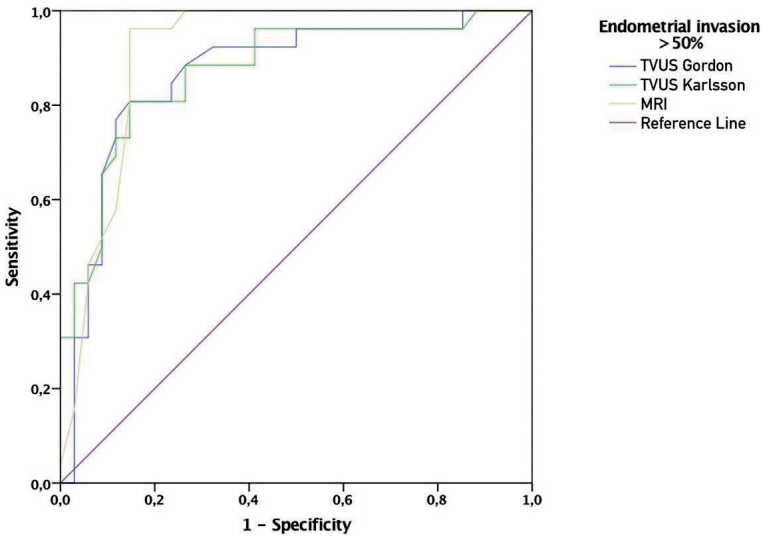

FIGURE 4. Receiver operating characteristics (ROC) analysis for percentage assessment of myometrial invasion (MI) with transvaginal ultrasound (TVUS) by Gordon's and Karlsson's, and with MRI

The depth of MI was correctly assessed by Karlsson's method in 48 (80%) cases, overestimated in four (6.6%) and underestimated in eight (13.3%) (Table 2). The concordance coefficient between TVUS and histopathology was statistically significant ($p < 0.001$) and kappa was 0.585. Accordingly, Karlsson's method calculating MI reached PPV of 82% and NPV of 79%, 69% sensitivity, 88% specificity, and 80% overall accuracy (Table 3).

MRI correctly assessed MI in 54 (90%) cases, overestimated it in five (8.3%) cases and underestimated it in one (1.6%) (Table 2). The concordance coefficient between MRI and histopathology was statistically significant ($p < 0.001$) and kappa was 0.80. Accordingly, MRI calculating MI reached PPV of 83% and NPV of 97%, 97% sensitivity, 85% specificity, and 90% overall accuracy (Table 3).

The diagnostic performance of two objective transvaginal ultrasonography methods assessment and MRI calculations in predicting deep MI as well as the statistical comparison of ultrasonography to MRI method are introduced in Table 3.

Differences in the performance of the two TVUS imaging modalities (Karlsson *vs.* Gordon) were not statistically significant ($p = 0.867$). Differences in the performance between the Gordon's method and MRI were not statistically significant ($p = 0.417$). Differences in the performance between of the Karlsson's method and MRI were not statistically significant ($p = 0.464$).

The prevalence of myometrial pathology was the same in the incorrectly classified patients in TVUS and MRI methods of assessment of MI. Of the 10 patients in whom infiltration was misclassified on TVUS and of the 6 patients misclassified on MRI, 5 (50%) and three (50%) had benign myometrial pathologies (adenomyosis and leiomyoma), respectively.

TVUS and MRI correctly estimated MI in 45 (75%) patients, underestimated it in one (1.6%) and overestimated it in two (3.3%). If we consider only the cases in which the two techniques were in agreement (48 cases), the concordance with histology was 80%.

Evaluation of diagnostic accuracy was performed through Receiver Operating Characteristics (ROC) analysis and for percentage assessment of MI with TVUS by Gordon's and Karlsson's method, and with MRI. A graphical representation of this analysis is given in Figure 4, and a tabelar representation of the areas below the ROC curve (AUC) in the Table 4.

As can be seen, the best diagnostic accuracy according to the ROC analysis had MRI with an AUC of 0.911 (total accuracy 91.1%), which is in correlation with the already performed diagnostic accuracy analyses.

TABLE 4. Representation of the areas below the receiver operating characteristics (ROC) curve (AUC) for percentage assessment of MI with transvaginal ultrasound (TVUS) by Gordon and Karlsson, and with MRI

Method of assessment	AUC	P	95% CI for AUC	
			Lower limit	Upper limit
TVUS (Gordon)	0.872	< 0.001	0.769	0.965
TVUS (Karlsson)	0.865	< 0.001	0.766	0.964
MRI	0.911	< 0.001	0.833	0.989

Discussion

In this prospective, comparative, ultrasonographer-blinded study on patients with EC two objective TVUS methods (Gordon's and Karlsson's) and MRI were compared for the MI assessment in the same cohort of patients. All three tested approaches were found to be statistically significant predictors of the MI, exceeding AUC value of 0.85 and reaching final p value < 0.001. We found that MRI assessment of MI is better than any objective TVUS measurement technique in all measures of the diagnostic tests, but without statistically significance.

Median age in our patients is similar to Pineda *et al.* study[17], 60 *vs*. 60.9, respectively, however there are studies with higher[1,4-6,8], and lower median age.[12,18]

Postmenopausal in recent study were 75% patients which correlate with other studies, where postmenopausal patients were in the range from 70.2% to 92%.[5-10,15,17,19] EC is disease of older and postmenopausal women, that was also confirmed by our study.[3]

Patients in recent study were obese with an median body mass index (BMI) of 32.05 which is similar to median BMI of 31 in Rei *et al.* study[8], however there are studies with higher[7,15] and lower median BMI.[4-6,17,19] Obesity is a proven risk factor for developing EC, what was also confirmed by recent study.[8]

The most frequently encountered histological grade in recent study was grade 2 (58%) which is the same percentage as in Karatasli *et al.* study.[15] In most of the reviewed studies, histological grade 1 is more common than other grades which agrees with the fact that endometrial cancer is usually a well-differentiated.[1,5-7,10,14,17]

In current study according to the gold standard, histopathological diagnostics, it is more common superficial MI (≤ 50%), which correlate with most reviewed studies and with fact that EC is detected at an early stage in most cases.[4-8,10-12,14,15,18,22,23]

Several studies evaluated objective measurements such as those proposed by Gordon *et al.* and Karlsson *et al*.[2,3]

Alcazar *et al.* in systematic review and meta-analysis found that the overall diagnostic performance of TVUS for Karlsson's and Gordon's method in detecting deep MI in women with EC gave a pooled sensitivity of 84 % and 85 %, pooled specificity of 82% and 80% which is higher sensitivity and lower specificity than in our study for both methods.[2] They observed that both methods were similar, without statistical differences, in terms of diagnostic performance, similar as in our study.[2]

In reviewed studies diagnostic performance for Gordon's method reached sensitivity from 69.6% to 92.3%, specificity from 65.9% to 79.2%, PPV from 56.7% to 61%, NPV from 77.1% to 96.1% and overall accuracy from 67.3% to 82.6%.[1,5]

Recent studies reported for Karlsson's method sensitivity from 56.3% to 86.8%, specificity from 64.4% to 76.4%, PPV from 62.8% to 83.6%, NPV from 70% to 71.2% and overall accuracy 68.1%.[5,6,19,21]

Besides, current study did not find statistical differences between Gordon's and Karlsson's method. Although both TVUS objective calculations, Gordon's and Karlsson's method, had similar accuracy, the approach published by Gordon *et al.* have better sensitivity and accuracy in preoperative assessment of MI in EC. However, in our opinion Gordon's method might be more difficult for assessment of MI.[5] On the other side, under or overestimation of MI by Karlsson's method is often caused by large polypoid EC, submucosal leiomyomas and adenomyosis which make longer anterio-posterior uterine diameter.[5]

In 2017 Alcazar *et al.* published a systematic review and meta-analysis based on preoperative detection of deep MI comparing TVUS and MRI on the same set of women.[3] However, they found out that sensitivity and specificity for diagnosing deep MI were 75% and 82% for TVUS, and 83% and 82% for MRI, respectively. MRI showed a better sensitivity than TVUS for detecting depth of MI in women with EC, but without statistical differences, as in our study.[3] However, none of these studies compared the three imaging methods altogether in one cohort of patients as is the case in our comparative study.

In analysed studies diagnostic performance for MRI reached sensitivity from 70% to 92.6%, specificity from 71% to 95%, PPV from 65% to 92.2%, NPV from 70% to 98%, and overall accuracy from 74% to 89%.[7-10,12-15,20-22]

We have shown that two imaging modalities (contrast-enhanced MRI and TVUS) perform equally well in the assessment of MI, differences in the performance were not statistically significant.

Cubo-Abert *et al.* obtained similar results as in our study, when it comes to the diagnostic accuracy of TVUS *versus* MRI in estimating the depth of MI, with the difference that they used the TVUS method based on the measurement of the minimal distance to the uterine serosa.[24]

Costas *et al.* in systematic review and meta-analysis have not found a satisfying number of studies about the comparison of 2D-TVUS and 3D-TVUS methods for MI assessment in EC.[25] They have identified lack of knowledge and studies regarding the objective methods used for 3D-TVUS assessment and their comparison with subjective 3D-TVUS methods.[25]

Although the definitive staging of endometrial cancer is based on histopathology, an accurate preoperative assessment of MI by TVUS and/or MRI provides the opportunity for surgical planning to provide an adequate type of surgery, the need of a multidisciplinary team, time management in the operating room, and avoid morbidity associated with unnecessary lymphadenectomy.[8,9,23]

Causes of over or understaging were similar for the TVUS and MRI: a polypoid EC, large exophytic tumors with distension and thinning of the myometrium with regular endometrial junction and without MI, fibromatosis, adenomyosis, leiomyomata, deep MI, small isolated glandular foci, uterine anomalies, uterine prolapse or retroversion, short time after previous endometrial biopsy, poorly defined endometrial borders on TVUS, and disappearance of the junctional zone on MRI.[1,6,7,9,19]

Considering that there are no statistically significant differences in diagnostic performance between TVUS and MRI and the cost and availability of MRI, TVUS may have a role as the first imaging technique for assessing MI in women with EC, especially as it is implemented in the everyday practice of gynecologists.[1,2,4,8]

As Miklos *et al.* concluded the diagnostic accuracy of the TVUS depends more on the individual experience and professional potential of the examiner than diagnostic accuracy of the MRI.[1] Examiner experience, technological advances and different protocols for assessing MI among the studies, for both TVUS and MRI can contribute to the heterogeneity of published results of TVUS and MRI in the assessment of MI.[1,3,8] Expert TVUS and MRI were comparable and superior to non-expert TVUS for assessing MI in EC.[26]

MRI, which is more expensive, time consuming and difficult to access, could be employed as a second-line imaging technique in patients in whom TVUS gives images of poor quality in case of obesity and factors above mentioned that may cause over or understaging.[9]

MRI is currently recommended for preoperative imaging in some guidelines, as the imaging modality of choice and most appropriate for the assessment of disease extent in patients with newly diagnosed EC.[3,15,20]

Iitsuka *et al.* in their study and review of literature found that their data and the pooled analysis with previous studies indicate that the frozen section diagnosis is sensitive as MRI assessment in predicting deep MI, and has a higher specificity compared with MRI.[27]

Contraindications for MRI should also be kept in mind, when MRI cannot be performed such as metal foreign body, pathologic obesity, contrast allergies and claustrophobia.

The main strength of our study is that, to the best of our knowledge, this is the first study that compares prospectively the two objective TVUS methods (Gordon's and Karlsson's) and objective MRI method, for assessing MI in patients with endometrioid EC in the same set of patients. A strength of our study are the prospective design and the fact that the gynaecologists performing TVUS and the radiologists performing MRI were blinded to each other's results. Another strength is that all TVUS assessment of MI were made by the same physician, MRI assessment of MI by the same radiologist, and all surgeries and pathologic examinations were done at the same center. Strength of our study is also that we compared the three imaging methods altogether in one cohort of patients which is ideally, for comparing the diagnostic performance of different approaches to assess MI, and this is rarity in reviewed studies.

Limitations of our study are the relatively small number and short time of collection of participants, but this can be justified by the prospective design of the study, the strict inclusion and exclusion criteria, and in fact that the study was performed in the largest tertiary center in the country.

Conclusions

In conclusion, we found that objective TVUS assessment of myometrial invasion was performed with a diagnostic accuracy comparable to that of MRI in women with endometrial cancer. Further multi-centric studies with prospective designs and standardized protocols are needed to investigate which objective measurement techniques and MRI have the highest reproducibility, and how well they perform in the hands of examiners with more or less experience. In addition, studies evaluating inter-observer agreement as well as the impact of TVUS training would be of great interest.

Acknowledgments

This article is a part of research conducted within the doctoral dissertation of Anis Cerovac.

We are thankful to personnel of the Clinic for Gynecology and Obstetrics, Clinic for Radiology and Nuclear Medicine and Policlinic for Laboratory Diagnostics, University Clinical Center Tuzla for their cooperation.

We give our deep appreciation to all women who participated in this trial because with their participation they can help women with endometrial cancer, but also offer new diagnostic approach and opportunities for future generations.

References

1. Miklos P, Klacko M, Babala P, Masak L, Ondrus D, Waczulikova I. Transvaginal ultrasound examination of myometrial infiltration by endometrial cancer. *Bratisl Lek Listy* 2014; **115:** 14-18. doi: 10.4149/bll_2014_003
2. Alcázar JL, Orozco R, Martinez-Astorquiza Corral T, Juez L, Utrilla-Layna J, Mínguez JA, et al. Transvaginal ultrasound for preoperative assessment of myometrial invasion in patients with endometrial cancer: a systematic review and meta-analysis. *Ultrasound Obstet Gynecol* 2015; **46**: 405-13. doi: 10.1002/uog.14905
3. Alcázar JL, Gastón B, Navarro B, Salas R, Aranda J, Guerriero S. Transvaginal ultrasound versus magnetic resonance imaging for preoperative assessment of myometrial infiltration in patients with endometrial cancer: a systematic review and meta-analysis. *J Gynecol Oncol* 2017; **28:** e86. doi: 10.3802/jgo.2017.28.e86
4. Eriksson LSE, Lindqvist PG, Flöter Rådestad A, Dueholm M, Fischerova D, Franchi D, et al. Transvaginal ultrasound assessment of myometrial and cervical stromal invasion in women with endometrial cancer: interobserver reproducibility among ultrasound experts and gynecologists. *Ultrasound Obstet Gynecol* 2015; **45:** 476-82. doi: 10.1002/uog.14645
5. Frühauf F, Zikan M, Semeradova I, Dundr P, Nemejcova K, Dusek L, et al. The diagnostic accuracy of ultrasound in assessment of myometrial invasion in endometrial cancer: subjective assessment versus objective techniques. *Biomed Res Int* 2017; **2017:** 1318203. doi: 10.1155/2017/1318203
6. Mascilini F, Testa AC, Van Holsbeke C, Ameye L, Timmerman D, Epstein E. Evaluating myometrial and cervical invasion in women with endometrial cancer: comparing subjective assessment with objective measurement techniques. *Ultrasound Obstet Gynecol* 2013; **42:** 353-8. doi: 10.1002/uog.12499
7. Ozdemir S, Celik C, Emlik D, Kiresi D, Esen H. Assessment of myometrial invasion in endometrial cancer by transvaginal sonography, Doppler ultrasonography, magnetic resonance imaging and frozen section. *Int J Gynecol Cancer* 2009; **19:** 1085-90. doi: 10.1111/IGC.0b013e3181ad3eb6
8. Rei M, Rodrigues I, Condeco P, Igreja F, Verissimo C, Mendinhos G. Endometrial cancer: preoperative versus intraoperative staging. *J Gynecol Obstet Hum Reprod* 2019; 101647. doi: 10.1016/j.jogoh.2019.101647
9. Savelli L, Ceccarini M, Ludovisi M, Fruscella E, De Iaco PA, Salizzoni E, et al. Preoperative local staging of endometrial cancer: transvaginal sonography vs. magnetic resonance imaging. *Ultrasound Obstet Gynecol* 2008; **31:** 560-6. doi: 10.1002/uog.5295
10. Yin XH, Jia HY, Shi M, Wu H, Li YM. Magnetic resonance imaging for detection of depth of myometrial invasion and cervical invasion in patients with endometrial carcinoma. *Int J Clin Exp Med* 2015; **8:** 19501-5. PMCID: PMC4694500
11. Brocker KA, Radtke JP, Hallscheidt P, Sohn C, Schlemmer HP, Alt CD. Comparison of the determination of the local tumor extent of primary endometrial cancer using clinical examination and 3 Tesla magnetic resonance imaging compared to histopathology. *Arch Gynecol Obstet* 2019; **299:** 1391-8. doi: 10.1007/s00404-019-05072-5
12. Yang T, Tian S, Li Y, Tian X, Wang W, Zhao J, et al. Magnetic resonance imaging (MRI) and three-dimensional transvaginal ultrasonography scanning for preoperative assessment of high risk in women with endometrial cancer. *Med Sci Monit* 2019; **25:** 2024-31. doi: 10.12659/MSM.915276
13. Bi Q, Chen Y, Wu K, Wang J, Zhao Y, Wang B, et al. The diagnostic value of MRI for preoperative staging in patients with endometrial cancer: a meta-analysis. *Acad Radiol* 2020; **27:** 960-8. doi: 10.1016/j.acra.2019.09.018
14. Goel G, Rajanbabu A, Sandhya CJ, Nair IR. A prospective observational study evaluating the accuracy of MRI in predicting the extent of disease in endometrial cancer. *Indian J Surg Oncol* 2019; **10:** 220-4. doi: 10.1007/s13193-018-0832-9
15. Karataşlı V, Çakır I, Şahin H, Ayaz D, Sancı M. Can preoperative magnetic resonance imaging replace intraoperative frozen sectioning in the evaluation of myometrial invasion for early-stage endometrial carcinoma? *Ginekol Pol* 2019; **90:** 128-33. doi: 10.5603/GP.2019.0023
16. Rizzo S, Femia M, Buscarino V, Franchi D, Garbi A, Zanagnolo V, et al. Endometrial cancer: an overview of novelties in treatment and related imaging keypoints for local staging. *Cancer Imaging* 2018; **18:** 45. doi: 10.1186/s40644-018-0180-6
17. Pineda L, Alcázar JL, Caparrós M, Mínguez JA, Idoate MA, Quiceno H, et al. Agreement between preoperative transvaginal ultrasound and intraoperative macroscopic examination for assessing myometrial infiltration in low-risk endometrioid carcinoma. *Ultrasound Obstet Gynecol* 2016; **47:** 369-73. doi: 10.1002/uog.14909
18. Tatar B. Assessment of myometrial invasion of endometrial carcinoma with preoperative transvaginal sonography. *Eur J Gynaecol Oncol* 2021; **42:** 85-9. doi: 10.31083/j.ejgo.2021.01.2236
19. Capozzi VA, Merisio C, Rolla M, Pugliese M, Morganelli G, Cianciolo A, et al. Confounding factors of transvaginal ultrasound accuracy in endometrial cancer. *J Obstet Gynaecol* 2021; **41:** 779-84. doi: 10.1080/01443615.2020.1799342
20. Horváth K, Pete I, Vereczkey I, Dudnyikova A, Gődény M. Evaluation of the accuracy of preoperative MRI in measuring myometrial infiltration in endometrial carcinoma. *Pathol Oncol Res* 2014; **20:** 327-33. doi: 10.1007/s12253-013-9699-9
21. Gastón B, Muruzábal JC, Lapeña S, Modroño A, Guarch R, García de Eulate I, et al. Transvaginal ultrasound versus magnetic resonance imaging for assessing myometrial infiltration in endometrioid low grade endometrial cancer: a prospective study. *J Ultrasound Med* 2022. **41:** 335-42. doi: 10.1002/jum.15708
22. Wu WJ, Yu MS, Su HY, Lin KS, Lu KL, Hwang KS. The accuracy of magnetic resonance imaging for preoperative deep myometrium assessment in endometrial cancer. *Taiwan J Obstet Gynecol* 2013; **52:** 210-4. doi: 10.1016/j.tjog.2013.04.010
23. Sobočan M, Ogrizek AM, Ledinek T, Takač I, Knez J. Importance of preoperative ultrasound examination and pathological tumour evaluation in the management of women with endometrial cancer. *Eur J Obstet Gynecol Reprod Biol* 2021; **257:**121-6. doi: 10.1016/j.ejogrb.2020.12.029
24. Cubo-Abert M, Díaz-Feijoo B, Bradbury M, Rodríguez-Mías NL, Vera M, Pérez-Hoyos S, et al. Diagnostic performance of transvaginal ultrasound and magnetic resonance imaging for preoperative evaluation of low-grade endometrioid endometrial carcinoma: prospective comparative study. *Ultrasound Obstet Gynecol* 2021; **58:** 469-75. doi: 10.1002/uog.23607
25. Costas T, Belda R, Alcazar JL. Transvaginal three-dimensional ultrasound for preoperative assessment of myometrial invasion in patients with endometrial cancer: a systematic review and meta-analysis. *Med Ultrason* 2021. [Ahead of print]. doi: 10.11152/mu-2961
26. Dueholm M, Hjorth IM, Dahl K, Marinovskij E, Ørtoft G. Preoperative prediction of high-risk endometrial cancer by expert and non-expert transvaginal ultrasonography, magnetic resonance imaging, and endometrial histology. *Eur J Obstet Gynecol Reprod Biol* 2021; **263:** 181-91. doi: 10.1016/j.ejogrb.2021.05.041
27. Iitsuka C, Asami Y, Hirose Y, Nagashima M, Mimura T, Miyamoto S, et al. Preoperative magnetic resonance imaging versus intraoperative frozen section diagnosis for predicting the deep myometrial invasion in endometrial cancer: our experience and literature review. *J Obstet Gynaecol Res* 2021; **47:** 3331-8. doi: 10.1111/jog.14891

research article

Bladder paraganglioma: CT and MR imaging characteristics in 16 patients

Jing Zhang[1], Xu Bai[2], Jing Yuan[3], Xiaojing Zhang[1], Wei Xu[1], Huiyi Ye[1], Haiyi Wang[1]

[1] Department of Radiology, First Medical Center, Chinese PLA General Hospital, Beijing, China
[2] Department of Radiology, Fifth Medical Center, Chinese PLA General Hospital, Beijing, China
[3] Department of Pathology, Tianjin Nankai Hospital, Tianjin, China

Radiol Oncol 2022; 56(1): 46-53.

Received 3 August 2021
Accepted 24 November 2021

Correspondence to: Haiyi Wang M.D., Department of Radiology, First Medical Centre, Chinese PLA General Hospital, No. 28 Fuxing Road, Haidian District, Beijing 100853, China. E-mail: wanghaiyi301@outlook.com

Jing Zhang and Xu Bai contributed equally.

Disclosure: No potential conflicts of interest were disclosed.

Background. Bladder paraganglioma (BPG) is a rare extra-adrenal pheochromocytoma with variable symptoms and easy to be misdiagnosed and mishandled. The aim of the study was to document the imaging features of BPG using computed tomography (CT) and magnetic resonance imaging (MRI).

Patients and methods. We retrospectively enrolled consecutive patients with pathology-proven BPG, who underwent CT or MRI examinations before surgery between October 2009 and October 2017. The clinical characteristics, CT, and MRI features of the patients were described and analysed.

Results. A total of 16 patients with 16 bladder tumours (median age 51 years, 9 females) were included. Among them, 13 patients underwent CT examinations and eight patients underwent MRI examinations preoperatively. Tumour diameters ranged from 1.6−5.4 cm. Most of the tumours grew into the bladder cavity (n = 11) with oval shapes (n = 10) and well-defined margins (n = 14). Intratumour cystic degeneration or necrosis (n = 2) was observed. Two lesions showed peripheral tissue invasion, suggesting malignant BPGs. All 13 lesions imaged with CT exhibited slight hypoattenuation and moderate to marked enhancement. Compared to the *gluteus maximus*, all lesions showed slight hyperintensity in T2-weighted images, hyperintensity on diffusion-weighted images (DWI), hypointensity on apparent diffusion coefficient maps, hyperintensity on T1-weighted images and a "fast in and slow out" enhanced pattern on contrast-enhanced MRI images.

Conclusions. BPGs are mostly oval-shaped, broadly-based and hypervascular bladder tumours with hypoattenuation on non-contrast CT, T2 hyperintensity, slight T1 hyperintensity compared to the muscle, marked restricted diffusion on DWI. Peripheral tissue invasion can suggest malignancy of the BPGs. All of these features contribute to preoperative decision-making.

Key words: paraganglioma; urinary bladder; computed tomography; magnetic resonance imaging

Introduction

Paragangliomas are rare neoplasms of extra-adrenal chromaffin cells that belong to the family of neuroendocrine tumours.[1] They account for 15–20% of pheochromocytomas and occur in a variety of locations such as the head and neck, paraspinal region, chest, abdomen, and pelvis. The bladder is the most common site of paragangliomas in the genitourinary system (79.2%).[2]

Bladder paragangliomas (BPGs) are exceedingly rare and constitute only 0.06% of bladder tumours and 1% of all paragangliomas.[3] BPG is an extra-adrenal pheochromocytoma that arises from the chromaffin tissue of the sympathetic nervous system associated with the bladder wall and has

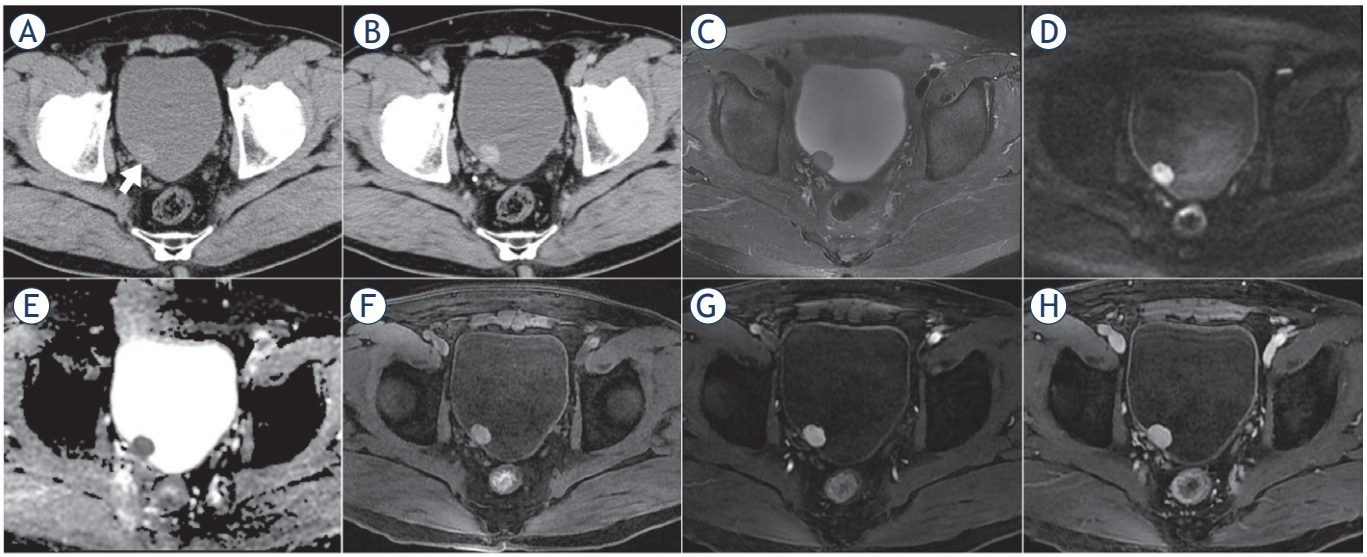

FIGURE 1. CT and MR images of a 61-year-old male patient with bladder paraganglioma. The tumour was located in the posterior bladder wall, oval, well-defined margin, protruding into the bladder cavity with broad-base attachment to the bladder wall (short arrow). The lesion showed slight hypodensity and obvious enhancement on axial pre- and post-contrast-enhanced CT images **(A, B)**, homogenous slight hyperintensity on T2-weighted images (T2WI) **(C)**, marked hyperintensity on diffusion-weighted images (DWI) **(D)**, hypointensity on apparent diffusion coefficient (ADC) maps (mean ADC value, 0.870 × 10^{-3} mm^2/s) **(E)**, hyperintensity compared to the *gluteus maximus* on T1-weighted images (T1WI) **(F)** and "fast in and slow out" on dynamic contrast-enhanced MRI **(G, H)**.

the potential to secrete catecholamines (norepinephrine, epinephrine, and dopamine).[2] The surgical preparation and procedure therefore needs to be effectively formulated to avoid life-threatening malignant cardiovascular events caused by a burst release of catecholamines.[4] Due to its rarity and symptomatic variability[5], the disorder can easily be misdiagnosed and mishandled. Thus, accurate preoperative diagnosis is crucial.

In the present study, a series of 16 patients with BPG treated in our institution over an eight-year period were retrospectively reviewed and the computed tomography (CT) and magnetic resonance imaging (MRI) characteristics of BPG were analysed.

Patients and methods

The study was conducted in accordance with the Declaration of Helsinki and was approved by the Institutional Review Board of The First Medical Center of Chinese PLA General Hospital. Written informed consent was obtained from all patients. A computerized search of the hospital's pathology databases for BPGs from October 2009 to October 2017 was performed. During this period, there were 29 adult patients (age > 18 years) with 29 pathology-proven BPGs. This list of patients was then cross referenced with the institutional radiology database to identify the patients who underwent preoperative pelvic CT and/or MRI examinations. This yielded 16 patients with BPGs, which comprised our study population. Among them, 13 underwent contrast-enhanced CT examinations, eight underwent non-enhanced (n = 1) and dynamic contrast-enhanced (n = 7) MRI examinations, and five underwent both CT and MR preoperative examinations.

CT examinations were performed with GE Light Speed 16-row scanner (Milwaukee, WI, USA) (n = 3), Siemens Somatom 64-row scanner (Erlangen, Germany) (n = 5), Siemens Sensation Cardiac 64-row scanner (Erlangen, Germany) (n = 3) and GE Optima CT660 128-row spiral scanner (Milwaukee, WI, USA) (n = 2). All examinations were performed using similar scanning parameters with a slice thickness of 5 mm, 1.5 mm reconstruction, 120 kVp, and 500 mA. Nonionic contrast agents (Ultravist, Bayer HealthCare, Berlin, Germany; Iohexol, Beilu, Beijing, China) were used, dose 90–100 ml, injection rate 3.5 ml/s. Contrast-enhanced CT images were only acquired in the arterial phase (30~35s after contrast agent injection). The patients fasted for 4–6 h and were

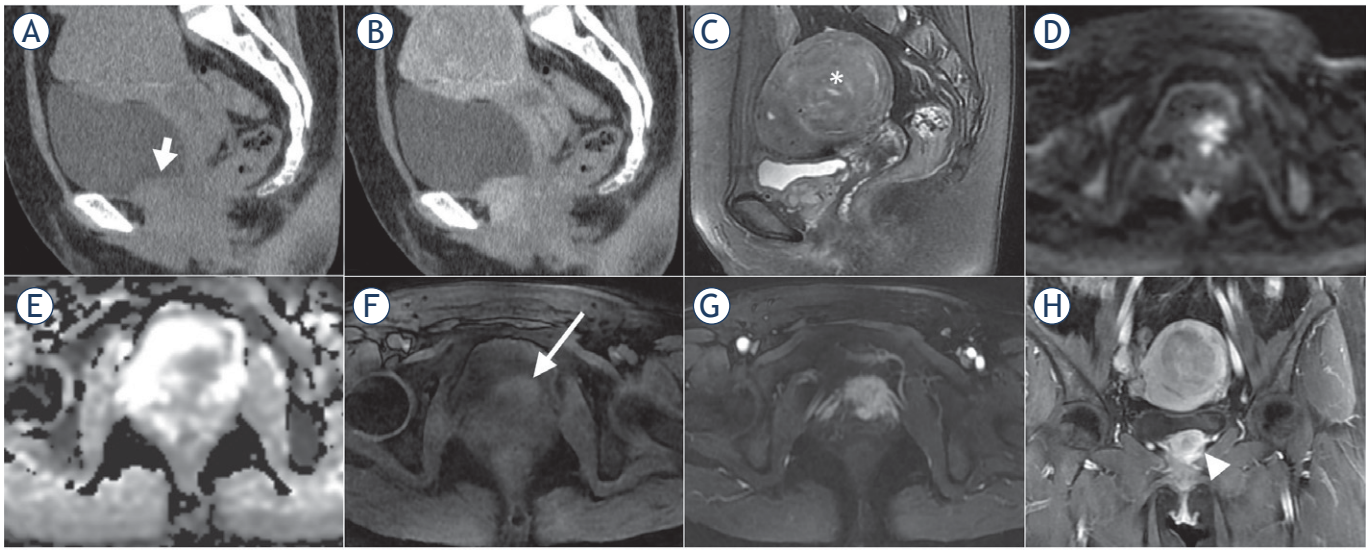

FIGURE 2. CT and MR images of a 47-year-old female with malignant bladder paraganglioma. The bladder tumour was located in the inferior bladder wall with an irregular shape and ill-defined margin, invading the adjacent tissues (short arrow). The tumour showed iso-density and moderate enhancement on sagittal pre- and post-contrast enhanced CT images **(A, B)**, inhomogenous hyperintensity on sagittal T2-weighted images (T2WI) **(C)**, hyperintensity on diffusion-weighted images (DWI) **(D)**, hypointensity on apparent diffusion coefficient (ADC) maps (mean ADC value, 0.852 × 10^{-3} mm^2/s) **(E)**, inhomogenous slight hyperintensity compared to the *gluteus maximus* on T1-weighted images (T1WI) (long arrow) **(F)**, heterogenous marked enhancement on arterial phase **(G)** and coronal contrast-enhanced images (arrowhead) **(H)**. In addition, a uterine fibroid on the posterior wall of the uterus was also found (asterisk on sagittal T2WI).

TABLE 1. Clinical characteristics of patients with bladder paraganglioma

Characteristics	Number (%) of patients
Median age in years (interquartile range)	51 (40, 63)
Sex	
Male	7 (43.8)
Female	9 (56.2)
Clinical manifestations	
Postmicturition syndrome*	6 (37.5)
Hypertension	3 (18.8)
Hematuria or progressive dysuria	3 (18.7)
24-h urinary VMA and CA level	
Not measured	11 (68.8)
Normal	4 (25.0)
Elevated	1 (6.2)
Tumor number	
Single	14 (87.5)
Multiple	2 (12.5)
Surgical approach	
Partial cystectomy	7 (43.8)
Local resection of bladder tumor**	9 (56.2)
Imaging methods	
Computerized tomography	13 (81.3)
Magnetic resonance imaging	8 (50.0)

CA = catecholamine; VMA = vanillylmandelic acid;

* postmicturition syndrome includes symptoms of catecholamine release such as sweating, palpitations, headaches, hypertension and syncope;
** local resections include transurethral laser and electric resection of bladder tumor

given water 30 min before the examination. The acquisition was performed with the bladder full of urine, from the inferior symphysis pubis to the apex of the bladder.

MRI examinations were performed with GE Signa Excite 1.5T and 3.0T MR imaging system (Milwaukee, WI, USA) (n = 5), and GE Signa HDxt 3.0T MR imaging system (Milwaukee, WI, USA) (n = 3). Patients were imaged in the supine position using an eight-channel surface phased-array coil. Pelvic MRI sequences and parameters were as follows: axial, sagittal and coronal fast spin echo (FSE) T2-weighted images (T2WI): repetition time (TR) / echo time (TE), infinite / 90–105 ms; field of view (FOV), 36×44cm; slice thickness / interlayer distance, 5.0 mm / 0.5 mm; and matrix, 320 × 224. Diffusion-weighted images (DWI) using single-shot echo planar imaging (SE-EPI): b values, 0 / 800 s/mm^2; TR / TE, 2500–5000 / 60–65 ms; FOV, 36×44 cm; slice thickness / interlayer distance, 5.0 mm / 0.5 mm; and matrix, 128×128. Axial gradient recalled echo (GRE) T1-weighted images (T1WI): TR / TE, 3.2–4.5 / 1.5–2.2 ms; FOV, 36×44 cm; slice thickness / interlayer distance, 5.0 mm / −2.5 mm; and matrix, 288 × 224. Dynamic contrast enhanced T1WI was performed in the axial plane during the arterial phase, venous phase, and delayed phase. Gadobenate dimeglumine (MultiHance; Bracco

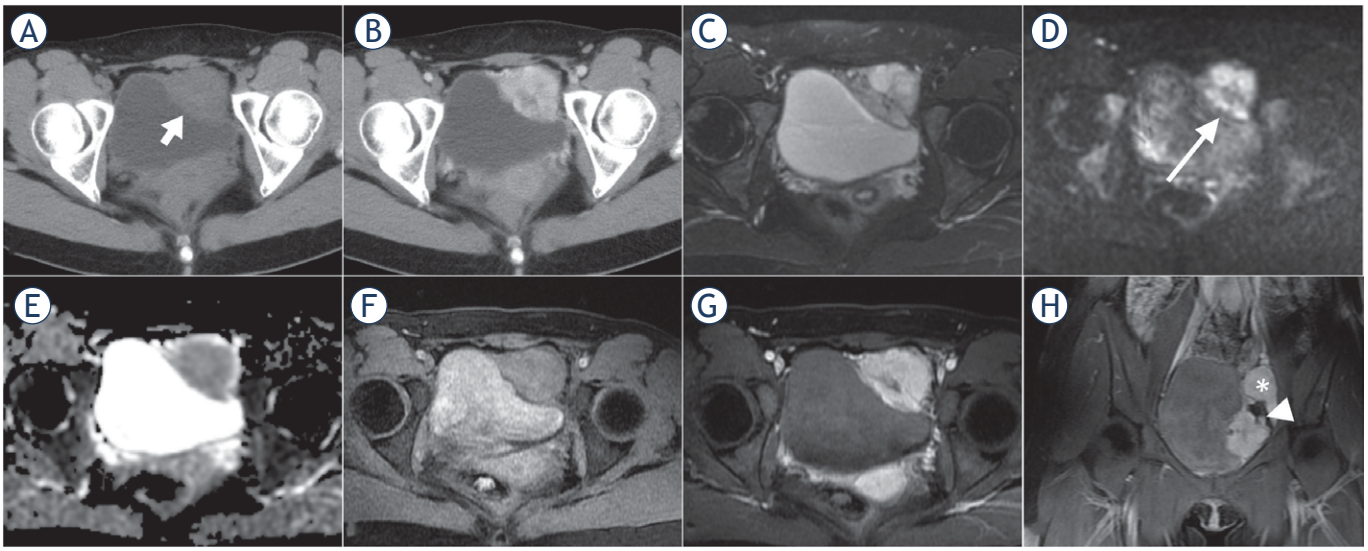

FIGURE 3. CT and MR images of a 25-year-old female with malignant bladder paraganglioma. The tumour was located in the left bladder wall with irregular shape, presenting heterogenous hypodensity (short arrow) and obvious enhancement on axial pre- and post-contrast enhanced CT images **(A, B)**, heterogenous slight or marked hyperintensity on T2-weighted images (T2WI) **(C)**, heterogenous hyperintensity on diffusion-weighted images (DWI) (long arrow) **(D)**, hypointensity on apparent diffusion coefficient (ADC) maps (mean ADC value, 0.997×10^{-3} mm^2/s) **(E)**, slight hyperintensity compared to the gluteus maximus on T1WI (**F**) and early marked enhancement on arterial phase images **(G)**. Coronal enhanced MRI showed the lesion encased the left iliac artery branch (arrowhead); a similar enhanced lesion was located next to the left iliac vessels (asterisk), suggesting multiple paraganglioma **(H)**.

Sine, Shanghai, China) was injected intravenously at a dosage of 0.1 mmol/kg as a rapid bolus injection at a rate of 2 mL/s with a power injector (Spectris Solaris EP, Medrad, Indianola, PA, USA), followed by a 20 mL saline flush.

Two experienced abdominal radiologists (Huiyi Ye and Haiyi Wang, with 30 and 20 years of experience, respectively) at our institution reviewed the CT or MR image characteristics of each lesion, and reached a consensus on imaging analysis. The imaging parameters observed included the location, size, shape, margin, density / signal intensity, enhancement pattern, cystic degeneration/necrosis, haemorrhage, and calcification. On pre- / post-contrast enhanced CT and MR images, the density and signal intensity relative to the *gluteus maximus* at the same layer were measured. The area of interest (ROI) was determined based on avoiding cystic degeneration and necrosis in the lesion. The mean apparent diffusion coefficient (ADC) value was measured by drawing a ROI over the most hypointense area within the tumour on the ADC maps

Blind to the image findings, all specimens were reviewed by an experienced uropathologist (Jing Yuan with 15 years of experience) according to the World Health Organization Classification of Tumours of Endocrine Organs.[6]

TABLE 2. Location and morphological characteristics of bladder paraganglioma

Characteristics	Number (%) of patients
Mean maximum diameter of tumour (cm)*	2.6 ± 1.0
Location	
Anterior wall	3 (18.7)
Posterior wall	4 (25.0)
Left wall	1 (6.3)
Right wall	3 (18.7)
Dome	2 (12.5)
Bottom	3 (18.8)
Spatial relationship with the bladder wall	
Protruding into the bladder cavity	11 (68.7)
Protruding into the pelvic cavity	1 (6.3)
Protruding into the bladder and pelvic cavities	4 (25.0)
Morphological characteristics	
Oval	10 (62.5)
Lobulated	4 (25.0)
Fusiform	2 (12.5)
Tumor margin	
Well-defined	14 (87.5)
Ill-defined	2 (12.5)

* Data are means ± standard deviations

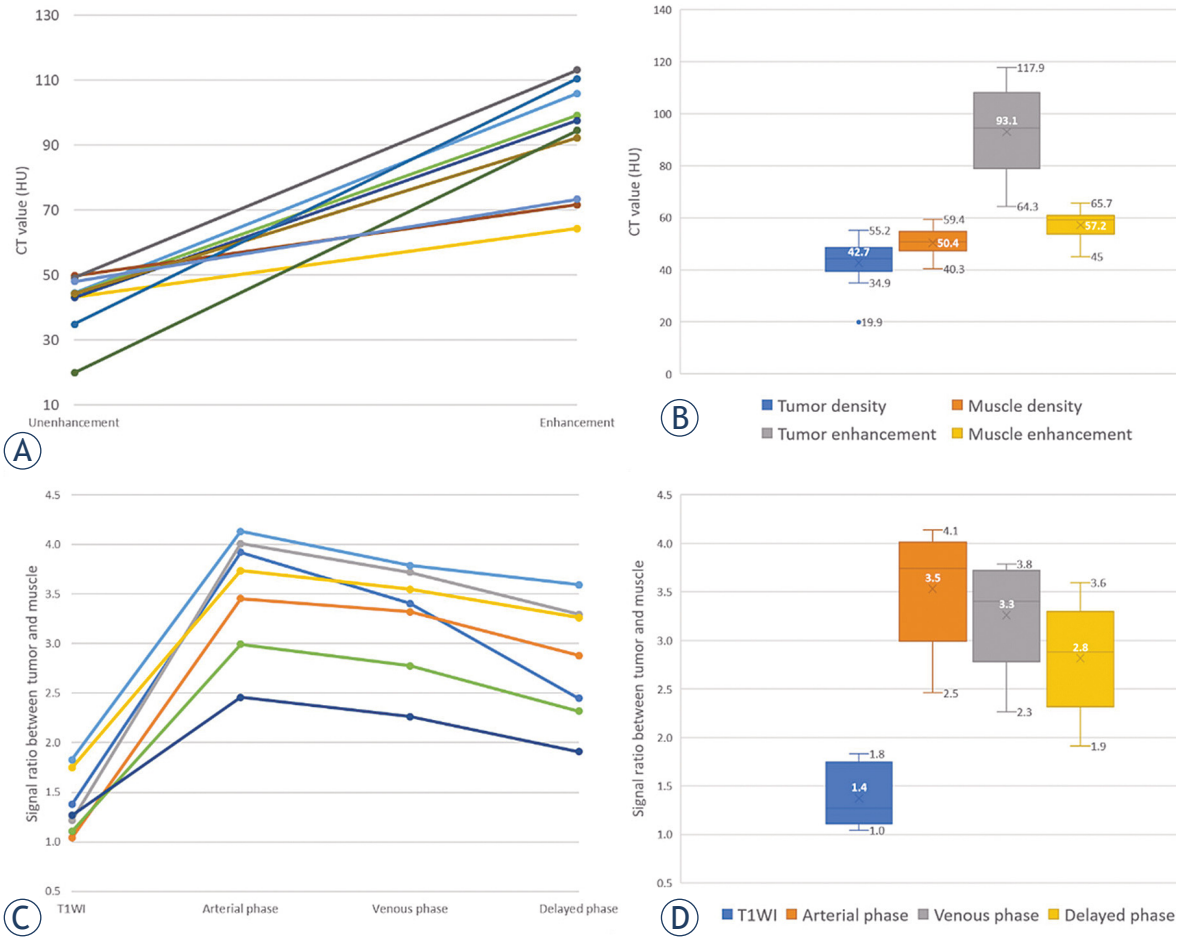

FIGURE 4. Enhancement trend charts of bladder paragangliomas on CT and MR images. **(A)** Broken line graph of enhancement trend on CT images; **(B)** Box plot of density distribution on pre- and post-contrast enhanced CT images (arterial phase); **(C)** Broken line graph of dynamic enhancement trend on MR images; **(D)** Box plot of signal distribution on unenhanced and dynamic contrast-enhanced MR images.

Results

Among the 16 patients enrolled (median age 51 years, interquartile range 40–63; 9 female), 12 patients had preoperative clinical symptoms, including six with typical symptoms related to micturition before surgery (increased blood pressure, headache, dizziness, pale complexion, chest tightness, palpitations, hyperhidrosis, abdominal pain), three had a long history of hypertension, two had haematuria and one had a progressive dysuria (tumour close to the trigone). The 24 h urinary vanillylmandelic acid (VMA) and urinary catecholamine concentrations were measured for five of the patients with typical symptoms, and only one patient had an elevated VMA concentration (429 nmol / 24 h; standard range, 59.1–266 nmol / 24 h). Twelve patients were accurately diagnosed as BPG (five of them took phenoxybenzamines for 1 to 2 weeks before surgery), and the remaining four patients were misdiagnosed preoperatively because of negative hormonal activity or atypical manifestation. Based on pathological confirmation, multiple paraganglioma was found in two cases (one with two lesions located in the bladder wall and the left adrenal gland and the other with two lesions located in the bladder wall and next to the left iliac vessels). (Table 1)

The maximum diameters of the BPGs ranged from 1.6 to 5.4 cm. The lesions were distributed in different locations of the bladder wall, and most of them grew into the bladder cavity (11/16) with broad-based attachment to the wall. The tumours mostly exhibited oval in shape (10/16) and well-defined margins (14/16) (Table 2). One of the two BPGs with ill-defined margins invaded the upper middle urethra and the anterior wall of the vagina

while the other encased the left iliac vein branch. (Figure 1–3)

On non-contrast CT images, the lesions mainly demonstrated homogeneous and soft-tissue density, with CT values ranging from 19.9 to 55.2 Hounsfield Units (HU). Intra-tumoural cystic degeneration or necrosis was rare (2/16). All lesions showed moderate to marked enhancement in the arterial phase of contrast-enhanced CT images (Table 3), with CT values of 64.3–117.9 HU, which were about 2.3 times that of the CT value on pre-contrast enhanced images (Figure 4A–B). In the two patients with multiple paragangliomas, the density and enhancement pattern of lesions in the non-bladder sites were similar to those in the bladder.

On T2WI, the lesions demonstrated homogenous hyperintensity (10/16), higher than the *gluteus maximus* and lower than the urine in the bladder, without typical "pepper and salt" sign. Due to the restricted diffusion, the lesions showed hyperintensity on DWI and hypointensity on ADC maps (mean ADC value ± standard deviation, 0.883 ± 0.126×10^{-3} mm^2/s). On T1WI, the lesions showed hyperintensity and averaged 1.4 times higher than that of the *gluteus maximus* at the same layer. Following MRI enhancement, the BPGs all had obvious enhancement in the arterial phase (an average of 2.5 times higher than the tumour signal intensity on T1WI), slightly decreased enhancement in the venous phase and the delayed phase (an average of 2.4 and 2.0 times higher than the tumour signal intensity on T1WI, respectively), exhibiting a "fast in and slow out" enhanced pattern (Table 3, Figure 4C–D). Similar to CT findings, the two patients with multiple paragangliomas showed comparable MRI findings between the bladder and non-bladder lesions.

Pathological examination revealed that the tumours were of varying sizes, nodular, with a greyish-tan cut surface and medium hardness. Microscopic examination showed polygonal or oval tumour cells that were rich in basophil granular cytoplasm and arranged in a sheet or organoid arrangement, which had abundant sinuses and capillaries. Immunohistochemical staining showed that the tumour cells were positive for chromogranin A (Figure 5).

TABLE 3. CT and MR image characteristics*

Computerized tomography (n = 13)	
Density	Moderate or slightly lower density
Enhancement characteristics	Moderate to marked enhancement
Calcification	None
Cystic degeneration or necrosis	Rare (n = 2)
Haemorrhage	None
Magnetic resonance imaging (n = 8)	
T2-weighted imaging	Slight hyperintensity
Diffusion-weighted imaging	Hyperintensity
Apparent diffusion coefficient (ADC) map	Hypointensity (ADC value, 0.883±0.126×10^{-3} mm^2/s)**
T1-weighted imaging	Slight hyperintensity
Enhancement characteristics	"Fast in and slow out" pattern
Cystic degeneration or necrosis	Rare (n = 2)
Haemorrhage	None

* The density and signal intensity of the tumours were reported with reference to those of the *gluteus maximus* in the same layer; ** data are means ± standard deviations

Discussion

BPG is a rare neuroendocrine neoplasm with potential hormonal activity derived from the medullary tissue of the bladder wall sympathetic nervous system.[7] Better surgical preparation and effective perioperative anaesthetics management is required to avoid potentially fatal consequences, such as hypertensive crisis. In this study, the clinical and imaging characteristics of 16 patients with BPG were documented and analysed.

Several typical BPG symptoms caused by catecholamine release, such as hypertension, headache, palpitations, and perspiration, were present in 83% of BPG patients.[8] Because of the special location of BPGs, the above symptoms may be caused by over distension of the bladder, micturition or defecation.[7] In this study, 75% of patients had typical symptoms, which was consistent with previous literature. Similar to other paragangliomas, BPGs can usually be diagnosed by biochemical tests, such as 24 h urine measurements of catecholamines or metabolites. However, some BPGs showed no biochemical abnormalities, as were the lesions in this study, which may be due to the small size of the tumour at diagnosis or the transient hormone-release during micturition.[2]

BPGs have the predilection age of 30–50 years with no gender difference. Primary lesions can occur in any part of the bladder wall and mainly have cavity growth with a size ranging from 1.2–5.0 cm.[9] The ages and tumour sizes of the 16 patients were compatible with the reported information. BPGs are prone to attach to the bladder wall with a broad base. This morphological characteristic was observed in all 16 lesions, which may be

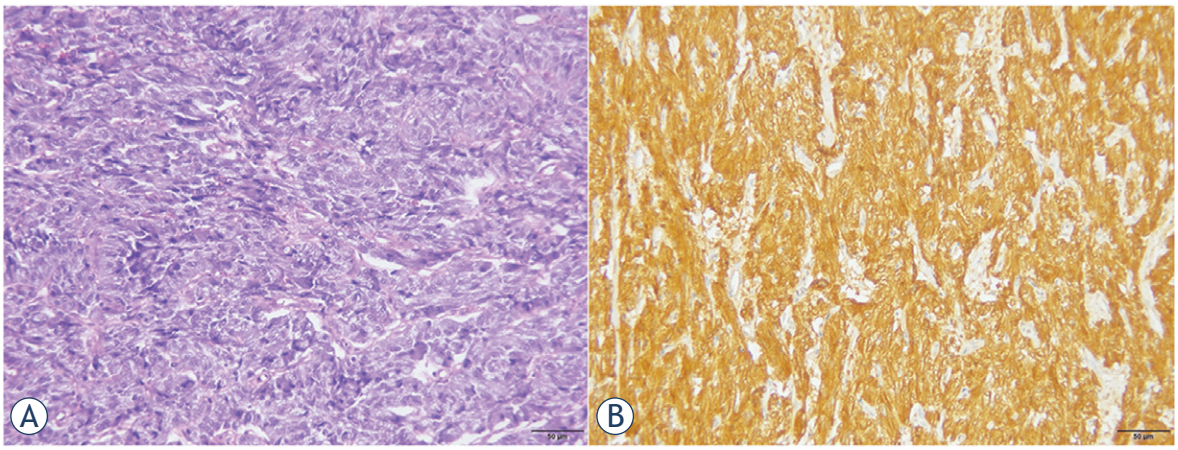

FIGURE 5. Microscopic examination of paraganglioma. **(A)** Polygonal or oval tumour cells were rich in basophil granular cytoplasm and arranged in a sheet or organoid arrangement. (Hematoxylin and eosin staining, × 400). **(B)** Immunohistochemical staining of tumours cells was positive for chromogranin A (CgA) (EnVision × 200).

pathologically based on the tendency of BPGs to infiltrate and grow along the muscularis.[10] Lu *et al.* suggested that intramural (located in the muscular layer) and subserosal (protruding from the serosa) tumours often had systemic symptoms caused by catecholamine release. Furthermore, the tumours with typical manifestations were larger than those without typical manifestations.[7] In this study, 50% and 100% of the intramural and subserosal tumours showed systemic manifestations, respectively, but the correlation between symptoms and sizes was not observed.

Imaging methods are primarily used for localization of the paraganglioma.[11] In the absence of typical clinical manifestations and negative biochemical tests, imaging can also be used as a complementary approach for qualitative diagnosis. CT has a high sensitivity (82%) in detecting extra-adrenal pheochromocytoma.[9] We demonstrated that most BPGs are typically present as a solitary lesion protruding into or out of the bladder cavity, with an oval shape, soft tissue density, well-defined margin and a broad-base attachment to the bladder wall. The tumour exhibits slightly lower density and early marked enhancement on the contrast-enhanced CT images. Contrary to the previous literature, T2WI showed that BPGs are mostly homogeneous and high-intensity, without the typical "pepper and salt" appearance.[12,13] The homogenous nature may be due to the fact that the lesion was still small when it was detected, and intratumoural degeneration has not yet occurred. Similar to bladder cancer, BPGs show marked hyperintensity on DWI and hypointensity on ADC maps due to restricted diffusion of water molecules.[14] The tumours presented slight hyperintensity on T1WI and "fast in and slow out" enhanced pattern on contrast-enhanced images, which may be distinctive MRI features of BPGs.[10,15] The potential pathological bases for the above imaging findings are that the tumour cells are large with abundant cytoplasm and the intercellular stromata are rich in blood vessels showing fissure or haemangioma-like dilatation.[16]

The malignant rate of BPGs is estimated to be 10–15%.[9] Because no reliable pathological evidence exists for early differentiation between benign and malignant tumours, direct invasion of adjacent tissues or distant metastases are considered to represent potential malignancy.[17] In this study, two lesions showed features of peripheral tissue invasion, suggesting malignancy. At present, dynamic contrast-enhanced MRI incorporating non-fat suppression T2WI with small FOV and high resolution, by means of the natural contrast between pelvic fat and urine in bladder, is the preferred imaging method for recognition of possible malignant tumours.[18] In addition to CT and MRI, functional imaging is recommended to detect multi-focal and metastatic disease, such as ^{123}I-metaiodobenzylguanidine (^{123}I-MIBG) SPECT and ^{68}Gallium-labeled somatostatin analogues (^{68}Ga-DOTA-SSA) PET/CT. Depending on specific ligands that target specific cell membrane transporters or vesicular catecholamine transport systems, this modality can provide greater diagnostic specificity.[12,19]

Due to their rarity and symptomatic variability, BPGs, especially malignant BPGs, should be differentiated from bladder carcinoma, the most

common malignant tumour of the bladder. The latter is more likely to occur in older men, related to smoking, and includes common symptoms of painless gross haematuria and progressive dysuria. Bladder carcinoma mostly shows hypointensity on T1WI compared to the appearance of muscle and no early marked enhancement. This may be the crucial difference between these two kinds of tumours. Other infrequent tumours of the bladder, such as lymphoma leiomyoma and haemangioma, cannot be ignored and they can be distinguished from BPGs by comprehensive analysis of CT and MRI characteristics.

This study has limitations. It is a retrospective series of a small study population, imaging with CT and MRI was not available in all patients, and contrast-enhanced CT contained only plain and arterial phase images. Although we attempted to objectively describe the image characteristics by calculating tumour-muscle signal ratio, due to the different scanners, inconsistent image acquisition time and subjective observation, the features observed require further validation in more cases.

In conclusion, on CT and MRI, BPGs are mostly oval-shaped, well-defined and broadly-based bladder tumours with hypoattenuation on non-contrast CT, T2 hyperintensity, slight T1 hyperintensity compared to the muscle, marked restricted diffusion on DWI and "fast in and slow out" enhanced pattern on contrast-enhanced images. Preoperative CT and MRI can be used to determine the location of the tumours, but can also assist in qualitative diagnosis, malignant risk assessment and operative proposal formulation.

Acknowledgement

We acknowledge financial support from the National Natural Science Foundations of China (Grant No. 81971580 and No. 81471641-JT); the Medical Big Data Research and Development Project supported by Chinese PLA General Hospital (Grant No. 2018MBD-023).

Reference

1. Lenders JW, Duh QY, Eisenhofer G, Gimenez-Roqueplo AP, Grebe SK, Murad MH, et al. Pheochromocytoma and paraganglioma: an endocrine society clinical practice guideline. *J Clin Endocrinol Metab* 2014; **99:** 1915-42. doi: 10.1210/jc.2014-1498

2. Beilan JA, Lawton A, Hajdenberg J, Rosser CJ. Pheochromocytoma of the urinary bladder: a systematic review of the contemporary literature. *BMC Urol* 2013; **13:** 22. doi: 10.1186/1471-2490-13-22

3. Qin J, Zhou G, Chen X. Imaging manifestations of bladder paraganglioma. *Ann Palliat Med* 2020; **9:** 346-51. doi: 10.21037/apm.2020.03.09

4. Sharma AP, Bora GS, Mavuduru RS, Panwar VK, Mittal BR, Singh SK. Management of bladder pheochromocytoma by transurethral resection. *Asian J Urol* 2019; **6:** 298-301. doi: 10.1016/j.ajur.2018.05.010

5. Tevosian SG, Ghayee HK. Pheochromocytomas and paragangliomas. *Endocrinol Metab Clin North Am* 2019; **48:** 727-50. doi: 10.1016/j.ecl.2019.08.006

6. International Agency for Research on Cancer. World Health Organization. *WHO classification of tumours of endocrine organs*. 4th edition. Lloyd RV, Osamura RY, Klöppel G, Rosai J, editors. Lyon, France: IARC; 2017. p. 78-80.

7. Lu H, Male M, Jiang K, Ye Z, Song D, Xia D. Clinical significance of functional and anatomical classifications in paraganglioma of the urinary bladder. *Urol Oncol* 2019; **37:** 354.e9-17. doi: 10.1016/j.urolonc.2019.01.027

8. Jain A, Baracco R, Kapur G. Pheochromocytoma and paraganglioma-an update on diagnosis, evaluation, and management. *Pediatr Nephrol* 2020; **35:** 581-94. doi: 10.1007/s00467-018-4181-2

9. Henderson SJ, Kearns PJ, Tong CM, Reddy M, Khurgin J, Bickell M, et al. Patients with urinary bladder paragangliomas: a compiled case series from a literature review for clinical management. *Urology* 2015; **85:** e25-9. doi: 10.1016/j.urology.2014.11.006

10. Liu F, Xiao H, Wang H, Fang Z, Yu Y, Li Y, et al. [The imaging analysis and diagnosis of the paraganglioma of the urinary bladder]. [Chinese]. *Oncoradiology* 2020; **29:** 181-6. doi: 10.19732/j.cnki.2096-6210.2020.02.018

11. Sbardella E, Grossman AB. Pheochromocytoma: an approach to diagnosis. *Best Pract Res Clin Endocrinol Metab* 2020; **34:** 101346. doi: 10.1016/j.beem.2019.101346

12. Aygun N, Uludag M. Pheochromocytoma and paraganglioma: from clinical findings to diagnosis. *Sisli Etfal Hastan Tip Bul* 2020; **54:** 271-80. doi: 10.14744/SEMB.2020.14826

13. Liang JP, Li HG, Gao LK, Yin L, Yin L, Zhang JW. Bladder paraganglioma: Clinicopathology and magnetic resonance imaging study of five patients. *Urol J* 2016; **13:** 2605-11. doi: 10.22037/uj.v13i2.3140

14. Al Johi RS, Seifeldein GS, Moeen AM, Aboulhagag NA, Moussa EM, Hameed DA, et al. Diffusion weighted magnetic resonance imaging in bladder cancer, is it time to replace biopsy? *Cent European J Urol* 2018; **71:** 31-7. doi: 10.5173/ceju.2017.1427

15. Wang H, Ye H, Guo A, Wei Z, Zhang X, Zhong Y, et al. Bladder paraganglioma in adults: MR appearance in four patients. *Eur J Radiol* 2011; **80:** e217-20. doi: 10.1016/j.ejrad.2010.09.020

16. Fan DG, Wu CL, Huang HJ, Wu L, Lin SY. [Paraganglioma of urinary bladder: a clinicopathological features analysis of 23 cases]. [Chinese]. *Zhonghua Bing Li Xue Za Zhi* 2020; **49:** 311-6. doi: 10.3760/cma.j.cn112151-20190928-00535

17. Quist EE, Javadzadeh BM, Johannesen E, Johansson SL, Lele SM, Kozel JA. Malignant paraganglioma of the bladder: a case report and review of the literature. *Pathol Res Pract* 2015; **211:** 183-88. doi: 10.1016/j.prp.2014.10.009

18. Raza SA, Jhaveri KS. MR imaging of urinary bladder carcinoma and beyond. *Radiol Clin North Am* 2012; **50:** 1085-110. doi: 10.1016/j.rcl.2012.08.011

19. Lenders JWM, Eisenhofer G. Update on modern management of pheochromocytoma and paraganglioma. *Endocrinol Metab (Seoul)* 2017; **32:** 152-61. doi: 10.3803/EnM.2017.32.2.152

research article

Diagnostic performance of apparent diffusion coefficient values for the differentiation of intrahepatic cholangiocarcinoma from gastrointestinal adenocarcinoma liver metastases

Temel Fatih Yilmaz[1], Mehmet Ali Gultekin[1], Hacı Mehmet Turk[2], Mehmet Besiroglu[2], Dilek Hacer Cesme[1], Melih Simsek[2], Alpay Alkan[1], Huseyin Toprak[1]

[1] Departments of Radiology, Faculty of Medicine, Bezmialem Vakif University, Istanbul, Turkey
[2] Departments of Medical Oncology, Faculty of Medicine, Bezmialem Vakif University, Istanbul, Turkey

Radiol Oncol 2022; 56(1): 54-59.

Received 29 July 2021
Accepted 4 November 2021

Correspondence to: Asist. Prof. Temel Fatih Yilmaz, M.D., Department of Radiology, Faculty of Medicine, Bezmialem Vakif University, Istanbul, Turkey. Phone: 90 212 4531700; Fax: 90 212 6217580; E-mail: temelfatihyilmaz@gmail.com

Disclosure: No potential conflicts of interest were disclosed.

Background. We aimed to investigate whether there is a difference between intrahepatic cholangiocarcinoma (IHCC) and liver metastases of gastrointestinal system (GIS) adenocarcinoma in terms of apparent diffusion coefficient (ADC) values.

Patients and methods. From January 2018 to January 2020, we retrospectively examined 64 consecutive patients with liver metastases due to gastrointestinal system adenocarcinomas and 13 consecutive IHCC in our hospital's medical records. After exclusions, fifty-three patients with 53 liver metastases and 10 IHCC were included in our study. We divided the patients into two groups as IHCC and liver metastases of GIS adenocarcinoma. For mean apparent diffusion coefficient (ADC_{mean}) values, the region of interests (ROI) was placed in solid portions of the lesions. ADC_{mean} values of groups were compared.

Results. The mean age of IHCC group was 62.50 ± 13.49 and mean age of metastases group was 61.15 ± 9.18. ADC_{mean} values were significantly higher in the IHCC group compared to the metastatic group ($p < 0.001$). ROC curves method showed high diagnostic accuracy (AUC = 0.879) with cut-off value of < 1178 x 10^{-6} mm^2/s for ADC_{mean} (Sensitivity = 90.57, Specificity = 70.0, positive predictive value [PPV] = 94.1, negative predictive value [NPV] = 58.3) in differentiating adenocarcinoma metastases from IHCC.

Conclusions. The present study results suggest that ADC values have a potential role for differentiation between IHCC and GIS adenocarcinoma liver metastases which may be valuable for patient management.

Key words: cholangiocarcinoma, gatrointestinal system; liver metastases; apparent diffusion coefficient; diffusion weighted image; MRI

Introduction

Intrahepatic cholangiocarcinoma (IHCC) is the second most common primary malignant lesion of the liver after hepatocellular cancer and estimated 15% of primary liver cancer worldwide. The incidence of IHCC has been increasing recently.[1] According to macroscopic appearance, cholangiocarcinoma (CC) is divided into three types: mass forming type, periductal infiltrative type and intraductal grow-

ing type.[1-2] Mass forming type CC is the most common type with a rate of 60%.[3] Diffusion weighted image (DWI) usually is added to standard abdomen protocols, because it is a rapid technique and talented of detecting most liver masses in patients with supposed malignant disease. It may be difficult to differentiate between IHCC and gastrointestinal system (GIS)-derived adenocarcinoma even when contrast is given, and DWI can be helpful in differential diagnosis in these cases.[4]

DWI provides diagnostic value in differentiation of benign and malignant liver masses. It gives information about cellularity of tissues and integrity of cell membranes. DWI increases the sensitivity of detection for liver metastases when combined with dynamic contrast enhanced upper abdomen MRI. DWI has been used in characterization of metastatic and primary liver tumors.[5] The sensitivity of using DWI in addition to routine imaging in detecting malignancy was reported as 94.9% and the specificity as 97.8%.[6] To avoid unnecessary diagnostic and therapeutic interventions, differentiation between IHCC and metastases of adenocarcinomas is very significant, because they have different treatment options and prognosis. It would be valuable to precisely differentiate the liver metastases of GIS from IHCC based on apparent diffusion coefficient (ADC) values. Because it's sometimes hard to differentiate even based on the histological analysis since all these tumors are adenocarcinomas. We aimed to investigate whether there is a difference between IHCC's and adenocarcinoma liver metastases from GIS origin in terms of ADC values.

The goal of this study was to evaluate the value of DWI, using the mean ADC value for distinguishing IHCC from liver metastases of adenocarcinomas originating in the gastrointestinal tract.

Patients and methods

Patients

We consecutively reviewed medical records of patients who had a diagnosis or an imaging study showing IHCC or metastasis between January 2018 to January 2020. Inclusion criteria were determined as histopathological confirmation of the primary or metastatic lesion GIS adenocarcinoma arising from stomach, colon, and pancreas with liver metastases at the initial diagnosis, and CC with no history of chemotherapy at initial imaging and the presence of pretreatment MRI of the abdomen with a proper DWI.

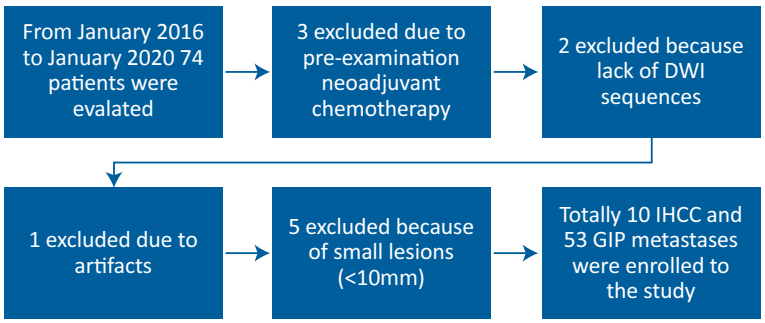

FIGURE 1. Flow-chart of the study showing the exclusion criteria of the patients.

Exclusion criteria were determined as pre-examination neoadjuvant chemotherapy for the primary tumor (n = 3), lack of DWI sequence (n = 2), heavy image artefacts and technical reasons (n = 1), and lesions smaller than 10 mm with difficult to measure ADC values (n = 5). We only included one major metastatic lesion from each patient to provide study homogeneity. Finally, a total of 53 patients with 53 liver metastases and 10 patients with IHCC were included in our study (Figure 1). We divided the patients into two groups as IHCC's (n = 10 patients) and liver metastases of GIS adenocarcinoma (n = 53 patients with 53 lesions). In our study group, there were no underlying chronic liver diseases and no metastases contained mucinous components in it.

The study protocol was approved by our institution's ethics committee. All procedures performed in the studies involving human participants were in accordance with the ethical standards of the institutional and/or national research committee and with the 1964 Helsinki Declaration and its later amendments or comparable ethical standards. Informed consent was obtained from all individual participants included in the study.

Histopathologic analysis

Diagnosis of all IHCCs and primary GIS adenocarcinomas were confirmed histopathologically. For IHCC's, primary tumor sites were right hepatic lobe (n = 4), and left hepatic lobe (n = 6), Histopathological diagnosis was obtained by percutaneous tru-cut biopsy.

For the metastasis group, primary tumor sites were colorectal (n = 32), gastric (n = 9), and pancreas (n = 12). Tissue samples of colorectal and gastric adenocarcinomas were obtained through endoscopic biopsy samples. For pancreatic adenocarcinomas, endosonographic-guided fine needle

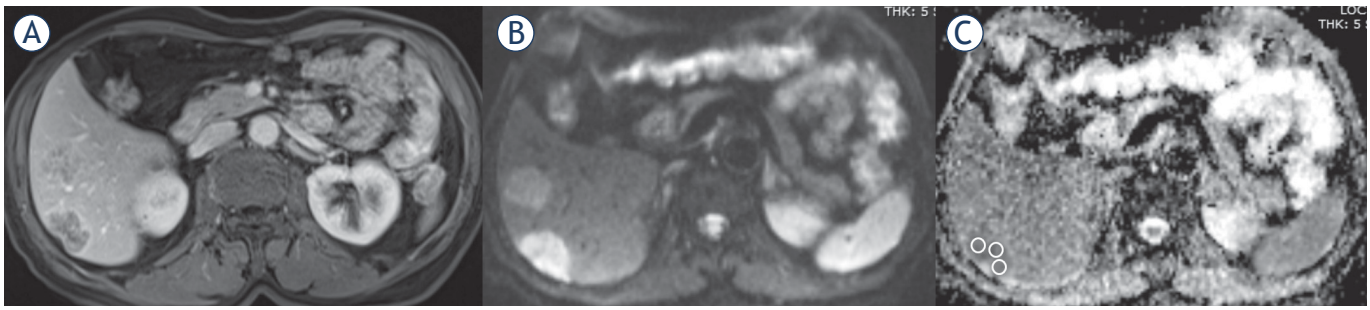

FIGURE 2. 59-year-old male with liver metastases due to colorectal adenocarcinoma. Contrast-enhanced axial T1-weighted (T1W) **(A)**, diffusion weighted image (DWI) obtained at b value of 800 s/mm^2 **(B)** and apparent diffusion coefficient (ADC) maps **(C)** with free hand ROI placement technique.

aspiration biopsy (n = 7), percutaneous tru-cut biopsy of metastatic liver lesions (n = 3), and surgical biopsy (n = 2) were done.

MRI protocol

All patients underwent MRI using a 1.5-T system (Siemens, Avanto, Erlangen, Germany). T1-W in- and out-of-phase (TR/TE, 128/4.90 and 128/2.37; NEX, 1; the FOV of 38 to 50 cm; 5 mm thickness and 2 mm intersection gap), T2-weighted axial (TR/TE, 2000/120; NEX, 1; the FOV of 38 to 50 cm; 5 mm thickness and 2 mm intersection gap), fast spin echo T2-W axial (TR/TE, 2000/117; NEX, 1; the FOV of 38 to 50 cm; 5 mm section thickness and 2 mm intersection gap) and T2-W coronal images were performed (TR/TE, 1400/106; NEX, 1; the FOV of 38 to 50 cm; 5 mm section thickness and 1 mm intersection gap). The DWI images were obtained at b-values of 50, 400, and 800 s/mm^2 (TR/TE, 7300/78; NEX, 2; FOV 38-50 cm; slice thickness 5 mm and no intersection gap). Pre and postcontrast fat-saturated T1-W axial (VIBE) (TR/TE, 4.90/2.39; NEX, 1; and the FOV of 38 to 50 cm; 3 mm section thickness and no intersection gap) were performed. Dynamic imaging was performed after a rapid bolus of gadolinium-diethylenetriamine pentaacetic acid, 0.1 mmol/kg body weight, intravenously at a rate of 1.5 mL/s, followed by a 30 mL saline flush using a power injector. Contrast-enhanced dynamic images were performed in arterial phase, portal venous phase, and interstitial phase in the axial plane and in interstitial phase in the coronal plane.

Image analysis

Image analysis and region of interests (ROI) placement was made by two abdominal radiologists who had ten and eleven years' experience of abdominal radiology. The morphological features were evaluated as follows: 1- lesion size, measurements were made in the axial plane on contrast enhanced T1-weighted (T1W) images at the largest diameter. 2-lesion localization (right or left lobe of the liver). 3-ADC values of the metastases and IHCC's. For ADC_{mean} values, the ROIs were placed over the three different enhancing solid portions of the lesions on contrast enhanced T1W images blinded to ADC maps. Conventional T2-weighted (T2W) and contrast enhanced T1W images were used as reference to determine the enhanced portions of the lesion areas and to avoid the cystic or necrotic parts of the lesions. Final ADC_{mean} values were calculated as the average of the ADC values obtained from 3 different ROIs (Figure 2–3). We used synapse 3D® (Fujifilm Medical, Tokyo, Japan) and Leonardo console (software version 2.0, Siemens) to evaluate metastatic liver lesions and to calculate ADC values of metastatic liver lesions.

Statistical analysis

Statistical analysis was performed using the IBM SPSS Statistics 26.0 statistical software (Armonk, NY: IBM Corp.). The Kolmogorov-Smirnov test was used for normality. non-parametric Mann-Whitney-U test was used in the comparison of the ADC_{mean} values of the IHCC and adenocarcinoma groups from the enhanced solid metastases and the lesion sizes. Descriptive statistics are presented as median (50%) and interquartile range (IQR = Q3(75%)-Q1(25%)) values. p value below 0.05 was accepted as statistically significant. ROC curves were evaluated to determine the cut-off value to differentiate between ADC_{mean} values of IHCC and adenocarcinoma metastases.

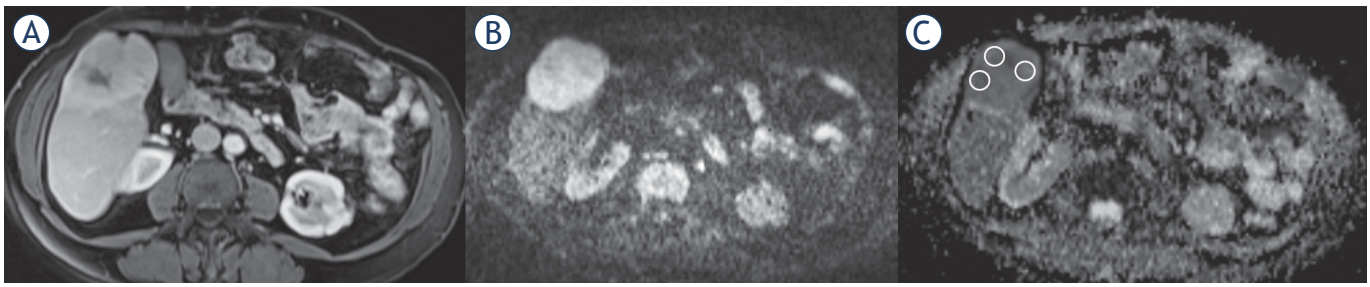

FIGURE 3. 58-year-old female with an expansile liver mass with central hypovascular fibrous stroma and peripheral contrast enhancement on contrast-enhanced axial T1-weighted (T1W) **(A)** images. diffusion weighted image (DWI) obtained at b value of 800 s/mm^2 **(B)** and apparent diffusion coefficient (ADC) maps **(C)** with region of interests (ROI) placement with three different contrast enhancing area for calculating ADC_{mean} values.

Results

IHCC was diagnosed in 10 patients with 10 lesions and adenocarcinoma was diagnosed in 53 patients with 53 liver metastases. There was no statistically significant difference between IHCC and adenocarcinoma in terms of age. Demographic features were summarized at Table 1.

ADC_{mean} values were significantly higher in the IHCC group compared to the adenocarcinoma group ($p < 0.001$) (Figure 4). These results are summarized in Table 2.

ROC curves method showed diagnostic accuracy for ADC_{mean} (AUC = 0.879). Cut-off value was < 1178 x 10^{-6} mm^2/s for ADC_{mean} (Sensitivity = 90.57%, Specificity = 70.0%, positive predictive value [PPV] = 94.1, negative predictive value [NPV] = 58.3) in differentiating adenocarcinoma metastases from IHCC's with the 95% confidence interval (Figure 5). The AUC rates showed that ADC_{mean} values were statistically significant in differentiating the two groups ($p < 0.0001$).

Discussion

Gastrointestinal cancer is from the most common malignant tumors worldwide with rising incidence.[7] Surgery is now the primary treatment for gastrointestinal cancer. Liver metastasis occurs in approximately 45% of patients.[8]

IHCC originates from small intrahepatic bile ducts and grows through adjacent liver parenchyma. IHCC typically occurs as a large mass, which is difficult to differentiate from a metastatic focus of adenocarcinoma. The only curative treatment of IHCC is surgery and even with surgery its 5-year survival rates remain at 39–41%.[9] In contrast there is no surgical treatment option for some metastatic GIS tumors.[10]

IHCC is hypointense on T1-weighted (T1W), and hyperintense on T2W imaging relative to liver parenchyma. The grade of hyperintensity on T2W imaging frequently depends on the quantity of fibrosis, necrosis, and mucin within the tumor.[11] The imaging features of IHCC have been further described, with the targetoid appearance being one of the most common characteristics.[12]

Magnetic resonance (MR) DWI is a technique that provides image contrast by free water mol-

TABLE 1. Univariate analysis of patient characteristics for gastrointestinal system (GIS) liver metastases and intrahepatic cholangiocarcinoma (IHCC)

Patient characteristics	Number of patients (n = 63)	IHCC (n = 10)	Liver metastases (n = 53)	P value
Age (years)	61.4 ± 9.93	62.50 ± 13.49	61.15 ± 9.18	0.679
Gender				**< 0.001**
Male	35	2	33	
Female	28	8	20	
Diameter (mm)	47 ± 31.27	82.70 ± 28.58	40.26 ± 27	**< 0.001**
Location				**< 0.001**
Right lobe	24	2	38	
Left lobe	43	8	15	

TABLE 2. Apparent diffusion coefficient (ADC) values of intrahepatic cholangiocarcinoma (IHCC) and gastrointestinal system (GIS) liver metastases

Patient Groups	ADC x 10^{-6}mm/sn^2 (median, IQR)
IHCC	(1293.0), (1422.0–951.75)
GIS metastases	(861.0), (1053.0–695.0)

IQR = interquartile range

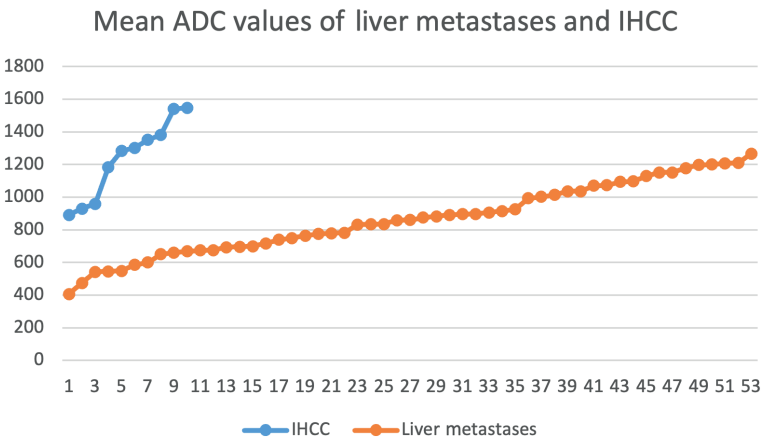

FIGURE 4. Mean apparent diffusion coefficient (ADC_{mean}) values of liver metastases of gastrointestinal system adenocarcinomas and intrahepatic cholangiocarcinoma (IHCC).

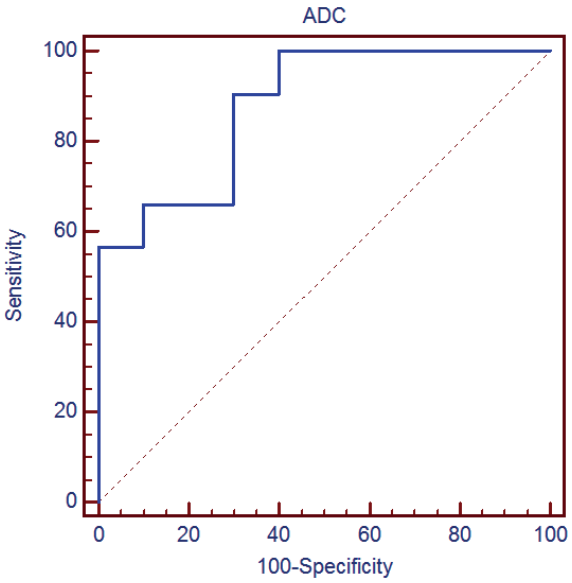

FIGURE 5. Receiver operating characteristic curve of the apparent diffusion coefficient (ADC) mean values.

ecule movement within tissue and the ADC (expressed in mm2/s), is a numerical parameter of DWI. ADC values give information about cellularity of tissues and integrity of cell membranes.[12] Biopsy is required before surgical or oncological treatment in cases where IHCC is considered by imaging.

It is sometimes difficult to distinguish liver metastases from IHCC with routine abdominal MRI. It is not possible to differentiate especially in solitary or hypovascular metastases. DWI must be added to routine abdominal MR imaging since it is very sensitive to detect liver malignancies. ADC is a measure of the magnitude of diffusion within tissue and is commonly clinically calculated using DWI. ADC values reflect the structure of masses and vary in different tumor types. Lower ADC values may reflect the hypercellularity of these tumors, and decreased intra and extracellular space.

Mungai *et al.* reported mean ADC values of CC as 0.970 x 10^{-3}mm/sn^2 and metastases as 0.947 x 10^{-3}mm^2/sn and these results were not statistically significant.[4] This may be a result of evaluation of metastases arising from any origin and the evaluation of all subtypes of CC. In our study we have found median ADC value of IHCC 1293 x 10^{-6}mm^2/sn and mean ADC value of metastases of GIS 861 x 10^{-6}mm^2/sn and this was statistically significant ($p < 0.0001$). Decreased ADC values in GIS liver metastases may be attributed to hypercellularity. However increased ADC values in IHCC may be the result of decreased cellularity due to fibrotic changes compared to metastases.

Drevelegas *et al.* demonstrated that mean ADC value in 12 patients with liver CC was 1.34 ± 0.27 x 10^{-3}mm^2/s and 1.11 ± 0.295 x 10^{-3}mm^2/s in 51 patients with secondary liver malignancy.[13] They only concluded that primary liver tumors have higher ADC values than secondary ones. The result of this study supports our outcomes.

Namimoto *et al.* found the mean ADC value of 1.51 ± 0.47 x 10^{-3}mm^2/s in IHCC and 1.23 ± 0.32 x 10^{-3}mm^2/s in metastatic liver lesions. These results are in accordance with the results in our study.[6]

Lee *et al.* in their study on 91 patients, stated good prognosis and survival of IHCCs when areas with diffusion restriction are dominant.[14] But they do not provide ADC values of masses in their study. Yamada *et al.* notified that low ADC value is associated with poor differentiation and prognosis which has rich fibrotic stroma. The researchers, who divided the patients into two groups as high or low ADC, showed that the prognosis was poor in the tumors with decreased ADC. This result conflicts with the results of previous studies by Lee *et al.*[15]

In our study, we did not make prognostic grouping of our IHCC patients. In our study, we found significantly higher ADC values in IHCC patients compared to GIS adenocarcinoma liver metastases. We distinguished these tumors with a cut off ADC_{mean} value of 1178 x 10–6 mm^2/s and 90.57% sensitivity. We speculated that the rich desmoplastic stroma of IHCC is effective in revealing the ADC difference in the differentiation from liver metastases of GIS.

In a recent study, Kovac *et al.* investigated the contribution of ADC values in the differentiation between solitary hypovascular liver metastases and IHCC.[16] They reported lower ADC values in the peripheral enhancing areas and higher in the central parts in IHCC compared to solitary hypovascular metastases. Authors explained that high ADC values in the central part of IHCC are related to rich fibrous tissue.[16] In our study, ADC values were obtained from enhancing solid area and we found higher ADC values compared to GIS metastases. High ADC values in IHCC could be attributed to desmoplastic stromal changes and decreased cellularity within the tumor.

We thought that the reproducibility of ADC measurement may be limited or needs more effort in clinical practice, but it provides significant diagnostic clues in differential diagnosis of such liver malignancies.

There were several limitations in the current study. First this is a retrospective study and has relatively small sample size, especially for the IHCC group because of the rarity of these tumors. Second, the fibrous intensity and differentiation levels of tumors was not assessed by histopathologically. Furthermore, the manual placement of ROI, as a known limitation in all ROI-based studies, may have led to biased results. In addition, the histopathological confirmation of liver metastases was made from primary tumor localization. But this situation was ignored because of low probability of synchronous IHCC and GIS metastases.

Conclusions

As far as we know, this is the first study that particularly demonstrates the utility of ADC values in differentiation of IHCC from GIS adenocarcinoma liver metastases. Our study results suggest that ADC values have a potential role for differentiation between IHCC and GIS liver metastases which may be valuable for patient management. Further larger-scale studies are needed to establish the relationship between IHCC and different tumor origins in terms of ADC values.

References

1. Shin HR, Oh JK, Masuyer E, Curado MP, Bouvard V, Fang YY, et al. Epidemiology of cholangiocarcinoma: an update focusing on risk factors. *Cancer Sci* 2010; **101:** 579-85. doi: 10.1111/j.1349-7006.2009.01458.x
2. Zhou Y, Zhou G, Gao X, Xu C, Wang X, Xu P. Apparent diffusion coefficient value of mass-forming intrahepatic cholangiocarcinoma: a potential imaging biomarker for prediction of lymph node metastasis. *Abdom Radiol* 2020; **45:** 3109-18. doi: 10.1007/s00261-020-02458-x.
3. Lim JH. Cholangiocarcinoma: morphologic classification according to growth pattern and imaging findings. *AJR Am J Roentgenol* 2003; **181:** 819-27. doi: 10.2214/ajr.181.3.1810819
4. Mungai F, Morone M, Villanacci A, Bondioni MP, Mazzoni LN, Grazioli L, et al. Diffusion weighted MR and apparent diffusion coefficient measurement in classification and characterization of noncystic focal liver lesions: does a clinical role exist? *Medicine (Baltimore)* 2014; **93:** e40. doi: 10.1097/MD.0000000000000040
5. Shenoy-Bhangle A, Baliyan V, Kordbacheh H, Guimaraes AR, Kambadakone A. Diffusion weighted magnetic resonance imaging of liver: Principles, clinical applications and recent updates. *World J Hepatol* 2017; **9:** 1081-91. doi: 10.4254/wjh.v9.i26.1081
6. Namimoto T, Nakagawa M, Kizaki Y, Itatani R, Kidoh M, Utsunomiya D, et al. Characterization of liver tumors by diffusion-weighted imaging: Comparison of diagnostic performance using the mean and minimum apparent diffusion coefficient. *J Comput Assist Tomogr* 2015; **39:** 453-61. doi: 10.1097/RCT.0000000000000228
7. Rawla P, Barsouk A. Epidemiology of gastric cancer: global trends, risk factors and prevention. *Prz Gastroenterol* 2019; **14:** 26-38. doi: 10.5114/pg.2018.80001
8. Zheng DX, Ning AY, Levoska MA, Xiang L, Wong C, Scott JF, et al. Predicting liver metastasis of gastrointestinal tract cancer by diffusion-weighted imaging of apparent diffusion coefficient values. *World J Gastroenterol* 2016; **22:** 3031-7. doi: 10.3748/wjg.v22.i10.3031
9. Wang K, Zhang H, Xia Y, Liu J, Shen F. Surgical options for intrahepatic cholangiocarcinoma. *Hepatobiliary Surg Nutr* 2017; **6:** 79-90. doi: 10.21037/hbsn.2017.01.06
10. Vanderveen KA, Hussain HK. Magnetic resonance imaging of cholangiocarcinoma. *Cancer Imaging* 2004; **4:** 104-15. doi: 10.1102/1470-7330.2004.0018
11. Maetani Y, Itoh K, Watanabe C, Shibata T, Ametani F, Yamabe H, et al. MR imaging of intrahepatic cholangiocarcinoma with pathologic correlation. *AJR Am J Roentgenol* 2001; **176:** 1499-507. doi: 10.2214/ajr.176.6.1761499
12. Kele PG, van der Jagt EJ. Diffusion weighted imaging in the liver. *World J Gastroenterol* 2010; **16:** 1567-76. doi: 10.3748/wjg.v16.i13.1567
13. Drevelegas K, Nikiforaki K, Constantinides M, Papanikolaou N, Papalavrentios L, Stoikou I, et al. Apparent diffusion coefficient quantification in determining the histological diagnosis of malignant liver lesions. *J Cancer* 2016; **7:** 730-5. doi: 10.7150/jca.14197
14. Lee J, Kim SH, Kang TW, Song KD, Choi D, Jang KT. Mass-forming intrahepatic cholangiocarcinoma: diffusion-weighted imaging as a preoperative prognostic marker. *Radiology* 2016; **281:** 119-28. doi: 10.1148/radiol.2016151781
15. Yamada S, Morine Y, Imura S, Ikemoto T, Arakawa Y, Saito Y, et al. Prognostic prediction of apparent diffusion coefficient obtained by diffusion-weighted MRI in mass-forming intrahepatic cholangiocarcinoma. *J Hepatobiliary Pancreat Sci* 2020; **27:** 388-95. doi: 10.1002/jhbp.732
16. Kovač JD, Galun D, Đurić-Stefanović A, Lilić G, Vasin D, Lazić L, et al. Intrahepatic mass-forming cholangiocarcinoma and solitary hypovascular liver metastases: is the differential diagnosis using diffusion-weighted MRI possible? *Acta Radiol* 2017; **58:** 1417-26. doi: 10.1177/0284185117695666

research article

Assessment of hyperbaric oxygenation treatment response in parotid glands by T_2 mapping following radiotherapy for head and neck tumours

Jernej Vidmar[1,2,3], Ksenija Cankar[1], Maja Groselj[4], Zarko Finderle[1], Igor Sersa[1,2]

[1] University of Ljubljana, Faculty of medicine Institute of physiology, Ljubljana, Slovenia
[2] Jožef Stefan Institute, Ljubljana, Slovenia
[3] Institute of Radiology, University Medical Center Ljubljana, Ljubljana, Slovenia
[4] University of Ljubljana, Faculty of medicine Department of Dental Diseases and Normal Dental Morphology, Ljubljana, Slovenia

Radiol Oncol 2022; 56(1): 60-68.

Received 23 September 2021
Accepted 10 December 2021

Correspondence to: Assist. Prof. Jernej Vidmar, M.D., Ph.D., Institute of Physiology, Faculty of Medicine, University of Ljubljana, Zaloška 4, SI-1000 Ljubljana, Slovenia. E-mail: jernej.vidmar@mf.uni-lj.si

Disclosure: No potential conflicts of interest were disclosed.

Background. The study was designed to evaluate the influence of hyperbaric oxygenation therapy (HBOT) on the parotid gland in patients following radiotherapy for head and neck tumours.

Patients and methods. HBOT response was monitored by 3T magnetic resonance imaging (MRI) using T_2 mapping and subsequent measurement of mean T_2 and T_2 variability as well as by salivary tests (salivary flow, buffer capacity, and pH). Eighteen patients previously treated with irradiation doses between 50 and 80 Gy as well as 18 healthy gender and age matched controls were enrolled. MRI was performed prior to HBOT (40.2 ± 20 months after radiotherapy) and after 20 daily HBOT at 2.5 ATA (absolute atmosphere). Each HBOT consisted of breathing 100% oxygen for 90 minutes.

Results. Significant differences in mean T_2 prior to HBOT were observed between the ipsilateral irradiated (121 ± 20 ms), contralateral parotids (107 ± 21) and control group (96 ± 12 ms). A positive correlation in patients between T_2 variability and irradiation dose was detected in contralateral parotids before HBOT ($R = 0.489$, $p = 0.0287$). In addition, negative correlations were observed between mean T_2 in the ipsilateral as well as the contralateral gland and salivary flow before and after HBOT. Negative correlations between mean T_2, T_2 variability and pH of unstimulated saliva were also observed in the sides of parotid before and after HBOT.

Conclusions. The study confirmed that T_2 mapping had a potential for monitoring the differences between irradiated and normal parotid glands. It could also be useful in the assessment of the glandular tissue response to HBOT.

Key words: salivary glands; MRI; T_2 mapping; hyperbaric oxygenation therapy

Introduction

The main method of treatment of the malignant head and neck tumours is surgical removal and/or radiation therapy with therapeutic doses between 50 and 70 Gy.[1,2] Doses above 40 Gy results in irreversible changes in the salivary glands – atrophy and necrosis[3,4] – which leads to the reduction of the flow of saliva and the development of xerostomia when salivary glands are in the field of irradiation[4-6]; the latter is probably due to the apoptosis of salivary tissue, as observed in other

tissues under radiation therapy.[7-9] Consequently, both stimulated and unstimulated salivary flow, salivary pH and buffer capacity are reduced[6,10] and the ion composition of saliva is also changed.[11,12] These changes cause the accumulation of plaque and an increased number of microorganisms in the saliva[13-15] which may result in rapidly progressing radiation caries.[16,17] In addition, the reduced excretion of saliva causes complaints associated with oral dryness in patients. It effects the use of oral prostheses as well as speech and taste. The quality of life is also compromised.[16,17] Effective treatments of radiation-induced xerostomia are warranted.[18,19]

Hyperbaric oxygenation therapy (HBOT) is an acceptable method of treatment for the prevention of osteoradionecrosis and soft tissue necrosis in the oral cavity.[20] It improves blood circulation in post-ischemic tissues[21], reduces oedema formation[22], increases diffusion of oxygen in the tissues[23], and accelerates activation of stem cells.[24] The likely cause of the beneficial effect of HBOT against the long-term negative effects of radiotherapy is the accelerated angiogenesis and revascularization of tissues.[25] Until now, there has been no studies that objectively measured the impact of HBOT on salivary gland tissue.

Multiparametric MRI is already a common diagnostic tool for the parotid gland tumours[26, 27], since it enables the optimization of contrast among various soft tissues based on the values of T_1 and T_2 relaxation times of various tissues and organs. T_2 mapping is specifically a magnetic resonance imaging technique used to calculate the T_2 relaxation times of the specific tissues and displaying them voxel-vice on a parametric map. It has been used for tissue characterization in various types of tissue (e.g. myocardium).[28] The T_2 relaxation time, also referred to as the spin-spin or transverse relaxation, is a time constant for the decay of transverse magnetization and is tissue-specific with regards to its ability to differentiate the abnormal tissues from the normal ones. T_2 values reflect water content in the respective tissue and are mainly used for the evaluation of oedema, e.g., in myocardial inflammation or infarction as in other pathologies. In addition, T_2 mapping and mDIXON Quant imaging proved to be useful for non-invasive evaluation of the radiation-induced parotid damage.[29] Consequently, the mapping of the transversal relaxation time (T_2-mapping) enables good differentiation among different stages of soft tissue inflammation without the need of contrast medium and would be an appropriate method for the early detection of salivary gland tissue changes due to radiation and HBOT.

In the present *in vivo* study, the patients with head and neck tumours who had undergone radiation therapy were scanned by the T_2 mapping MRI technique before and after HBOT. The obtained T2 maps were further correlated with the standard clinical salivary tests (salivary flow, pH, and buffering capacity).

Patients and methods

Patient group

The study was carried out on 18 patients (2 females and 16 males) with the head and neck tumours previously treated with radiotherapy. The mean age of the patients was 60.9 ± 11.7 years. Patients had been diagnosed with different types of tumours, the majority of which were located in the oral cavity. In all patients, the salivary glands were in the radiation field. The patients received irradiation doses from 50 to 80 Gy (mean irradiation dose 64.3 ± 6.3 Gy). Each patient included in the study received 20 daily HBOT in a hyperbaric chamber at 2.5 ATA (absolute atmosphere) where patients breathed 100% oxygen for 90 minutes each day. Patients were examined by MRI as well as salivary function testing twice; the first MRI examination was performed at baseline before the first HBO therapy (40.2 ± 20 months after radiation therapy) and the second 3 to 7 days after the last HBOT to avoid possible acute effects of higher oxygen levels. All patients were able to perform routine daily activities prior to each MRI examination.

Contraindications to MRI such as an implanted pacemaker constituted exclusion criteria. All participants provided written informed consent approved by the Ethical Committee of the National Ministry of Health (Approval number 0120-41/2017/13) to participate in this protocol and conformed to the STROBE guidelines. The clinical study was undertaken with the understanding and written consent of each subject according to the Declaration of Helsinki (version 2008).

Control group

The control group was composed of 18 healthy gender- and age-matched participants (mean age: 56.7 ± 11.8 years; 2 females and 16 males), who were enrolled in the study as volunteers and did not receive any HBOT. All the measurements in the control group (MRI measurements as well as salivary

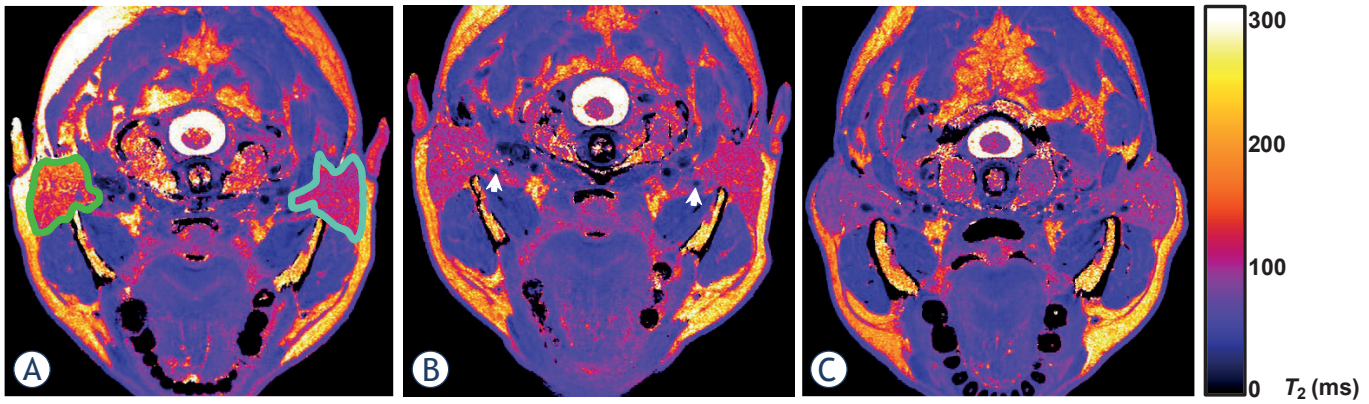

FIGURE 1. Representative T_2 maps of parotid glands in a single transversal slice in a patient following radiotherapy for head and neck tumour before **(A)** and after hyperbaric oxygenation therapy (HBOT) **(B)** and in healthy control **(C)**. Region of interest (ROI) on the ipsilateral side is encircled by green and on the contralateral side by the white-blue colour. Retromandibular veins (white arrows in B) were always carefully omitted from the ROI.

function testing) were performed only once in the same manner as in the patient group. Specifically, analysis of the MRI measurements was performed in both parotid glands. The results of the control group were used as a reference.

MR image acquisition

The MR imaging of the parotid glands was performed on a 3T MRI system (TX Achieva, Philips, Netherlands) with a maximum gradient strength of 80 mT/m and use of a 32-channel receive head coil. The MR images were acquired using a multi-spin-echo (MSE) MRI sequence with parameters: TR = 2000 ms; TE = 7.8, 16, 24, 32, 40, 47 ms; field of view (FOV) 160 × 160 mm^2; slice thickness 2 mm; image acquisition/reconstruction matrix 380 × 311/560 × 560; acquisition/reconstruction voxel size 0.42 × 0.51 × 2.5/0.29 × 0.29 × 2.5 mm^3; single slice; bandwidth 290 Hz/pixel; no signal acquisition acceleration; and acquisition time for all 6 echoes was equal to 10 min 24 s. The imaging plane was oriented so that it contained most of the parotid glad, *i.e.*, in the transversal orientation.

MR data analysis

A central slice in the transversal plane, covering the largest area of the parotid gland tissue, was used for T_2 mapping analysis. T_2 map was calculated using pixel-wise least-square fitting analysis of a set of T_2-weighted images with TE values as specified above. The fitting analysis implemented in the MRI for the calculation of T_2 maps used Analysis Calculator plugin (ImageJ, National Institutes of Health, USA) that utilizes a mono-exponential T_2 signal decay function $S_{i,j}(TE) = S_{0\ i,j} \exp(-TE / T_{2\ i,j})$ as the model function for the analysis and the pair (i,j) denotes the pixel coordinate. From the calculated T_2 maps, mean and variability of T_2 values in the region of interest (encircled in Figure 1) were determined in the ipsilateral as well as the contralateral parotid gland of the subjects in the study. The variability of T_2 values was used for a quantitative assessment of tissue heterogeneity.

Salivary function testing

Tests for the evaluation of the functioning of the salivary glands were always performed between 11-12 a.m. The patients were instructed to clean their teeth in the morning and not to drink, eat or smoke for two hours before the measurements. Unstimulated salivary flow was determined by a 5-minute saliva collection. Saliva production was then stimulated with a 5-minute chewing of a paraffin block. The paraffin blocks (each weighting 1g and with a melting point of 48 °C) were part of the CRT buffer test provided by Ivoclar Vivadent (Liechtenstein). During this time, patients were not allowed to swallow saliva. After the stimulation, the salivary flow was determined. The buffering capacity was determined only in stimulated saliva with a CRT buffer (Ivoclar Vivadent, Liechtenstein) due to the negligible amount of unstimulated saliva. After five minutes, the colour of the pad was compared with the colour chart. The salivary pH was determined by a pH-meter (Iskra, Slovenia). In order to exclude the influence of saliva enhancement and disinfection procedures on

TABLE 1. Mean T_2 and T_2 variability values of parotid glands in patients following radiotherapy for head and neck tumours before and after hyperbaric oxygenation therapy (HBOT) and in healthy controls

	Ipsilateral side (N = 18)		Contralateral side (N = 18)		Controls (N = 18)
	before HBOT	after HBOT	before HBOT	after HBOT	
MEAN T_2 (ms)	121 ± 20†	113 ± 16†*	107 ± 21**	103 ± 14	96 ± 12
T_2 VARIABILITY (ms)	30 ± 8	25 ± 8*	21 ± 8	19 ± 6	16 ± 4

†-statistically significant difference with healthy controls

*-statistically significant change in response to HBOT

**-statistically significant difference between ipsilateral and contralateral side

the results of the study, instructions regarding oral hygiene and saliva flow enhancement were also provided after the saliva evaluation at the end of HBOT.

Protocol for HBOT

Patients were treated in a multi-place hyperbaric chamber (Kovinarska P&P, Slovenia). For each patient, 20 dives were held consecutively on each working day of the week. Each individual dive in the hyperbaric chamber filled with air at a pressure of 2.5 ATA (absolute atmosphere) lasted 90 min. The patients breathed 100-percent oxygen through a mask at a pressure of 2.5 ATA. For each patient, MRI as well as saliva tests before the start and 3 to 7 days after the last HBOT were performed.

Statistical analysis

The results were expressed as mean and standard deviation in the case of a passed Shapiro-Wilk test or as the median value and the interquartile range (IQR) in the case of a failed Shapiro-Wilk test, both with the criterion of significance at $p < 0.05$.

The mean $T_2$and T_2 variability values of the patients' parotid glands were compared by Analysis of Variance (ANOVA) with repeated measures using 19 degrees of freedom and a Bonferroni's post-hoc test. The obtained mean T_2 and T_2 variability values in the patient group (ipsilateral and contralateral gland respectively) were compared with values obtained in healthy controls with a Student t-test. The values of the salivary flow and pH of unstimulated as well as stimulated saliva in patients before and after the end of HBOT were compared with a paired t-test. To assess the magnitude and direction of change in the buffer capacity at the beginning and at the end of HBOT, the Wilcoxon signed-rank test was used.

Correlation tests between mean T_2 and T_2 variability values from the ipsilateral as well as the contralateral gland and saliva test parameters (i.e. salivary flow, pH and buffering capacity) and with irradiation doses in patients were made by a linear regression (Pearson correlation coefficient).

Results

MRI analysis

At the beginning of HBO therapy, significantly higher mean T_2 value was observed in the examined slice of the ipsilateral parotid when compared to the mean T_2 value on the contralateral gland ($p = 0.007$, Table 1). Furthermore, significant difference was observed between mean T_2 values in the parotid glands of healthy controls and in ipsilateral parotid glands of patients before HBO therapy ($p = 0.0004$). In contrast, no significant difference was observed between mean T_2 in the contralateral parotid glands of patients and healthy controls. In addition, no significant differences in T_2 variability of parotid glands of patients before HBOT and healthy controls were observed.

A significant higher mean T_2 on the ipsilateral gland was found in patients after the end of HBOT when compared to healthy controls ($p = 0.002$). In contrast, no difference was observed on the contralateral side. On the ipsilateral side, statistically significant decrease in mean T_2 and T_2 variability was observed in patient as a response to HBOT. In contrast, no significant change in mean T_2 and T_2 variability of contralateral parotid glands was observed in patients in response to HBOT.

Analysis of salivary tests

The salivary flow and pH value of unstimulated and stimulated saliva were significantly lower in

TABLE 2. Salivary flow, pH, and buffer capacity in patients following radiotherapy for head and neck tumours before and after hyperbaric oxygenation therapy (HBOT) and in healthy controls

	before HBOT (N = 18)	after HBOT (N = 18)	Controls (N = 18)
Unstimulated salivary flow (mL/min) (median and IQR)	0.22 (0.04-0.54) †	0.32 (0.08-0.70)*†	0.61 (0.49-0.99)
pH of unstimulated saliva (mean ± SD)	6.61± 0.69†	6.72 ± 0.71†	7.56 ± 0.53
Stimulated salivary flow (mL/min) (mean ± SD)	0.82 ± 0.60†	0.90 ± 0.64†	2.04 ± 0.91
pH of stimulated saliva (mean ± SD)	7.38 ± 0.74†	7.48 ± 0.51†	8.00 ± 0.28
Buffering capacity of stimulated saliva (median and IQR)	2.00 (1.75-3.00)	3.00 (2.00-3.00)*	3.00 (2.00-3.00)

†-statistically significant difference with healthy controls

*-statistically significant change in response to HBOT

IQR = interquartile range; SD = standard deviation

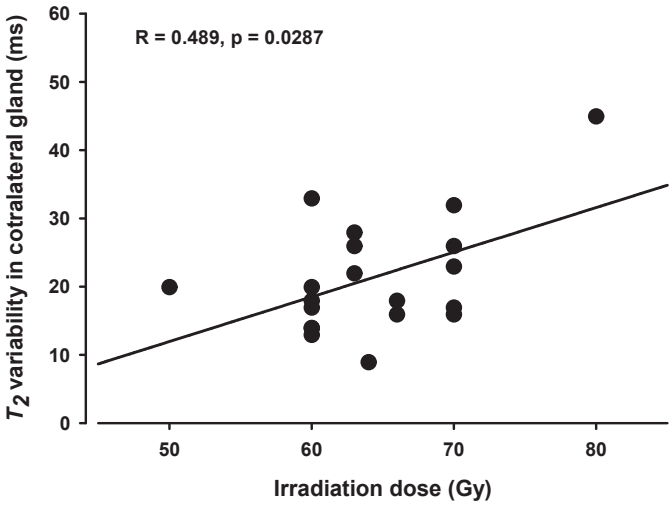

FIGURE 2. A correlation between an irradiation dose and variability of T_2 values in contralateral parotid glands before hyperbaric oxygenation therapy (HBOT).

patients prior to and after the end of HBOT when compared to the values obtained in healthy controls (Table 2, $p < 0.01$). In contrast, no significant difference in the buffering capacity of stimulated saliva was observed between patients and controls. Statistically significant increase in the unstimulated salivary flow as well as in the buffering capacity of stimulated saliva was observed in patients in response to HBOT. In contrast, no significant change was found in other measured salivary parameters.

Correlation between MRI parameters, irradiation dose and salivary tests

A significant positive correlation between T_2 variability of the contralateral parotid gland and the irradiation dose was observed before HBOT (Figure 2). In contrast, no significant correlation between mean T_2 on either ipsilateral or contralateral gland or T_2 variability in ipsilateral parotid glands before HBOT and the irradiation dose was found.

On the ipsilateral side, a significant negative correlation was observed between mean T_2 and stimulated salivary flow before HBOT (Figure 3A) and between mean T_2 and unstimulated salivary flow after HBOT (Figure 3B). On the contralateral side a negative correlation between mean T_2 and unstimulated (Figure 4A) as well as stimulated salivary flow (Figure 4B) was observed after the HBOT.

In addition, significant negative correlations between mean T_2 and T_2 variability and pH of unstimulated saliva were observed in ipsilateral parotid glands in patients before and after HBOT (Table 3). On the contralateral side negative correlations were also observed except for the correlation between T_2 variability and pH of unstimulated saliva before HBOT. No correlations were found between mean T_2 or T_2 variability and pH of stimulated saliva.

Discussion

In the present study, the structural and functional response to HBOT in parotid glands of the patients after the radiotherapy of head and neck tumours was monitored by T_2 mapping and functional salivary test. Two of the MRI parameters obtained from the T_2 maps, *i.e.* mean T_2 and T_2 variability were used for the assessment of tissue structure after radiotherapy, prior to and after HBOT. Mean T_2 was used to assess tissue oedema and T_2 variability

TABLE 3. Correlations between mean T_2 or T_2variability and pH of unstimulated saliva before and after hyperbaric oxygenation therapy (HBOT) (R-correlation coefficients and p-values)

	Ipsilateral side (N = 18)				Contralateral side (N = 18)			
	before HBOT		after HBOT		before HBOT		after HBOT	
	R	p	R	p	R	p	R	p
Mean T_2 (ms)	-0.647	0.0037	-0.571	0.0133	-0.557	0.0164	-0.675	0.0021
T_2 variability (ms)	-0.595	0.0092	-0.506	0.0323	-0.130	0.607	-0.588	0.0133

for the assessment of structural changes in the tissue, *e.g.*, tissue heterogeneity. Mean T_2 is strongly dependent on the free water content and its mobility in the tissue; however, it lacks more detailed information about the tissue structure heterogeneity, otherwise visualized on the T_2 maps of the examined slice. Therefore, mean T_2 values were complemented with T_2 variability.

Prior to HBOT, consistent high mean T_2 values were observed in the examined slices with the parotid gland on the ipsilateral side compared to the values obtained from the glands on the contralateral side of the same patients as well as healthy controls. The most plausible explanation for this phenomenon is the onset of radiation induced parenchymal changes in the affected parotid glands in patients following radiotherapy.[26,29] Therefore, the augmented T_2 values in the parotid glands on the side of radiation can be explained by the prolonged effect of the inflammation along with glandular oedema. T_2 variability values in parotid glands are also the highest in the ipsilateral irradiated parotid glands and somewhat lower on the contralateral side in patients before HBOT when compared to the control group. This can be explained by a different structural tolerance of parotid glands to the received radiation. Due to the proximity of the ipsilateral side to the radiation source, a relatively high radiation dose was accumulated, causing scarring and narrowing of the blood vessels with more severe parenchymal atrophy.[30] The latter resulted in a more heterogeneous structure, as seen in T_2 maps of the parotid glands on the ipsilateral side, and consequently in a relatively high T_2 variability. It should be emphasized that the MRI assessment of parotid glands performed at the late time prior to HBOT might represent late radiation effects (LRE) resulting in tissue oedema as well as chronic tissue changes.[31]

After the HBOT, a decrease in mean T_2 and T_2 variability in the patients' ipsilateral gland was observed. This can be explained by HBOT effects on LRE through a complex series of changes in the affected tissues. Tissue oedema is probably improved through an osmotic effect of oxygen while the onset of a steep oxygen gradient across an irradiated tissue margin is a powerful stimulus for

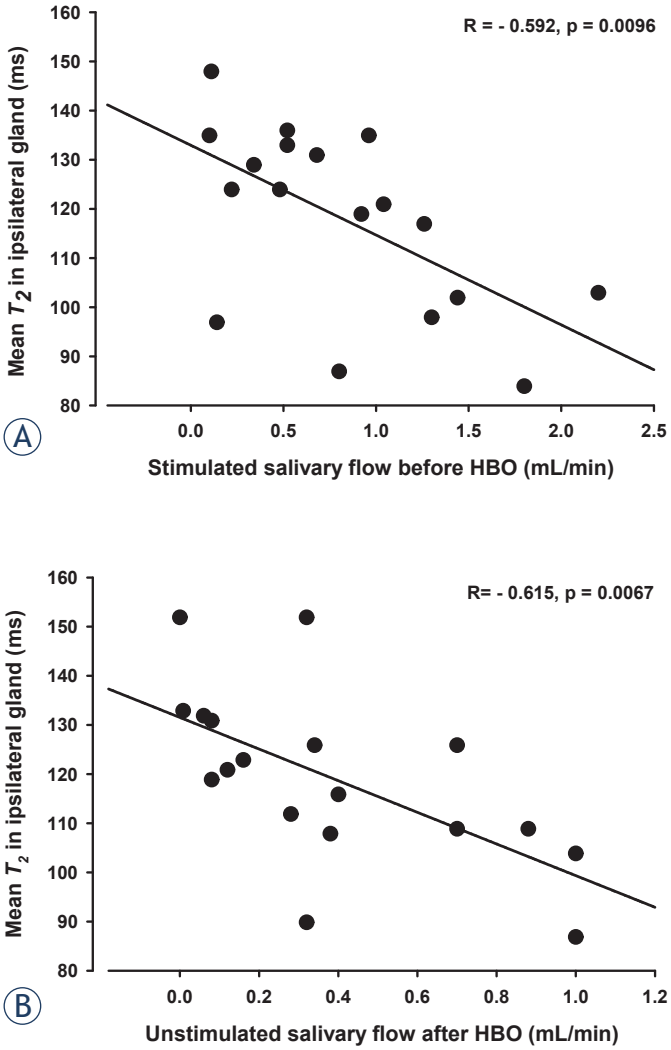

FIGURE 3. A correlation between the mean T_2 values in ipsilateral parotid glands and stimulated salivary flow before hyperbaric oxygenation therapy (HBOT) **(A)** and unstimulated salivary flow after HBOT **(B)**.

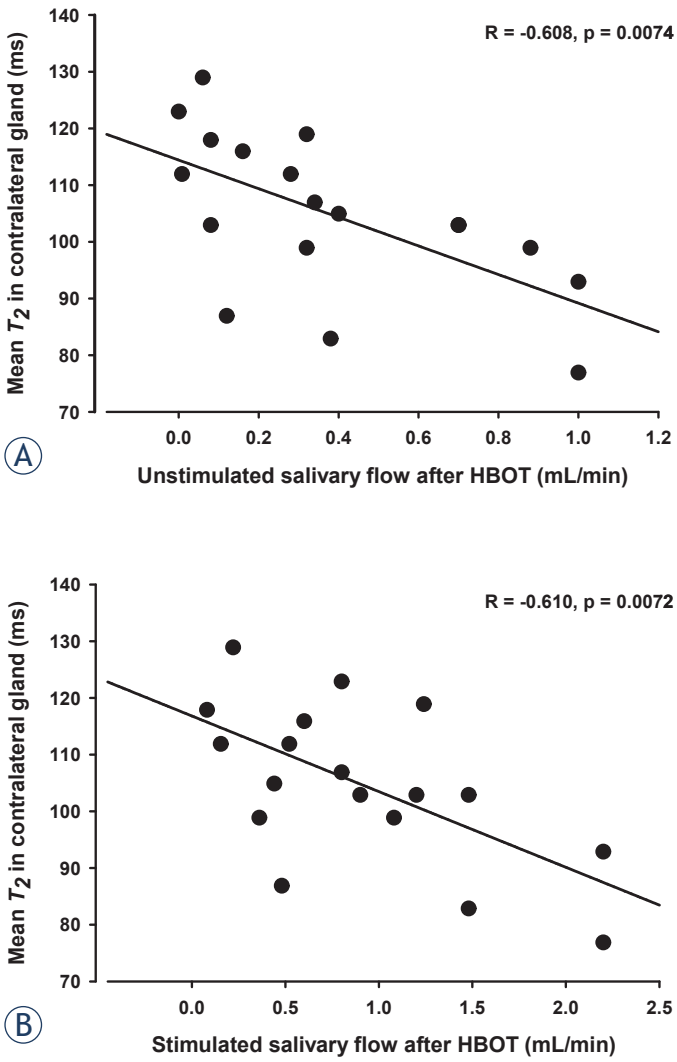

FIGURE 4. A correlation between the mean T_2 values in contralateral parotid glands and unstimulated **(A)** and stimulated salivary flow **(B)** after hyperbaric oxygenation therapy (HBOT).

the growth of new blood vessels and subsequent tissue neovascularisation. In addition, an increase in oxygen levels, improves white cell and fibroblast function, thus enabling further enhancement of wound healing and tissue quality improvement.[32] The effect of HBOT was slightly more pronounced on the ipsilateral side due to the more severe structural changes.

A positive correlation between T_2 variability and the irradiation dose was observed only in contralateral parotid glands prior to HBOT. This confirms that the contralateral side could also be affected with higher doses of radiation. In contrast, absence of any significant correlation on the ipsilateral side could be attributed to rather comparable cumulative radiation doses between patients, *i.e.*, most of them were exposed to doses between 60 to 70 Gy. Furthermore, mean T_2 and T_2 variability were also relatively high on the ipsilateral side and would probably require enrolment of more patients with doses ranging from relatively low (~50 Gy) to relatively high (~80 Gy) to obtain a significant correlation.

Previous studies on the effects of radiation on the function of salivary glands have shown that the reduction of salivary gland activity depends on the dose of radiation and the volume of irradiated tissues.[33] Namely, doses above 60 Gy result in a dramatic decrease in salivary flow rate.[4] The latter is in agreement with the results of functional salivary tests in our patient group prior to HBOT. Since the radiation doses were nearly the same in all patients, we could not find any correlation between the radiation doses received and salivary flow. As a response to HBOT, a significant improvement of salivary gland function was observed in all measured salivary parameters. The results confirm the findings of previous studies demonstrating a subjective reduction of problems related to swallowing, taste sensation and saliva quantity.[34]

A negative correlation between mean T_2 and T_2 variability in the examined slice of ipsilateral parotid glands and unstimulated saliva pH as well as stimulated salivary flow was observed in patients prior to and after HBOT. These correlations can be attributed to the fact that structural changes in glandular tissues influence the function of all gland and subsequent cumulative saliva secretion. In addition, these results are also in agreement with another MRI study showing an increase in apparent diffusion coefficient (ADC) of salivary glands due to radiation injury as well as a correlation between ADC, stimulated salivary flow and xerostomia questionnaire scores.[35]

The present study has several limitations, mainly due to MRI scanning time as well as the comparison of MRI results with the functional salivary tests. Firstly, the achievable resolution in our experimental setup was limited by a reasonable MRI scanning time, *e.g.*, approximately ten minutes per scan for T_2 mapping, therefore allowing only T_2 mapping in the central slice of the parotid gland. Consequently, only a T_2 map of the slice with the largest proportion of glandular tissue was measured and analysed. For the purpose of more in-depth analysis of the parotid structure, the whole area of the parotid gland should be scanned for T_2 mapping; however, this would require unreasonably prolonged scanning time. Secondly, we

analysed parotid glands on both sides. Because of limitations in the experimental setup, allowing only single slice T_2 mapping and clinically applicable salivary tests, only single-sided T_2 values from ipsilateral and contralateral parotid gland were correlated with the salivary tests in each patient. Such analysis does not enable accurate correlation between a single-sided T_2 values with functional salivary testing, which includes the cumulative function of all glands. Namely, in the case of hypofunction of one gland, its function deficit may be compensated by the glands on the contralateral side. Since structural changes observed in T_2 maps on both glandular sides were proportional prior to and after HBOT, this is less likely, suggesting that the function of both glands was affected to some extent and our approach seems still reasonable. Ideally, this could be avoided by using advanced MRI methods, combing T_2 mapping or even ADC mapping with MR functional salivary flow imaging (MR dynamic sialography). However, such complex scanning results in excessively long scanning time.[36]

Conclusions

The results of the present study confirm that T_2 mapping has a potential for the evaluation of the differences between irradiated and normal parotid glandular tissue. In this study, it is shown that T_2 mapping could also be useful in the evaluation of the glandular tissue response to HBOT.

Acknowledgement

This work was supported by Grant No.: P3-0019, Ministry of Higher Education, Science and Technology, Slovenia.

References

1. Palme CE, Gullane PJ, Gilbert RW. Current treatment options in squamous cell carcinoma of the oral cavity. *Surg Oncol Clin N Am* 2004; **13:** 47-70. doi: 10.1016/S1055-3207(03)00123-6
2. Lefebvre JL. Current clinical outcomes demand new treatment options for SCCHN. *Ann Oncol* 2005; **16(Suppl 6):** vi7-vi12. doi: 10.1093/annonc/mdi452
3. Han P, Lakshminarayanan P, Jiang W, Shpitser I, Hui X, Lee SH, et al. Dose/volume histogram patterns in salivary gland subvolumes influence xerostomia injury and recovery. *Sci Rep* 2019; **9:** 3616. doi: 10.1038/s41598-019-40228-y
4. Sim C, Soong YL, Pang E, Lim C, Walker GD, Manton DJ, et al. Xerostomia, salivary characteristics and gland volumes following intensity-modulated radiotherapy for nasopharyngeal carcinoma: a two-year follow up. *Aust Dent J* 2018; **63:** 217-23. doi: 10.1111/adj.12608
5. Burlage FR, Coppes RP, Meertens H, Stokman MA, Vissink A. Parotid and submandibular/sublingual salivary flow during high dose radiotherapy. *Radiother Oncol* 2001; **61:** 271-4. doi: 10.1016/s0167-8140(01)00427-3
6. Moller P, Perrier M, Ozsahin M, Monnier P. A prospective study of salivary gland function in patients undergoing radiotherapy for squamous cell carcinoma of the oropharynx. *Oral Surg Oral Med Oral Pathol Oral Radiol Endod* 2004; **97:** 173-89. doi: 10.1016/s1079-2104(03)00473-6
7. Konings AW, Coppes RP, Vissink A. On the mechanism of salivary gland radiosensitivity. *Int J Radiat Oncol Biol Phys* 2005; **62:** 1187-94. doi: 10.1016/j.ijrobp.2004.12.051
8. Gupta A, Epstein JB, Sroussi H. Hyposalivation in elderly patients. *J Can Dent Assoc* 2006; **72:** 841-6. PMID: 17109806
9. Arsenian MA. Cardiovascular sequelae of therapeutic thoracic radiation. *Prog Cardiovasc Dis* 1991; **33:** 299-311. doi: 10.1016/0033-0620(91)90022-e
10. Cankar K, Finderle Z, Jan J. The effect of hyperbaric oxygenation on postradiation xerostomia and saliva in patients with head and neck tumours. *Caries Res* 2011; **45:** 136-41. doi: 10.1159/000324811
11. Almstahl A, Wikstrom M. Electrolytes in stimulated whole saliva in individuals with hyposalivation of different origins. *Arch Oral Biol* 2003; **48:** 337-44. doi: 10.1016/s0003-9969(02)00200-5
12. Chambers MS, Garden AS, Kies MS, Martin JW. Radiation-induced xerostomia in patients with head and neck cancer: pathogenesis, impact on quality of life, and management. *Head Neck* 2004; **26:** 796-807. doi: 10.1002/hed.20045
13. Meng L, Liu J, Peng B, Fan M, Nie M, Chen Z, et al. The persistence of Streptococcus mutans in nasopharyngeal carcinoma patients after radiotherapy. *Caries Res* 2005; **39:** 484-9. doi: 10.1159/000088184
14. Eliasson L, Carlen A, Almstahl A, Wikstrom M, Lingstrom P. Dental plaque pH and micro-organisms during hyposalivation. *J Dent Res* 2006; **85:** 334-8. doi: 10.1177/154405910608500410
15. Almstah IA, Wikstrom M, Stenberg I, Jakobsson A, Fagerberg-Mohlin B. Oral microbiota associated with hyposalivation of different origins. *Oral Microbiol Immunol* 2003; **18:** 1-8. doi: 10.1034/j.1399-302x.2003.180101.x
16. Vissink A, Jansma J, Spijkervet FK, Burlage FR, Coppes RP. Oral sequelae of head and neck radiotherapy. *Crit Rev Oral Biol Med* 2003; **14:** 199-212. doi: 10.1177/154411130301400305
17. Moore C, McLister C, Cardwell C, O'Neill C, Donnelly M, McKenna G. Dental caries following radiotherapy for head and neck cancer: a systematic review. *Oral Oncol* 2020; **100:** 104484. doi: 10.1016/j.oraloncology.2019.104484
18. Shiboski CH, Hodgson TA, Ship JA, Schiodt M. Management of salivary hypofunction during and after radiotherapy. *Oral Surg Oral Med Oral Pathol Oral Radiol Endod* 2007; **103(Suppl):** S66 e1-19. doi: 10.1016/j.tripleo.2006.11.013
19. Dirix P, Nuyts S, Vander Poorten V, Delaere P, Van den Bogaert W. The influence of xerostomia after radiotherapy on quality of life: results of a questionnaire in head and neck cancer. *Support Care Cancer* 2008; **16:** 171-9. doi: 10.1007/s00520-007-0300-5
20. Annane D, Depondt J, Aubert P, Villart M, Gehanno P, Gajdos P, et al. Hyperbaric oxygen therapy for radionecrosis of the jaw: a randomized, placebo-controlled, double-blind trial from the ORN96 study group. *J Clin Oncol* 2004; **22:** 4893-900. doi: 10.1200/JCO.2004.09.006
21. Buras JA, Reenstra WR. Endothelial-neutrophil interactions during ischemia and reperfusion injury: basic mechanisms of hyperbaric oxygen. *Neurol Res* 2007; **29:** 127-31. doi: 10.1179/016164107X174147
22. Mychaskiw G 2nd, Pan J, Shah S, Zubkov A, Clower B, Badr A, et al. Effects of hyperbaric oxygen on skin blood flow and tissue morphology following sciatic nerve constriction. *Pain Physician* 2005; **8:** 157-61. PMID: 16850069
23. Plafki C, Carl UM, Glag M, Hartmann KA. The treatment of late radiation effects with hyperbaric oxygenation (HBO). *Strahlenther Onkol* 1998; **174(Suppl 3):** 66-8. PMID: 9830461
24. Thom SR, Bhopale VM, Velazquez OC, Goldstein LJ, Thom LH, Buerk DG. Stem cell mobilization by hyperbaric oxygen. *Am J Physiol Heart Circ Physiol* 2006; **290:** H1378-86. doi: 10.1152/ajpheart.00888.2005
25. Bennett MH, Feldmeier J, Hampson N, Smee R, Milross C. Hyperbaric oxygen therapy for late radiation tissue injury. *Cochrane Database Syst Rev* 2005**:** CD005005. doi: 10.1002/14651858.CD005005.pub2

26. Burke CJ, Thomas RH, Howlett D. Imaging the major salivary glands. *Br J Oral Maxillofac Surg* 2011; **49:** 261-9. doi: 10.1016/j.bjoms.2010.03.002

27. Gokce E. Multiparametric magnetic resonance imaging for the diagnosis and differential diagnosis of parotid gland tumors. *J Magn Reson Imaging* 2020; **52:** 11-32. doi: 10.1002/jmri.27061

28. Bohnen S, Radunski UK, Lund GK, Ojeda F, Looft Y, Senel M, et al. Tissue characterization by T1 and T2 mapping cardiovascular magnetic resonance imaging to monitor myocardial inflammation in healing myocarditis. *Eur Heart J-Card Img* 2017; **18:** 744-51. doi: 10.1093/ehjci/jex007

29. Zhou N, Chu C, Dou X, Chen W, He J, Yan J, et al. Early evaluation of radiation-induced parotid damage in patients with nasopharyngeal carcinoma by T2 mapping and mDIXON Quant imaging: initial findings. *Radiat Oncol* 2018; **13:** 22. doi: 10.1186/s13014-018-0970-9

30. Ortholan C, Mornex F. [Normal tissue tolerance to external beam radiation therapy: lung]. [French]. *Cancer Radiother* 2010; **14:** 312-8. doi: 10.1016/j.canrad.2010.02.009

31. Stone HB, Coleman CN, Anscher MS, McBride WH. Effects of radiation on normal tissue: consequences and mechanisms. *Lancet Oncol* 2003; **4:** 529-36. doi: 10.1016/s1470-2045(03)01191-4

32. Feldmeier JJ, Davolt DA, Court WS, Onoda JM, Alecu R. Histologic morphometry confirms a prophylactic effect for hyperbaric oxygen in the prevention of delayed radiation enteropathy. *Undersea Hyperb Med* 1998; **25:** 93-7. PMID: 9670434

33. Eisbruch A, Ten Haken RK, Kim HM, Marsh LH, Ship JA. Dose, volume, and function relationships in parotid salivary glands following conformal and intensity-modulated irradiation of head and neck cancer. *Int J Radiat Oncol Biol Phys* 1999; **45:** 577-87. doi: 10.1016/s0360-3016(99)00247-3

34. Gerlach NL, Barkhuysen R, Kaanders JH, Janssens GO, Sterk W, Merkx MA. The effect of hyperbaric oxygen therapy on quality of life in oral and oropharyngeal cancer patients treated with radiotherapy. *Int J Oral Maxillofac Surg* 2008; **37:** 255-9. doi: 10.1016/j.ijom.2007.11.013

35. Shi D, Qian JJ, Fan GH, Shen JK, Tian Y, Xu L. Salivary gland function in nasopharyngeal carcinoma before and late after intensity-modulated radiotherapy evaluated by dynamic diffusion-weighted MR imaging with gustatory stimulation. *BMC Oral Health* 2019; **19:** 288. doi: 10.1186/s12903-019-0951-x

36. Tanaka T, Ono K, Ansai T, Yoshioka I, Habu M, Tomoyose T, et al. Dynamic magnetic resonance sialography for patients with xerostomia. *Oral Surg Oral Med Oral Pathol Oral Radiol Endod* 2008; **106:** 115-23. doi: 10.1016/j.tripleo.2008.03.012

research article

Comparison of local recurrence in transcatheter arterial chemoembolization of hepatocellular carcinoma with or without accumulation of iodized oil beyond corona enhancement area: Short-term results

Yukinobu Watanabe, Masahiro Ogawa, Masahiro Kaneko, Mariko Kumagawa, Midori Hirayama, Naoki Matsumoto, Hiroshi Nakagawara, Toshiki Yamamoto, Mitsuhiko Moriyama

Department of Gastroenterology and Hepatology, Nihon University School of Medicine, Tokyo, Japan

Radiol Oncol 2022; 56(1): 69-75.

Received 12 August 2021
Accepted 1 October 2021

Correspondence to: Prof. Yukinobu Watanabe, Department of Gastroenterology and Hepatology, Nihon University Hospital, 1-6 Kanda, Surugadai, Chiyoda-ku, Tokyo 101-8309, Japan. E-mail: koushin0809@yahoo.co.jp

Disclosure: No potential conflicts of interest were disclosed.

Background. Local tumor recurrence of hepatocellular carcinoma (HCC) often occurs in blood drainage areas. Corona enhancement is determined by computed tomography during hepatic arteriography (CTHA) and is considered to represent the blood drainage area. This study aimed to investigate the relationship between embolization of corona enhancement area and local tumor recurrence of patients with HCC who underwent transcatheter arterial chemoembolization (TACE).

Patients and methods. The study retrospectively selected 53 patients with 60 HCC nodules that showed corona enhancement area on late-phase CTHA and showed homogenous accumulation of iodized oil throughout the nodule on non-contrast-enhanced CT performed immediately after TACE. We divided the nodules into two groups, according to whether the accumulation of iodized oil covered the entire corona enhancement area (group A) or not (group B). Local tumor recurrence was compared between the two groups.

Results. The cumulative local tumor recurrence rates for group A (n = 36) were 2.8%, 2.8%, 8.3% at 3, 6, and 12 months, respectively, whereas the recurrence rates for group B (n = 24) were 20.8%, 45.8%, 75% at 3, 6, and 12 months, respectively. The cumulative local tumor recurrence rates for group A were significantly lower than those for group B (hazard ratio, 0.079; 95% confidence interval, 0.026–0.24; $p < 0.001$).

Conclusions. The results of the study suggest that the corona enhancement area may be an accurate safety margin in TACE which should be performed until the embolic area covers the entire corona enhancement area.

Key words: corona enhancement; transcatheter arterial chemoembolization; computed tomography during hepatic arteriography; hepatocellular carcinoma

Introduction

Hepatocellular carcinoma (HCC) is the most common primary liver malignancy and is the third leading cause of cancer death worldwide.[1] Transcatheter arterial chemoembolization (TACE) has been widely used to treat unresectable HCC.[2-5] According to the Barcelona Clinic Liver Cancer staging system, TACE is the first-line treatment for patients with intermediate-stage HCC[6], underlining the importance of TACE in the treatment of HCC.

HCC often has satellite lesions that cannot be diagnosed by imaging modalities, and the local tumor recurrences may occur because of untreated satellite lesion.[7,8] Therefore, it is necessary to treat not only the tumor itself but also the area around the tumor in the treatment of HCC. Previous studies reported that the adequate safety margin of iodized oil in TACE also affects microsatellite lesions around the tumor, which resulted in a lower rate of local tumor recurrence.[9-11]

Corona enhancement is one of the characteristic findings of hypervascular HCC, and it results in perinodular enhancement with bright branching structures depicted on late-phase computed tomography during hepatic arteriography (CTHA).[12-16] The corona enhancement area has been proposed as the blood drainage area of HCC and a previous study reported that satellite lesions of HCC existed in the blood drainage area.[17] The corona enhancement area is expected to be an accurate safety margin in the treatment of HCC. However, there have been no studies that have evaluated the association between embolization of corona enhancement area and local tumor recurrence following TACE.

The aim of this retrospective study was to investigate the relationship between local recurrence following TACE and embolization of corona enhancement area.

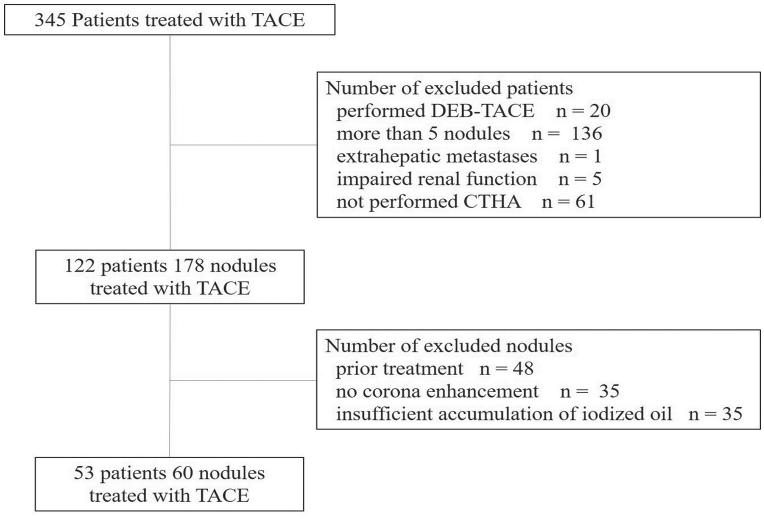

FIGURE 1. Flow diagram of patients' and nodules' selection.

CTHA = computed tomography during hepatic arteriography; DEB-TACE = drug-eluting beads transcatheter arterial chemoembolization; RFA = radiofrequency ablation; TACE = transcatheter arterial chemoembolization

Patients and methods

This study was conducted in accordance with the guidelines of the Declaration of Helsinki and was approved by our institutional ethics committee (protocol number 20200502). Informed consent was waived by the committee because this study was a retrospective study.

Study population

Between April 2016 and October 2019, TACE procedures were performed on 345 patients with HCC at our hospital. TACE was done because patients were ineligible for surgery or they refused to undergo surgical resection. Radiofrequency ablation (RFA) procedures were not performed due to the location of the tumor, where ablation may cause insufficient therapeutic effects and/or adverse effects on adjacent organs. The diagnosis of HCC was confirmed by at least 2 of the following modalities: contrast-enhanced computed tomography (CECT), contrast-enhanced ultrasonography, and/or gadolinium-ethoxybenzyl-diethylenetriamine pentaacetic acid (Gd-EOB-DTPA)-enhanced magnetic resonance imaging (MRI). Eligibility criteria for this study were as follows: (a) the presence of fewer than five nodules; (b) nodules treated with balloon-occluded TACE (B-TACE); (c) nodules that showed corona enhancement on late-phase CTHA; and (d) nodules showing dense accumulation of iodized oil throughout the tumor on non-contrast-enhanced CT performed immediately after TACE. The exclusion criteria were as follows: (a) the nodules with prior treatment; (b) impaired renal function, a contraindication for CECT; and (c) extrahepatic metastases. Fifty-three patients with a total of 60 nodules were enrolled in this study. A flow diagram of patient and nodule selection is shown in Figure 1.

The nodules were retrospectively divided into two groups based on the degree of iodized oil accumulation identified on non-contrast-enhanced CT performed immediately after TACE. In group A, a dense accumulation of iodized oil covered the whole tumor and the entire corona enhancement area. In group B, a dense accumulation of iodized oil covered the whole tumor but did not cover the entire corona enhancement area.

CTHA procedure

Double-phase CTHA was performed in all patients prior to TACE. After left brachial artery puncture, A 4-Fr catheter (FNSAC IV, Angiomaster; Terumo,

Tokyo, Japan) was selectively inserted into the proper, common, or replaced hepatic artery and CTHA was performed to identify tumor staining, corona enhancement, and the feeding arteries of the tumor. Examinations were performed using a 64 multidetector-row CT scanner (Aquilion CX; Canon, Tokyo, Japan). The imaging CT parameters were rotation time 0.5 s, beam collimation 64 × 0.5 mm, 0.5 mm slice thickness at 0.4 mm intervals, a tube voltage 120 kV, and volume EC. Helical scanning was initiated 6 or 7 s after the infusion of 13 ml iomeprol (iodine concentration 350 mg/mL; Iomeron, Eisai, Tokyo, Japan) diluted with 26 ml of saline into the common, proper, or replaced hepatic artery at a rate of 3 or 3.5 ml/s. The late-phase scanning was performed 40 s after the initiation of the infusion.

TACE procedure

All patients had a B-TACE using a 1.8-Fr microballoon catheter (Attendant Delta, Terumo, Tokyo, Japan) through a 4-Fr catheter. The microballoon catheter was placed as close to the tumor feeding artery as possible, and miriplatin (MIRIPLA; Dainippon-Sumitomo Pharmaceutical, Tokyo, Japan) suspended in iodized oil (Ultra-Fluid; Dainippon-Sumitomo Pharmaceutical) was injected into the tumor feeding artery under balloon occlusion. The doses of miriplatin were determined on the basis of tumor size, however. injections of miriplatin were stopped immediately before the flow ceased completely. The total amount of miriplatin per session was limited to 120 mg. This stage was followed by embolization with 1-mm gelatin sponge particles (Gerpart; Nippon Kayaku, Tokyo, Japan) crushed by pumping ten times with two 2.5-mL syringes and a three-way stopcock. If several tumor feeding arteries were confirmed, B-TACE was also performed through each artery.

Image evaluation

Double-phase CTHA images were evaluated to determine whether corona enhancement was depicted around the hypervascular tumor. When intranodular enhancement was observed on the early-phase CTHA and subsequently perinodular enhancement appeared on the late phase of CTHA, we determined that corona enhancement was positive in this study. we also measured the thickness of corona enhancement. Based on previous report[16], perinodular enhancement with or without irregular protrusions that was greater than 2 mm thickness was classified as thick corona enhancement, and flat perinodular enhancement that was less than or equal to 2 mm thick was classified as thin corona enhancement. In all patients, an unenhanced CT was performed immediately after TACE to check for iodized oil accumulation in the target nodules and the nodules were divided into group A or B based on the degree of iodized oil accumulation. Contrast-enhanced CT was performed 4 weeks after TACE for evaluation of the treatment effect. If no local tumor recurrence was identified, then contrast-enhanced CT or Gd-EOB-DTPA-enhanced MRI was performed every 3–4 months thereafter. Local tumor recurrence was judged when identifiable nodular enhancement in the arterial phase was seen in or adjacent to the treated tumor. In this study, two board-certified hepatologists (> 10 years of experience in abdominal CT) independently assessed the images of unenhanced CT, contrast-enhanced CT, Gd-EOB-DTPA enhanced MRI, and CTHA. If two hepatologists had different assessments, the final result of that particular investigation was obtained by consensus through discussion of them.

Statistical analysis

Data analyses were performed using EZR (Saitama Medical Center, Jichi Medical University, Saitama, Japan), a graphical user interface for R (The R Foundation for Statistical Computing, Vienna, Austria).

The significance of differences in background parameters was evaluated by the Mann-Whitney U test and Fisher exact test. Univariate and multivariate logistic regression analyses were performed to identify the factors correlated with local tumor recurrence. The main objective of this study was to investigate the relationship between embolization including corona enhancement area and local tumor recurrence in TACE, and thus, tumor recurrence rates were compared between group A and group B. The cumulative local recurrence rate was calculated using the Kaplan-Meier method and evaluated using the log-rank test. p values of less than 0.05 were considered to be a statistically significant difference.

Results

Group A had 36 cases and group B had 24 cases. The clinical characteristics of nodules are summarized in Table 1. Except for des-gamma-carboxy

TABLE 1. Clinical characteristics of nodules in group A and B

Clinical characteristics	Group A (n = 36)	Group B (n = 24)	*p* value
Age, years*	74 (70–79)	71 (64–79)	0.149
Gender, male/female	8/28	6/18	0.999
Etiology (HCV/HBV/Alcohol/Unknown)	16/8/8/4	9/5/6/4	0.912
Child-Pugh classification (A/B)	31/5	19/5	0.569
BCLC stage(0/A/B)	11/20/5	5/17/2	0.545
Size of tumor, mm*	14.5 (12–21.3)	15.5 (11–22)	0.757
Thickness of corona enhancement(≤ 2mm/>2mm)	17/19	10/14	0.793
AFP, ng/ml*	4.9 (2.6–10.6)	5.9 (2.7–14.1)	0.419
DCP, mAU/mL*	26.4 (17.0–49.2)	48.8 (25.3–153.9)	0.021
Usage of miriplatin, mg*	28 (20–38.5)	30 (22.4–51.5)	0.310

AFP = alpha-fetoprotein; BCLC = The Barcelona Clinic Liver Cancer Classification; DCP = des-gamma-carboxy prothrombin; HBV = hepatitis B virus; HCV = hepatitis C virus;

* = data are the median (interquartile range)

prothrombin, the baseline characteristics did not differ significantly between groups A and B.

In the total sample, local tumor recurrence was observed in 22 out of 60 cases (36.7%) and the cumulative 3-, 6-, 12-month tumor local recurrence rates for all cases were 10%, 20%, and 35% respectively. The median time to local recurrence was 167 days (range, 32–375 days). In group B, local tumor recurrence was observed in 18 out of 24 cases (75%) (Figure 2). Meanwhile, in group A, lo-

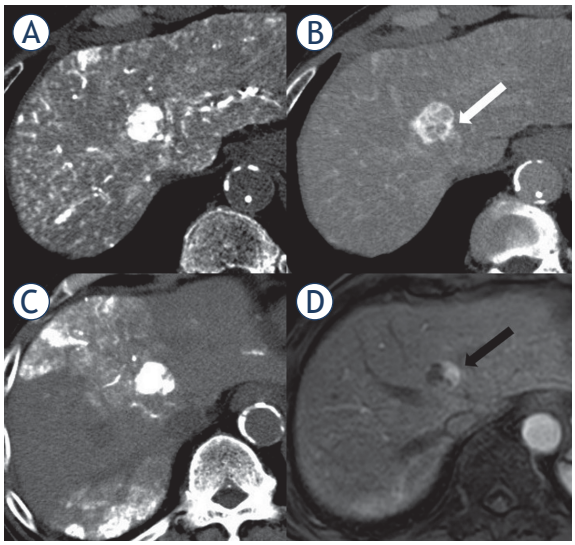

FIGURE 2. Local tumor recurrence after transcatheter arterial chemoembolization (TACE) in an 82-year-old patient with a hepatocellular carcinoma. **(A)** Early-phase computed tomography during hepatic arteriography (CTHA) demonstrated a hypervascular nodule in S5. **(B)** Late-phase CTHA demonstrated the corona enhancement around the tumor (white arrow). **(C)** Non-contrast-enhanced computed tomography performed immediately after TACE showed dense accumulation of iodized oil throughout the tumor, but not in the entire corona enhancement area. **(D)** In contrast enhanced magnetic resonance images obtained 4 months after TACE, local recurrence developed around the tumor (black arrow).

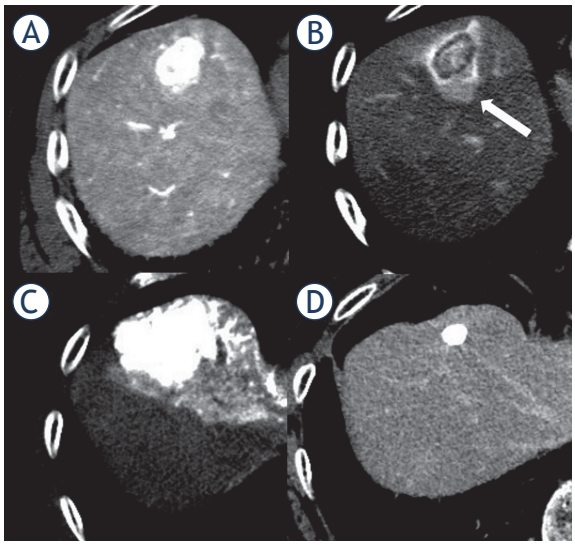

FIGURE 3. Complete response after transcatheter arterial chemoembolization (TACE) in a 77-year-old patient with a hepatocellular carcinoma. **(A)** Early-phase computed tomography during hepatic arteriography (CTHA) demonstrated a hypervacular nodule in S4. **(B)** Late-phase CTHA demonstrated the corona enhancement around the tumor (white arrow). **(C)** Non-contrast-enhanced computed tomography performed immediately after TACE showed dense accumulation of iodized oil beyond corona enhancement area. **(D)** Contrast-enhanced computed tomography performed 15 months after TACE showed no enhancement around the tumor.

TABLE 2. Univariate and multivariate logistic regression analysis for factor affecting local tumor recurrence

Factor	Univariate analysis		Multivariate analysis	
	Odds ratio (95% CI)	*p* value	Odds ratio (95% CI)	*p* value
Size of tumor (< 20 vs. ≥ 20 mm)	0.67 (0.20–2.32)	0.577		
AFP (< 10 vs. ≥ 10 ng/mL)	0.45 (0.13–1.61)	0.242		
DCP (< 40 vs. ≥ 40 mAU/mL)	0.59 (0.18–1.92)	0.417		
Usage of miriplatin (< 30 vs. ≥ 30 mg)	0.70 (0.17–1.89)	0.420		
Thickness of corona enhancement (≤ 2mm/ > 2mm)	0.97 (0.30–3.20)	0.999		
Degree of iodized oil accumulation (Group A vs. B)	0.045 (0.0080–0.20)	< 0.001	0.042 (0.010–0.17)	< 0.001

AFP = alpha-fetoprotein; CI = confidence interval; DCP = des-gamma-carboxy prothrombin

cal tumor recurrence was observed in only 4 out of 36 cases (11.1%), and most nodules had no local tumor recurrence (Figure 3). The cumulative 3-, 6-, 12-month tumor local recurrence rates were 2.8%, 2.8%, 8.3%, respectively for group A, and 20.8%, 45.8%, 75%, respectively for group B. The cumulative local tumor recurrence rates in group A were significantly lower than those in group B (hazard ratio [HR], 0.079; 95% confidence interval [CI], 0.026–0.24; $p < 0.001$) (Figure 4).

Univariate logistic regression analysis for prognostic factors affecting local tumor recurrence was performed for the following factors: the size of tumors, serum alpha-fetoprotein level, serum des-gamma-carboxy prothrombin level, usage of miriplatin, thickness of corona enhancement, and the degree of iodized oil accumulation (Group A or B). The degree of iodized oil accumulation only showed p values < 0.05 in univariate analysis. Multivariate analysis identified the degree of iodized oil accumulation as independent prognostic factors of local tumor recurrence ($p < 0.001$) (Table 2).

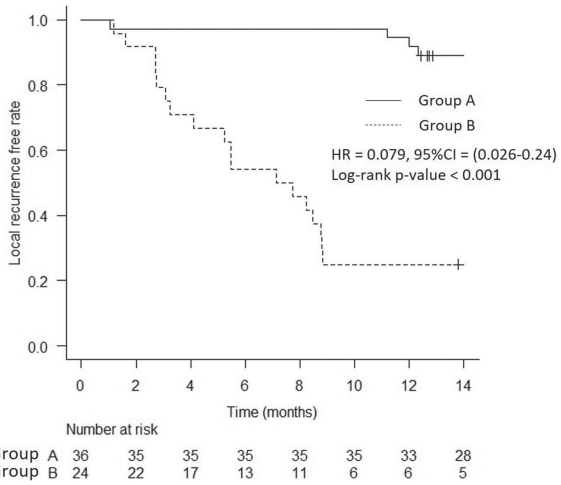

FIGURE 4. Local tumor recurrence-free rate according to the range of the embolization for transcatheter arterial chemoembolization (TACE). The cumulative 3-, 6-, 12-month tumor local recurrence rates were 2.8%, 2.8%, 8.3%, respectively, for cases with embolization of the entire corona enhancement area, and 20.8%, 45.8%, 75%, respectively, for cases without embolization of the entire corona enhancement area (hazard ratio [HR], 0.079; 95% confidence interval [CI], 0.026–0.24; $p < 0.001$).

Discussion

In this study, we investigated whether the embolization of not only the tumor but also the corona enhancement area could provide a better therapeutic effect for TACE. Our findings showed that the group with a dense embolization of HCC including the corona enhancement area had a significantly lower local tumor recurrence rate and a higher therapeutic effect than the group with a dense embolization of HCC itself but not including the corona enhancement area. Our study demonstrated a relationship between local recurrence following TACE and embolization of corona enhancement area.

HCC often has satellite lesions that cannot be diagnosed by imaging modalities.[7,8] Previous histopathological research reported that microsatellite lesions found in 46% of HCCs were smaller than 5 cm, and in 29% of HCCs, the lesions were smaller than 2.5 cm.[18] Another study reported that 28 of 149 resected specimens exhibited microsatellite lesions.[7] These reports indicate that it is important to embolize the tumor and the surrounding tissues by TACE. Miyayama *et al*. reported that local tumor recurrence developed in 29.1% of the sufficient margin group and 66.7% of the insufficient margin group after TACE, and embolization of the safety margin was important for local tumor control by

TACE.[9] Several other studies also reported that the safety margin of iodized oil during TACE resulted in a lower rate of local tumor recurrence.[10,11,19] Corona enhancement area determined by CTHA was reported to reflect the blood drainage area of HCC[16,20], and this finding served as the basis for this study. We considered that the corona enhancement area would be an accurate safety margin for TACE. Hirooka *et al*. reported that the cumulative local recurrence rate was significantly lower in the group that ablated the entire blood drainage area, depicted as the area of corona enhancement on CTHA, than in the group that did not by RFA (0, 0, and 1.5% *vs*. 3.8, 17.0, and 22.8% at 1, 3, and 5 years).[21] Although there are differences in the procedures of RFA and TACE, the results of this previous study are similar to those of our study, indicating that the corona enhancement area can be an accurate margin for HCC treatment. The thicker the corona enhancement, the larger the drainage area that requires embolization, but thickness of corona enhancement wasn't identified as independent prognostic factors of local tumor recurrence in this study. Therefore, we consider that the size of the drainage area cannot be a factor that makes embolization of the entire drainage.

The usefulness of CTHA, including cone-beam CTHA during the TACE procedure, has been reported because of its ability to offer relevant information for tumor identification, assessment of tumor feeding artery, and navigation guidance.[22-24] Moreover, it has become possible for the accurate identification of tumor feeding arteries in combination with guidance software[19], suggesting that CTHA will be performed more frequently during TACE. By performing not only the early phase of CTHA but also the late phase of CTHA and depicting the corona-like deep stain, CTHA can be used not only for tumor vessel identification and navigation guidance but also for determination of safety margin. As it requires two CT scans, in the early phase and in the delayed phase, it has the disadvantage of increasing the radiation exposure. However, since the therapeutic effect of TACE can be expected to increase, we consider that the benefits outweigh the risks for the patient. If conventional CT or cone-beam CT is performed before the end of the TACE procedure and accumulation of iodized oil to the corona enhancement area is insufficient, we believe that additional embolization should be performed considering the possibility of inadequate drug administration or the presence of the feeding artery. Whether the additional embolization will improve the treatment effect is an issue for further study.

Our study had several limitations. First, our study population was small and the study was retrospective. This limitation could have led to some patient selection bias. Moreover, as many tumors with relatively small diameters have been enrolled and only four tumors were larger than 30 mm in diameter in this study, it is unclear whether the same results as this study apply to large diameter tumors. Therefore, confirmation of our findings would require additional studies on large numbers of patients, including patients with large diameter tumors. Second, the observation period after TACE was relatively short. Longer-term observations may increase local recurrence rates. However, there was a large difference in local recurrence rates between the two groups, and it is considered that there is a significant difference between the two groups even after long-term observation. Third, as late-phase CTHA was not performed at a single-slice level, assessment of corona enhancement area may be slightly incorrect. In the nodules in which local tumor recurrence was recognized despite the assessment that the embolization was obtained throughout the corona enhancement area, the corona enhancement area may have been underestimated.

In conclusion, local tumor recurrence was significantly lower when embolizing not only the tumor itself but also the corona enhancement area, and corona enhancement area may be an accurate safety margin in TACE. Our results suggested that TACE should be continued until the embolic area covers the entire corona enhancement area.

References

1. Forner A, Reig M, Bruix J. Hepatocellular carcinoma. *Lancet* 2018; **391:** 1301-14. doi: 10.1016/S0140-6736(18)30010-2
2. Stefanini GF, Amorati P, Biselli M, Mucci F, Celi A, Arienti V, et al. Efficacy of transarterial targeted treatments on survival of patients with hepatocellular carcinoma. *Cancer* 1995; **75:** 2427-34. doi: 10.1002/1097-0142(19950515)75:10<2427::aid-cncr2820751007>3.0.co;2-j
3. Llovet JM, Bruix J. Systematic review of randomized trials for unresectable hepatocellular carcinoma: chemoembolization improves survival. *Hepatology* 2003; **37:** 429-42. doi: 10.1053/jhep.2003.50047
4. Lo CM, Ngan H, Tso WK, Liu CL, Lam CM, Poon RT, et al. Randomized controlled trial of transarterial lipiodol chemoembolization for unresectable hepatocellular carcinoma. *Hepatology* 2002; **35:** 1164-71. doi: 10.1053/jhep.2002.33156
5. Llovet JM, Real MI, Monyana X, Planas R, Coll S, Aponte J, et al. Arterial embolization or chemoembolization versus symptomatic treatment in patients with unresectable hepatocellular carcinoma: a randomized controlled trial. *Lancet* 2002; **359:** 1734-9. doi: 10.1016/S0140-6736(02)08649-X

6. European Association for the Study of the Liver. EASL Clinical Practice Guidelines: management of hepatocellular carcinoma. *J Hepatol* 2018, **69:** 182-236. doi: 10.1016/j.jhep.2018.03.019

7. Okusaka T, Okada S, Ueno H, Ikeda M, Shimada K, Yamamoto J, et al. Satellite lesions in patients with small hepatocellular carcinoma with reference to clinicopathologic features. *Cancer* 2002; **95:** 1931-7. doi: 10.1002/cncr.10892

8. Nakashima Y, Nakashima O, Tanaka M, Okuda K, Nakashima M, Kojiro M. Portal vein invasion and intrahepatic micrometastasis in small hepatocellular carcinoma by gross type. *Hepatol Res* 2003; **26:** 142-7. doi: 10.1016/s1386-6346(03)00007-x

9. Miyayama S, Yamashiro M, Hashimoto M, Hashimoto N, Ikuno M, Okumura K, et al. Comparison of local control in transcatheter arterial chemoembolization of hepatocellular carcinoma ≤ 6 cm with or without intraprocedural monitoring of the embolized area using cone-beam computed tomography. *Cardiovasc Intervent Radiol* 2014; **37:** 388-95. doi: 10.1007/s00270-013-0667-2

10. Kittipitch B, Keerati H, Teeravut T, Teerha P. Safety margin of embolized area can reduce local recurrence of hepatocellular carcinoma after superselective transarterial chemoembolization. *Clin Mol Hepatol* 2019; **25:** 74-85. doi: 10.3350/cmh.2018.0072

11. Kattipatanapong T, Nishiofuku H, Tanaka T, Sato T, Masada T, Tatsumoto S, et al. Improved local tumor control and survival rates by obtaining a 3D-safety margin in superselective transarterial chemoembolization for small hepatocellular carcinoma. *Cardiovasc Intervent Radiol* 2020; **43:** 423-33. doi: 10.1007/s00270-019-02365-9

12. Ueda K, Matsui O, Kawamori Y, Nakamura Y, Kadoya M, Yoshikawa J, et al. Hypervascular hepatocellular carcinoma: evaluation of hemodynamics with dynamic CT during hepatic arteriography. *Radiology* 1998; **206:** 161-6. doi: 10.1148/radiology.206.1.9423667

13. Ueda K, Matsui O, Kawamori Y, Kadoya M, Yoshikawa J, Gabata T, et al. Differentiation of hypervascular hepatic pseudolesions from hepatocellular carcinoma: value of single-level dynamic CT during hepatic arteriography. *J Comput Assist Tomogr* 1998; **22:** 703-8. doi: 10.1148/radiology.206.1.9423667

14. Inoue E, Fujita M, Hosomi N, Sawai Y, Hashimoto T, Kuroda C, et al. Double phase CT arteriography of the whole liver in the evaluation of hepatic tumors. *J Comput Assist Tomogr* 1998; **22:** 64-8. doi: 10.1097/00004728-199801000-00011

15. Matsui O, Ueda K, Kobayashi S, Sanada J, Terayama N, Gabata T, et al. Intra- and perinodular hemodynamics of hepatocellular carcinoma: CT observation during intra-arterial contrast injection. *Abdom Imaging* 2002; **27:** 147-56. doi: 10.1007/s00261-001-0091-y

16. Kitao A, Zen Y, Matsui O, Gabata T, Nakamura Y. Hepatocarcinogenesis: multistep changes of drainage vessels at CT during arterial portography and hepatic arteriography – radiologic-pathologic correlation. *Radiology* 2009; **252:** 605-14. doi: 10.1148/radiol.2522081414

17. Sakon M, Nagano H, Nakamori S, Dono K, Umeshita K, Murakami T, et al. Intrahepatic recurrences of hepatocellular carcinoma after hepatectomy: analysis based on tumor hemodynamics. *Arch Surg* 2002; **137:** 94-9. doi: 10.1001/archsurg.137.1.94

18. Sasaki A, Kai S, Iwashita Y, Hirano S, Ohta M, Kitano S. Microsatellite distribution and indication for locoregional therapy in small hepatocellular carcinoma. *Cancer* 2005; **103:** 299-306. doi: 10.1002/cncr.20798

19. Miyayama S, Yamashiro M, Sugimori N, Ikeda R, Okimura K, Sakuragawa. Outcomes of patients with hepatocellular carcinoma treated with conventional transarterial chemoembolization using guidance software. *J Vasc Interv Radiol* 2019; **30:** 10-8. doi: 10.1016/j.jvir.2018.08.009

20. Matsui O, Kobayashi S, Sanada J, Kouda W, Ryu Y, Kozaka K, et al. Hepatocellular nodules in liver cirrhosis: hemodynamic evaluation (angiography-assisted CT) with special reference to multi-step heptocarcinogenesis. *Abdom Imaging* 2011; **36:** 264-72. doi: 10.1007/s00261-011-9685-1

21. Hirooka M, Ochi H, Koizumi Y, Tokumoto Y, Hiraoka A, Kumagi T, et al. Local recurrence of hepatocellular carcinoma in the tumor blood drainage area following radiofrequency ablation. *Mol Clin Oncol* 2014: **2:** 182-6. doi: 10.3892/mco.2013.229

22. Takayasu K, Muramatsu Y, Maeda T, Iwata R, Furukawa H, Muramatsu Y, et al. Targeted transarterial oily chemoembolization for small foci of hepatocellular carcinoma using a unified helical CT and angiography system: analysis of factors affecting local recurrence and survival rates. *Am J Roentgenol* 2001; **176:** 681-8. doi: 10.2214/ajr.176.3.1760681

23. Tacher V, Radaelli A, Lin M, Geschwind JF. How I do it: conebeam CT during transarterial chemoembolization for liver cancer. *Radiology* 2015; **274:** 320-34. doi: 10.1148/radiol.14131925

24. Lee JH, Lee IJ, Kim HB, Park B, Kim BH, Park JW, et al. Efficacy and safety of transarterial chemoembolisation with cone-beam CT in patients with hepatocellular carcinoma within the Milan criteria: a retrospective cohort study. *Clin Radiol* 2019; **74:** 407.e19-407.e28. doi: 10.1016/j.crad.2019.01.024

25. Chiaradia M, Izamis ML, Radaelli A, Prevoo W, Maleux G, Schlachter T, et al. Sensitivity and reproducibility of automated feeding artery detection software during transarterial chemoembolization of hepatocellular carcinoma. *J Vasc Intervent Radiol* 2018; **29:** 425-31. doi: 10.1016/j.jvir.2017.10.025

research article

Pre-treatment risk assessment of women with endometrial cancer: differences in outcomes of molecular and clinical classifications in the Slovenian patient cohort

Jure Knez[1,2], Monika Sobocan[1,2], Urska Belak[1], Rajko Kavalar[3], Mateja Zupin[4], Tomaz Büdefeld[4], Uros Potocnik[4,5], Iztok Takac[1,2]

[1] Divison of Gynecology and Perinatology, University Medical Centre Maribor, Maribor, Slovenia
[2] Department of Obstetrics and Gynecology, Faculty of Medicine, University of Maribor, Maribor, Slovenia
[3] Department of Pathology, University Medical Centre Maribor, Maribor, Slovenia
[4] Centre for Human Molecular Genetics and Pharmacogenomics, Faculty of Medicine, University of Maribor, Maribor, Slovenia
[5] Faculty of Chemistry and Chemical Engineering, University of Maribor, Maribor, Slovenia

Radiol Oncol 2022; 56(1): 76-82.

Received 13 May 2021
Accepted 20 August 2021

Correspondence to: Assist. Monika Sobočan, M.D., Division for Gynecology and Perinatology, University Medical Centre Maribor, Ljubljanska ulica 5, SI-2000 Maribor, Slovenia. E-mail: monika.sobocan@gmail.com

Disclosure: No potential conflicts of interest were disclosed.

Background. The aim of this study was to evaluate changes in prognostic risk profiles of women with endometrial cancer by comparing the clinical risk assessment with the integrated molecular risk assessment profiling.

Patients and methods. This prospective study recruited patients with biopsy proven endometrial cancer treated at the University Medical Centre Maribor between January 2020 to February 2021. Patient clinical data was assessed and categorized according to the currently valid European Society of Gynaecological Oncology, European SocieTy for Radiotherapy and Oncology, and European Society of Pathology (ESGO/ESTRO/ESP) guidelines on endometrial cancer. Molecular tumour characterization included determination of exonuclease domain of DNA polymerase-epsilon (POLE) mutational status by Sanger sequencing and imunohistochemical specimen evaluation on the presence of mismatch repair deficiencies (MMRd) and p53 abnormalities (p53abn).

Results. Fourty-five women were included in the study. Twenty-two tumours were of non-specific mutational profile (NSMP) (56.4%), 13 were classified as MMRd (33.3%), 3 were classified as p53abn (7.7%) and 1 was classified as POLE mutated (2.6%). Six tumours (15.4%) had multiple molecular classifiers, these were studied separately and were not included in the risk assessment. The clinical risk-assessment classified 21 women (53.8%) as low-risk, 5 women (12.8%) as intermediate risk, 2 women as high-intermediate risk (5.1%), 10 women (25.6%) as high risk and 1 patient as advanced metastatic (2.6%). The integrated molecular classification changed risk for 4 women (10.3%).

Conclusions. Integrated molecular risk improves personalized risk assessment in endometrial cancer and could potentially improve therapeutic precision. Further molecular stratification with biomarkers is especially needed in the NSMP group to improve personalized risk-assessment.

Key words: endometrial cancer; molecular classification; risk assessment

Introduction

Endometrial cancer is the most common gynaecological malignancy, with an increasing incidence in the developed world.[1] Most endometrial carcinoma occur in post-menopausal women, however in rare cases they can also affect young women.[2] In most cases it is diagnosed in early disease stages. With current therapeutic approaches, patients achieve an overall survival (OS) from 74% to 91%.[1] Recently

published data[3] on 5-year OS of women with endometrial cancer in Slovenia shows a modest increase in survival between the years 2012–2016 (80.6%) as compared to between the years 1997–2001 (79.8%).[3] Endometrial carcinoma are divided, based on their histopathological characteristics, into Type I and Type II carcinoma. Type I carcinomas represent the majority of EC and are of endometrioid subtype. Type II carcinomas are a more hetereogenous group of histopathological subtypes and include clear-cell, serous, mixed histology tumours and carcinosarcomas.[4]

There is a constant need to improve the risk assessment for improved precision in endometrial cancer treatment. An important aim is to identify patients that experience disease reccurrence regardless of the primary early stage endometrial cancer diagnosis. In the last decade, the molecular classification of endometrial cancer has emerged as a feasible possibility to stratify risk in women with endometrial cancer.[5] The evaluated molecular classification showed, that determining the status of endometrial carcinoma tumours for: i) pathogenic variants of the exonuclease domain of DNA polymerase-epsilon *(POLE)*, ii) mismatch repair deficiency (MMRd) and iii) copy-number high *TP53* mutations, enables the determination of specific molecular endometrial cancer subtypes[6] that could be used in the risk of recurrence assessment.[4] Clinical trials showed that patients with *POLE* ultramutated (POLEmut) tumours had a 100% 10-year recurrence free survival (RFS) versus 80.1% in *POLE* wild type (POLEwt) patients.[7] The recent individual patient meta-analysis has shown that the outcome of POLEmut tumours is good regardless of traditional risk classifiers.[8] The prognosis is intermediate in MMRd tumours and significantly worse in p53 aberrant tumours.[9] This led to the incorporation of molecular classification to the recently updated European Society of Gynaecological Oncology, European SocieTy for Radiotherapy and Oncology, and European Society of Pathology (ESGO/ESTRO/ESP) guidelines for endometrial cancer. The current guidelines recommend the use of clinical risk assessment or an integrated clinico-molecular risk assessment, if available.[4]

The molecular risk assessment has been applied for interventions and assessments of adjuvant therapy management decisions.[9] Based on the current ESGO-ESTRO-ESP guidelines, women with low-risk EC do not need additional adjuvant therapy. For intermediate risk, radiotherapy has been suggested as the optimal course of treatment. In high-intermediate or some cases of intermediate risk, chemotherapy can be considered in addition to radiotherapy. The guidelines recommend for women with high risk EC to undergo radiotherapy with concurrent chemotherapy.[4] Abdulfatah *et al*., reported also the use of molecular classification on biopsy specimens which showed a high level of concordance to hysterectomy specimens and outperformed pre-treatment risk assessment based on histological specimen sample and grade.[10]

Based on the currently available guidelines we aimed to assess the changes that clinical and integrated molecular risk assessment represent in terms of primary patient management.

Patients and methods

Patients

This single centre study prospectively recruited consecutive women treated at the University Medical Centre Maribor (UMC Maribor), Slovenia. Participants were recruited from February 2020 to February 2021. Women were eligible to participate in this study if they had a biopsy-proven EC diagnosis and were candidates for surgical treatment.

Informed consent was obtained prior to surgical treatment from all study participants. This study was approved by the Slovenian Ethics Committee for Research in Medicine under the registration number 0120-40/2020/4 and was carried out in accordance to the Declaration of Helsinki.

Management plan and risk assessment

All included women underwent complete diagnostic work-up at our centre, which routinely includes a comprehensive transvaginal ultrasound (TVUS) scan to assess for disease extent. Based on the clinical assessment of myometrial involvement and disease extent, as well as histopathological tumour assessment, a clinical risk prediction was made. Afterwards, they were presented to the interdisciplinary tumour board to plan the optimal treatment. Standard treatment of early stage endometrial cancer is surgical and is most commonly performed by minimally invasive surgery, but open surgical approach is also an option. This depends on the tumour type and patient characteristics. Surgical treatment usually consists of total hysterectomy with bilateral salpingo-oophorectomy. This is most commonly combined with sentinel lymph node biopsy (SLN) or pelvic/paraaortic lymph node dissection (LND).

Molecular classification of endometrial cancer

The molecular risk-profile was determined according to current guidelines on endometrial cancer[4], based on determining the tumour *POLE* status, the mismatch repair decifiency status (MMRd) of the tumour as well as the p53 tumour expression status. For determining the *POLE* status of the tumour, DNA was isolated from tissue samples procured from the resected uterus by a pathologist. Tumor DNA was extracted from fresh frozen tissue using a QIAamp DNA Mini Kit (Qiagen GmbH, Hilden, Germany) according to the manufacturer's protocol. DNA purity and concentration were determined using a Synergy™ 2 spectrophotometer (Biotek, Winooski, VT, USA). Primers used for PCR amplification of selected exons 9, 12 and 13 of *POLE* were designed as described previously.[11] For amplification of target sequences, we used PCR technique which was performed using DreamTaq DNA Polymerase (Thermo Scientific, Vilnius, Lithuania). Briefly, 2 μL of 7 ng/ μL DNA was amplified using 8 μL mix of 1.0 μL DreamTaq buffer, 0.5 μL of each primer (10 μM), 0.2 μL dNTPs (10 mM each), 0.05 μL DreamTaq DNA polymerase (5 U/μL) and water in a final volume of 10 μL. Samples were subjected to incubation at 95°C for 5 min, then 38 amplification cycles of 95°C for 30 sec, 62°C for 30 sec and 72°C for 30 sec, and a final incubation at 72°C for 7 min using The *TProfessional Basic* Thermocycler (Biometra, Analytik Jena, Jena, Germany). The PCR products were visualised on 2% agarose gel electrophoresis excised from the gel and purified using a MinElute Gel Extraction Kit (Qiagen GmbH, Hilden, Germany) according to the manufacturer's protocol. Sanger sequencing was performed by Eurofins Genomics (Germany), and nucleotide sequences were manually analysed for the most frequent somatic mutations P286R, V411L, and S459F.[12]

MMRd status was determined by evaluating the immunohistochemical (IHC) markers (MLH1, MSH2, MSH6, PMS2). Previous research showed[13], that IHC markers represent an appropriate surrogate for screening for MMRd. The p53 protein expression status was evaluated using IHC expression according to current recommendations.[14]

Based on genetic and IHC data, women were grouped, according to the ESGO/ESTRO/ESP guidelines[5] into the following molecular classification groups: *POLE* mutated (POLEmut), MMRd, p53 abnormal (p53abn) or non-specific mutational profile (NSMP). If there were multiple molecular classifiers available for a patient, they were analysed separately.

Statistical analysis

Descriptive statistics were used to evaluate the distribution of each variable. Continuous variables were expressed as mean values with standard deviations. Categorical variables were reported as frequency or percentage. All statistical analyses were performed using SPSS software version 23.0 (IBM Corp., Armonk, NY, USA).

Results

Molecular characterisation was performed in all 45 women enrolled. Among them, 39 women (86.7%) were classified according to the current recommendations in one of the four molecular classification groups. Their characteristics are presented in Table 1. Six women (13.3%) had multiple molecular classifiers. The characteristics of these women are presented in Table 2.

Following the ESGO/ESTRO/ESP guidelines on risk assessment, women were classified according to the clinical risk assessment and the integrated molecular risk (Table 3). Most remained classified as low-risk endometrial cancer, reclassification changed for 4 women.

The risk profiles of three women decreased after integrated molecular risk classification: one was reclassified from high risk to high-intermediate risk and two from intermediate to low-risk. The risk profile of women changed from: i) intermediate to low risk as one woman had a POLEmut tumour, ii) from intermediate to low risk since it was of NSMP and iii) from high to high-intermediate (HIR) risk due to the MMRd classification. In one case, the risk profile increased from low to intermediate risk due to the detected p53abn mutation.

Primary surgical treatment

Surgical treatment was performed in all patients included in the study. The specifics of the treatment are presented in Table 4. Thirty women (77%) underwent a laparoscopic procedure and 9 women (23%) an open surgical procedure. The multidisciplinary (MDT) recommendation in cases of pre-operatively persumed low-risk disease is to perform sentinel lymph node biopsy (SLN). If the lymph nodes are not visualized, further LND is generally omitted. In cases of persumed intermediate risk,

the recommendation in case of SLN visualization failure is to perform LND.

The impact of molecular classification on treatment decisions

In the post-operative period two women (5.1%) died. Two women (5.1%) rejected the recommended adjuvant therapy. The final analysis was performed for 37 women as depicted in Figure 1.

Our study was observational and the molecular classification did not impact the MDT decision making. Two women which were re-classified from intermediate to low risk by the molecular classification received radiation therapy and one women that has been reclassified from high risk to HIR received radiotherapy and chemotherapy. One patient for whom the risk assesment increased from low to intermediate risk has been recommended no adjuvant treatment. In one patient of the intermediate risk group, the presence of co-morbidities led the MDT to suggest follow-up as the optimal strategy.

Discussion

In this study we assessed the risk of endometrial cancer for women using the clinical classification and the integrated molecular classification as suggested by the recent ESGO/ESTRO/ESP guide-

TABLE 1. Patient characteristics

Age at time of diagnosis (n = 39)		65.2 years (min 32 – max 86)
Body Mass Index at time of diagnosis (n = 36)		31 (17–43)
Reproductive history	Parity (median, range)	2 (0–5)
	Spontaneuos abortion (median, range)	0 (0–2)
Menopausal status	Pre-menopausal	5 (12.8%)
	Post-menopausal	34 (87.2%)
Tumour marker levels	CA125 (n = 32)	136.3 (min 2 – max 2084)
	CEA (n = 32)	3.4 (min 2 – max 17)
FIGO stage (n = 39)	IA	21 (54%)
	IB	8 (20.5%)
	II	1 (2.6%)
	IIIA	2 (5.1%)
	IIIB	2 (5.1%)
	IIIC1	3 (7.7%)
	IIIC2	1 (2.6%)
	IV	1 (2.6%)
Tumour type	Type 1	36 (92.3%)
	Type 2	3 (7.7 %)
Molecular tumour classification	POLEmut	1 (2.6%)
	MMRd	13 (33.3%)
	NSMP	22 (56.4%)
	p53abn	3 (7.7%)

MMRd = mismatch repair deficient tumour; NSMP = non-specific molecular profile tumour; p53abn = p53 expression abnormal tumour; POLE = DNA polymerase-epsilon; POLEmut = POLE ultramutated tumour

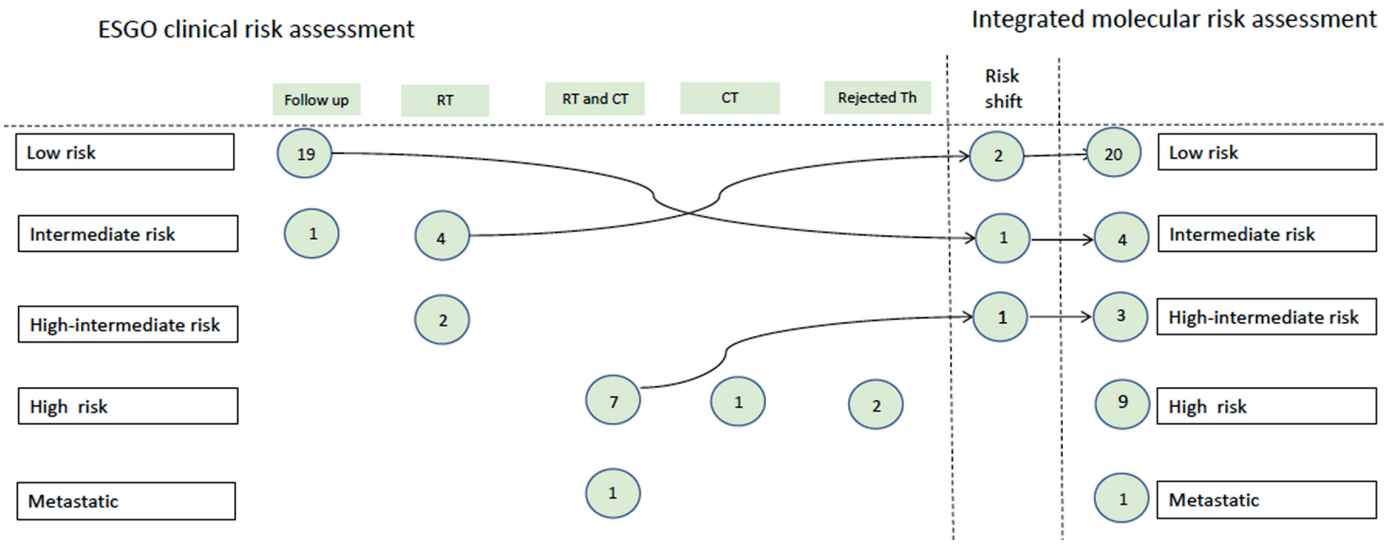

FIGURE 1. Potential impact of risk shifts on adjuvant therapy. Depicted in circles are the absolute numbers of women with endometrial cancer and their adjuvant therapy recommendations. Arrows point to a potential risk shift impacting therapy with the use of the molecular classification.

CT = chemotherapy; RT = radiotherapy

TABLE 2. Characteristics of patients with multiple molecular classifiers

	Age at time of diagnosis	Multiple-classifier EC	POLE variant	Tumor type	FIGO stage	Lymphovascular invasion	Clinical risk assessment
Patient 1	76	POLEmut and p53abn	P286R	endometrioid	IIIC2	Yes	High
Patient 2	75	POLEmut and p53abn	P286R	carcinosarcoma	IB	Yes	High
Patient 3	70	MMRd and p53abn	wild-type	endometrioid	IA	No	Low
Patient 4	87	MMRd and p53abn	wild-type	endometrioid	IIIB	Yes	High
Patient 5	53	POLEmut and p53abn	P286R	endometrioid	IA	No	Low
Patient 6	52	POLEmut and p53abn	P286R	endometrioid	IA	No	Intermediate

MMRd = mismatch repair deficient tumour; p53abn = p53 expression abnormal tumour; POLE = DNA polymerase-epsilon; POLEmut = POLE ultramutated tumour

TABLE 3. Risk assessment

		Number of patients (%)
ESGO Clinical Risk Group	Low risk	21 (53.8%)
	Intermediate risk	5 (12.8%)
	High-intermediate risk	2 (5.1%)
	High risk	10 (25.6%)
	Advanced metastatic	1 (2.6%)
Integrated molecular risk	Low risk	22 (56.4%)
	Intermediate risk	4 (10.3%)
	High-intermediate risk	3 (7.7%)
	High risk	9 (23.1%)
	Advanced metastatic	1 (2.6%)

ESGO = European Society of Gynaecological Oncology

lines. Out of 45 women enrolled in our study, the risk evaluation through integrated molecular risk groups was possible for 39 women. Six women had multiple molecular classifiers, which precluded further risk assessment using the current molecular classification. In the remaining group, assessment of molecular risk decreased in three and increased in one woman.

The classification of women with endometrial cancer into risk groups based on clinical and molecular data aims to improve individualised treatment according to the tumour biological potential. According to the currently valid guidelines[4], histopathological characteristics, including lymphvascular space invasion (LVSI) are the cornerstone of risk stratification. This is one of the reasons that shifts in risk groups between clinical and integrated molecular groups were present, as LVSI has been identified as an important marker of prognosis in low-risk endometrial cancer and is associated with adverse outcomes.[15] In comparison with a study of Oberndorfer *et al*.[16] which compared molecular risk with the guidelines on clinical risk assessment in endometrial cancer published in 2016[17], there were less shifts in the clinical risk assessment in our study. Therefore, by using the newly implemented clinical or integrated molecular risk assessment, comparable risk assessment is achieved. Our study is the first to compare the clinical and molecular risk stratification in the cohort of Slovenian patients. The clinical value of this approach needs to be verified in further prospective studies.

The nature of our study was observational and the molecular subtype was not taken into consideration for decision-making in regards to surgical

TABLE 4: Analysis of surgical treatment of women based on ESGO Clinical Risk Group assesment. SLN – sentinel lymph node biopsy, LND - lymphadenectomy

ESGO integrated molecular risk	Total number of women	Open surgery	Laparoscopic	SLN	LND	Unilateral SNB and contralateral LND	No LN treatment
Low risk	22 (56.4%)	2 (5.1%)	20 (51.3%)	18 (46.2%)	0	0	4 (10.3%)
Intermediate	4 (10.3%)	0	4 (10.3%)	3 (7.7%)	1 (2.6%)	0	0
HIR	3 (7.7%)	1 (2.6%)	2 (5.1%)	0	2 (5.1%)	1 (2.6%)	0
High	9 (23.1%)	5 (12.8%)	4 (10.3%)	2 (5.1%)	5 (12.8%)	2 (5.1%)	1 (2.6%)
Advanced	1 (2.6%)	1 (2.6%)	0	0	0	0	1 (2.6%)

HIR = high-intermediate risk; LND = lymphadenectomy; SLN = sentinel lymph node biopsy

or adjuvant therapy. Table 4 represents the surgical approach taken for women based on the pre-treatment assessment and the final ESGO Risk Group classification. The body of knowledge on using the integrated molecular classification for decision making on surgical treatment is scarce. Histopathological pre-operative evaluation might not always be concordant with post-operative diagnosis[18,19] and could potentially impact the MDT to suggest less invasive surgical procedures. This is especially true in recognizing serous EC. In these instances based on the molecular characteristics such as *TP53* mutations[20], integrated molecular evaluation could potentially enable individualized therapy already in the primary surgical setting.

Considering the changes in risk assessment for patients within our study, if using the integrated molecular assessment, two patients would most likely been recommended follow-up instead of radiotherapy, thus de-escalating their therapy based on their individual biological features. One patient would have been, based on her biological characteristics upgraded from low to intermediate risk. Especially in the low-intermediate and intermediate-high risk group, it is important to identify the patients correctly. Without appropriate adjuvant therapy, these patients were found to be at a approximately 30% higher risk than if adjuvant therapy was offered.[21] One of our patients was downgraded from high risk to the HIR risk group. While this individual has received radiotherapy and chemotherapy, this is also a valid strategy of treatment in the HIR risk group[4] and the decision process most likely would have not changed for her. Participants in our study have been mostly classified as NSMP (56.4%). NSMP tumours are currently classified in the low-risk or intermediate risk[4] based on a combination with other histopathological characteristics. As NSMP represents the largest group of currently classified tumours this shows the need for further refinements of molecular risk stratification.[22,23] A potential additional marker which has shown potential prognostic value, especially in the intermediate risk groups, is L1CAM expression[23,24] and in low risk endometrial cancer also mutation of *CTNNB1*.[25] Further evaluation of these and other novel markers could enable us to further individualise and stratify risk assessment in this large and clinically diverse group.[26]

An important consideration in our study is how to evaluate and incorporate risk assessment for women with multiple classifiers. There were six women with multiple classifiers in which four tumours were p53abn and POLEmut. Multiple classifiers MMRd and p53abn were present in two women. Recently, Leon-Castilo *et al*.[27] published data on their cohort of patients with multiple-classifier endometrial cancer. They supported the bioinformatic clustering of TCGA data which stated that MMRd-p53abn tumours mostly clustered around MMRd tumours and p53-POLEmut tumours mostly clustered around POLEmut tumours. Clinical outcomes showed that patients with MMRd-p53abn had a 5-year recurrence free survival (RFS) of 92.2% and patients with POLEmut-p53abn endometrial cancer a 5-year RFS of 94.1%.[27] This also supports the hypothesis that these tumours are biologically less aggressive than single classifier p53abn tumors, which had a 5-year RFS of 48%.[28] Further research and biomarker development is therefore needed to evaluate the appropriate approaches for patient treatment in cases of non-specific mutational profiles and multiple-classifiers.

The strength of our study is that it is the first prospectively designed study to evaluate the implementation of molecular risk stratification to endometrial cancer patients in Slovenia. The limitation is the low number of patients included. The follow-up data is not yet available and the clinical implications of this approach are yet to be determined.

Conclusions

The introduction of molecular risk stratification in the management of women with endometrial cancer represents a significant shift from the established clinical practice. Several adjustments to the routine workflow and significant additional resources are necessary in order to implement this approach to the clinics. Our data shows that in comparison to the current clinical risk stratification based on clinical and histopathological data, this may lead to change in management in a small proportion of women. The clinical value of this remains to be proven in further prospective studies. It is also important to note that the molecular risk stratification is not applicable to all women and refinements of the current classification with additional biomarkers are likely to improve and further de-escalate treatment in certain subtypes of endometrial cancer in the future.

Acknowledgement

The project was funded by the Institutional Research funding of UMC Maribor, reg. no IRP-

2019/02-13 and by the Slovenian Research Agency (research core funding P3-0067).

References

1. Morice P, Leary A, Creutzberg C, Abu-Rustum N, Darai E. Endometrial cancer. *Lancet* 2016; **387:**1094-108. doi: 10.1016/S0140-6736(15)00130-0
2. Repše-Fokter A. Endometrial cancer in young woman. *Acta Medico–Biotechnica* 2020; **13:** 60-4.
3. Zadnik V, Zagar T, Lokar K, Tomsic S, Konjevic AD, Zakotnik B. Trends in population-based cancer survival in Slovenia. *Radiol Oncol* 2021; **55:** 42-9. doi: 10.2478/raon-2021-0003
4. Concin N, Matias-guiu X, Vergote I, Cibula D, Mirza MR, Marnitz S, et al. ESGO / ESTRO / ESP Guidelines for the management of patients with endometrial carcinoma. *Int J Gynecol Cancer* 2021; **31:** 12-39. doi: 10.1136/ijgc-2020-002230
5. Urick ME, Bell DW. Clinical actionability of molecular targets in endometrial cancer. *Nat Rev Cancer* 2019; **19:** 510-21. doi: 10.1038/s41568-019-0177-x
6. Cancer Genome Atlas Research Network, Kandoth C, Schultz N, et al. Integrated genomic characterization of endometrial carcinoma. *Nature* 2013; **497:** 67-73. doi: 10.1038/nature12113
7. Wortman BG, Creutzberg CL, Putter H, Jürgenliemk-Schulz IM, Jobsen JJ, Lutgens LCHW, et al. Ten-year results of the PORTEC-2 trial for high-intermediate risk endometrial carcinoma: improving patient selection for adjuvant therapy. *Br J Cancer* 2018; **119:** 1067-74. doi: 10.1038/s41416-018-0310-8
8. McAlpine JN, Chiu DS, Nout RA, Church DN, Schmidt P, Lam S, et al. Evaluation of treatment effects in patients with endometrial cancer and POLE mutations: An individual patient data meta-analysis. *Cancer* 2021; **26:** 5400-10. doi: 10.1002/cncr.33516
9. Vermij L, Smit V, Nout R, Bosse T. Incorporation of molecular characteristics into endometrial cancer management. *Histopathology* 2020; **76:** 52-63. doi: 10.1111/his.14015
10. Abdulfatah E, Wakeling E, Sakr S, Al-Obaidy K, Bandyopadhyay S, Morris R, et al. Molecular classification of endometrial carcinoma applied to endometrial biopsy specimens: Towards early personalized patient management. *Gynecol Oncol* 2019; **154:** 467-74. doi: 10.1016/j.ygyno.2019.06.012
11. Malentacchi F, Turrini I, Sorbi F, Projetto E, Castiglione F, Vergoni F, et al. Identification of a gene panel for endometrioid endometrial cancer: a possible prognostic value? *Reprod Sci* 2020; **27:** 592-8. doi: 10.1007/s43032-019-00059-8
12. McAlpine J, Leon-Castillo A, Bosse T. The rise of a novel classification system for endometrial carcinoma; integration of molecular subclasses. *J Pathol* 2018; **244:** 538-49. doi: 10.1002/path.5034
13. Raffone A, Travaglino A, Cerbone M, Guida M, Insabato L, Zannoni GF, et al. Diagnostic accuracy of immunohistochemistry for mismatch repair proteins as surrogate of microsatellite instability molecular testing in endometrial cancer. *Pathol Oncol Res* 2020; **26:** 1417-27. doi: 10.1007/s12253-020-00811-5
14. Köbel M, Ronnett BM, Singh N, Soslow RA, Gilks CB, McCluggage WG. Interpretation of P53 immunohistochemistry in endometrial carcinomas. *Int J Gynecol Pathol* 2019; **38:** S123-S131. doi: 10.1097/PGP.0000000000000488
15. Ayhan A, Şahin H, Sari ME, Yalçin I, Haberal A, Meydanli MM. Prognostic significance of lymphovascular space invasion in low-risk endometrial cancer. *Int J Gynecol Cancer* 2019; **29:** 505-12. doi: 10.1136/ijgc-2018-000069
16. Oberndorfer F, Moling S, Hagelkruys LA, Grimm C, Polterauer S, Sturdza A, et al. Risk reclassification of patients with endometrial cancer based on tumor molecular profiling: First real world data. *J Pers Med* 2021; **11:** 1-11. doi: 10.3390/jpm11010048
17. Colombo N, Creutzberg C, Amant F, Cibula D, Mirza MR, Marnitz S, et al. ESMO-ESGO-ESTRO consensus conference on endometrial cancer. *Int J Gynecol Cancer* 2016; **26:** 2-30. doi: 10.1097/igc.0000000000000609
18. Han G, Sidhu D, Duggan MA, Arseneau J, Cesari M, Clement PB, et al. Reproducibility of histological cell type in high-grade endometrial carcinoma. *Mod Pathol* 2013; **26:** 1594-604. doi: 10.1038/modpathol.2013.102
19. Sobočan M, Ogrizek AM, Ledinek T, Takač I, Knez J. Importance of preoperative ultrasound examination and pathological tumour evaluation in the management of women with endometrial cancer. *Eur J Obstet Gynecol Reprod Biol* 2021; **257:** 121-126. doi: 10.1016/j.ejogrb.2020.12.029
20. Bogani G, Ray-Coquard I, Concin N, Ngoi NYL, Morice P, Enomoto T, et al. Uterine serous carcinoma. *Gynecol Oncol* 2021; 1**62:** 226-34. doi: 10.1016/j.ygyno.2021.04.029
21. Van Den Heerik ASVM, Horeweg N, De Boer SM, Bosse T, Creutzberg CL. Adjuvant therapy for endometrial cancer in the era of molecular classification: radiotherapy, chemoradiation and novel targets for therapy. *Int J Gynecol Cancer* 2021; **31:** 594-604. doi: 10.1136/ijgc-2020-001822
22. Talhouk A, McConechy MK, Leung S, Li-Chang HH, Kwon JS, Melnyk N, et al. A clinically applicable molecular-based classification for endometrial cancers. *Br J Cancer* 2015; **113:** 299-310. doi: 10.1038/bjc.2015.190
23. Kommoss FKF, Karnezis AN, Kommoss F, Talhouk A, Taran FA, Staebler A, et al. L1cam further stratifies endometrial carcinoma patients with no specific molecular risk profile. *Br J Cancer* 2018; **119:** 480-6. doi: 10.1038/s41416-018-0187-6
24. Weinberger V, Bednarikova M, Hausnerova J, Ovesna P, Vinklerova P, Minar L, et al. A novel approach to preoperative risk stratification in endometrial cancer: The added value of immunohistochemical markers. *Front Oncol* 2019; **9:** 1-13. doi: 10.3389/fonc.2019.00265
25. Imboden S, Tapia C, Scheiwiller N, Kocbek V, Altermatt HJ, Janzen J et al. Early-stage endometrial cancer, CTNNB1 mutations, and the relation between lymphovascular space invasion and recurrence. *Acta Obstet Gynecol Scand* 2020; **99:** 196-203. doi: 10.1111/aogs.13740
26. Kolehmainen A, Pasanen A, Tuomi T, Koivisto-Korander R, Butzow R, Loukovaara M. Clinical factors as prognostic variables among molecular subgroups of endometrial cancer. *PLoS One* 2020; **15:**1-12. doi: 10.1371/journal.pone.0242733
27. León-Castillo A, Gilvazquez E, Nout R, Smit VT, McAlpine JN, McConechy M, et al. Clinicopathological and molecular characterisation of 'multiple-classifier' endometrial carcinomas. *J Pathol* 2020; **250:** 312-22. doi: 10.1002/path.5373
28. Leon-Castillo A, De Boer SM, Powell ME, Mileshkin LR, Mackay HJ, Leary A, et al. Molecular classification of the PORTEC-3 trial for high-risk endometrial cancer: Impact on prognosis and benefit from adjuvant therapy. *J Clin Oncol* 2020; **38:** 3388-97. doi: 10.1200/JCO.20.00549

research article

Cystatin C and cystatin SN as possible soluble tumor markers in malignant uveal melanoma

Maria A. Dikovskaya[1,2], Galina S. Russkikh[3], Konstantin V. Loktev[4], Thomas P. Johnston[5], Margarita M. Gevorgyan[1], Natalya P. Voronina[1], Valery V. Chernykh[2], Alexander N. Trunov[2,4], Tatiana A. Korolenko[1]

[1] Scientific Research Institute of Neurosciences and Medicine, Novosibirsk, Russia
[2] The S. Fyodorov Eye Microsurgery Federal State Institution, Novosibirsk Branch. Novosibirsk, Russia
[3] Federal Research Center of Fundamental and Translational Medicine, Institute of Biochemistry, Novosibirsk, Russia
[4] Federal State Budget Scientific Institution, Federal Research Center of Fundamental and Translational Medicine, Novosibirsk, Russia
[5] Division of Pharmacology and Pharmaceutical Sciences, School of Pharmacy, University of Missouri-Kansas City, Kansas City, Missouri, USA

Radiol Oncol 2022; 56(1): 83-91.

Received 16 August 2021
Accepted 21 October 2021

Correspondence to: Prof. Tatiana A. Korolenko, Ph.D., Scientific Research Institute of Neurosciences and Medicine. Timakov St., 4, 630117 Novosibirsk, Russia. E-mail: t.a.korolenko@physiol.ru

Disclosure: No potential conflicts of interest were disclosed.

Background. The aim of the study was to determine the concentration of endogenous cystatin C and cystatin SN, as potential tumor biomarkers, in the serum and biological fluids of the eye in both healthy controls and patients with uveal melanoma.

Patients and methods. The concentration of both cystatins was determined in the intraocular fluid (IOF), tear fluid, and serum of patients with uveal melanoma and compared to baseline measurements in IOF, tears, serum, cerebral spinal fluid, saliva and urine of healthy controls.

Results. The concentration of cystatin C in all the biological matrices obtained from healthy controls significantly exceeded the concentration of cystatin SN and was independent of gender. Cystatin C concentrations in the tear fluid of patients with uveal melanoma (both the eye with the malignancy, as well as the contralateral, non-affected eye), were significantly greater than cystatin C concentrations in the tear fluid of healthy controls and was independent of tumor size. The concentration of cystatin SN in IOF of patients with uveal melanoma was significantly less than the corresponding concentration of cystatin SN in healthy controls.

Conclusions. The ratio of cystatins (CysC:CysSN) in both the serum and tear fluid, as well as the concentration of cystatin SN in IOF, would appear to strongly suggest the presence of uveal melanoma. It is further suggested that multiple diagnostic criteria be utilized if a patient is suspected of having uveal melanoma, such as determination of the cystatin C and cystatin SN concentrations in serum, tears, and IOF, ocular fundus and ultrasound imaging, and biopsy with histopathological evaluation.

Key words: uveal melanoma; cystatins; biomarkers; diagnosis

Introduction

Uveal melanoma frequently leads to progression of the malignancy and subsequent metastasis, which often results in death in patients with metastatic disease. The methods developed for the treatment of uveal melanoma consist of either removing the affected eye (enucleation), or complex ocular therapies (brachytherapy, laser photocoagulation, heat therapy, proton therapy, *etc.*).[1,2]

Despite advances in the diagnosis and treatment of uveal melanoma, mortality 5 years after enucleation of the eye is 16.5%; after 10 years, it is 58%. Extra-scleral germination significantly worsens the prognosis; in fact, in these patients, the mortality reaches 69–73% after 10 years.[3,4] According to recent results of large-scale studies in the United States with more than 7500 patients with uveal melanoma, the risk of metastasis and death increases significantly with each stage of cancer diagnosis. For example, Stage T1 (2 times), Stage T2 (4 times), and Stage T3 (8 times).[5,6]

Uveal melanoma, arising from melanocytes in the stroma, is the most common primary intraocular tumor in adults.[7,8] Detection of specific proteins allows for the identification of possible molecular markers of malignancy in several eye diseases. Specific tear proteins (~ 64 of 491 proteins), studied by proteome analysis and gel electrophoresis, are classified as proteases and protease inhibitors and carry special significance in the context of eye malignancies. Mammalian cystatins (to date, there are 12 known human cystatins) include a large family of proteins that have the ability to inhibit cysteine proteases[9,10], which are further divided into three types based on their molecular structure and distribution in the body.[11]

As just mentioned, cystatins can be categorized into three types. The first type (*e.g.*, cystatins A and B) are intracellular cystatins (stefins). The second type (*e.g.*, cystatins C, D, E/M, F, G, S, SN, SA) are extracellular cystatins. Finally, the third type of cystatins (*e.g.*, L-kininogen, H-kininogen) are intravascular proteins.[12] Cystatin SN has not been thoroughly studied to date[13], whereas, the most well-known cystatin, cystatin C, was the first to be identified and its amino acid sequence determined.[14,15] Subsequently, the functions of cystatin C, as an inhibitor of cysteine proteases, was investigated, as well as its role in cell proliferation, migration, aging, and cell death.[16,17]

Cystatins are endogenous and reversible inhibitors of cysteine peptidases that are important players in cancer progression.[18-20] Importantly, cystatin C plays a significant role in the physiological functions of eye fluids[12], as well as in the pathological processes associated with a number of eye tumors.[21-23] As an example, in 2009, Paraoan *et al*. reported that for one particular lysosomal cysteine protease (cathepsin S), there was an increase in the active form of this protease that was not counterbalanced by the expression of its strongest endogenous inhibitor (cystatin C) in an aggressive, highly-metastatic form of uveal melanoma.[24] The imbalance in cathepsin S and its inhibitor (cystatin C) is both relevant and important in the context of uveal melanoma, because it may provide a link to therapeutic anti-cancer strategies based on targeting the elastolytic and collagenolytic activity of cysteine cathepsins, as well as add to our understanding of the dysregulation in proteolytic activity that occurs in uveal melanoma.[24]

As previously mentioned, a large number of proteases and protease inhibitors have been identified among the 491 proteins in the tear fluid proteome.[25] Changes in the composition of tear proteins are associated with a number of inflammatory, degenerative, and malignant eye diseases.[26,27] In fact, the balance between proteases and protease inhibitors is important for controlling the rates of cellular metabolism and the barrier function of the eye cornea.[25] Furthermore, changes in the biological fluids of the eye are related to the ratio of proteases and protease inhibitors[27-29], which can affect the composition of proteins and peptides in the lacrimal fluid. Thus, it would seem reasonable to assume that the identification of specific proteins in the biological fluids of the eye may make it possible to identify new molecular markers for several eye diseases.

The precise role of cysteine protease inhibitors in the development of eye tumors has not been fully elucidated to date.[30-32] This is significant to ophthalmology, because some of these inhibitors may be of therapeutic benefit for the treatment of eye tumors. Thus, the aim of this study was to investigate the concentration of endogenous inhibitors of cysteine proteases; namely, cystatin C and cystatin SN, in the serum and the biological fluids of the eye in both healthy controls and patients with uveal melanoma.

Patients and methods

Patients and the collection of various biological matrices/fluids

All studies were carried out with informed consent of patients and in accordance with the ethical norms of the Helsinki Declaration (2000) and local regulations (Russian Council of Medical Research). The protocols were approved by the Institutional Review Board of biomedical ethics of the S. Fyodorov Eye Microsurgery Federal State Institution, Novosibirsk Branch (Protocol N4, 15.11.2017). Lastly, all the patients gave their informed consent for laboratory tests, as well as consent to process their personal data for scientific purposes.

Fifty-seven patients (mean age = 56.6 ± 2.4 years) with a diagnosis of choroidal melanoma in the Novosibirsk Branch of the S. Fyodorov Eye Microsurgery Federal State Institution were included in this investigation. The control group consisted of 37 healthy individuals (medical staff of the clinic and students of the Medical University, with a mean age = 31.0 ± 4.1 years for the subjects ≤ 60 years old [*i.e.*, n = 28 (n = 13 healthy controls ≤ 40 years old + n = 15 healthy controls 41–60 years old)]. Of the 37 healthy controls, 20 were men and 17 were women, with 9 control subjects over 60 years old. Since the literature indicates that the serum levels of cystatin C increase with age in normal healthy individuals, and especially after the age of 60 years[33-36], we selected a subgroup of the healthy individuals (41–60 years; mean age = 53.1 ± 3.4 years; n = 15) as an age-matched control group to facilitate appropriate statistical comparisons with choroidal melanoma patients. Intraocular fluid (IOF) was obtained from 7 control patients (3 men and 4 women) close to, but not exceeding 60 years of age, undergoing an uncomplicated cataract removal procedure and submitted for biochemical analysis.

Tears from the conjunctival sac were collected by microcannulas and blood from the ulnar vein. Specifically, the tear fluid was obtained from the lower conjunctival arch of the eye and placed into a dry, sealed tube of 300–500 microliters. To evaluate the IOF in patients with ocular melanoma, moisture in the anterior chamber of the enucleated eye was obtained during the operation.

Samples of cerebrospinal fluid were obtained from 8 additional patients in the Federal State Budget Institute ("Federal Neurosurgical Center", Novosibirsk, Russia) as part of a standard examination for neurosurgical patients without tumors.

An exclusion-criteria relevant to this study was the value of the estimated glomerular filtration rate (eGFR). Since the levels of cystatin C in various biological fluids could potentially be affected by overall kidney function, patients with an eGFR value less than 90 mL/min/1.73 m^2 were excluded from the present study to control for this variable.

Analysis of cystatins in biological fluids

The concentration of cystatin C in biological fluids was evaluated using ELISA kits for human cystatin C (BioVendor, Czechia). The measurements were performed using a biochemical analyzer AU 480 (Beckman Coulter, USA).

The concentration of cystatin SN was also determined using commercial ELISA kits for human cystatin SN (Cusabio, China). The measurements were conducted using a Stat Fax 2100 microplate reader for enzyme immunoassay (Awareness Technology Inc., USA) at 450 nm.

TABLE 1. Concentrations of cystatin C and cystatin SN in biological fluids of healthy individuals as a function of age (Mean ± s.d.)

Groups	Inhibitor	Serum (ng/mL)	Tears (ng/mL)	IOF (ng/mL)
Healthy (≤ 40 years) [n = 13]	Cystatin C Cystatin SN	561 ± 10.0 2.24 ± 0.20	296 ± 11.1 0.49 ± 0.30	-
Healthy (41–60 years) [n = 15]	Cystatin C Cystatin SN	539 ± 111 2.96 ± 0.70	256 ± 82.3 0.6 ± 0.35	414 ± 28 2.7 ± 1.40
Healthy (61–80 years) [n = 9]	Cystatin C Cystatin SN	[a]1,341 ± 177 [b]4.77 ± 0.10	382 ± 116 0.75 ± 0.14	[a]844 ± 113 2.18 ± 0.20

a = significantly greater ($p < 0.01$) cystatin C concentration in serum and IOF compared to individuals ≤ 60 years; b = significantly greater ($p < 0.01$) cystatin SN concentration in serum compared to individuals ≤ 60 years; IOF = Intraocular fluid; s.d. = standard deviation

Statistical analysis

All acquired data were reported as the mean ± the standard deviation (s.d.). Mean values were analyzed for statistically significant differences with the software program STATISTICA 10.0 using a one-way, analysis-of-variance (ANOVA). *Post-hoc* analysis of ANOVA testing was performed using the Least Significant Difference (LSD) test. When comparing only two mean values, we used the Student's *t*-test to identify a difference that was statistically significant. All statistical results using either ANOVA, or the Student's *t*-test, in which $p < 0.05$ were deemed statistically significantly different and were noted in the Figures, as well as in Table 1.

Results

Eye imaging

Figure 1A shows a typical image of the ocular fundus of a normal eye as compared to an eye with a choroidal melanoma having a thickness of 2.4 mm and a diameter of 8 mm. The thickness of the choroidal melanoma was also determined from an ultrasound image as shown in Figure 1B and was determined to be 3.1 mm.

Concentration of cystatin C and cystatin SN in various biological matrices in healthy individuals (controls)

Figure 2 shows the concentration of cystatin C in various biological matrices (cerebral spinal

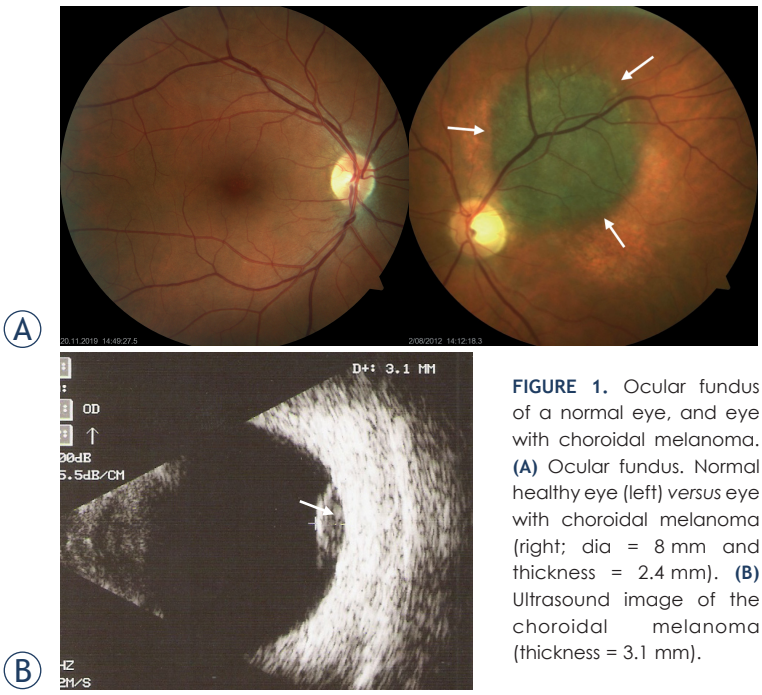

FIGURE 1. Ocular fundus of a normal eye, and eye with choroidal melanoma. **(A)** Ocular fundus. Normal healthy eye (left) *versus* eye with choroidal melanoma (right; dia = 8 mm and thickness = 2.4 mm). **(B)** Ultrasound image of the choroidal melanoma (thickness = 3.1 mm).

fluid [CSF], saliva, serum, IOF, tears, and urine) in healthy individuals, while Figure 3 depicts the concentration of cystatin SN in these same biological matrices. In general, it was found that the concentration of cystatin C in all the biological matrices significantly exceeded the concentration of cystatin SN in the same matrices (Figure 2 *vs.* Figure 3). Additionally, the rank order of cystatin C concentrations in the various biological fluids followed the order CSF > saliva > serum > IOF > tears > urine (Figure 2), whereas, for cystatin SN, the rank order was saliva > urine > CSF > serum > IOF > tears (Figure 3).

The concentration of cystatin C and cystatin SN in three relevant biological fluids (serum, tears, and IOF) was determined for three different age groups to assess whether there was an age-dependent variation in the concentration of these two inhibitors (Table 1). As was determined with the concentrations of cystatin C and cystatin SN in the six biological fluids of healthy individuals (Figure 2 and 3), there was a significantly greater concentration of cystatin C relative to cystatin SN in the serum, tears, and IOF (Table 1). While we determined that there was no gender difference observed between the concentration of each inhibitor in each age group for each of the three biological fluids mentioned above, there was a significant ($p < 0.01$) elevation in the serum concentration of both cystatins in healthy individuals (age 61–80 years) when compared to individuals less than or equal to 60 years of age (Table 1). This finding was also observed for IOF, but only for cystatin C and not cystatin SN (Table 1).

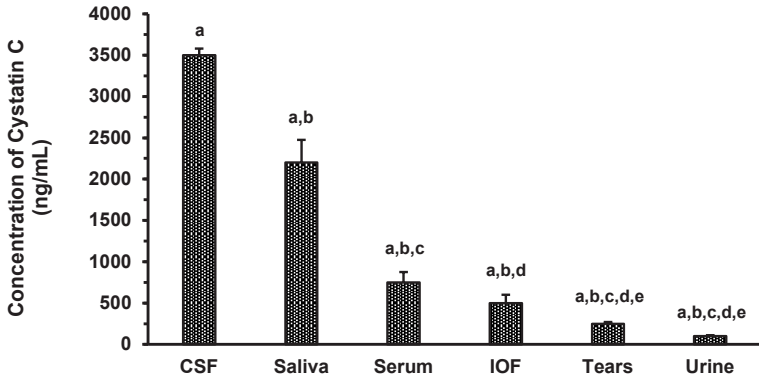

FIGURE 2. Cystatin C concentration in various biological matrices in healthy individuals. Concentration of cystatin C in each biological fluid (mean ± standard deviation [s.d.]; n = 28 [n = 13 healthy controls ≤ 40 years old + n = 15 healthy controls 41–60 years old]), since Table 1 shows a significant increase in cystatin C concentrations in serum and intraocular fluid (IOF) in 61–80 year old healthy controls, and thus, this age group was not included; cerebral spinal fluid (CSF) was obtained from an additional and separate group of cancer-free neurosurgical patients (n = 8) for the determination of the cystatin C concentration as described in the Materials and methods section.

[a] Significant difference ($p < 0.001$) from mean values indicated with the same letter.

[b] Significant difference ($p < 0.001$) from mean values indicated with the same letter.

[c] Significant difference ($p < 0.01$) from mean values indicated with the same letter.

[d] Significant difference ($p < 0.01$) from mean values indicated with the same letter.

[e] Significant difference ($p < 0.01$) from the mean value indicated with the same letter.

Cystatin C and cystatin SN concentrations and their ratio in the serum and tear fluid of patients with uveal melanoma

Cystatin C levels were significantly ($p < 0.01$) greater in both serum and tear fluid in patients with uveal melanoma when compared to healthy controls (Figure 4A). However, with regard to the concentration of cystatin SN in these same two biological fluids, there was only a significant ($p < 0.01$) decrease in the concentration of cystatin SN in the serum of patients with uveal melanoma compared to healthy controls (Figure 4B). Importantly, the ratio of cystatin C to cystatin SN (CysC:CysSN) in both serum and tear fluid was significantly ($p < 0.001$) increased in patients with uveal melanoma when compared to corresponding mean values of this ratio in healthy controls (Figure 4C).

As an aside, we also determined the inhibitor with higher concentrations in all biological fluids tested in this study; namely, cystatin C, for its prevalence in the tear fluid of patients with dif-

ferent size uveal melanoma tumors. The cystatin C concentrations in the tear fluid of patients with uveal melanoma (both the eye with the malignancy, as well as the contralateral, non-affected eye), were significantly ($p < 0.05$) greater than cystatin C concentrations determined in the tear fluid of healthy controls (*i.e.*, range of 450–500 ± 60 ng/mL in the diseased eye with uveal melanoma *vs.* 250 ± 25 ng/mL in both eyes of healthy controls) and was independent of tumor size. Moreover, at the time of clinical presentation, there was no significant difference between the cystatin C concentration in the tear fluid of the malignant eye *versus* the corresponding concentration of cystatin C in the tear fluid of the contralateral, non-affected eye regardless of tumor size (data not shown).

Concentration of cystatin C and cystatin SN in IOF of patients with uveal melanoma versus healthy controls

Figure 5A shows the concentrations of cystatin C in IOF in healthy controls and patients with uveal melanoma, while Figure 5B shows the concentration of cystatin SN in these same two patient cohorts. There was no significant difference between the concentration of cystatin C in IOF of healthy controls and patients with uveal melanoma, but there was a significant ($p < 0.001$) reduction in the concentration of cystatin SN in IOF of patients with uveal melanoma when compared to this same parameter in healthy controls.

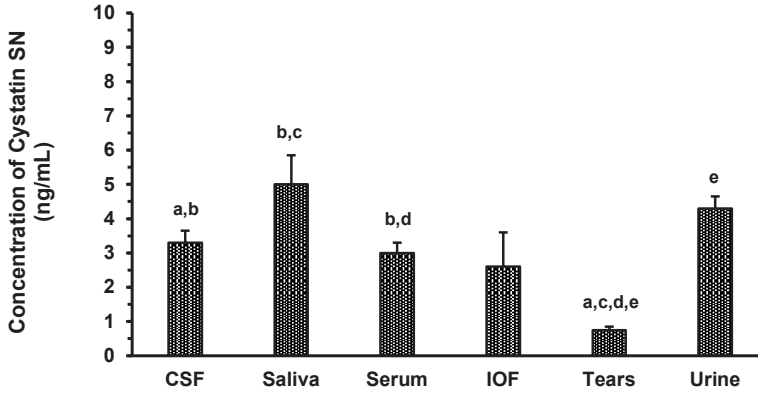

FIGURE 3. Cystatin SN concentration in various biological matrices in healthy individuals. Concentration of cystatin SN in each biological fluid (mean ± standard deviation [s.d.]; n = 28 [n = 13 healthy controls ≤ 40 years old + n = 15 healthy controls 41–60 years old]), since Table 1 shows a significant increase in the cystatin SN concentration in the serum of 61–80 year old healthy controls, and thus, this age group was not included; cerebral spinal fluid (CSF) was obtained from an additional and separate group of cancer-free neurosurgical patients (n = 8) for the determination of the cystatin SN concentration as described in the Materials and methods section.

[a] Significant difference ($p < 0.001$) from the mean value indicated with the same letter.

[b] Significant difference ($p < 0.05$) from mean values indicated with the same letter.

[c] Significant difference ($p < 0.001$) from the mean value indicated with the same letter.

[d] Significant difference ($p < 0.01$) from the mean value indicated with the same letter.

[e] Significant difference ($p < 0.001$) from the mean value indicated with the same letter.

Discussion

The present study has addressed the question as to whether cystatin C and/or cystatin SN may potentially function as biomarkers in uveal melanoma. Clearly, our work has shown that the concentration of each cysteine proteinase inhibitor (cystatin C and cystatin SN) is perturbed in uveal melanoma in various biological fluids. We first briefly describe the role of each cystatin, and then their use as potential biomarkers in cancer.

Cysteine proteinase inhibitors, cystatins, are involved in mechanisms controlling intracellular and extracellular protein degradation.[11,37] Cystatin

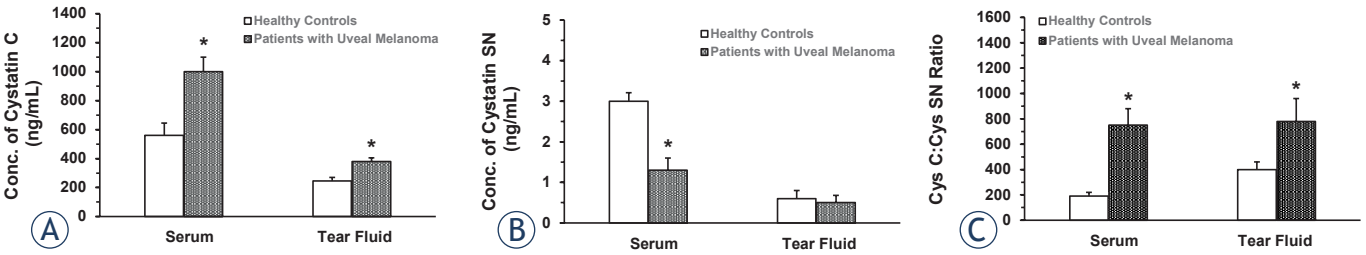

FIGURE 4. Cystatin C **(A)** and cystatin SN **(B)** concentrations and their ratio **(C)** in the serum and tear fluid of patients with uveal melanoma. **(A)** Values represent the mean ± standard deviation (s.d.) of n = 15 healthy controls (mean age = 53.1 ± 3.4 years) and n = 51 of 57 total patients with uveal melanoma (mean age = 51.7 ± 2.8 years; 6 patients were > 60 years old and were therefore not included). **(B)** Values represent the mean ± s.d. of n = 15 healthy controls (mean age = 53.1 ± 3.4 years) and n = 51 of 57 total patients with uveal melanoma (mean age = 51.7 ± 2.8 years; 6 patients were > 60 years old and were therefore not included). **(C)** Values represent the mean ± s.d. of n = 15 healthy controls (mean age = 53.1 ± 3.4 years) and n = 51 of 57 total patients with uveal melanoma (mean age = 51.7 ± 2.8 years; 6 patients were > 60 years old and were therefore not included).

* = significant difference ($p < 0.001$) from the mean value for healthy controls in each biological matrix

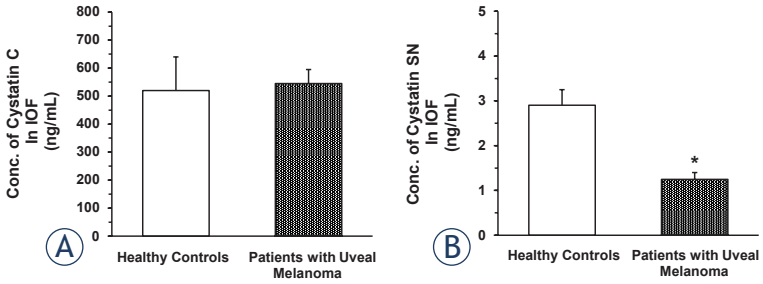

FIGURE 5. Concentration of cystatin C **(A)** and cystatin SN **(B)** in intraocular fluid of patients with uveal melanoma *versus* healthy controls. **(A)** Values represent the mean ± standard deviation (s.d.) of n = 7 healthy controls (mean age = 57.5 ± 1.9 years) and n = 18 of 57 total uveal melanoma patients selected based on an age close to the mean age of the 7 healthy controls (mean age = 55.9 ± 3.2 years; n = 18). **(B)** Values represent the mean ± s.d. of n = 7 healthy controls (mean age = 57.5 ± 1.9 years) and n = 18 of 57 total uveal melanoma patients selected based on an age close to the mean age of the 7 healthy controls (mean age = 55.9 ± 3.2 years; n = 18).

* = significant difference ($p < 0.001$) from mean value for healthy controls; IOF = intraocular fluid

C is a secreted cysteine protease inhibitor, which is abundantly expressed in body fluids and possibly regulated at both the transcriptional and post-translational levels.[38,39] Production of cystatin C from hematopoietic cell lineages contributes significantly to the overall systemic pool of cystatin C.[40] This particular cystatin is the most abundant and potent member[21,27] of the cystatin family, which is important due to the fact that the activity of various cysteine proteases, both inside and outside of cells, requires careful regulation or control by endogenous inhibitors such as cystatin C. The levels of cystatin C in the systemic circulation (serum) are typically different from the concentration of cystatin C in biological fluids of the eye, such as IOF and tears.[29,41] In fact, according to our data, the concentration of cystatin C in serum was significantly greater than in both IOF and tears. It has been suggested that tears may function as a pool, or reservoir, for biomarkers of various pathological eye conditions, as well as for diseases beyond just ocular disorders.[42]

Cystatin C is involved in numerous diseases, including atherosclerosis and cancer, as well as the aging process.[17,29,41] Importantly, cystatin C is believed to prevent tumor progression by inhibiting the activities of a family of lysosomal cysteine cathepsins. Using cystatin C-deficient animals, Huh *et al.* reported that cystatin C concentrations *in vivo* might influence tumor metastasis in some tissues.[43] Interestingly, cystatin C is downregulated in prostate cancer and may prevent tumor progression by inhibiting the activities of a family of lysosomal cysteine proteases.[44] However, Hammouda *et al.*[45] suggested that although serum cystatin C levels may potentially represent a novel biomarker that reflects tumor burden (based on the fact that cystatin C levels were significantly more elevated in diffuse large B-cell lymphoma patients than in controls), there was no prognostic value regarding overall survival. Jiang *et al.* have recently reported that both serum and urine cystatin C levels are elevated, and the cystatin C gene is upregulated nearly 50-fold, in patients with multiple myeloma, which suggests it use as a diagnostic biomarker in multiple myeloma.[31] Additionally, Leto and Sepporta[32] suggested the use of cystatin C as a predictive biomarker for breast cancer. Lastly, it is worth noting that Kos *et al.* considers cystatin C to be a potential anticancer agent.[41]

Next, we turn to the other cysteine protease inhibitor evaluated in the present study; namely, cystatin SN. Cystatin SN, along with cystatins S and SA, belongs to the second type of extracellular cystatins (in this case, salivary cystatins), which has not been as thoroughly studied as cystatin C. While cystatin SN is not as prevalent as cystatin C in normal mammalian tissues[46], it is a member of the cystatin family that inhibits the proteolytic activity of cysteine proteases. In fact, univariate and multivariate analyses have indicated that cystatin SN possibly acts as a marker for cancer prognosis.[13] For example, cystatin SN has been shown to be a tumor biomarker that provides useful information for the diagnosis of esophageal[47-49], gastric, pancreatic, and colorectal cancers[30,50], as well as neuroblastomas and melanomas.[12]

As it pertains to cancer progression, cystatin SN is thought to be involved in several malignant tumors.[51] For instance, it was recently reported by Cui *et al.* that upregulation of this inhibitor promoted the progression of hepatocellular carcinoma.[51] Of note, knockdown of cystatin SN significantly reduced the expression of proliferation-related proteins p-AKT and PCNA[10], which indicates a more complex role of cystatins in tumor growth and progression beyond their role as inhibitors of cysteine cathepsins. Lastly, a survival study in patients with surgically-resected, non-small cell lung cancer revealed an association between elevated expression levels of cystatin SN and poor prognosis.[46] Specifically, the study indicated that significantly increased expression of cystatin SN was directly correlated with a higher rate of cancer recurrence, metastatic risk, and poor overall survival.[46]

The present study focused on the use of cystatin C and cystatin SN as potential biomarkers

in the context of uveal melanoma. We successfully showed that the concentrations of cystatin C and cystatin SN were significantly elevated, and reduced, respectively, in the serum of patients with uveal melanoma compared to healthy controls. While there was a significant increase in the concentration of cystatin C in the tear fluid of patients with uveal melanoma when compared to healthy controls, there was no significant difference in the concentration of cystatin SN in the tear fluid between these same two patient cohorts. However, we would suggest that the value of the CysC:CysSN ratio in both biological matrices (*i.e.*, serum and tears) may potentially be a better indicator of uveal melanoma than either inhibitor (cystatin) alone, since the ratio was very significantly increased in both matrices.

The change in the concentration of cystatin SN in another ocular fluid; specifically, IOF, may serve as further evidence to suggest the presence of uveal melanoma, since the concentration of this cystatin was significantly reduced in patients with uveal melanoma when compared to corresponding concentrations of cystatin SN in healthy controls. This finding may argue for a combined determination of the concentrations of both cystatin C and cystatin SN in serum, tear fluid, and IOF to assist ophthalmologists that have a preliminary suspicion concerning the presence of uveal melanoma, especially when combined with both ocular fundus and ultrasound imaging. However, it is important to mention that there are other ocular disorders (*e.g.*, AMD) that may perturb the concentrations of cystatins in various biological fluids, which is why it is important to have multiple diagnostic criteria to confirm the presence of uveal melanoma. For example, a variant of cystatin C (*i.e.*, variant B, cystatin C) differs from the wild-type protein by a single amino acid (A25T) and is associated with decreased plasma cystatin C levels and an increased risk of developing AMD, which potentially raises the prospect of cystatin C replacement therapy for patients homozygous for variant B.[52]

In conclusion, the present investigation has documented changes in the concentrations of cystatin C and cystatin SN in various biological fluids in both healthy controls and patients with uveal melanoma, which may possibly serve as potential biomarkers of uveal melanoma, especially when the value of the CysC:CysSN ratio is determined in both the serum and tear fluid. That is, the value of the CysC:CysSN ratio may be a better indicator of the possibility of uveal melanoma than either cystatin alone. We would also suggest that the profound reduction in the concentration of cystatin SN in IOF may provide further support for the possible presence of uveal melanoma. However, it is imperative for ophthalmologists to utilize multiple diagnostic criteria if they suspect that a patient has uveal melanoma, including, but not limited to, the concentrations of cystatin C and cystatin SN in serum, tears, and IOF, together with ocular fundus and ultrasound imaging.

Lastly, as it pertains to the present findings described herein, we further suggest that the concentrations of cystatin C and cystatin SN in serum, tears, and IOF, as well as diagnostic ocular imaging studies, be combined with tissue biopsy and subsequent evaluation by surgical pathology to differentiate between malignant and benign eye tumors, since Dikovskaya *et al.* reported that the level of cystatin C in tears was significantly elevated (relative to the concentration of cystatin C in the tears of healthy controls) in both malignant and benign eye tumors.[27] That is, the concentration of cystatin C in the tear fluid of patients with both malignant and benign eye tumors was significantly elevated relative to this same measurement in healthy control patients, but was not significantly different ($p > 0.05$) between patients with either a malignant, or benign, eye tumor.[27] It is for the latter reason that a tissue biopsy with histopathological evaluation is absolutely necessary to distinguish a malignant eye tumor from one that is benign, although, as mentioned directly above and verified in the present study, cystatin C levels in the serum and tears of patients with uveal melanoma are profoundly elevated relative to cystatin C levels in these same two biological fluids in healthy controls, and thus, is certainly suggestive of possible uveal melanoma. Reliance on multiple diagnostic criteria is critically important for uveal melanoma, since surgery to remove the melanoma and a small area of healthy tissue is reserved for small melanomas, whereas enucleation is typically required for large eye tumors.

Acknowledgements

The authors would like to gratefully acknowledge the assistance of Prof. Kuleshova Olga Nikolaevna (S. Fyodorov Eye Microsurgery Federal State Institution, Novosibirsk, Russia) with the clinical portion of this work. We are also grateful to Professor J. Kos (Slovenia) for support and Dr. I.N. Ignatik (AquaTest, St. Petersburg) for providing assistance with the determination of human cystatin C in biological samples.

The present study was supported with funding provided by the Institute of Neurosciences and Medicine, Novosibirsk, Russia (2017–2021) for basic scientific research.

References

1. Kaliki S, Shields CL. Uveal melanoma: relatively rare but deadly cancer. *Eye (Lond)* 2017; **31:** 241-57. doi: 10.1038/eye.2016.275
2. Elder DE, Bastian BC, Cree IA, Massi D, Scolyer RA. The 2018 World Health Organization classification of cutaneous, mucosal, and uveal melanoma: detailed analysis of 9 distinct subtypes defined by their evolutionary pathway. *Arch Pathol Lab Med* 2020; **144:** 500-22. doi: 10.5858/arpa.2019-0561-RA
3. Sathe S, Sakata M, Beaton AR, Sack RA. Identification, origins and the diurnal role of the principal serine protease inhibitors in human tear fluid. *Curr Eye Res 1998*; **17:** 348-62. doi: 10.1080/02713689808951215
4. Saakyan SV, Tsygankov AY, Moiseeva NI, Karamysheva AF, Garri DD. Assessment of the chemosensitivity of uveal melanoma cells *ex vivo*. *Bull Exp Biol Med* 2020; **170:** 142-7. doi: 10.1007/s10517-020-05020-3
5. Shah SU, Mashayekhi A, Shields CL, Walia HS, Hubbard GB 3rd, Zhang J, et al. Uveal metastasis from lung cancer: clinical features, treatment, and outcome in 194 patients. *Ophthalmology* 2014; **121:** 352-7. doi: 10.1016/j.ophtha.2013.07.014
6. Valsecchi ME, Orloff M, Sato R, Chervoneva I, Shields CL, Shields JA, et al. Adjuvant sunitinib in high-risk patients with uveal melanoma: comparison with institutional controls. *Ophthalmology* 2018; **125:** 210-7. doi: 10.1016/j.ophtha.2017.08.017
7. Spagnolo F, Caltabiano G, Queirolo P. Uveal melanoma. *Cancer Treat Rev* 2012; **38:** 549-53. doi: 10.1016/j.ctrv.2012.01.002
8. Luke JJ, Triozzi PL, McKenna KC, Van Meir EG, Gershenwald JE, Bastian BC, et al. Biology of advanced uveal melanoma and next steps for clinical therapeutics. *Pigment Cell Melanoma Res* 2015; **28:** 135-47. doi: 10.1111/pcmr.12304
9. Turk V, Stoka V, Turk D. Cystatins: biochemical and structural properties, and medical relevance. *Front Biosci* 2008; **13:** 5406-20. doi: 10.2741/3089
10. Breznik B, Mitrović A, Lah T, Kos J. Cystatins in cancer progression: more than just cathepsin inhibitors. *Biochimie* 2019; **166:** 233-50. doi: 10.1016/j.biochi.2019.05.002
11. Wu H, Du Q, Dai Q, Ge J, Cheng X. Cysteine protease cathepsins in atherosclerotic cardiovascular diseases. *J Atheroscler Thromb* 2018; **25:** 111-23. doi: 10.5551/jat.RV17016
12. Wallin H, Bjarnadottir M, Vogel LK, Wassélius J, Ekström U, Abrahamson M. Cystatins – extra- and intracellular cysteine protease inhibitors: high-level secretion and uptake of cystatin C in human neuroblastoma cells. *Biochimie* 2010; **92:** 1625-34. doi: 10.1016/j.biochi.2010.08.011
13. Liu Y, Yao J. Research progress of cystatin SN in cancer. *Onco Targets Ther* 2019; **12:** 3411-9. doi: 10.2147/OTT.S194332
14. Grubb AO. Cystatin C – properties and use as diagnostic marker. *Adv Clin Chem* 2000; **35:** 63-99. doi: 10.1016/s0065-2423(01)35015-1
15. Abrahamson M, Alvarez-Fernandez M, Nathanson CM. Cystatins. *Biochem Soc Symp* 2003; **70:** 179-99. doi: 10.1042/bss0700179
16. Poteryaeva ON, Falameyeva OV, Korolenko TA, Kaledin VI, Djanayeva SJ, Nowicky JW, et al. Cysteine proteinase inhibitor level in tumor and normal tissues in control and cured mice. *Drugs Exp Clin Res* 2000; **26:** 301-6. PMID: 11345042
17. Keppler D. Towards novel anti-cancer strategies based on cystatin function. *Cancer Lett* 2006; **235:** 159-76. doi: 10.1016/j.canlet.2005.04.001
18. Lah TT, Kokalj-Kunovar M, Drobnic-Kosorok M, Babnik J, Golouh R, Vrhovec I, et al. Cystatins and cathepsins in breast carcinoma. *Biol Chem Hoppe Seyler* 1992; **373:** 595-604. doi: 10.1515/bchm3.1992.373.2.595
19. Cox JL. Cystatins and cancer. *Front Biosci (Landmark Ed)* 2009; **14:** 463-74. doi: 10.2741/3255. PMID: 19273078
20. Jakoš T, Pišlar A, Jewett A, Kos J. Cysteine cathepsins in tumor-associated immune cells. *Front Immunol* 2019; **10:** 2037. doi: 10.3389/fimmu.2019.02037
21. Svechnikova IG, Korolenko TA, Stashko JuF, Kaledin VI, Nikolin VP, Nowicky JW. The influence of Ukrain on the growth of HA-1 tumor in mice: the role of cysteine proteinases as markers of tumor malignancy. *Drugs Exp Clin Res* 1998; **24:** 261-9. PMID: 10190085
22. Korolenko TA, Cherkanova MS, Gashenko EA, Johnston T. Cystatin C, atherosclerosis and lipid-lowering therapy by statins. In: Cohen JB, Ryseck LP, editors. *Cystatins: protease inhibitors, biomarkers and immunomodulators.* New York, USA: Nova Science Publishers; 2011. p. 187-204.
23. Korolenko TA, Pisareva EE, Filyushina EE, Johnston TP, Machova E. Serum cystatin C and chitotriosidase in acute P-407 induced dyslipidemia: can they serve as potential early biomarkers for atherosclerosis? *Exp Toxicol Pathol* 2015; **67:** 459-66. doi: 10.1016/j.etp.2015.06.003
24. Paraoan L, Gray D, Hiscott P, Garcia-Finana M, Lane B, Damato B, et al. Cathepsin S and its inhibitor cystatin C: imbalance in uveal melanoma. *Front Biosci (Landmark Ed.)* 2009; **14:** 2504-13. doi: 10.2741/3393
25. De Souza GA, Godoy LM, Mann M. Identification of 491 proteins in the tear fluid proteome reveals a large number of proteases and protease inhibitors. *Genome Biol* 2006; **7:** R72. doi: 10.1186/gb-2006-7-8-R72
26. Balasubramanian SA, Wasinger VC, Pye DC, Willcox MD. Preliminary identification of differentially expressed tear proteins in keratoconus. *Mol Vis* 2013; **19:** 2124-34. eCollection 2013. PMID: 24194634
27. Dikovskaya MA, Trunov AN, Chernykh VV, Korolenko TA. Cystatin C and lactoferrin concentrations in biological fluids as possible prognostic factors in eye tumor development. *Int J Circumpolar Health* 2013; **72(Suppl 1):** 21087. doi: 10.3402/ijch.v72i0.21087. eCollection 2013
28. Korolenko TA, Tuzikov FV, Cherkanova MS, Johnston TP, Tuzikova NA, Loginova VM, et al. Influence of atorvastatin and carboxymethylated glucan on the serum lipoprotein profile and MMP activity of mice with lipemia induced by poloxamer 407. *Can J Physiol Pharmacol* 2012; **90:** 141-53. doi: 10.1139/y11-118
29. Pišlar A, Jewett A, Kos J. Cysteine cathepsins: their biological and molecular significance in cancer stem cells. *Semin Cancer Biol* 2018; **53:** 168-77. doi: 10.1016/j.semcancer.2018.07.010
30. Jiang J, Liu HL, Liu ZH, Tan SW, Wu B. Identification of cystatin SN as a novel biomarker for pancreatic cancer. *Tumor Biol* 2015; **36:** 3903-10. doi: 10.1007/s13277-014-3033-3
31. Jiang Y, Zhang J, Zhang C, Hong L, Jiang Y, Lu L, et al. The role of cystatin C as a proteosome inhibitor in multiple myeloma. *Hematology* 2020; **25:** 457-63. doi: 10.1080/16078454.2020.1850973
32. Leto G, Sepporta MV. The potential of cystatin C as a predictive biomarker in breast cancer. *Expert Rev Anticancer Ther* 2020; **20:** 1049-56. doi: 10.1080/14737140.2020.1829481
33. Ognibene A, Mannucci E, Caldini A, Terreni A, Brogi M, Bardini G, et al. Cystatin C reference values and aging. *Clin Biochem* 2006; **39:** 658-61. doi: 10.1016/j.clinbiochem.2006.03.017
34. Odden MC, Tager IB, Gansevoort RT, Bakker SJ, Katz R, Fried LF, et al. Age and cystatin C in healthy adults: a collaborative study. *Nephrol Dial Transplant* 2010; **25:** 463-9. doi: 10.1093/ndt/gfp474
35. Edinga BE, Yakam AT, Nansseu JR, Bilong C, Belinga S, Minkala E, et al. Reference intervals for serum cystatin C and serum creatinine in an adult sub-Saharan African population. *BMC Clin Pathol* 2019; **19:** 4. doi: 10.1186/s12907-019-0086-7
36. Groesbeck D, Köttgen A, Parekh R, Selvin E, Schwartz GJ, Coresh J, et al. Age, gender, and race effects on cystatin C levels in US adolescents. *Clin J Am Soc Nephrol* 2008; **3:** 1777-85. doi: 10.2215/CJN.00840208
37. Zou J, Chen Z, Wei X, Chen Z, Fu Y, Yang X, et al. Cystatin C as a potential therapeutic mediator against Parkinson's disease via VEGF-induced angiogenesis and enhanced neuronal autophagy in neurovascular units. *Cell Death Dis* 2017; **8:** e2854. doi: 10.1038/cddis.2017.240
38. Keppler D, Zhang J, Bihani T, Lin AW. Novel expression of CST1 as candidate senescence marker. *J Gerontol A Biol Sci Med Sci* 2011; **66:** 723-31. doi: 10.1093/gerona/glr033
39. Wang R, Chen Z, Fu Y, Wei X, Liao J, Liu X, et al. Plasma cystatin C and high-density lipoprotein are important biomarkers of Alzheimer's disease and vascular dementia: a cross-sectional study. *Front Aging Neurosci* 2017; **9:** 26. doi: 10.3389/fnagi.2017.00026

40. Xu Y, Ding Y, Li X, Wu X. Cystatin C is a disease-associated protein subject to multiple regulation. *Immunol Cell Biol* 2015; **93:** 442-51. doi: 10.1038/icb.2014.121

41. Kos J, Mitrović A, Mirković B. The current stage of cathepsin B inhibitors as potential anticancer agents. *Future Med Chem* 2014; **6:** 1355-71. doi: 10.4155/fmc.14.73

42. Pieragostino D, D'Alessandro M, Di Ioia M, Di Ilio C, Sacchetta P, Del Boccio P. Unraveling the molecular repertoire of tears as a source of biomarkers: beyond ocular diseases. *Proteomics Clin Appl* 2015; **9:** 169-86. doi: 10.1002/prca.201400084

43. Huh CG, Håkansson K, Nathanson CM, Thorgeirsson UP, Jonsson N, Grubb A, et al. Decreased metastatic spread in mice homozygous for a null allele of the cystatin C protease inhibitor gene. *Mol Pathol* 1999; **52:** 332-40. doi: 10.1136/mp.52.6.332

44. Wegiel B, Jiborn T, Abrahamson M, Helczynski L, Otterbein L, Persson JL, et al. Cystatin C is downregulated in prostate cancer and modulates invasion of prostate cancer cells via MAPK/Erk and androgen receptor pathways. *PLoS ONE* 2009; **4:** e7953. doi: 10.1371/journal.pone.0007953

45. Hammouda NE, Salah El-Din MA, El-Shishtawy MM, El-Gayar AM. Serum cystatin C as a biomarker in diffuse large B-cell lymphoma. *Sci Pharm* 2017; **85:** 9. doi: 10.3390/scipharm85010009

46. Cao X, Li Y, Luo RZ, Zhang L, Zhang SL, Zeng J, et al. Expression of cystatin SN significantly correlates with recurrence, metastasis, and survival duration in surgically resected non-small cell lung cancer patients. *Sci Rep* 2015; **5:** 8230. doi: 10.1038/srep08230

47. Chen YF, Ma G, Cao X, Luo RZ, He LR, He JH, et al. Overexpression of cystatin SN positively affects survival of patients with surgically resected esophageal squamous cell carcinoma. *BMC Surg* 2013; **13:** 15. doi: 10.1186/1471-2482-13-15

48. Oh SS, Park S, Lee KW, Madhi H, Park SG, Lee HG, et al. Extracellular cystatin SN and cathepsin B prevent cellular senescence by inhibiting abnormal glycogen accumulation. *Cell Death Dis* 2017; **8:** e2729. doi: 10.1038/cddis.2017.153

49. Oh BM, Lee SJ, Cho HJ, Park YS, Kim JT, Yoon SR, et al. Cystatin SN inhibits auranofin-induced cell death by autophagic induction and ROS regulation via glutathione reductase activity in colorectal cancer. *Cell Death Dis* 2017; **8:** e2682. doi: 10.1038/cddis.2017.100

50. Yoneda K, Iida H, Endo H, Hosono K, Akiyama T, Takahashi H, et al. Identification of cystatin SN as a novel tumor marker for colorectal cancer. *Int J Oncol* 2009; **35:** 33-40. doi: 10.3892/ijo_00000310

51. Cui Y, Sun D, Song R, Zhang S, Liu X, Wang Y, et al. Upregulation of cystatin SN promotes hepatocellular carcinoma progression and predicts a poor prognosis. *J Cell Physiol* 2019; **234:** 22623-34. doi: 10.1002/jcp.28828

52. Paraoan L, Hiscott P, Gosden C. Cystatin C in macular and neuronal degenerations: Implications for mechanism(s) of age-related macular degeneration. *Vision Research* 2010; **50:** 737-42. doi: 10.1016/j.visres.2009.10.022

research article

Clinical impacts of copy number variations in B-cell differentiation and cell cycle control genes in pediatric B-cell acute lymphoblastic leukemia: a single centre experience

Klementina Crepinsek[1,2], Gasper Marinsek[1], Marko Kavcic[2,3], Tomaž Prelog[3], Lidija Kitanovski[3], Janez Jazbec[2,3], Marusa Debeljak[1,2]

[1] Clinical Institute for Special Laboratory Diagnostics, University Children's Hospital, University Medical Centre Ljubljana, Ljubljana, Slovenia

[2] Faculty of Medicine, University of Ljubljana, Ljubljana, Slovenia

[3] Department of Oncology and Haematology, University Children's Hospital, University Medical Centre Ljubljana, Ljubljana, Slovenia

Radiol Oncol 2022; 56(1): 92-101.

Received 7 September 2021
Accepted 5 November 2021

Correspondence to: Assist. Prof. Maruša Debeljak, Ph.D., Clinical Institute for Special Laboratory Diagnostics, University Children's Hospital, University Medical Centre Ljubljana, Vrazov trg 1, 1000 Ljubljana, Slovenia. E-mail: marusa.debeljak@kclj.si

Disclosure: No potential conflicts of interest were disclosed.

Background. *IKZF1* gene deletions have been identified as a poor prognostic factor in pediatric B-cell acute lymphoblastic leukemia (B-ALL), especially in the presence of co-occurring deletions (*IKZF1*^{plus} profile). This study aimed to determine the frequency of *IKZF1* deletions and deletions in other B-cell differentiation and cell cycle control genes, and their prognostic impact in Slovenian pediatric B-ALL patients.

Patients and methods. We studied a cohort of 99 patients diagnosed with B-ALL from January 2012 to December 2020 and treated according to the ALL IC-BFM 2009 protocol. Eighty-eight bone marrow or peripheral blood samples were analysed for copy number variations (CNVs) using the SALSA MLPA P335 ALL-IKZF1 probemix.

Results. At least one CNV was detected in more than 65% of analysed samples. The most frequently altered genes were *PAX5* and *CDKN2A/B* (30.7%, 26.1%, and 25.0%, respectively). Deletions in *IKZF1* were present in 18.2% of analysed samples and were associated with an inferior 5-year event-free survival (EFS; 54.8% *vs*. 85.9%, p = 0.016). The *IKZF1*^{plus} profile was identified in 12.5% of the analysed samples, and these patients had an inferior 5-year EFS than those with deletions in *IKZF1* only and those without deletions (50.8% *vs*. 75.0% *vs*. 85.9%, respectively, p = 0.049). Overall survival (OS) was also worse in patients with the *IKZF1*^{plus} profile than those with deletions in *IKZF1* only and those without deletions (5-year OS 76.2% *vs*. 100% *vs*. 93.0%, respectively). However, the difference between the groups was not statistically significant.

Conclusions. Our results are in concordance with the results obtained in larger cooperative clinical trials. Copy number variations analysis using the SALSA MLPA kit is a reliable tool for initial diagnostic approach in children with B-ALL, even in smaller institutions in low- and middle-income countries.

Key words: B-acute lymphoblastic leukemia; *IKZF1* deletions; *IKZF1*^{plus}; MLPA; pediatric; copy number variations (CNVs)

Introduction

Improvements in risk stratification and new therapeutic approaches have dramatically improved treatment outcomes in pediatric B-cell acute lymphoblastic leukemia (B-ALL). In developed countries, the overall survival for these patients is approaching 90%.[1,2] Nevertheless, some genetic

subtypes still imply poor outcomes, and 10–20% of patients experience a relapse that is often accompanied by treatment resistance and failure.[3,4] Therefore, the need for new diagnostic and prognostic markers remains of paramount importance.

In the previous years, deletions in the *IKZF1* gene have been identified as an important predictor of relapse in B-ALL.[5-9] *IKZF1* gene is located on chromosome 7p12.2 and consists of 8 exons, and of those, exons 2–8 are protein-coding. The gene codes for the transcription factor IKAROS, which regulates the expression of genes that control cell cycle progression and cell survival. It is involved in the development of all lymphoid lineages, especially in the differentiation of B-progenitor cells. Exons 4–6 encode four zinc finger DNA-binding domains that are essential for the tumour-suppressive function of IKAROS, and exon 8 encodes two zinc fingers that are responsible for the homo- or heterodimerization of IKAROS.[10,11] Genomic deletions in *IKZF1* occur in around 15% of pediatric B-ALL cases.[5,6,8,12-14] Their occurrence is exceptionally high in *BCR-ABL1*-positive (70%)[15,16] and *BCR-ABL1*-like (40%)[13,17] B-ALL, and have been associated with poor treatment response and an increased risk of relapse.[5–9] Deletions are most common in exons 4–7 or affect the whole gene, however, other less common lesions may also be present (e. g. deletions in exons 2–8, 2–7), and they are all associated with an unfavourable outcome in pediatric B-ALL.[6,18] Therefore, some study groups on B-ALL treatment have decided to include *IKZF1* deletion status into their risk stratification protocols. Others, however, did not, as there was hesitation on whether the prognostic impact of these deletions was strong enough to justify treatment intensification.[14,19,20]

Recently, another, minimal residual disease (MRD) dependent prognostic profile *IKZF1*^{plus} with an immensely poor prognostic value was identified. This profile is defined by additional deletions in genes involved in cell differentiation and cell cycle regulation. *IKZF1* deletions that co-occur with deletions in *CDKN2A, CDKN2B, PAX5*, or the PAR1 region (deletions of *CSF2RA* and *IL3RA*, but not *CRLF2*) in the absence of *ERG* deletions are associated with the worst event-free and overall survival.[21] This profile is already being used in the current AIEOP-BFM ALL 2017 trial as a high-risk criterion.[20] Copy number variations (CNVs) in some aforementioned genes (*PAX5*, *CDKN2A, CDKN2B*) also seem to be independently associated with poor prognosis, however, the results remain conflicting.[19,22-25] The inclusion of the CNV status of these genes may significantly improve risk stratification in B-ALL, but more studies are needed to elucidate their true prognostic effect.

Deletions in *IKZF1* are mostly observed in high-risk pediatric ALL subtypes. Many studies have confirmed the association of *IKZF1* deletions and *IKZF1*^{plus} profile with poor treatment outcomes. In Slovenia, no studies have been done yet to determine the frequency of *IKZF1* deletions and CNVs in other cell differentiation and cell cycle regulation genes in pediatric B-ALL patients and treatment outcomes for these patients. Due to the importance of these alterations in the prognosis and choosing the best treatment approach, it is of great importance to determine their presence. Therefore, the study aimed to analyze bone marrow samples from Slovenian pediatric patients diagnosed with B-ALL from January 2012 to December 2020 for the presence of these CNVs and to determine their prognostic value.

Patients and methods

Patients and samples

In total, 99 children with B-ALL that were treated at the University Children's Hospital, University Medical Centre Ljubljana between January 2012 and December 2020 according to the ALL IC-BFM 2009 protocol were included in this study. Diagnoses were established following standard clinical, cytomorphological, and immunological criteria.

We obtained bone marrow samples for 92 patients as part of the diagnostic procedure before starting treatment. For 7 patients, bone marrow samples were not available, therefore, peripheral blood samples were obtained for the analysis. For four patients, there was no sufficient material available to perform the multiplex ligation-dependent probe amplification (MLPA) assay, 3 samples contained less than 40% of blasts and were excluded from analysis, and for an additional four, the assay failed due to poor sample quality. Therefore, data analysis was performed on 88 patient samples (82 bone marrow and 6 peripheral blood). The bone marrow samples contained 77.4 ± 16.7% of blast in average, and for the peripheral blood samples this value was 77.8 ± 16.0%. For survival analysis, patient samples from the year 2020 were excluded, due to the short follow-up period. Therefore, the survival analysis was carried out on 72 patients diagnosed between January 2012 and December 2019.

Informed consent was obtained from all subjects involved in the study, or their parents. The

TABLE 1. The demographic and clinical characteristics of Slovenian B-ALL patients included in the study

Characteristic	
Nr. of patients	99
Sex	
Male	54 (54.5%)
Female	45 (45.5%)
Primary genetic abnormalities	
ETV6-RUNX1	28 (28.3%)
BCR-ABL1	7 (7.1%)
KMT2A rearrangements	4 (4.0%)
TCF3-PBX1	4 (4.0%)
Hyperdiploidy	27 (27.3%)
Hypodiploidy	3 (3.0%)
iAMP21	2 (2.0%)
No recurrent abnormalities	24 (24.2%)
Age at diagnosis	
< 1	3 (3.0%)
1–5	57 (57.6%)
≥ 6	39 (39.4%)
Risk group	
Standard risk	17 (17.2%)
Intermediate risk	59 (59.6%)
High risk	23 (23.2%)
FC- minimal residual disease	
Day 15	
< 0.1%	35 (35.4%)
0.1–10%	48 (48.5%)
> 10%	13 (13.1%)
Unknown	3 (3.0%)
Day 33	
< 0.01%	73 (73.7%)
0.01–1%	20 (20.2%)
> 1%	3 (3.0%)
Unknown	3 (3.0%)

study was conducted according to the guidelines of the Declaration of Helsinki, and approved by the Ethics Committee of the Republic of Slovenia (reference number KME 51/03/11).

DNA extraction

Genomic DNA was extracted from bone marrow or peripheral blood samples using the FlexiGene DNA Kit 250 (QIAGEN®, Hilden, Germany) according to the manufacturer's instructions. All samples were quantified using DS-11 FX+ Spectrophotometer (DeNovix, Wilmington, USA), and stored at 4°C. Before analysis, the DNA concentration was established at 25 ± 1 ng/μL for the MLPA assay.

Analysis of copy number alterations

DNA was analysed for copy number alterations using the SALSA MLPA P335 ALL-IKZF1 probemix, according to the manufacturer's instructions (MRC Holland, Amsterdam, the Netherlands). The P335 probemix allows for the detection of deletions and duplications in B-cell differentiation and cell cycle control genes (*IKZF1, CDKN2A/B, PAX5, EBF1, ETV6, BTG1*, and *RB1*), as well as in genes from the X/Y PAR1 region (*CRLF2, CSF2RA, SHOX, IL3RA*, and *P2RY8*). It also contains 13 reference probes that function as internal controls. Additionally, analysis for copy number alterations for the determination of *ERG* status was carried out on samples that carried deletions in *IKZF1* and at least one additional gene (namely *CDKN2A, CDKN2B, PAX5, CSF2RA*, and *IL3RA*) with the SALSA MLPA P327 iAMP21-ERG probemix. The P327 probemix is used for the detection of deletions, duplications or amplifications of specific sequences on chromosome 21, including intragenic deletions of ERG. It contains 59 MLPA probes that bind to several regions on chromosome 21, including the *ERG* gene, and 13 reference probes. DNA samples from healthy donors were used as controls.

MLPA reactions were carried out on a 96-well PCR thermocycler SimpliAmp Thermal Cycler (Applied Biosystems, Thermo Fisher, Massachusetts, USA), and the products were separated by capillary electrophoresis on an ABI-3500 genetic analyser (Applied Biosystems, Thermo Fisher, Massachusetts, USA). The resulting peak intensities were analysed using Coffalyser software (MRC-Holland) which performed the intrasample and intersample normalization of the peaks with the manufacturer's reference probes and normal control DNA, respectively. Values above 1.3 were considered as gain, between 1.3 and 0.75 normal, between 0.75 and 0.25 heterozygous loss, and below 0.25 homozygous loss.

Statistical analysis

All statistical analyses were performed using SPSS 22.0 software (IBM Corp., Armonk, NY, USA).

Event-free survival (EFS; defined as the time between diagnosis and relapse or death) and overall survival (OS; defined as time between diagnosis and death or last follow-up) were analysed using the Kaplan-Meier method and the differences between multiple groups were analysed using the log-rank test. Multivariate analysis was performed using a Cox regression model, which was adjusted for other risk factors, namely sex, age at diagnosis, and risk group (HR *vs*. non-HR). Comparisons of categorical values were carried out using the Fischer's exact test, and for the comparison of numerical values, the Mann–Whitney U-test was used. The significance level for all the tests was 5% ($p < 0.05$ was considered to be statistically significant).

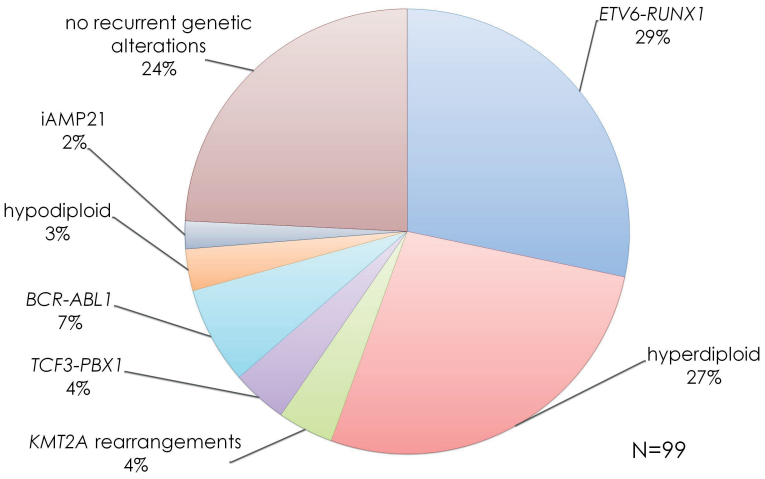

FIGURE 1. Prevalence of ALL subtypes in the Slovenian pediatric B-ALL cohort.

Results

Study group

The cohort included 54 males and 45 females (N = 99), with median age 4 years (range from 1 day to 23 years). Of these, 75 harboured recurrent genetic abnormalities (28 *ETV6-RUNX1*, 27 hyperdiploid karyotype, 7 *BCR-ABL1*, 4 *KMT2A* rearrangements, 4 *TCF3-PBX1*, 3 hypodiploid karyotype and 2 iAMP21), while no genetic alterations were identified in 24 patients (Figure 1). Based on age, white blood cell (WBC) count at diagnosis, blast cell counts on day 8, genetic abnormalities, and MRD at days 15 and 33, 17 patients were classified as standard risk (SR), 59 as intermediate risk (IR), and 23 as high risk (HR). The main patient characteristics are summed up in Table 1.

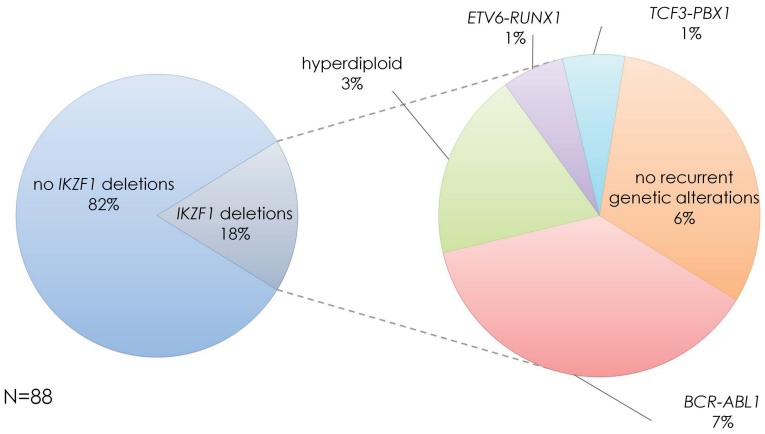

FIGURE 2. Primary genetic alterations in patients with *IKZF1* deletions.

Detection and analysis of *IKZF1* deletions by MLPA

Altogether, 92 patient samples and 5 controls were analysed by MLPA using the SALSA MLPA P335 ALL-IKZF1 probemix. Four patient samples failed the MLPA analysis. Out of the remaining 88 samples, *IKZF1* deletions were found in 16 (18.2%). The most common was the deletion of the whole gene, which was observed in eight patients (50%), others were focal deletions. The second most common deletion was the deletion of exons 4–8, which was found in four patients (25%). This deletion was described as rare in other studies. Other deletions that were also detected in our cohort were the deletion of exons 2–8 (two patients; 12.5%), 4–7 and 5 (both found in one patient; 6.3%). Eleven patients with *IKZF1* deletion had additional deletions present, which put them in the *IKZF1*^{plus} group. Of these, six

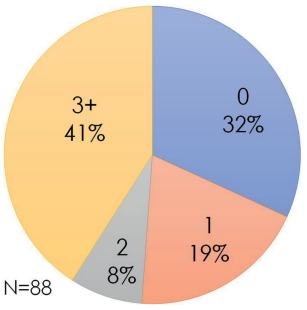

FIGURE 3. The number of CNVs present in Slovenian B-ALL samples.

carried additional deletions in *CDKN2A, CDKN2B* and *PAX5*, three in *CDKN2A* and *CDKN2B*, one in only *CDKN2B*, and one had deletions in the PAR1 region. *ERG* deletions were not found in any of these 11 samples.

The comparison of patient characteristics depending on *IKZF1* deletion is summarized in

TABLE 2. Patients' characteristics and response to treatment according to *IKZF1* deletion status in 91 Slovenian pediatric B-ALL patients

Characteristic	*IKZF1* status		
	No IKZF1 deletion	*IKZF1 deletion only*	*IKZF1^{plus}*
Nr. of patients	72	5	11
Sex			
Male	34 (47.2%)	5 (100%)	9 (81.8%)
Female	38 (52.8%)	0 (0.0%)	2 (18.2%)
Primary genetic abnormalities			
ETV6-RUNX1	24 (33.3%)	0 (0.0%)	1 (9.1%)
BCR-ABL1	1 (1.4%)	2 (40.0%)	4 (36.4%)
KMT2A rearrangements	4 (5.6%)	0 (0.0%)	0 (0.0%)
TCF3-PBX1	3 (4.2%)	0 (0.0%)	1 (9.1%)
Hyperdiploidy	20 (27.8%)	2 (40.0%)	1 (9.1%)
Hypodiploidy	2 (2.8%)	0 (0.0%)	1 (9.1%)
iAMP21	1 (1.4%)	0 (0.0%)	0 (0.0%)
No recurrent abnormalities	18 (25.0%)	1 (20.0%)	3 (27.3%)
Age at diagnosis			
< 1	3 (4.2%)	0 (0.0%)	0 (0.0%)
1–5	41 (56.9%)	2 (40.0%)	5 (45.5%)
≥ 6	28 (38.9%)	3 (60.0%)	6 (54.5%)
Risk group			
Standard risk	13 (18.1%)	0 (0.0%)	0 (0.0%)
Intermediate risk	46 (63.9%)	2 (40.0%)	4 (36.4%)
High risk	13 (18.1%)	3 (60.0%)	7 (63.6%)
FC- minimal residual disease			
Day 15			
< 0.1%	30 (41.7%)	0 (0.0%)	1 (9.1%)
0.1–10%	33 (45.8%)	2 (40.0%)	6 (54.5%)
> 10%	6 (8.3%)	3 (60.0%)	4 (36.4%)
Unknown	3 (4.2%)	0 (0.0%)	0 (0.0%)
Day 33			
< 0.01%	56 (77.8%)	0 (0.0%)	8 (72.7%)
0.01–1%	13 (18.1%)	3 (60.0%)	2 (18.2%)
> 1%	2 (2.8%)	1 (20.0%)	0 (0.0%)
Unknown	1 (1.4%)	1 (20.0%)	1 (9.1%)

Table 2. Of the 16 patients that harboured *IKZF1* deletions, five patients had no recurrent genetic alterations. The presence of primary recurrent genetic abnormalities found in patients with *IKZF1* deletions is shown in Figure 2. *IKZF1* deletions were significantly more common in Ph+ patients than in Ph– patients (6/7, 85.7% *vs*. 10/81, 12.3%, p = 0.0001), and so was the presence of the *IKZF1^{plus}* profile (4/7, 57.1% *vs*. 7/81, 8.6%, p = 0.004).

The *IKZF1* deletions were significantly more common in males than in females (p = 0.0045), however, the presence of the *IKZF1^{plus}* profile did not significantly differ between the sexes (p = 0.0607). Patients with *IKZF1* deletions were also older at diagnosis than those without deletions (median age 6 years, interquartile range (IQR) = 8 years *vs*. median age 4 years, IQR = 3.25 years, p = 0.052), and so were the patients with *IKZF1^{plus}* profile in comparison to those who did not have this profile (median age 6 years, IQR = 8 years *vs*. median age 4 years, IQR = 4, p = 0.136), however the differences were not statistically significant. Patients with *IKZF1* deletions showed higher blast count values on the 8th day of chemotherapy treatment (median blast count 252 blasts/μL, IQR = 2018.5 blasts/μL *vs*. median blast cell count 17 blasts/μL, IQR = 192,5 blasts/μL, p = 0.0005), higher values of MRD on day 15 (median MRD15 6.15% IQR = 30.67% *vs*. median MRD15 0.184%, IQR = 1.24%, p = 0.0005), and 33 of treatment (median MRD33 0.001%, IQR = 0.15% *vs*. median MRD33 0.000%, IQR = 0.01%, p = 0.033) compared to those without deletions. Similarly, blast cell count and MRD15 values of patients with the *IKZF1^{plus}* profile were higher compared to patients without the profile (median blast cell counts 224 blasts/μL, IQR = 2112 blasts/μL *vs*. median blast cell count 24 blasts/μL, IQR = 220 blasts/μL, p = 0.006; median MRD15 3.8%, IQR = 17.6% *vs*. median MRD15 0.24%, IQR = 2.23%, p = 0.030), while the difference was not significant for MRD33. The deletions were also more common in the HR group than in the IR (10/23, 43.5% *vs*. 6/52, 11.5%, p = 0.0032) and the SR group (10/23, 43.5% *vs*. 0/13, 0%, p = 0.0045). Patients in the HR group also exhibited the *IKZF1^{plus}* profile more often than those in the IR (7/23, 30.4% *vs*. 4/52, 7.7%, p = 0.0160) and the SR group (7/23, 30.4% *vs*. 0/13, 0%, p = 0.0294).

In our cohort, 13 patients (14.8%) experienced an event (either relapse or death). Among these, four patients had no recurrent genetic alterations, three patients carried the *ETV6-RUNX1* fusion gene, two the *BCR-ABL1* fusion gene, two were hyperdiploid, one had a *KMT2A* rearrangement and one carried the *TCF3-PBX1* fusion gene. One patient was classified as SR, eight as IR and four as HR. In this group, five patients (5/13, 38.5%) carried an *IKZF1* deletion, and of those, four had additional deletions, but lacked the *ERG* deletions, which met the criteria for the *IKZF1^{plus}* profile. The presence of *IKZF1* deletions and the *IKZF1^{plus}* profile was

higher in the group of patients who experienced an event in comparison to those who did not, however the difference did not reach statistical significance (5/13 *vs*. 11/75, p = 0.055 and 4/13 *vs*. 7/75, p = 0.053, respectively).

Detection and analysis of other gene deletions and duplications by MLPA

The SALSA MLPA P335 ALL-IKZF1 probemix can detect deletions or duplications in the following B-cell differentiation and cell cycle control genes: *IKZF1, EBF1, CDKN2A/B, PAX5, ETV6, BTG1, RB1,* and in the PAR1 region (*SHOX* area, *CRLF2, CSF2RA, IL3RA* and *P2RY8* genes). At least one CNV was detected in 60 patient samples (68.2%). Of those, 60% carried three or more CNVs, 28.3% carried only one CNV, and 11.7% carried two CNVs (Figure 3).

The most common CNVs were those in the *PAX5* gene that were present in 30.7% of analysed samples, followed by *CDKN2A* and *CDKN2B* that were altered in 26.1% and 25.0% of analysed samples, respectively. In these genes, deletions were more common than amplifications. CNVs were also very common in the PAR1 region, 22.7% of analysed samples had at least one CNV present in this region, and in these genes, amplifications were observed more often than deletions. Detailed information about CNVs in all analysed genes are shown in Figure 4.

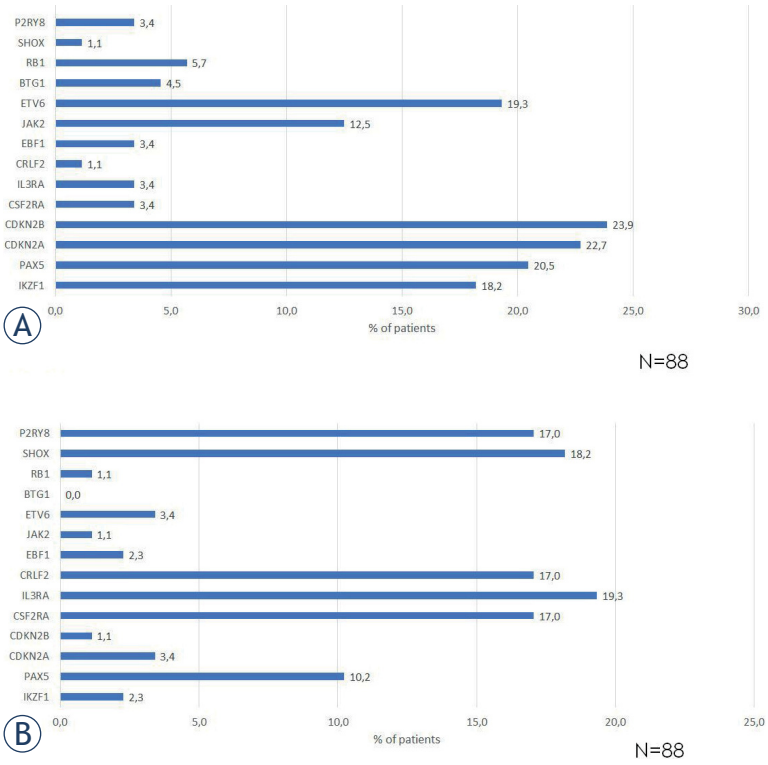

FIGURE 4. Frequency of copy number variations: **(A)** Gene deletions in the cohort. **(B)** Gene amplifications in the cohort.

BTG1 = BTG anti-proliferation factor 1; *CDKN2A/2B* = cyclin dependent kinase inhibitor 2A/2B; *CRLF2* = cytokine receptor-like factor 2; *CSF2RA* = colony-stimulating factor 2 receptor a subunit; *EBF1* = early B-cell factor 1; *ETV6* = ETS variant 6; *IKZF1* = IKAROS family zinc finger 1; *IL3RA* = interleukin 3 receptor subunit a; *JAK2* = Janus kinase 2; *PAX5* = paired box 5; *P2RY8* = purinergic receptor P2Y8; *SHOX* = short-stature homeobox gene; *RB1* = RB transcriptional corepressor 1

Prognostic significance of *IKZF1* deletions

First, the patients were divided into two groups, a group with and a group without *IKZF1* deletions. The 5-year EFS was significantly worse for patients harbouring *IKZF1* deletions, compared to those without the deletions (54.8% *vs*. 85.9%, p = 0.016) (Figure 5A). The 5-year OS was slightly worse as well for these patients, although the difference was not statistically significant (81.5% *vs*. 93.0%, p = 0.295) (Figure 5B).

The 5-year EFS and OS were also compared between groups with no *IKZF1* deletions, with deletions in the *IKZF1* gene only and with the *IKZF1*^{plus} profile. The difference in EFS between groups was statistically significant (p = 0.049). Pairwise comparison showed that patients in group *IKZF1*^{plus} had significantly poorer EFS in comparison to those in group with no *IKZF1* deletions (5-year EFS 50.8% *vs*. 85.9%, p = 0.016), while the difference was not significant between other groups (Figure 6A). The OS analysis between groups showed no differences between the groups (Figure 6B).

A multivariate Cox regression model was applied to this data to see, whether after adjusting for other relevant risk factors, *IKZF1* deletions profile retained a prognostic impact on event-free survival. We included the following variables in the model: sex, age at diagnosis, risk group (HR *vs*. nonHR) and the presence of *IKZF1* deletions. The overall model showed borderline significance (p = 0.05). When each separate variable was inspected, it was observed that both sex and the presence of the *IKZF1* deletions showed a certain trend (males having poorer survival than females (HR = 1.44), and those with the *IKZF1* deletions having poorer survival than those without the deletions (HR = 1.15)), however, they did not reach significance (p = 0.072 and p = 0.078, respectively). Similar results were obtained when this analysis was applied for the *IKZF1*^{plus} profile. This can most likely be attributed to the small sample size of our sample for survival analysis.

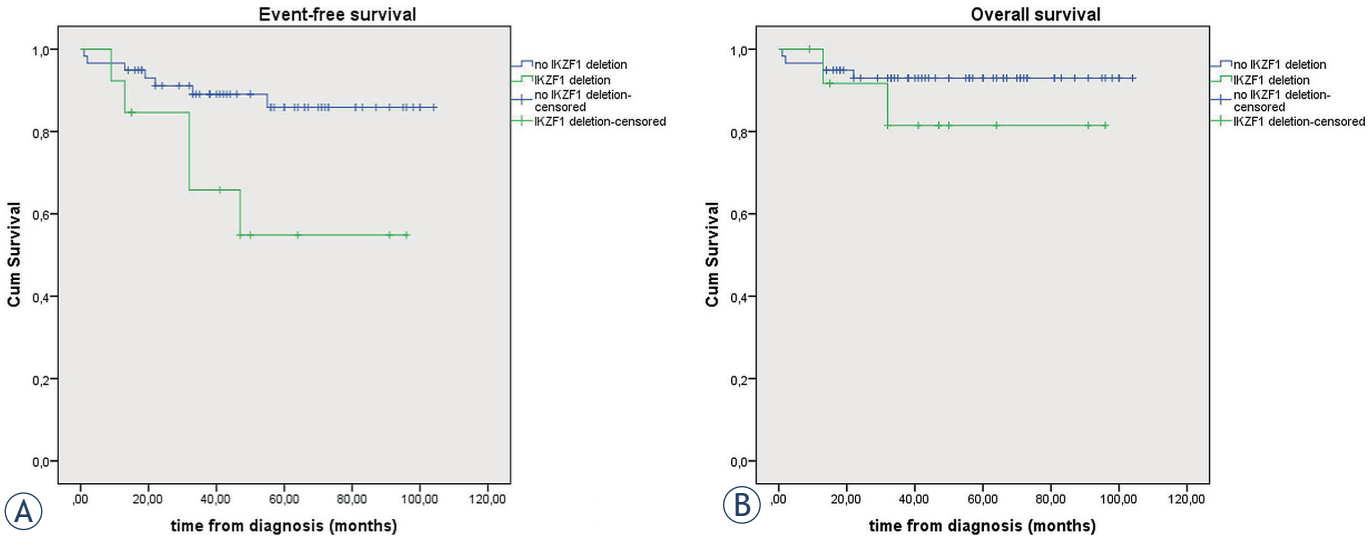

FIGURE 5. (A) Event-free survival in patients with or without *IKZF1* deletions (5-year event-free survival [EFS] 54.8% *vs*. 85.9%, p = 0.016). **(B)** Overall survival in patients with or without *IKZF1* deletions (5-year overall survival [OS] 81.5% *vs*. 93.0%, p = 0.295).

We further looked at the group of patients, classified as non-high risk (either SR or IR). In this group, six patients carried the *IKZF1* deletions, and of those, two patients experienced an event (2/6, 33.3%), and among the patients without the deletions, seven experienced an event (7/59, 11.9%) (p = 0.1907). The 5-year EFS for those without the deletions was 83.6%, while it was only 50% for those with the deletion. Once again, there is a certain trend to be seen, however, the difference was not statistically significant (p = 0.114). We also examined patients with the *IKZF1*^{plus} profile in the non-HR group. The frequency of events was higher amongst the patients with the profile compared to those without it (2/4, 50% *vs*. 7/61, 11.5%, p = 0.0890), and their EFS was poorer, although not significantly (50.0% *vs*. 83.7%, p = 0.087).

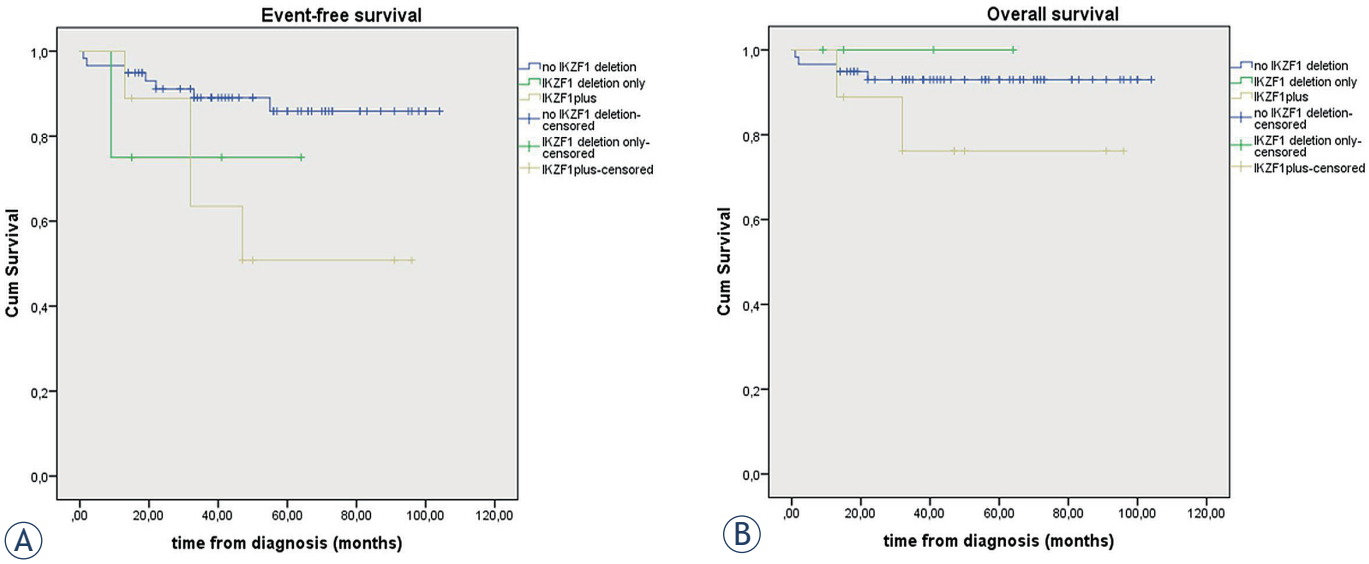

FIGURE 6. (A) Event-free survival in patients without IKZF1 deletions, with IKZF1 deletions only, and those with the IKZF1plus profile (5-year EFS 85.9% *vs*. 75.0% *vs*. 50.8%, p = 0.049). **(B)** Overall survival in patients without *IKZF1* deletions, with *IKZF1* deletions only and those with the *IKZF1*^{plus} profile (5-year OS 93.0% *vs*. 100% *vs*. 76.2%, p = 0.290).

Discussion

Various alterations in genes involved in cell differentiation and cell cycle regulation are a hallmark of B-ALL. The role of deletions in the *IKZF1* gene in B-ALL has previously been described as very prognostically revealing and predictive for relapse.[8,21] Due to their association with poorer treatment outcomes, it is important to detect them to adjust the treatment protocol accordingly. Moreover, alterations in other genes, such as *PAX5* and *CDKN2A/2B,* are also often present. However, information regarding their prognostic impact is still rather ambiguous[19,22,23,26], therefore, more studies need to be carried out to define their true value for patient risk stratification.

Our study was carried out on a smaller (88 patients), yet consecutive, unselected, and well-controlled population of pediatric patients with B-ALL. This is the first report about CNVs in cell differentiation and cell cycle regulation genes in Slovenian pediatric B-ALL patients. In our cohort, *IKZF1* deletions were identified in 18.2% of analysed samples. This is in concordance with reports of *IKZF1* deletions ranging from 10.7 to 15.9% in other studies that analysed unselected cohorts.[6,8,12–14,21] The *IKZF1* deletions were more common in the HR group when compared to the IR and SR groups, as was also shown in the study done by Dörge *et al*.[6] Six out of seven (86%) patients with the *BCR-ABL1* translocation also carried deletions in the *IKZF1* gene, four of those had the *IKZF1*^{plus} profile. As it was previously described, these deletions are very commonly, however not exclusively, present in *BCR-ABL1* ALL.[12,15,16,21] Some studies excluded patients with the *BCR-ABL1* translocation and determined the *IKZF1* status only in the *BCR-ABL1*-negative patients. These studies reported frequencies of *IKZF1* deletions from 9.4 to 16%.[7,27-30] Our results show that 12.3% of patients without *BCR-ABL1* in this cohort carried *IKZF1* deletions, which is again similar to previously published results.

The most common *IKZF1* deletion in our cohort was, as was also reported by other studies, the deletion of the whole gene (50%). Interestingly, however, the second most common deletion was that of exons 4–8 (25%), whereas this deletion was described as rare in other studies. The second most common deletion reported by other groups was that of exons 4–7 [6,8,18,31] which results in a dominant-negative isoform (IK6). This deletion occurred in only one patient in our cohort. Nevertheless, all *IKZF1* deletions, including the rare ones, have an important prognostic impact.[18] Therefore, all should be considered when selecting the appropriate treatment.

In our cohort, *IKZF1* deletions and the *IKZF1*^{plus} profile were more common amongst males and were associated with higher blast values on day 8 of chemotherapy, higher values of MRD15 and MRD33, and were more often found in the HR group. The presence of *IKZF1* deletions and the *IKZF1*^{plus} profile was higher amongst the patients who experienced an event (relapse or death) than those who did not, albeit this difference was not significant. Two of the patients who carried these deletions and experience a relapse also had the *BCR-ABL1* fusion gene, which placed them in the HR group. However, three others with these deletions and an event did not exhibit genetic alterations that would predict a poorer outcome – one patient carried the *ETV6-RUNX1* fusion, one was hyperdiploid and one had no recurrent genetic abnormalities. This shows that alterations in cell differentiation and cell cycle regulation genes may play a crucial role in disease development even in patients with primary genetic alterations that are thought to be favourable, which is in concordance with reports of these deletions being an independent prognostic factor.[6]

Previously published studies have shown a poorer event-free and overall survival of patients with *IKZF1* deletions in comparison to those without such aberrations[6,8,12,14,16,30], and Stanulla *et al*. discovered that patients with additional mutations in certain genes that define the *IKZF1*^{plus} profile have even more dismal outcomes.[21] Our study similarly confirmed the inferior event-free survival for patients with *IKZF1* deletions and the *IKZF1*^{plus} profile, however, the overall survival did not significantly differ between the groups. After adjusting for confounding factors, our data did not confirm the independent prognostic role of the *IKZF1* deletions, as well as *IKZF1*^{plus}, on EFS. However, the trend of poorer EFS in patients with the *IKZF1* deletions and the *IKZF1*^{plus} profile was observed. These discrepancies, as well as the high proportion of males presenting with the *IKZF1* mutations, are most likely the result our small sample size and short follow-up duration. When inspecting non-high-risk patients with the *IKZF1*^{plus} profile, the relative frequency of events among the patients with the profile was higher, and there was a trend of poorer EFS for these patients. The dismal outcomes for patients with the *IKZF1*^{plus} profile have previously been confirmed by other studies, and this profile is currently already being used in cer-

tain treatment protocols[20], and more are likely to follow.

The CNV analysis of other genes showed that the most common alterations were in the *PAX5* gene (30.7%), *CDKN2A,* and *CDKN2B* (26.1% and 25.0%, respectively). However, deletions in *CDKN2A/2B* were more common than deletions in *PAX5* which was also observed by Öfverholm *et al*.[31] and Mullighan *et al*.[9] Deletions in *PAX5* have previously been reported as much more common than intragenic amplifications in this gene, and the latter have mostly been reported only in isolated cases.[31-34] However, more recently, Schwab *et al*.[23] showed that *PAX5* amplifications occur in around 1% of B-ALL cases, out of which 40% experienced a relapse, suggesting that these alterations may play an important role in leukemogenesis. Interestingly, in our cohort, the amplifications were even more common, as they occurred in 10.2% of all B-ALL cases. Out of 27 patients with CNVs in *PAX5*, 9 (33.3%) carried amplifications. As already suggested by Schwab *et al*.[23], more studies need to be conducted to evaluate the prognostic impact of *PAX5* amplifications. The *PAX5* deletions were also more frequent in our cohort (20.5%) than previously described (10%).[35,36] Amongst the samples with *PAX5* deletion, a sizable amount (61.1%) also carried the *CDKN2A/2B* deletions. The frequent co-occurrence of these deletions has previously been described by Kim *et al*.[37]

In our cohort, amplifications in the PAR1 region were observed quite frequently. Altogether, 17 patients (19.3%) had at least one gene amplification in this region. This is due to the fact that our cohort is unselected, and therefore also includes patients with hyperdiploidy. In hyperdiploidy, gains in the X chromosome are very common (present in 70% of hyperdiploid childhood B-ALL cases)[38], and indeed, 14 out of our 17 patients with amplifications in PAR1 had a hyperdiploid karyotype. This karyotype is associated with a favourable outcome. However, the hyperdiploid patients in our cohort did not have a significantly better 5-year EFS, and the same was seen for the patients with amplifications in the PAR1 region that were identified with MLPA. Two patients carried deletions in this region (namely in *CSF2RA, IL3RA* and *P2RY8* genes), which resulted in the formation of the *P2RY8-CRLF2* fusion gene. This was confirmed with fluorescence *in situ* hybridization. While the *P2RY8-CRLF2* fusion is associated with a poorer treatment response and outcomes[39], the two patients in our cohort did not experience an event.

Despite the limitations of our study due to a lower number of analyzed samples and relatively short follow-up period, it produced results that are in concordance with the results obtained in larger cooperative clinical trials. We have shown that it is possible to provide comparable results regarding the presence of certain CNVs and their prognostic value in pediatric B-ALL patients even within a single-center experience. This study is only a starting point for the more comprehensive screening of patients diagnosed with B-ALL in Slovenia that we have planned for the future and will enable us to better evaluate and treat these patients.

Acknowledgments

The research was supported by the Slovenian Research Agency (ARRS) grant number P3-0343.

References

1. Roberts KG, Reshmi SC, Harvey RC, Chen IM, Patel K, Stonerock E, et al. Genomic and outcome analyses of Ph-like ALL in NCI standard-risk patients: a report from the children's oncology group. *Blood* 2018; **132:** 815-24. doi: 10.1182/blood-2018-04-841676

2. Hunger SP, Lu X, Devidas M, Camitta BM, Gaynon PS, Winick NJ, et al. Improved survival for children and adolescents with acute lymphoblastic leukemia between 1990 and 2005: a report from the children's oncology group. *J Clin Oncol* 2012; **30:** 1663-9. doi: 10.1200/JCO.2011.37.8018

3. Ward E, DeSantis C, Robbins A, Kohler B, Jemal A. Childhood and adolescent cancer statistics, 2014. *CA Cancer J Clin* 2014; **64:** 83-103. doi: 10.3322/caac.21219

4. Einsiedel HG, Von Stackelberg A, Hartmann R, Fengler R, Schrappe M, Janka-Schaub G, et al. Long-term outcome in children with relapsed ALL by risk-stratified salvage therapy: results of trial Acute Lymphoblastic Leukemia-Relapse Study of the Berlin-Frankfurt-Münster Group 87. *J Clin Oncol* 2005; **23:** 7942-50. doi: 10.1200/JCO.2005.01.1031

5. Olsson L, Ivanov Öfverholm II, Norén-Nyström U, Zachariadis V, Nordlund J, Sjögren H, et al. The clinical impact of IKZF1 deletions in paediatric B-cell precursor acute lymphoblastic leukaemia is independent of minimal residual disease stratification in Nordic Society for Paediatric Haematology and Oncology treatment protocols used between 1992 aand 1993. *Br J Haematol* 2015; **170:** 847-58. doi: 10.1111/bjh.13514

6. Dörge P, Meissner B, Zimmermann M, Möricke A, Schrauder A, Bouquin JP, et al. IKZF1 deletion is an independent predictor of outcome in pediatric acute lymphoblastic leukemia treated according to the ALL-BFM 2000 protocol. *Haematologica* 2013; **98:** 428-32. doi: 10.3324/haematol.2011.056135

7. Asai D, Imamura T, Suenobu S, Saito A, Hasegawa D, Deguchi T, et al. IKZF 1 deletion is associated with a poor outcome in pediatric B-cell precursor acute lymphoblastic leukemia in Japan. *Cancer Med* 2013; **2:** 412-9. doi: 10.1002/cam4.87

8. Kuiper RP, Waanders E, Van Der Velden VHJ, Van Reijmersdal SV, Venkatachalam R, Scheijen B, et al. IKZF1 deletions predict relapse in uniformly treated pediatric precursor B-ALL. *Leukemia* 2010; **24:** 1258-64. doi: 10.1038/leu.2010.87

9. Mullighan CG, Su X, Zhang J, Radtke I, Phillips LAA, Miller CB, et al. Deletion of IKZF1 and prognosis in acute lymphoblastic leukemia. *N Engl J Med* 2009; **360:** 470-80. doi: 10.1056/NEJMoa0808253

10. Georgopoulos K, Bigby M, Wang JH, Molnar A, Wu P, Winandy S, et al. The ikaros gene is required for the development of all lymphoid lineages. *Cell* 1994; **79:** 143-56. doi: 10.1016/0092-8674(94)90407-3

11. Molnar A, Wu P, Largespada DA, Vortkamp A, Scherer S, Copeland NG, et al. The Ikaros gene encodes a family of lymphocyte-restricted zinc finger DNA binding proteins, highly conserved in human and mouse. *J Immunol* 1996; **156:** 585-92. PMID: 8543809

12. Yang YL, Hung CC, Chen JS, Lin KH, Jou ST, Hsiao CC, et al. IKZF1 deletions predict a poor prognosis in children with B-cell progenitor acute lymphoblastic leukemia: a multicenter analysis in Taiwan. *Cancer Sci* 2011; **102:** 1874-81. doi: 10.1111/j.1349-7006.2011.02031.x

13. Van Der Veer A, Waanders E, Pieters R, Willemse ME, Van Reijmersdal S V., Russell LJ, et al. Independent prognostic value of BCR-ABL1-like signature and IKZF1 deletion, but not high CRLF2 expression, in children with B-cell precursor ALL. *Blood* 2013; **122:** 2622-9. doi: 10.1182/blood-2012-10-462358

14. Moorman A V., Enshaei A, Schwab C, Wade R, Chilton L, Elliott A, et al. A novel integrated cytogenetic and genomic classification refines risk stratification in pediatric acute lymphoblastic leukemia. *Blood* 2014; **124:** 1434-44. doi: 10.1182/blood-2014-03-562918

15. Mullighan CG, Miller CB, Radtke I, Phillips LA, Dalton J, Ma J, et al. BCR-ABL1 lymphoblastic leukaemia is characterized by the deletion of Ikaros. *Nature* 2008; **453:** 110-14. doi: 10.1038/nature06866

16. Van Der Veer A, Zaliova M, Mottadelli F, De Lorenzo P, Te Kronnie G, Harrison CJ, et al. IKZF1 status as a prognostic feature in BCR-ABL1-positive childhood ALL. *Blood* 2014; **123:** 1691-8. doi: 10.1182/blood-2013-06-509794

17. Roberts KG. The biology of Philadelphia chromosome-like ALL. *Best Pract Res Clin Haematol* 2017; **30:** 212-21. doi: 10.1016/j.beha.2017.07.003

18. Boer JM, Van Der Veer A, Rizopoulos D, Fiocco M, Sonneveld E, De Groot-Kruseman HA, et al. Prognostic value of rare IKZF1 deletion in childhood B-cell precursor acute lymphoblastic leukemia: an international collaborative study. *Leukemia* 2016; **30:** 32-38. doi: 10.1038/leu.2015.199

19. Steeghs EMP, Boer JM, Hoogkamer AQ, Boeree A, de Haas V, de Groot-Kruseman HA, et al. Copy number alterations in B-cell development genes, drug resistance, and clinical outcome in pediatric B-cell precursor acute lymphoblastic leukemia. *Sci Rep* 2019; **9:** 1-11. doi: 10.1038/s41598-019-41078-4

20. Stanulla M, Cavé H, Moorman A V. IKZF1 deletions in pediatric acute lymphoblastic leukemia: still a poor prognostic marker? *Blood* 2020; **135:** 252-60. doi: 10.1182/blood.2019000813

21. Stanulla M, Dagdan E, Zaliova M, Möricke A, Palmi C, Cazzaniga G, et al. IKZF1 plus defines a new minimal residual disease-dependent very-poor prognostic profile in pediatric b-cell precursor acute lymphoblastic leukemia. *J Clin Oncol* 2018; **36:** 1240-9. doi: 10.1200/JCO.2017.74.3617

22. Gu Z, Churchman ML, Roberts KG, Moore I, Zhou X, Nakitandwe J, et al. PAX5-driven subtypes of B-progenitor acute lymphoblastic leukemia. *Nat Genet* 2019; **51:** 296-307. doi: 10.1038/s41588-018-0315-5

23. Schwab C, Nebral K, Chilton L, Leschi C, Waanders E, Boer JM, et al. Intragenic amplification of PAX5: a novel subgroup in B-cell precursor acute lymphoblastic leukemia? *Blood Adv* 2017; **1:** 1473-7. doi: 10.1182/bloodadvances.2017006734

24. Zhang W, Kuang P, Liu T. Prognostic significance of CDKN2A/B deletions in acute lymphoblastic leukaemia: a meta-analysis. *Ann Med* 2019; **51:** 28-40. doi: 10.1080/07853890.2018.1564359

25. Carrasco Salas P, Fernández L, Vela M, Bueno D, González B, Valentín J, et al. The role of CDKN2A/B deletions in pediatric acute lymphoblastic leukemia. *Pediatr Hematol Oncol* 2016; **33:** 415-22. doi: 10.1080/08880018.2016.1251518

26. Zhang W, Kuang P, Liu T. Prognostic significance of CDKN2A/B deletions in acute lymphoblastic leukaemia: a meta-analysis. *Ann Med* 2019; **51:** 28-40. doi: 10.1080/07853890.2018.1564359

27. Yamashita Y, Shimada A, Yamada T, Yamaji K, Hori T, Tsurusawa M, et al. IKZF1 and CRLF2 gene alterations correlate with poor prognosis in japanese BCR-ABL1-negative high-risk B-cell precursor acute. *Pediatr Blood Cancer* 2013; **60:** 1587-92. doi: 10.1002/pbc

28. Palmi C, Valsecchi MG, Longinotti G, Silvestri D, Carrino V, Conter V, et al. What is the relevance of Ikaros gene deletions as a prognostic marker in pediatric Philadelphia-negative B-cell precursor acute lymphoblastic leukemia? *Haematologica* 2013; **98:** 1226-31. doi: 10.3324/haematol.2012.075432

29. Clappier E, Grardel N, Bakkus M, Rapion J, De Moerloose B, Kastner P, et al. IKZF1 deletion is an independent prognostic marker in childhood B-cell precursor acute lymphoblastic leukemia, and distinguishes patients benefiting from pulses during maintenance therapy: results of the EORTC Children's Leukemia Group study 58951. *Leukemia* 2015; **29:** 2154-61. doi: 10.1038/leu.2015.134

30. Vrooman LM, Blonquist TM, Harris MH, Stevenson KE, Place AE, Hunt SK, et al. Refining risk classification in childhood b acute lymphoblastic leukemia: results of DFCI ALL consortium protocol 05-001. *Blood Adv* 2018; **2:** 1449-58. doi: 10.1182/bloodadvances.2018016584

31. Öfverholm I, Tran AN, Heyman M, Zachariadis V, Nordenskjöld M, Nordgren A, et al. Impact of IKZF1 deletions and PAX5 amplifications in pediatric B-cell precursor ALL treated according to NOPHO protocols. *Leukemia* 2013; **27:** 1936-9. doi: 10.1038/leu.2013.92

32. Schwab CJ, Jones LR, Morrison H, Ryan SL, Yigittop H, Schouten JP, et al. Evaluation of multiplex ligation-dependent probe amplification as a method for the detection of copy number abnormalities in B-cell precursor acute lymphoblastic leukemia. *Genes Chromosom Cancer* 2010; **49:** 1104-13. doi: 10.1002/gcc

33. Schwab CJ, Chilton L, Morrison H, Jones L, Al-Shehhi H, Erhorn A, et al. Genes commonly deleted in childhood B-cell precursor acute lymphoblastic leukemia: association with cytogenetics and clinical features. *Haematologica* 2013; **98:** 1081-8. doi: 10.3324/haematol.2013.085175

34. Mullighan CG, Goorha S, Radtke I, Miller CB, Coustan-Smith E, Dalton JD, et al. Genome-wide analysis of genetic alterations in acute lymphoblastic leukaemia. *Nature* 2007; **446:** 758-64. doi: 10.1038/nature05690

35. Kim M, Choi JE, She CJ, Hwang SM, Shin HY, Ahn HS, et al. PAX5 deletion is common and concurrently occurs with CDKN2A deletion in B-lineage acute lymphoblastic leukemia. *Blood Cells, Mol Dis* 2011; **47:** 62-6. doi: 10.1016/j.bcmd.2011.04.003

36. Kawamata N, Ogawa S, Zimmermann M, Sanada M, Hemminki K, Yamatomo G, et al. Rearrangement and deletion of the PAX5 gene in pediatric acute B-cell lineage lymphoblastic leukemia. *Blood* 2007; **110:** 981. doi: 10.1182/blood.V110.11.981.981

37. Kim M, Choi JE, She CJ, Hwang SM, Shin HY, Ahn HS, et al. PAX5 deletion is common and concurrently occurs with CDKN2A deletion in B-lineage acute lymphoblastic leukemia. *Blood Cells, Mol Dis* 2011; **47:** 62-6. doi: 10.1016/j.bcmd.2011.04.003

38. Paulsson K, Johansson B. High Hyperdiploid childhood acute lymphoblastic leukemia. *Genes Chromosom Cancer* 2009; **48:** 637-60. doi: 10.1002/gcc.20671

39. Palmi C, Vendramini E, Silvestri D, Longinotti G, Frison D, Cario G, et al. Poor prognosis for P2RY8-CRLF2 fusion but not for CRLF2 over-expression in children with intermediate risk B-cell precursor acute lymphoblastic leukemia. *Leukemia* 2012; **26:** 2245-53. doi: 10.1038/leu.2012.101

research article

Percutaneous electrochemotherapy in primary and secondary liver malignancies – local tumor control and impact on overall survival

Hannah Spallek[1], Peter Bischoff[1], Willi Zhou[1], Francesca de Terlizzi[2], Fabian Jakob[3], Attila Kovàcs[1]

[1] Clinic for Diagnostic and Interventional Radiology and Neuroradiology, MediClin Robert Janker Klinik, Bonn, Germany
[2] IGEA Clinical Biophysics, Laboratory Carpy, Modena, Italy
[3] Clinic for Radiology and Nuclear Medicine, University Hospital Schleswig Holstein, Campus Luebeck, Luebeck, Germany

Radiol Oncol 2022; 56(1): 102-110.

Received 19 11 2021
Accepted 24 12 2021

Correspondence to: Attila Kovàcs, Clinic for Diagnostic and Interventional Radiology and Neuroradiology, MediClin Robert Janker Klinik, Bonn, Germany. E-mail: Attila.Kovacs@mediclin.de

Disclosure: No potential conflicts of interest were disclosed.

Background. Local nonsurgical tumor ablation currently represents a further option for the treatment of patients with liver tumors or metastases. Electrochemotherapy (ECT) is a welcome addition to the portfolio of local therapies. A retrospective analysis of patients with liver tumors or metastases treated with ECT is reported. Attention is given to the safety and efficacy of the treatment over time.

Patients and methods. Eighteen consecutive patients were recruited with measurable liver tumors of different histopatologic origins, mainly colorectal cancer, breast cancer, and hepatocellular cancer. They were treated with percutaneous ECT following the standard operating procedures (SOP) for ECT under general anaesthesia and muscle relaxation. Treatment planning was performed based on MRI preoperative images. The follow-up assessment included contrast-enhanced MR within at least 1–3 months after treatment and then after 5, 7, 9, 12, and 18 months until progression of the disease or death.

Results. Only mild or moderate side effects were observed after ECT. The objective response rate was 85.7% (complete response 61.9%, partial 23.8%), the mean progression-free survival (PFS) was 9.0 ± 8.2 months, and the overall survival (OS) was 11.3 ± 8.6 months. ECT performed best (PFS and OS) in lesions within 3 and 6 cm diameters ($p = 0.0242$, $p = 0.0297$). The effectiveness of ECT was independent of the localization of the lesions: distant, close or adjacent to vital structures. Progression-free survival and overall survival were independent of the primary histology considered.

Conclusions. Electrochemotherapy provides an effective valuable option for the treatment of unresectable liver metastases not amenable to other ablative techniques.

Key words: electrochemotherapy; liver metastases

Introduction

Globally, liver cancer ranks sixth for cancer incidence and fourth for cancer deaths, being the second leading cause of cancer-related years of life lost. During the next decade, a further increase in the number of new cases of primary liver cancer is predicted each year in most countries as a result of changes in risk factors.[1,2]

Globally, colon and rectal cancer ranks third for cancer incidence and second for cancer deaths.[1] Population-based studies have shown that 25–30% of patients diagnosed with colorectal cancer (CRC) develop liver metastases during the course of their

disease. Indications for curative-intended treatment of CRC liver metastases have expanded in recent years. Unfortunately, despite oncological and surgical advances, only 25% of patients affected are amenable to resection.[3,4]

Local nonsurgical interventional tumor ablation currently represents a further option for the treatment of cancer patients. Local treatments can be divided into thermal (radiofrequency or microwave ablation and cryoablation) and nonthermal treatments (high precision radiotherapy, brachytherapy and electroporation).

The European Society of Medical Oncology (ESMO) included local ablation procedures in the current consensus guidelines on the treatment of metastatic colorectal cancer (mCRC).[5]

The choice of therapy is determined by the number, size, configuration and location or environment of the target lesion. Thermal ablation techniques are emerging as alternative treatment options to open surgery for both primary and secondary hepatic tumors.[6] A disadvantage of RFA is the therapeutic limitation to smaller target lesions up to 3.5 cm in diameter; in the case of microwave and cryoablation, the ablation zone can be enlarged up to 5 cm in tumor diameter. However, hyperthermia-based technologies have some limitations, including heat sink effects in the proximity of large blood vessels, the risk of causing cholestasis when treating lesions close to the thermosensitive bile ducts or damaging critical structures if proximal to the hepatic portal Glisson's capsule or diaphragm, or if located on the intra-abdominal free surface.

A special form of local nonthermal ablation is internal radiation (interstitial brachytherapy), which uses radiation with a very limited range because it is limited in the proximity of organs vulnerable to radiation; it cannot be repeated, and furthermore, some tumor entities are not radiosensitive. In such cases, chemoablation, such as electrochemotherapy (ECT), is a welcome addition to the portfolio of local therapies.

ECT is a local ablative technique that utilizes electroporation for enhanced drug (bleomycin or cisplatin) delivery to cells by generating transient permeation structures in the cell membrane.[7,8] Over the past 20 years, ECT has been shown to have proven effectiveness in the treatment of cutaneous, subcutaneous, mucosal, or deep-seated tumors of various histologies and in different body sites.[9-11]

The international, multicenter clinical study European Standard Operating Procedures for Electrochemotherapy (ESOPE) developed the Standard Operating Procedures for ECT on cutaneous tumors with the Cliniporator™ Device (IGEA S.p.A., Carpi, Italy).[8] Based on its effectiveness for cutaneous tumors, ECT is now being developed and has been shown to be feasible, safe, and effective for deep-seated tumors, such as liver tumors. ECT can be used near collagenous structures such as vessels and bile ducts[12], and it is repeatable and suitable as a local therapy between chemotherapy cycles. ECT has the potential to close relevant gaps in the spectrum of local ablative therapies, enabling the treatment of i) lesions that are too large for thermal ablation, ii) nonradiation-sensitive tumors or iii) lesions located in the immediate vicinity of radiation- or temperature-vulnerable organs. ECT is specifically suitable for the treatment of liver metastases located centrally, close to the capsule or in proximity of the major vessels, which are not resectable and not suitable for radiofrequency ablation or microwave ablation due to the heat sink effect. The safety of ECT in the treatment of metastases located near large liver vessels was also proven in animal models.[13,14] In cancer patients, ECT is well tolerated, with few side effects and no relevant pain, nausea or systemic side effects.[15-18]

In this study, we present a retrospective analysis of patients with liver tumors or metastases treated with ECT at our institution. This is the first real-world clinical experience on percutaneous application of ECT in the liver in a large cohort of patients. Attention is given to the safety and efficacy of the treatment over time.

Patients and methods

In this cohort study, 18 patients with measurable liver tumors of different histopathologic origins were recruited: colorectal cancer, breast cancer, hepatocellular cancer, ovarian cancer, anal cancer, non-small cell lung cancer (NSCLC) and cancer of unknown primary origin (CUP). They were treated with ECT between June 2018 and June 2020. The study was conducted according to the Helsinki declaration. The patients signed an informed consent form. The study was approved by the Committee for Medical Ethics of the Institution.

Imaging

Standard pretreatment evaluation of patients with liver tumors included liver MRI with a hepatospecific contrast agent and CT of the thorax and abdomen, including the pelvis at least 1 month before ECT. MRI was performed using a GE Signa Hdxt

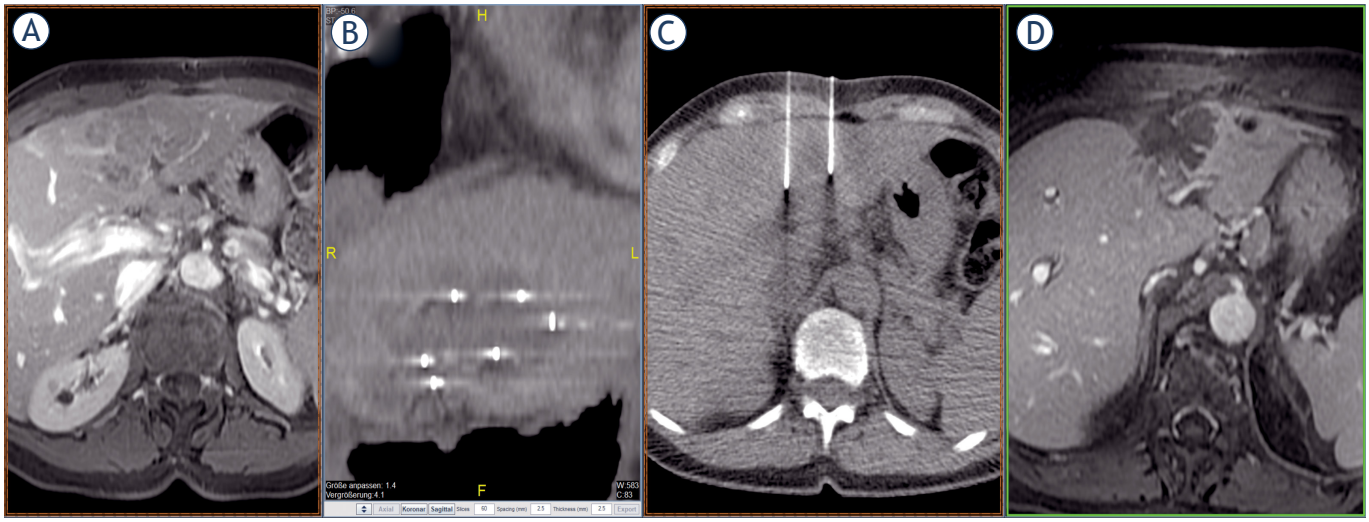

FIGURE 1. (A) Solitary liver metastasis from a breast carcinoma in a challenging location between the left and right lobes of the liver, not amenable to surgical resection and progressive under various lines of systemic chemotherapy. The dimensions of the metastasis in segment IVa/b adjacent to segment VIII were 4 x 7 x 5 cm (volume 70 cc). **(B)** Position of the electrodes in the coronary reconstruction. The aim is to achieve the most uniform coverage of the target lesion by the electrodes. **(C)** Position of the electrodes in axial cross-sectional imaging. This image shows another essential requirement for the therapeutic success of ECT – the parallelism of the electrodes. **(D)** The most recent imaging control, complete two years after the ECT procedure, shows complete chemoablation of the entire metastasis, thus formally complete remission of the target lesion without residual or marginal recurrence.

1.5T using standard imaging sequences for the liver: tra T2w fs, tra DWI, tra T1w nat, tra and cor ce T1w. The patients were reviewed by a multidisciplinary team. The follow-up assessment included contrast-enhanced MRI of the liver within at least 1–3 months after treatment and then after 5, 7, 9, 12, 18 months and/or until progression of the disease or death.

Electrochemotherapy

Freehand electrodes are used for the percutaneous therapy of parenchymatous organs or for intraoperative positioning. Depending on the size, configuration and localization of the target region, different active electrode tips, shaft lengths and thicknesses can be selected. A maximum of 6 probes can be operated synchronously. Therapy planning is software-based: the parallel positioning of the probes at a defined distance from each other plays an essential role in the optimal therapeutic coverage of the target lesion. The aim is to achieve a distance of 2.0 to 2.5 cm from each other and a voltage to be applied of approx. 1000 volts per cm. Treatment planning was performed based on MRI preoperative images. During ECT treatment, needle electrodes were percutaneously inserted based on the CT-fluoro guided planning images, and a distance of at least 0.5 and maximally 3.0 cm between the electrodes was ensured. Electrodes were freely positionable single needle probes with a diameter of 1.2 mm; a minimum of 2 and a maximum of 8 electrodes (median 6) were used per treatment (Table 2). In particular: in 8 patients electrodes 16 cm long and with an active part of 4 cm, in 6 patients electrodes 16 cm long with an active part of 3 cm, in 4 patients electrodes 20 cm long with 3 cm active part and in 1 patient electrodes 20 cm long with active part of 4 cm (IGEA, Carpi, Italy). The direction of electrode access was determined by the performing surgeon.

Since the pulses are delivered, among pairs of electrodes, the computation of the voltage to be applied was performed by the device for each pair of electrodes separately, and the appropriate electric field for each pair combined assured the complete coverage of a tumor. By sequentially activating the electrodes in this way, a larger tumor volume can be covered with sufficiently strong electric fields.[19] The goal was to ensure 100% coverage of the clinical target volume with an electric field above 400 V/cm and to limit the maximum current delivered to the tissue to be below 50 A (hardware limit of the IGEA Cliniporator Vitae pulse generator).[20]

ECT was performed using the same treatment protocol as defined by the SOP for ECT of cutaneous tumors regarding the drug dosage and electrical parameters (*i.e.*, pulse duration and number of

pulses) of electroporation.[8,21] The needle electrodes were percutaneously inserted into the lesions under CT-fluoro guidance. The electrodes were connected to an electric pulse generator (Cliniporator VITAE, IGEA SpA, Carpi, Italy). Thereafter, the patients were given 15,000 U/m^2 bleomycin intravenously in bolus. Eight electric pulses of 100 µs duration were delivered between pairs of electrodes 8 min after the bleomycin injection, when the maximal pharmacological peak of bleomycin in the tumors was expected. Complete coverage of the tumor by repositioning of the electrodes should possibly be completed by 40 minutes thereafter. Care is also taken to ensure that the electrical pulses are delivered only in the refractory phase of the heart by automatic ECG synchronization to avoid interferences with the heart rhythm. ECT treatment takes place under general anaesthesia and muscle relaxation as a minimally invasive, usually percutaneous, procedure (Figure 1).

Statistical analysis

Descriptive statistics are reported as the mean, standard deviation, median and range for continuous variables and absolute numbers and percentage for categorical variables. Comparisons between groups were performed by ANOVA (continuous variables) and contingency tables and chi square tests (for categorical variables). A P value lower than 0.05 was considered statistically significant. Statistical analysis was performed with NCSS 9 (NCSS 9 Statistical Software (2013)). NCSS, LLC. Kaysville, Utah, USA, ncss.com/software/ncss).

Results

Eighteen patients were treated with ECT in the period June 2018 – June 2020 and were followed for a median time of 9 months (mean 11.3 ± 8.6 months). One patient was lost to follow-up. Three patients were treated with 2 lesions, all the others in a single lesion of the liver.

The characteristics of the cohort of patients are reported in Table 1. The mean age was 64.3 ± 11.1 years (median 64, range 41–83 years).

Lesion sizes were 5.9 ± 2.5 cm in the LA (long axis) direction (median 4.6, range 1.5–11.2 cm) and 5.4 ± 2.1 cm in the SA (short axis) direction (median 5.5, range 1.5–10 cm). The overall mean volume was 129.6 ± 137.3 cm^3 (median 57, range 23–475 cm^3). Table 2 shows other characteristics of the lesions and the technical parameters of ECT treatment.

TABLE 1. Demographic

	N	%
PATIENTS	18	
GENDER		
M	8	44.4%
F	10	55.6%
DIAGNOSIS		
Colorectal cancer	7	38.9%
Breast cancer	4	22.2%
Hepatocellular cancer	2	11.1%
Ovarian cancer	2	11.1%
Anal cancer	1	5.6%
Cancer of unknown primary origin (CUP)	1	5.6%
Non-small cell lung cancer (NSCLC)	1	5.6%
TUMOURS TREATED	21	
LIVER METASTASES		
Synchronous	8	44.4%
Metachronous	8	44.4%
No	2	11.2%
METASTASES LOCATION		
Liver only	7	43.7%
Liver + lung	3	21.5%
Liver + bone	1	6.2%
Liver + kidney	1	6.2%
Liver + lung + bone + brain	1	6.2%
Liver + bone + peritoneum	1	6.2%
Liver + pleural + bone	1	6.2%
Liver + retroperitoneal	1	6.2%
PREVIOUS TREATMENTS		
Systemic therapy	16	88.8%
Liver surgery	4	22.2%
TACE	8	44.4%
TACE + RFA	1	5.6%
TACE + CP	1	5.6%
CRYOTH	1	5.6%
NO	7	38.9%
COMORBIDITIES*		
Cardiac diseases	6	33.3%
Pulmonary diseases	3	16.7%
Liver diseases	9	50.0%

* Cardiac diseases were cardiomyopathies, *status post* coronary bypass, *status post* aortocoronary venous bypass operation, valvular disease, pericardial effusion; pulmonary diseases were chronic obstructive pulmonary diseases; liver diseases were hematomas, ascites, cholestasis, hemochromatosis

CP = chemoperfusion; CRYOTH = cryotherapy; F = female; M = male; N = number; RFA = radiofrequency ablation; TACE = hepatic artery chemoembolization

Safety/toxicity

Only mild or moderate side effects were observed after ECT: in 16 of 21 patients, temporary (1st day) mild pain at the treated site; in 1 patient, CRP (C-reactive protein) elevation and leucocytosis were successfully treated with *i.v.* antibiotics; and in 1 patient, moderate pain due to a liver capsular hematoma, *w.o.* hemoglobin drop, successfully treated with ibuprofen/pantoprazole self-resolving after 10 days.

TABLE 2. Lesions and treatment description

	N	%
LESIONS	21	100%
PLANNING MRI	21	100%
TYPE		
Hypervascular	2	9.5%
Intermediate	14	71.4%
Hypovascular	5	19.0%
CHALLENGING LOCATION*		
Yes	19	90.5%
No	2	9.5%
VESSELS OR BILE DUCTS SURROUNDING THE METASTASES		
Distant (> 10 mm)	4	19.0%
Close (1 mm to 10 mm)	6	28.6%
Adjacent (< 1 mm)	11	52.4%
PREVIOUS LOCAL TREATMENT ON THE LESION		
Local ablative therapy (LAT)	0	0%
Transarterial chemoembolization (TACE)	6	28.6%
Chemoperfusion (CP)	1	4.8%
Treatment-naive	14	66.7%
TECHNICAL SUCCESS		
Yes	20	95.2%
No	1	4.8%
# ELECTRODES PER TREATMENT		
2	1	4.8%
3	2	9.5%
4	1	4.8%
6	16	76.2%
8	1	4.8%

* Challenging location represented in liver were liver dome, vicinity of portal vein main trunk, vicinity of main bile duct

Response to treatment

The response to treatment was evaluated between 1 and 3 months after the ECT session; the overall response is reported in Table 3. Objective response rate was 85.7%.

Mean progression-free survival (PFS) was 9.0 ± 8.2 months. Three patients progressed during follow-up after 3, 5, and 7 months. The first underwent TACE and was in complete response (CR) after 6 months; the second underwent interstitial brachytherapy and was in CR after 2 months; the last underwent TACE + CRYO and was in CR after 11 months.

Mean overall survival (OS) was 11.3 ± 8.6 months. Three patients died for reasons related to liver metastases (14.3%), 11 patients (52.4%) died for other reasons, and 7 (33.3%) were still alive.

Furthermore, response to treatment, PFS and OS were evaluated according to lesion size, histology of the primary tumor and location of the liver lesions. The results are shown in Table 4.

Discussion

Interventional oncology is the fastest developing area of interventional radiology. Minimally invasive, image-guided procedures are playing an increasingly important role in multimodal cancer therapy.[22-24]

In this study, we evaluated the effect of percutaneous ECT on liver tumors of different pathologic origins. Percutaneous ECT treatments of 21 lesions in 18 patients were included in the analysis. The lesions were close to the capsule or in proximity of the major vessels, not suitable for radiofrequency or microwave ablation due to the heat sink effect, and not surgically resectable. In 90.5% of cases, the lesions were in a challenging location (liver dome, near portal vein main trunk, near main bile duct).

The mean volume of treated lesions was 129.59 ± 137.31 cm^3, which is definitely larger than the volumes usually accessible for other minimally invasive procedures.

The most important advantage of minimally invasive technologies is that, in combination with standard therapies, they significantly increase overall survival compared to standard treatment alone. This has been proven in 2 different studies: the CLOCC[22] and the SABR-COMET[25] trials. In the CLOCC trial, patients with nonresectable colorectal cancer liver metastases were randomized either to receive systemic chemotherapy or a combination of systemic and minimally invasive therapies; the overall survival at 8 years was significantly improved in the combined arm versus the standard therapies arm (36% *vs.* 8%). In the same way, the SABR-COMET study analyzed the impact of stereotactic ablative radiotherapy (SABR) in combination with standard of care in the treatment of different oligometastatic patients from various cancers (breast, lung, colorectal, prostate) in comparison with standard of care alone. The first arm showed a superior 5-year survival (42.3% *vs.* 17.7%). Other advantages of minimally invasive technologies are good tolerability, less impact on quality of life, fewer systemic side effects and tissue preservation when compared to classical surgery. Furthermore, except for radiotherapy, minimally invasive technologies are also repeatable.

Thermo and radioablative techniques are limited in some situations, for example, when target lesions have a size that exceeds the safe ablation zone of thermal procedures, usually estimated at 3.5 cm in diameter.[26] On the other hand, radioablation is limited near radiation-sensitive organs. In these cases, ECT can truly be a valuable option, as it is

TABLE 3. Response of target lesions evaluated between 1 and 3 months

RESPONSE	N	%
Complete response (CR)	13	61.9%
Partial response (PR)	5	23.8%
Stable disease (SD)	1	4.8%
Progressive disease (PD)	0	0%
Lost to follow-up	2	9.5%

a combined tumor therapy that enhances the local effect of a systemically administered chemotherapeutic drug by reversible electroporation.[26] The most commonly used chemotherapeutic agent is bleomycin, which, when combined with electroporation, has the major advantage of being cytotoxic regardless of the tumor's histology.

The aim of minimally invasive, local ablative procedures is to destroy primary and secondary malignancies efficiently and gently at the same time using image guidance. These novel techniques can be used for diverse applications ranging from curative intent for small localized tumors, down staging of large tumors for resection, or locoregional control and palliation of advanced disease. The choice of therapy is determined by the parameters "number, size and location" of the target lesions. Given that all standard local ablative procedures were available at the hospital that conducted the present study, a proactive decision was made to perform ECT in each individual case. Due to the aforementioned limitations of each procedure, it was most often the size, location and immediate environment of the target lesions that contraindicated thermal ablation or compromised its efficacy in the first place. In most decisions, from the therapist's point of view, ECT seemed to us to be the only alternative.

This technique has already been shown to be effective on cutaneous, subcutaneous and mucosal lesions[10,11], with a response rate of 70–80%, and to be particularly effective on basal cell carcinoma, with a complete remission of treated lesions up to 91%.[11]

ECT has also shown convincing results with deep-seated tumors. In a prospective multicenter study[27], Campanacci *et al.* evaluated ECT in the treatment of symptomatic bone metastases. The results on 102 patients from 11 European centers demonstrated that ECT is a safe and effective treatment for painful bone metastases resistant to other local treatments. Furthermore, a significant decrease in pain intensity and significantly better quality of life were observed after the ECT session and at later follow-up.

Several pilot studies on intraoperative ECT on liver metastases[16,28-30], hepatocellular carcinoma[31,32], perihilar cholangiocarcinoma[33,34], vulvar cancer[35–37], and renal cancer[38] are available in the literature.

In a recently published phase II study on ECT in the treatment of colorectal liver metastases, the objective response rate (OR) per lesion was 75%, with 63% complete response (CR) and 12% partial response (PR), while OR, CR and PR per patient were 59%, 44% and 15%, respectively. The median response time was 20.8 months for metastases in CR and 9.8 months for metastases in PR. There was no difference in treatment response with regard to the location of the metastases, e.g., metastases in the central *vs*. peripheral location. The median overall survival of patients after ECT was 29.0 months.[16] The histopathological assessment of some of these colorectal liver metastases after ECT treatment showed that most vessels (> 5 mm) and biliary structures remained intact, while smaller blood vessels were damaged. This study shows that ECT can be safely applied to treat metastases in the immediate vicinity of the large blood vessels in the liver.[12]

Regarding hepatocellular carcinoma (HCC), a prospective phase II study was recently published on 24 patients with 32 HCC lesions not suitable for other curative treatments according to the BCLC classification or refractory to previous surgery and different local ablative techniques. In this study, the treatment was proven to be equally effective for tumors located centrally and peripherally, with a median response rate per patient of 95.8% (79.2% CR and 16.6% PR). The overall survival over 5 years of observation was 72.0%.[31]

In these studies, ECT treatment was performed intraoperatively as part of an open procedure. To the best of our knowledge, the present study is the largest case series about ECT on liver tumors with a percutaneous approach.

To date, only a few studies with a percutaneous approach to liver tumors using ECT have been published.[15] Tarantino *et al.* 2017 demonstrated the efficiency and effectiveness of ECT in the treatment of six patients with portal vein thrombosis at the hepatic hilum, resulting in two patients with regained complete patency of the portal vein and three patients with a persistent avascular nontumoral shrinked thrombus; none of these patients developed a local recurrence.[39] The same group

TABLE 4. Response to treatment, progression-free survival and overall survival according to different subgroups of analysis

	CR	PR	SD	PD	NE	PFS (mo)	OS (mo)
	N (%)	N (%)	N (%)	N (%)	N (%)	Mean ± s.d.	Mean ± s.d.
SIZE							
< 6 cm	9 (90.0%)	0	0	0	1 (10.0%)	12.0 ± 9.2	15.1 ± 8.0
> 6 cm	4 (36.4%)	5 (45.4%)	1 (9.1%)	0	1 (9.1%)	4.7 ± 5.4	7.9 ± 7.9
P value			0.0483			0.0209	0.0322
HISTOLOGY							
Colorectal cancer	4 (50.0%)	2 (25.0%)	0	0	2 (25.0%)	7.3 ± 12.1	12.1 ± 12.1
Breast cancer	4 (80.0%)	1 (20.0%)	0	0	0	9.8 ± 7.5	10.6 ± 6.9
Hepatocellular cancer	1 (33.3%)	2 (66.7%)	0	0	0	10.3±10.1	15.0 ± 7.2
P-value			0.3615			0.8781	0.8379
LOCATION							
Distant (> 10 mm)	2 (100%)	0	0	0	0	6.5 ± 3.5	8.5 ± 0.7
Close (> 1 mm)	5 (62.5%)	1 (12.5%)	1 (12.5%)	0	1 (12.5%)	8.0 ± 7.4	10.7 ± 7.3
Adjacent (< 1 mm)	6 (54.5%)	4 (36.3%)	0	0	1 (9.2%)	8.8 ± 9.8	10.2 ± 10.5
P-value			0.6643			0.9364	0.9539

CR = comlete response; NE = no evidence, lost to follow up; OS = overall survival; PFS = progression-free survival; PR = partial response; s.d. = standard deviation; SD = stable disease

also successfully treated patients with perihilar cholangiocarcinoma with minimally invasive ECT treatment.[33]

In our study, we showed that ECT performed best (in terms of progression-free survival and overall survival) in lesions < 6 cm in diameter compared to lesions > 6 cm in diameter ($p = 0.0209$ and $p = 0.0322$, respectively). These results demonstrate that the technique is effective even in lesions of large size, up to 6 cm, significantly larger than lesions addressable with thermal ablation techniques.

Furthermore, we proved that the effectiveness of ECT is independent of the localization of the lesions: distant, close or adjacent to vital structures, with the latter being devoid of therapeutic options.

We observed that progression-free survival and overall survival in our cohort of patients were similar for all primary histologies considered: colorectal metastases, breast cancer metastases, and hepatocellular cancer ($p = 0.8781$ and $p = 0.8379$, respectively). This result demonstrates the effectiveness of ECT and bleomycin independent of the histology of the treated lesions.

Apart from its effectiveness, one of the most important advantages of ECT is that it spares collagenous healthy structures such as vessels and bile ducts.[26] ECT is repeatable and suitable as a local therapy even if performed between chemotherapy cycles. In conclusion, ECT has the potential to close relevant gaps in the local ablative therapy field: ECT allows the treatment of lesions too large for thermal ablation, nonradiation-sensitive tumors, and lesions adjacent to radiation-vulnerable organs.

The various thermo, radio- and chemoablative procedures as well as endovascular and percutaneous therapies do not compete with each other but complement each other and are used supplementarily in the hands of experienced interventionalists. Radiological-interventional expertise implies that a broad spectrum of procedures and technologies must be mastered. Too many evidence-based recommendations for sequencing minimally invasive procedures do not yet exist. The scarce knowledge is limited to the combination of TACE and RFA in larger HCCs, where thermal ablation alone is limited.[40] It can be considered an imperative task of the interventional community to generate this same evidence as soon as possible.

In our study, we demonstrated that ECT was well tolerated by the patients, and no serious ad-

verse events were observed during the procedure or in the follow-up; side effects were limited in number and intensity, and no relevant pain or systemic side effects were observed.

This study has several limitations: a retrospective design, the limited number of cases and their heterogeneity in terms of diagnosis of primary tumor, localization, and previous treatments. This is a first experience conducted in our center and therefore includes all patients treated in the observation period. Moreover, this study well represents the variety of the cohort of patients, which can benefit from the application of ECT in clinical practice.

In one case, where 100% technical success could not be achieved, a plastic bile duct stent was placed at the margin of the target lesion. The generator reported inadequate discharges at the two electrodes closest to the biliary stent. Although several discharge cycles were performed, residual contrast uptake in this area was documented in the postinterventional MR control after 48 hours. However, it cannot be concluded from this single case observation that bile duct stents per se represent a limitation to ECT.

In addition to these limitations, our study provides further evidence on the effectiveness of ECT in the treatment of liver metastases of different origins, different sizes and locations. This treatment provides long-term local tumor control as well as long progression-free survival (mean progression-free survival of 9.0 ± 8.2 months). ECT, therefore, provides an effective valuable option for the treatment of unresectable liver metastases not amenable to other ablative techniques.

References

1. Global Burden of Disease Cancer Collaboration; Fitzmaurice C, Allen C, Barber RM, Barregard L, Bhutta ZA, Brenner H, et al. Global, regional, and national cancer Incidence, mortality, years of life lost, years lived with disability, and disability-adjusted life-years for 32 cancer groups, 1990 to 2015: a systematic analysis for the Global Burden of Disease Study. *JAMA Oncol* 2017; **3:** 524. doi: 10.1001/jamaoncol.2016.5688
2. Valery PC, Laversanne M, Clark PJ, Petrick JL, McGlynn KA, Bray F. Projections of primary liver cancer to 2030 in 30 countries worldwide. *Hepatology* 2018; **67:** 600-11. doi: 10.1002/hep.29498
3. Engstrand J, Nilsson H, Strömberg C, Jonas E, Freedman J. Colorectal cancer liver metastases – a population-based study on incidence, management and survival. *BMC Cancer* 2018; **18:** 78. doi: 10.1186/s12885-017-3925-x
4. Hackl C, Neumann P, Gerken M, Loss M, Klinkhammer-Schalke M, Schlitt HJ. Treatment of colorectal liver metastases in Germany: a ten-year population-based analysis of 5772 cases of primary colorectal adenocarcinoma. *BMC Cancer* 2014; **14:** 810. doi: 10.1186/1471-2407-14-810
5. Van Cutsem E, Cervantes A, Adam R, Sobrero A, Van Krieken JH, Aderka D, et al. ESMO consensus guidelines for the management of patients with metastatic colorectal cancer. *Ann Oncol* 2016; **27:** 1386-422. doi: 10.1093/annonc/mdw235
6. Goldberg SN, Gazelle GS, Mueller PR. Thermal ablation therapy for focal malignancy: a unified approach to underlying principles, techniques, and diagnostic imaging guidance. *Am J Roentgenol* 2000; **174:** 323-31. doi: 10.2214/ajr.174.2.1740323
7. Glass LF, Jaroszeski M, Gilbert R, Reintgen DS, Heller R. Intralesional bleomycin-mediated electrochemotherapy in 20 patients with basal cell carcinoma. *J Am Acad Dermatol* 1997; **37:** 596-9. doi: 10.1016/S0190-9622(97)70178-6
8. Marty M, Sersa G, Garbay JR, Gehl J, Collins CG, Snoj M, et al. Electrochemotherapy – an easy, highly effective and safe treatment of cutaneous and subcutaneous metastases: results of ESOPE (European Standard Operating Procedures of Electrochemotherapy) study. *Eur J Cancer Suppl* 2006; **4:** 3-13. doi: 10.1016/j.ejcsup.2006.08.002
9. Clover AJP, de Terlizzi F, Bertino G, Curatolo P, Odili J, Campana LG, et al. Electrochemotherapy in the treatment of cutaneous malignancy: outcomes and subgroup analysis from the cumulative results from the pan-European International Network for Sharing Practice in Electrochemotherapy database for 2482 lesions in 987 patients (2008–2019). *Eur J Cancer* 2020; **138:** 30-40. doi: 10.1016/j.ejca.2020.06.020
10. Plaschke CC, Bertino G, McCaul JA, Grau JJ, de Bree R, Sersa G, et al. European Research on Electrochemotherapy in Head and Neck Cancer (EURECA) project: results from the treatment of mucosal cancers. *Eur J Cancer* 2017; **87:** 172-81. doi: 10.1016/j.ejca.2017.10.008
11. Bertino G, Sersa G, De Terlizzi F, Occhini A, Plaschke CC, Groselj A, et al. European Research on Electrochemotherapy in Head and Neck Cancer (EURECA) project: results of the treatment of skin cancer. *Eur J Cancer* 2016; **63:** 41-52. doi: 10.1016/j.ejca.2016.05.001
12. Gasljevic G, Edhemovic I, Cemazar M, Brecelj E, Gadzijev EM, Music MM, et al. Histopathological findings in colorectal liver metastases after electrochemotherapy. *PLoS ONE* 2017; **12:** e0180709. doi: 10.1371/journal.pone.0180709
13. Brloznik M, Boc N, Sersa G, Zmuc J, Gasljevic G, Seliskar A, et al. Radiological findings of porcine liver after electrochemotherapy with bleomycin. *Radiol Oncol* 2019; **53:** 415-26. doi: 10.2478/raon-2019-0049
14. Zmuc J, Gasljevic G, Sersa G, Edhemovic I, Boc N, Seliskar A, et al. Large Liver Blood Vessels and Bile Ducts Are Not Damaged by Electrochemotherapy with Bleomycin in Pigs. *Sci Rep* 2019; **9:** 3649. doi: 10.1038/s41598-019-40395-y
15. Cornelis FH, Korenbaum C, Ben Ammar M, Tavolaro S, Nouri-Neuville M, Lotz JP. Multimodal image-guided electrochemotherapy of unresectable liver metastasis from renal cell cancer. *Diagn Interv Imag* 2019; **100:** 309-11. doi: 10.1016/j.diii.2019.01.001
16. Edhemovic I, Brecelj E, Cemazar M, Boc N, Trotovsek B, Djokic M, et al. Intraoperative electrochemotherapy of colorectal liver metastases: a prospective phase II study. *EJSO* 2020; **46:** 1628-33. doi: 10.1016/j.ejso.2020.04.037
17. Mali B, Gorjup V, Edhemovic I, Brecelj E, Cemazar M, Sersa G, et al. Electrochemotherapy of colorectal liver metastases - an observational study of its effects on the electrocardiogram. *BioMed Eng OnLine* 2015; **14(Suppl 3):** S5. doi: 10.1186/1475-925X-14-S3-S5
18. Jarm T, Krmac T, Magjarevic R, Kos B, Cindric H, Miklavcic D. Investigation of safety for electrochemotherapy and irreversible electroporation ablation therapies in patients with cardiac pacemakers. *BioMed Eng OnLine* 2020; **19:** 85. doi: 10.1186/s12938-020-00827-7
19. Boc N, Edhemovic I, Kos B, Marolt Music M, Brecelj E, Trotovsek B, et al. Ultrasonographic changes in the liver tumors as indicators of adequate tumor coverage with electric field for effective electrochemotherapy. *Radiol Oncol* 2018; **52:** 383-91. doi: 10.2478/raon-2018-0041
20. Bertacchini C. Cliniporator: medical electroporation of tumors. In: Miklavcic D, editor. *Handbook of Electroporation.* Cham: Springer International Publishing; 2017. p. 1-36.
21. Gehl J, Sersa G, Matthiessen LW, Muir T, Soden D, Occhini A, et al. Updated standard operating procedures for electrochemotherapy of cutaneous tumours and skin metastases. *Acta Oncol* 2018; **57:** 874-82. doi: 10.1080/0284186X.2018.1454602
22. Ruers T, Van Coevorden F, Punt CJ, Pierie JE, Borel-Rinkes I, Ledermann JA, et al. Local treatment of unresectable colorectal liver metastases: results of a randomized phase ii trial. *J Natl Cancer I* 2017; **109:** djx015. doi: 10.1093/jnci/djx015

23. Slovak R, Ludwig JM, Gettinger SN, Herbst RS, Kim HS. Immuno-thermal ablations - boosting the anticancer immune response. *J Immunother Cancer* 2017; **5:** 78. doi: 10.1186/s40425-017-0284-8

24. Camacho JC, Petre EN, Sofocleous CT. Thermal ablation of metastatic colon cancer to the liver. *Semin Intervent Radiol* 2019; **36:** 310-8. doi: 10.1055/s-0039-1698754

25. Olson R, Mathews L, Liu M, Schellenberg D, Mou B, Berrang T, et al. Stereotactic ablative radiotherapy for the comprehensive treatment of 1–3 Oligometastatic tumors (SABR-COMET-3): study protocol for a randomized phase III trial. *BMC Cancer* 2020; **20:** 380. doi: 10.1186/s12885-020-06876-4

26. Kovács A, Bischoff P, Haddad H, Kovács G, Schaefer A, Zhou W, et al. Personalized image-guided therapies for local malignencies: interdisciplinary options for interventional radiology and interventional radiotherapy. *Front Oncol* 2021; **11:** 616058. doi: 10.3389/fonc.2021.616058

27. Campanacci L, Bianchi G, Cevolani L, Errani C, Ciani G, Facchini G, et al. Operating procedures for electrochemotherapy in bone metastases: results from a multicenter prospective study on 102 patients. *Eur J Surg Oncol* 2021; **47:** 2609-17. doi: 10.1016/j.ejso.2021.05.004

28. Edhemovic I, Gadzijev EM, Brecelj E, Miklavcic D, Kos B, Zupanic A, et al. Electrochemotherapy: a new technological approach in treatment of metastases in the liver. *Technol Cancer Res Treat* 2011; **10:** 475-85. doi: 10.7785/tcrt.2012.500224

29. Edhemovic I, Brecelj E, Gasljevic G, Marolt Music M, Gorjup V, Mali B, et al. Intraoperative electrochemotherapy of colorectal liver metastases. *J Surg Oncol* 2014; **110:** 320-7. doi: 10.1002/jso.23625

30. Coletti L, Battaglia V, De Simone P, Turturici L, Bartolozzi C, Filipponi F. Safety and feasibility of electrochemotherapy in patients with unresectable colorectal liver metastases: a pilot study. *Int J Surg* 2017; **44:** 26-32. doi: 10.1016/j.ijsu.2017.06.033

31. Djokic M, Cemazar M, Popovic P, Kos B, Dezman R, Bosnjak M, et al. Electrochemotherapy as treatment option for hepatocellular carcinoma, a prospective pilot study. *EJSO* 2018; **44:** 651-7. doi: 10.1016/j.ejso.2018.01.090

32. Djokic M, Dezman R, Cemazar M, Stabuc M, Petric M, Smid LM, et al. Percutaneous image guided electrochemotherapy of hepatocellular carcinoma: technological advancement. *Radiol Oncol* 2020; **54:** 347-52. doi: 10.2478/raon-2020-0038

33. Tarantino L, Busto G, Nasto A, Nasto RA, Tarantino P, Fristachi R, et al. Electrochemotherapy of cholangiocellular carcinoma at hepatic hilum: a feasibility study. *EJSO* 2018; **44:** 1603-9. doi: 10.1016/j.ejso.2018.06.025

34. Granata V, Palaia R, Albino V, Piccirillo M, Venanzio Setola S, Petrillo A, et al. Electrochemotherapy of cholangiocellular carcinoma at hepatic hilum: a case report. *Eur Rev Med Pharmacol Sci* 2020; **24:** 7051-7. doi: 10.26355/eurrev_202006_21698

35. Corrado G, Cutillo G, Fragomeni SM, Bruno V, Tagliaferri L, Mancini E, et al. Palliative electrochemotherapy in primary or recurrent vulvar cancer. *Int J Gynecol Cancer* 2020; **30:** 927-31. doi: 10.1136/ijgc-2019-001178

36. Perrone AM, Galuppi A, Pirovano C, Borghese G, Covarelli P, De Terlizzi F, et al. Palliative Electrochemotherapy in vulvar carcinoma: preliminary results of the ELECHTRA (Electrochemotherapy Vulvar Cancer) multicenter study. *Cancers* 2019; **11:** 657. doi: 10.3390/cancers11050657

37. Perrone AM, Ferioli M, Argnani L, De Terlizzi F, Pirovano C, Covarelli P, et al. Quality of life with vulvar carcinoma treated with palliative electrochemotherapy: The ELECHTRA (ELEctroCHemoTherapy vulvaR cAncer) Study. *Cancers* 2021; **13:** 1622. doi: 10.3390/cancers13071622

38. Andresciani F, Faiella E, Altomare C, Pacella G, Beomonte Zobel B, Grasso RF. Reversible electrochemotherapy (ECT) as a treatment option for local RCC recurrence in solitary kidney. *Cardiovasc Intervent Radiol* 2020; **43:** 1091-4. doi: 10.1007/s00270-020-02498-2

39. Tarantino L, Busto G, Nasto A, Fristachi R, Cacace L, Talamo M, et al. Percutaneous electrochemotherapy in the treatment of portal vein tumor thrombosis at hepatic hilum in patients with hepatocellular carcinoma in cirrhosis: A feasibility study. *WJG* 2017; **23:** 906. doi: 10.3748/wjg.v23.i5.906

40. Liu F, Chen M, Mei J, Xu L, Guo R, Lin X, et al. Transarterial chemoembolization combined with radiofrequency ablation in the treatment of stage B1 intermediate hepatocellular carcinoma. *J Oncol* 2019; **2019:** 1-7. doi: 10.1155/2019/6298502

research article

The learning curve of laparoscopic liver resection utilising a difficulty score

Arpad Ivanecz[1,2], Irena Plahuta[1], Matej Mencinger[3,4,5], Iztok Perus[2,6], Tomislav Magdalenic[1], Spela Turk[1], Stojan Potrc[1,2]

[1] Clinical Department of Abdominal and General Surgery, University Medical Centre Maribor, Maribor, Slovenia
[2] Department of Surgery, Faculty of Medicine, University of Maribor, Maribor, Slovenia
[3] Faculty of Civil Engineering, Transportation Engineering and Architecture, University of Maribor, Maribor, Slovenia
[4] Centre of Applied Mathematics and Theoretical Physics, University of Maribor, Maribor, Slovenia
[5] Institute of Mathematics, Physics and Mechanics, Ljubljana, Slovenia
[6] Faculty of Natural Science and Engineering, University of Ljubljana, Ljubljana, Slovenia

Radiol Oncol 2022; 56(1): 111-118.

Received 2 June 2021
Accepted 16 July 2021

Correspondence to: Assist. Prof. Arpad Ivanecz, M.D., Ph.D., Clinical Department of Abdominal and General Surgery, University Medical Centre Maribor, Ljubljanska ulica 5, 2000 Maribor, Slovenia. E-mail: arpad.ivanecz@ukc-mb.si

Disclosure: No potential conflicts of interest were disclosed.

Background. This study aimed to quantitatively evaluate the learning curve of laparoscopic liver resection (LLR) of a single surgeon.

Patients and methods. A retrospective review of a prospectively maintained database of liver resections was conducted. 171 patients undergoing pure LLRs between April 2008 and April 2021 were analysed. The Halls difficulty score (HDS) for theoretical predictions of intraoperative complications (IOC) during LLR was applied. IOC was defined as blood loss over 775 mL, unintentional damage to the surrounding structures, and conversion to an open approach. Theoretical association between HDS and the predicted probability of IOC was utilised to objectify the shape of the learning curve.

Results. The obtained learning curve has resulted from thirteen years of surgical effort of a single surgeon. It consists of an absolute and a relative part in the mathematical description of the additive function described by the logarithmic function (absolute complexity) and fifth-degree regression curve (relative complexity). The obtained learning curve determines the functional dependency of the learning outcome versus time and indicates several local extreme values (peaks and valleys) in the learning process until proficiency is achieved.

Conclusions. This learning curve indicates an ongoing learning process for LLR. The proposed mathematical model can be applied for any surgical procedure with an existing difficulty score and a known theoretically predicted association between the difficulty score and given outcome (for example, IOC).

Key words: learning curve; difficulty score; laparoscopy; hepatectomy; intraoperative complication

Introduction

Interest in laparoscopic liver resection (LLR) has grown since the publication of the International Louisville Statement on laparoscopic liver surgery.[1] Since then, the number of LLRs performed worldwide has increased exponentially.[2]

The laparoscopic approach must not compromise the technical quality of the liver resection. The message from the second Morioka consensus conference in 2014 was the need for a formal structure of education for those interested in performing LLR.[3] The need for the organisation of LLR was achieved by the establishment of the

International Laparoscopic Liver Society in 2016.[4] In Southampton, 2017, the third consensus meeting has produced a set of clinical practice guidelines to direct the speciality's continued safe progression and dissemination.[5] A few difficulty scoring systems have been proposed to rate the difficulty of LLR, and the need for validating the existing tools before the clinical application has been highlighted.[6-9] Halls *et al.*[10] developed and internally validated a difficulty score estimating the risk of intraoperative complications (IOC) during LLR, which was externally validated by the authors of the present study.[11]

Along with the evolution of LLR, its learning curves (LCs) have received increased attention.[12-14] The idealised model of the LC has been described, demonstrating continuous result improvement along with experience.[15] Recently, the LC has been reported to resemble a true model, in which alternating periods of progression and regression occurred until mastery was achieved.[16]

The present study was based on a thirteen-years single-centre experience and was designed to analyse the real LC of LLR. To the best of our knowledge, it is the only study quantitatively presenting the LC of LLR.

Patients and methods

Patients

Study subjects were identified from a prospectively maintained database of patients who underwent liver resections at the Department of Abdominal and General Surgery, University Medical Centre Maribor, Slovenia. This institution has been a tertiary referral centre specialised in hepato-pancreato-biliary surgery, where the first LLR was performed in April 2008. The study included all the patients in whom a pure laparoscopic liver procedure was performed (intention-to-treat analysis) until 31st March 2021. For the present study, patients who underwent laparoscopic cyst fenestration, liver biopsies, and radiofrequency ablation were excluded.

Only pure LLR were performed; no hand-assisted or hybrid procedures were used. All patients were operated by the same surgeon (AI). He had expertise in open hepato-pancreatico-biliary and laparoscopic surgery but no experience in LLR before this series. Perioperative definitions were provided elsewhere.[11] The surgical technique for LLR has been extensively described by others[17] and performed as reported previously.[18-20]

At the time of the operation all patients had given their written consent that anonymous data can be used for research purposes. Patient records were anonymized and de-identified before analysis. Ethical approval for this study was obtained from the local institutional review board.

Statistical analysis

IBM SPSS for Windows Version 26.0 (IBM Corp., Armonk, NY, USA) and Wolfram Mathematica for Windows Version 10.4 (Wolfram Research, Inc., Champaign, IL, USA) were used for statistical computations.

Categorical variables were reported as frequency (percentages). Continuous variables were reported as mean and standard deviation when data distribution was normal; otherwise, they were reported as median (minimum-maximum, interquartile range). The chi-square and the paired samples t-test were used. Percentages were listed to one decimal place, and a difference in the P-value of <0.05 was considered statistically significant.

Mathematical modelling of the learning curve

The Halls difficulty score (HDS)[10] was applied. Its parameters (neoadjuvant chemotherapy, previous open liver resection, benign or malignant lesion, lesion size, and classification of resection) were captured from the institutional database. Each LLR was retrospectively scored from 0 to 15.

In the proposed model, IOC was used as a sensible measure of the complexity of the resection.[10] IOC's key markers were blood loss over 775 mL, unintentional damage to the surrounding structures and conversion to open approach.[10] The conversion was defined as the requirement for laparotomy at any time of the procedure, except for the extraction of the resected specimen.[10]

In[11], the authors searched for functorial dependence between IOC and HDS using the first 128 patients of the observed cohort. The best-fit-dependency was found to be the Weibull cumulative distribution function[21] of the form

$$p_{IOC_{theoretical}}(x) = 1 - e^{(x/\lambda)^k}$$

with $\lambda = 8.085$ and $k = 2.871$. Here x represents the HDS, and $p_{IOC_{theoretical}}(x)$ represents the predicted probability of IOC occurrence. This functional dependence will be referred as the theoretical probability of IOC[11] and is graphically represented in

Figure 1. This figure is rendered here for the self-sufficiency of this article.

The Weibull curve in Figure 1 is monotonically increasing. Regarding the LC, we assume that a procedure with a higher difficulty score must be graded better than a procedure with a lower difficulty score if the resection is done without IOC. Therefore, the difference between the theoretically predicted probability of IOC and obtained IOC is greater if the difficulty score is higher (if IOC = 0). On the other hand, if IOC was detected (if IOC = 1), the difference between the theoretically predicted probability of IOC and obtained IOC is negative (implying a lower grade for a surgeon) if the difficulty score is low. Thus, the learning outcome is proportional to the share of IOC caused by the surgeon obtained in each of the ten classes.

We wanted to test if the time dependency of HDS is (on average) an ascending function. Therefore, resections were divided into three (time) sequential classes (each consisting of 57 patients), and the number of obtained IOC in each class was counted.

HDS[10] was used in the analysis of LC. Its dependency was proven to be (on average) an increasing function (Figure 1).

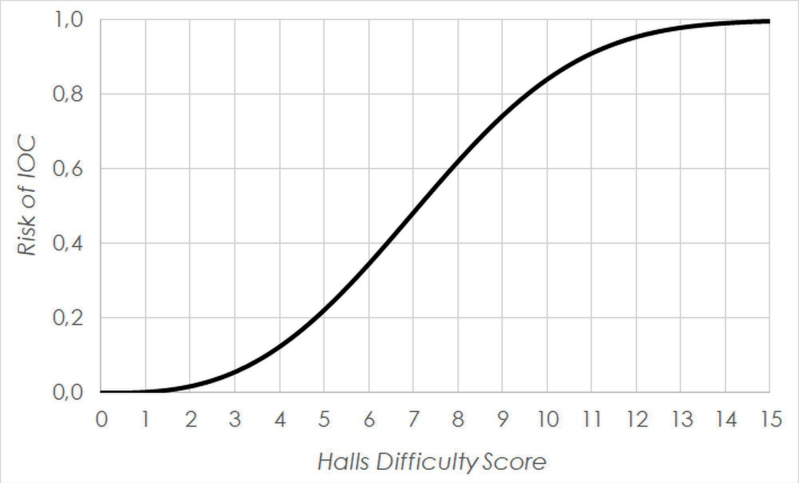

FIGURE 1. The continuous mean risk curve of intraoperative complication (IOC) as a function of the Halls difficulty score: the theoretical probability of intraoperative complication.[11]

The proposed mathematical model of a learning curve

The probability (the share of IOC in the time-dependent class) of IOC depends on HDS. The share of IOC in a time-dependent class measures the complexity of resections. Therefore, a novel model for presenting the learning outcome in the case of LLR with existing theoretical dependence between HDS and (the probability of) IOC was introduced.

We assume that the learning outcome consists of two additive components. The first represents the absolute complexity of the resection according to time (which is proportional to effort). The second (additive) component is obtained by comparing the share of IOC to the theoretically predicted (probability of) IOC depending on the HDS of the patient. Components share the same *physical* units; therefore, the addition is justified. The sum of components results in the learning outcome for any patient and finally in the LC. The first component reflects the absolute complexity of the resections within the same class, while the second one reflects the relative complexity (comparing to the theoretically predicted HDS), which can be interpreted as the surgeon's efficiency.

At this point, we mathematically define the objectives determining the learning outcomes, and consequently, the LC. The cohort of 171 patients is divided into ten sequential classes (the last class contains 17+1 patient). By n, we denote the sequential number of the patient. By N, we denote the sequential number of the class (for every class, its cardinality $\#N$ is equal to 17).

Our main assumptions and proposals are the following:

1. Since the resections were listed chronologically, we may assume that the sequential number of the patient corresponds to the effort of the surgeon (the correspondence is monotonically increasing).
2. For every class N, the absolute complexity (ac) of the tasks in the class is proportional to the ratio of the IOC cases.

$$ac(N) = \sum_{n_i \in N} p_{IOC_{theoretical}}(n_i)$$

The non-smooth dependency $(N_i, ac(N_i));\ i = 1,2,\dots,10$ was fitted to smooth logarithmic function $\mathrm{ac}(N) = f(N)$. Additionally, it was modified to absolute complexity for each sequential patient (AC)

$$AC(n) = f\left(\frac{n+16}{17}\right).$$

3. For every class N, the relative complexity (rc) or efficiency of the surgeon is proportional to the sum of differences between the theoretically predicted probabilities of IOC and the obtained probabilities of IOC

$$rc(N) = \sum_{n_i \in N} p_{IOC_{theoretical}}(n_i) - p_{IOC_{obtained}}(n_i)$$

Interpolating the data $(N_i, rc(N_i))$; $i = 1,2,\ldots,10$ to a polynomial of degree five, one gets a smooth function $rc(N)$ obtained by Mathematica command *SplineFit* using option *Cubic*.

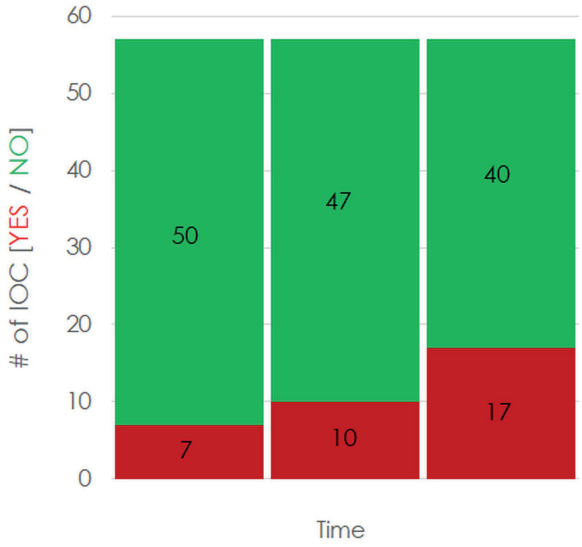

FIGURE 2. Histogramic time classes dependency of intraoperative complication (IOC) (yes/no) on the observed cohort.

TABLE 1. Baseline characteristics of 171 patients who underwent laparoscopic liver resection

Baseline characteristics	N[a,b]
Male sex[a]	104 (60.8%)
Age (years)[b]	64 (20-86, 15)
BMI (kg/m²)[b]	27 (18-50, 4.8)
ASA score[a]	1 44 (25.7%) 2 73 (42.7%) 3 51 (29.8%) 4 3 (1.8%)
Liver cirrhosis Child-Pugh (22)[a]	A 33 (19.3%) B 4 (2.3%)
Previous abdominal surgery[a]	41 (24.0%)
Previous liver resection[a]	8 (4.6%)
Malignant tumour[a]	128 (74.9%)
Neoadjuvant chemotherapy[a]	25 (14.6%)
Max. diameter (mm)[b]	38 (2-160, 33)
Number of tumours[a]	1 (1-10, 0).
Deep location within liver[a]	50 (29.2%)
Posterosuperior liver segments[a]	49 (28.7%)

[a] = categorical variables; [b] = continuous variables have been reported as median (minimum-maximum, interquartile range); ASA = American Society of Anaesthesiologists; BMI = body mass index

Additionally, $rc = rc(N)$ was finally modified to relative complexity (RC) for each sequential patient

$RC(n) = rc\left(\frac{n+16}{17}\right)$.

4. Adding both components, we get the learning curve (LC) of the surgeon: $LC(n) = AC(n) + RC(n)$

Results

The presentation of the cohort

Between April 2008 and April 2021, 171 patients underwent pure LLR. Their baseline characteristics are presented in Table 1.

Perioperative outcomes are given in Table 2.

Two patients (1.2%) suffered from unintentional laceration of the transverse colon, sutured laparoscopically. The procedure was completed laparoscopically in 147 (86.0%) patients. The reasons for conversion to laparotomy in 24 (14.0%) patients were diffuse parenchymal bleeding (N = 3), inability to proceed due to the large liver or dense adhesions (N = 6), and oncological concern (N = 15). The decision to proceed to conversion was not made upon life-threatening bleeding. The indication for liver resection in converted cases was malignant tumours. Three (1.8%) patients died – one bled out from ruptured oesophageal varices, and two died of liver failure; they all had hepatocellular carcinoma and liver cirrhosis Child-Pugh B.

Learning curve analysis results

The analysis of the learning curve was motivated by the increasing time dependency of HDS. Therefore, resections were divided into three sequential classes of 57 resections, and the number of obtained IOC in each class was counted. The results are graphically presented in Figure 2.

On $\alpha = 5\%$ significance level the p-value for Chi Square test is slightly above 5% ($p = 0.055$). However, for linear-by-linear (Mantel Haenszel) test for trend, the p-value is < 0.05.

HDS[10] was used in the analysis of LC. The risk-of-IOC dependency was proven to be (on average) an increasing function in terms of HDS (Figure 1). A time-dependent and increasing trend can also be seen in Figure 3 (see the red linear trend-line for HDS; the blue chart represents actual data).

The sequential number of the patient corresponds to the effort of the surgeon (the correspondence is monotonically increasing). In the first class,

the average time difference between sequential surgeries was 117 days (with a standard deviation of 132 days), while in the last class, the time difference was 13 days with a standard deviation of 12 days. The paired samples t-test shows that (at the level of confidence of 95%) the two means are not equal ($p < 0.05$).

The final result of our LC data analysis is presented in Figure 4. Ten consecutive classes of 17 patients are given on abscissa. The height of the columns represents the share of the IOC in the time class. Two types of LCs for the observed cohort and the surgeon under consideration are given. The orange line represents the logarithmic regression curve based on absolute complexity for data $(N_i, ac(N_i))$. The green line represents the sum of the orange curve and the quintic regression line of relative complexity for data $(N_i, rc(N_i))$. This green line represents our LC.

Discussion

Like any other human activity, where individuals perform more difficult and intricated tasks over time, surgeons have been interested in their LC when performing LLR.[16] The obtained learning curve has resulted from thirteen years of surgical effort of a single surgeon. It consists of an absolute and a relative part in the mathematical description of the additive function described by the logarithmic function (absolute complexity) and fifth-degree regression curve (relative complexity). The obtained LC determines the functional dependency of the learning outcome versus time and indicates several local extreme values (peaks and valleys) in the learning process until proficiency is achieved.

A typical LC graphically represents the relationship between the learning effort and achievement. LC consists of a measure of learning which usually lies on the ordinate (y-axis), a measure of effort, which usually lies on the abscissa (x-axis) and a mathematical linking function. The shapes of this mathematical (functorial) dependence can vary depending on the nature and difficulty of the learning outcomes and difficulty of the task.[26,27]

It may be assumed that LC should be increasing in time (*i.e.*, with effort). There are several typical LCs for learning different skills whose shape depends on the complexity of the task. When learning simple skills, S-shaped or logistic curves appear. The logistic curve admits a single inflexion point (indicating the point when half of the knowledge was acquired) and a horizontal asymptote (representing the cap to be acquired). In surgical procedures for more complex skills, often a logarithmic LC without a cap appears. However, when interpreting a paediatric ankle radiograph, the LC turns out to be logarithmic.[27] The zig-zag shape can appear as well.[27] A steep LC is rare in medicine since the skills are associated with difficult and complex procedures.[26,27]

We have considered the LC of a single surgeon in a technically demanding LLR. When implementing a new surgical procedure, a surgeon already has some fundamental knowledge. The learning outcome is assumed to be proportional to the share of IOC made by the surgeon, *i.e.* we learn from our

TABLE 2. Perioperative outcomes of 171 patients who underwent laparoscopic liver resection

Intraoperative details and postoperative course	N[a,b]
Anatomic resection (23) [a]	101 (59.1%)
Anatomically major resection (23) [a]	27 (15.8%)
Technically major resection (24)[a]	29 (17.0%)
Operation time (min)[b]	160 (25-450, 90)
Blood loss (mL)[b]	150 (0-2200, 180)
Intraoperative complication (10)[c]	**34 (19.9%)**
Conversion to open approach[a]	24 (14.0%)
Blood loss > 775 mL[a]	12 (7.0%)
Unintentional damage to the surrounding structures[a]	2 (1.2%)
Hepatic pedicle clamping[a]	45 (26.3%)
Total hepatic pedicle clamping time (min)[b]	8 (0-75, 10)
Transfusion required[a]	20 (11.7%)
Pathohistological diagnosis	
Colorectal liver metastases	53 (31%)
Hepatocellular carcinoma	46 (29.6%)
Intrahepatic cholangiocarcinoma	14 (8.2%)
Other metastases	11 (6.4%)
Hepatic cysts	10 (5.8%)
Hepatic adenoma	6 (4.7%)
Focal nodular hyperplasia	8 (4.7%)
Haemangioma	6 (3.5%)
Other pathology	15 (8.8%)
R0 resection	163 (95.3%)
Major morbidity CD 3a–4b (25)[a]	21 (12.3%)
Hospital stay (days)[b]	6 (2-79, 4)

[a] = categorical variables; [b] = continuous variables have been reported as median (minimum-maximum, interquartile range); [c] = intraoperative complication was defined as blood loss over 775 mL, unintentional damage to the surrounding structures and conversion to open approach

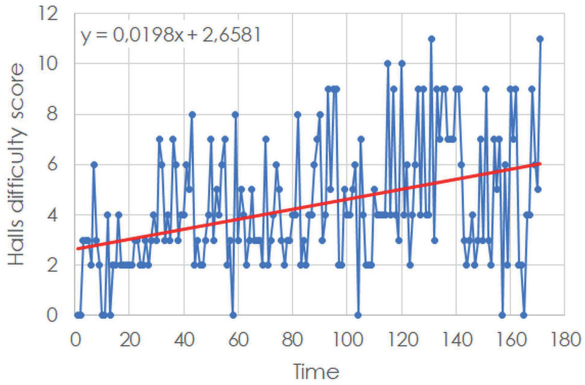

FIGURE 3. Time dependency of the Halls difficulty score on the observed cohort (blue points) and its regression (trend) line (red line).

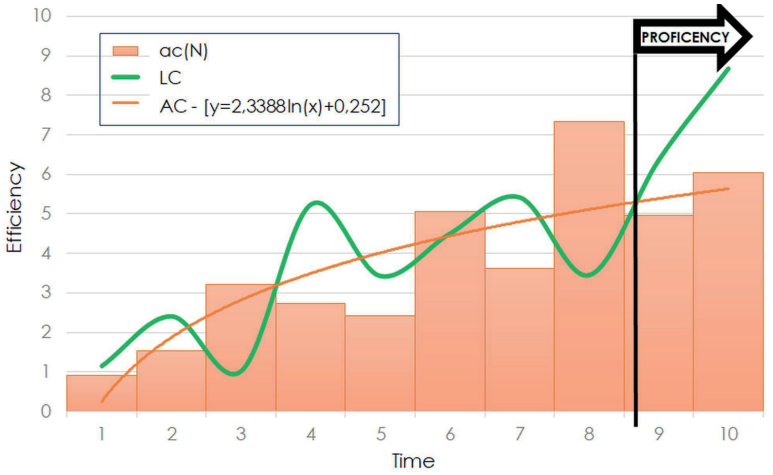

FIGURE 4. Two types of learning curves for observed cohort and the surgeon under consideration. The orange line (AC) represents the logarithmic regression curve based on absolute complexity. The green line (LC) represents the sum of the orange curve and the quintic regression line of relative complexity. This line represents our learning curve.

AC = absolute complexity; ac (N) = absolute complexity expressed by the number of intraoperative complications; LC = learning curve

mistakes (IOC). However, LLR has not been a single procedure, and the complexity of operations varies from wedge resections to extended major hepatectomies. This fact contributes to the difficulties during learning and assessing the LC.[12-16] In the beginning, solitary and peripherally located symptomatic benign tumours in anterolateral segments were resected.[28] With growing experience, the laparoscopic approach was implemented regardless of tumour location and its characteristics.[1,5] The time difference between sequential surgeries in time classes shortened from 117 days to 13 days. Therefore, one could reasonably assume this was a part of the learning strategy.

It is assumed that a higher level of (the sum of) theoretically predicted probability of IOC (within a particular class) reflects a higher level of gained knowledge (higher grade for the LC). This may be justified because the average HDS is also increasing with time (Figure 4). Therefore, HDS affects the relative complexity of the case. The orange line represents the basic LC. The relative complexity depends on the subjective decision made by the surgeon according to previously successfully finished cases with no IOC. LLR has been encompassing different procedures, each with its own anatomic and procedural considerations. Komatsu *et al.*[13] demonstrated an ideal learning curve effect for the left lateral sectionectomy and left hepatectomy, but it was not observed for the right hepatectomy. The more successive cases with no IOC encouraged the surgeon to do more cases with increased HDS.

When analysing IOC, the conversion rate of 14% was consistent with the reported ones, counting from 1% to 17%.[15,29] An increased risk of conversion has been associated with neoadjuvant chemotherapy, previous open liver resection, malignant tumours, their size, anatomically major and technically major resection.[30] Patients who had an elective conversion for an unfavourable intraoperative finding had better outcomes than patients who had an emergency conversion secondary to an adverse intraoperative event.[30] All our converted cases occurred in malignant tumours. None of the cases was related to life-threatening bleeding. The most common indications for conversion were the inability to proceed and oncological concern, respectively. A chosen method does not change the principle of the surgery. Therefore, an oncologically uncompromised resection has been more crucial than the laparoscopic completion of the procedure. The overall major morbidity and mortality rates of 12.3% and 1.8% followed reports in the literature.[13,14,16] To sum up, this conversion rate reflected the surgeon's reliance on the open method when dealing with adverse intraoperative findings.[20]

Although the first anatomical LLR was performed in 1996[31], the first difficulty score was published not earlier than 2014.[32] Our first LLR was performed in 2008, and the surgeon had to lean on his experience from open liver surgery. It would be riveting to study the results of the surgeon's trainees who could benefit from the evolution of techniques, learning modules[12,16,33], and difficulty scores.[6-8,10]

The main shortcoming of the presented research is a relatively low number of patients. Therefore, in future research, a larger number of patients should

be involved to show the robustness of the presented LC. Furthermore, its retrospective manner is another limitation.

The proposed LC and used methodology could guide the trainee surgeons and monitor their performance. In this sense, practitioners should be provided with a statistically independent set of patients with a constant increase (*i.e.*, a constant gradient) of HDS over time. Thus, more difficult cases would be taken over by more qualified surgeons. A newly created application would randomly select patients with the appropriate HDS for each practitioner. It would enable control of the (accidental) variability in HDS and its consequences on IOC, which could not be completely avoided in practice. Under the supervision of a qualified operator, the objective evaluation of the LC would avoid deeper *valleys* in it (higher number of IOCs than theoretically expected) and thus ensure the most optimal learning. Given the basic assumption that we learn from our mistakes (see section *A mathematical modelling of a learning curve*), the maximal acceptable number and type of mistakes in the learning process should be objectively evaluated through further research.

To conclude, our LC is closer to a true model in which alternating periods of progression and regression occurred until mastery was achieved.[16] Furthermore, the method presented in this paper can be applied to any (surgical) procedure with a difficulty score and given outcome (for example IOC), if a theoretically predicted probability dependence for the given outcome is available. From this point of view, the method is novel.

Acknowledgement

This work was supported by University Medical Centre Maribor (grant number IRP-2019/01-03). The funding source has no role in the design, practice, or analysis of this study.

References

1. Buell JF, Cherqui D, Geller DA, O'Rourke N, Iannitti D, Dagher I, et al. The international position on laparoscopic liver surgery: The Louisville Statement, 2008. *Ann Surg* 2009; **250:** 825-30. doi: 10.1097/sla.0b013e3181b3b2d8
2. Ciria R, Cherqui D, Geller DA, Briceno J, Wakabayashi G. Comparative short-term benefits of laparoscopic liver resection: 9000 cases and climbing. *Ann Surg* 2016; **263:** 761-77. doi: 10.1097/sla.0000000000001413
3. Wakabayashi G, Cherqui D, Geller DA, Buell JF, Kaneko H, Han HS, et al. Recommendations for laparoscopic liver resection: a report from the second international consensus conference held in Morioka. *Ann Surg* 2015; **261:** 619-29. doi: 10.1097/sla.0000000000001184
4. Cherqui D, Wakabayashi G, Geller DA, Buell JF, Han HS, Soubrane O, et al. The need for organization of laparoscopic liver resection. *J Hepatobiliary Pancreat Sci* 2016; **23:** 665-67. doi: 10.1002/jhbp.401
5. Abu Hilal M, Aldrighetti L, Dagher I, Edwin B, Troisi RI, Alikhanov R, et al. The Southampton consensus guidelines for laparoscopic liver surgery: from indication to implementation. *Ann Surg* 2018; **268:** 11-8. doi: 10.1097/sla.0000000000002524
6. Wakabayashi G. What has changed after the Morioka consensus conference 2014 on laparoscopic liver resection? *Hepatobiliary Surg Nutr* 2016; **5:** 281-9. doi: 10.21037/hbsn.2016.03.03
7. Hasegawa Y, Wakabayashi G, Nitta H, Takahara T, Katagiri H, Umemura A, et al. A novel model for prediction of pure laparoscopic liver resection surgical difficulty. *Surg Endosc* 2017; **31:** 5356-63. doi: 10.1007/s00464-017-5616-8
8. Kawaguchi Y, Fuks D, Kokudo N, Gayet B. Difficulty of laparoscopic liver resection: proposal for a new classification. *Ann Surg* 2018; **267:** 13-7. doi: 10.1097/sla.0000000000002176
9. Hallet J, Pessaux P, Beyfuss KA, Jayaraman S, Serrano PE, Martel G, et al. Critical appraisal of predictive tools to assess the difficulty of laparoscopic liver resection: a systematic review. *Surg Endosc* 2019; **33:** 366-76. doi: 10.1007/s00464-018-6479-3
10. Halls MC, Berardi G, Cipriani F, Barkhatov L, Lainas P, Harris S, et al. Development and validation of a difficulty score to predict intraoperative complications during laparoscopic liver resection. *Br J Surg* 2018; **105:** 1182-91. doi: 10.1002/bjs.10821
11. Ivanecz A, Plahuta I, Magdalenić T, Mencinger M, Peruš I, Potrč S, et al. The external validation of a difficulty scoring system for predicting the risk of intraoperative complications during laparoscopic liver resection. *BMC Surg* 2019; **19:** 179. doi: 10.1186/s12893-019-0645-y
12. Guilbaud T, Birnbaum DJ, Berdah S, Farges O, Beyer Berjot L. Learning curve in laparoscopic liver resection, educational value of simulation and training programmes: a systematic review. *World J Surg* 2019; **43:** 2710-9. doi: 10.1007/s00268-019-05111-x
13. Komatsu S, Scatton O, Goumard C, Sepulveda A, Brustia R, Perdigao F, et al. Development process and technical aspects of laparoscopic hepatectomy: learning curve based on 15 years of experience. *J Am Coll Surg* 2017; **224:** 841-50. doi: 10.1016/j.jamcollsurg.2016.12.037
14. van der Poel MJ, Besselink MG, Cipriani F, Armstrong T, Takhar AS, van Dieren S, et al. Outcome and learning curve in 159 consecutive patients undergoing total laparoscopic hemihepatectomy. *JAMA Surg* 2016; **151:** 923-28. doi: 10.1001/jamasurg.2016.1655
15. Vigano L, Laurent A, Tayar C, Tomatis M, Ponti A, Cherqui D. The learning curve in laparoscopic liver resection: improved feasibility and reproducibility. *Ann Surg* 2009; **250:** 772-82. doi: 10.1097/SLA.0b013e3181bd93b2
16. Villani V, Bohnen JD, Torabi R, Sabbatino F, Chang DC, Ferrone CR. "Idealized" vs. "True" learning curves: the case of laparoscopic liver resection. *HPB (Oxford)* 2016; **18:** 504-9. doi: 10.1016/j.hpb.2016.03.610
17. Han HS, Cho JY, Yoon YS. Techniques for performing laparoscopic liver resection in various hepatic locations. *J Hepatobiliary Pancreat Surg* 2009; **16:** 427-32. doi: 10.1007/s00534-009-0118-2
18. Ivanecz A, Krebs B, Stozer A, Jagric T, Plahuta I, Potrc S. Simultaneous pure laparoscopic resection of primary colorectal cancer and synchronous liver metastases: a single institution experience with propensity score matching analysis. *Radiol Oncol* 2018; **52:** 42-53. doi: 10.1515/raon-2017-0047
19. Ivanecz A, Pivec V, Ilijevec B, Rudolf S, Potrč S. Laparoscopic anatomical liver resection after complex blunt liver trauma: a case report. *Surg Case Rep* 2018; **4:** 25. doi: 10.1186/s40792-018-0432-5
20. Ivanecz A, Plahuta I, Magdalenić T, Ilijevec B, Mencinger M, Peruš I, et al. Evaluation of the Iwate model for predicting the difficulty of laparoscopic liver resection: does tumor size matter? *J Gastrointest Surg* 2021; **25:** 1451-60. doi: 10.1007/s11605-020-04657-9
21. Weibull W. A statistical distribution function of wide applicability. *J Appl Mech* 1951; **18:** 293-97.
22. Pugh RN, Murray-Lyon IM, Dawson JL, Pietroni MC, Williams R. Transection of the oesophagus for bleeding oesophageal varices. *Br J Surg* 1973; **60:** 646-9. doi: 10.1002/bjs.1800600817
23. Strasberg SM, Belghiti J, Clavien PA, Gadzijev E, Garden JO, Lau WY, et al. The Brisbane 2000 terminology of liver anatomy and resections. *HPB* 2000; **2:** 333-39. doi: 10.1016/S1365-182X(17)30755-4

24. Kazaryan AM, Røsok BI, Marangos IP, Rosseland AR, Edwin B. Comparative evaluation of laparoscopic liver resection for posterosuperior and anterolateral segments. *Surg Endosc* 2011; **25:** 3881-9. doi: 10.1007/s00464-011-1815-x

25. Clavien PA, Barkun J, de Oliveira ML, Vauthey JN, Dindo D, Schulick RD, et al. The Clavien-Dindo classification of surgical complications: five-year experience. *Ann Surg* 2009; **250:** 187-96. doi: 10.1097/SLA.0b013e3181b13ca2

26. Hopper AN, Jamison MH, Lewis WG. Learning curves in surgical practice. *Postgrad Med J* 2007; **83:** 777-9. doi: 10.1136/pgmj.2007.057190

27. Pusic MV, Boutis K, Hatala R, Cook DA. Learning curves in health professions education. *Acad Med* 2015; **90:** 1034-42. doi: 10.1097/acm.0000000000000681

28. Nguyen KT, Gamblin TC, Geller DA. World review of laparoscopic liver resection-2,804 patients. *Ann Surg* 2009; **250:** 831-41. doi: 10.1097/SLA.0b013e3181b0c4df

29. Costi R, Scatton O, Haddad L, Randone B, Andraus W, Massault PP, et al. Lessons learned from the first 100 laparoscopic liver resections: not delaying conversion may allow reduced blood loss and operative time. *J Laparoendosc Adv Surg Tech A* 2012; **22:** 425-31. doi: 10.1089/lap.2011.0334

30. Halls MC, Cipriani F, Berardi G, Barkhatov L, Lainas P, Alzoubi M, et al. Conversion for unfavorable intraoperative events results in significantly worse outcomes during laparoscopic liver resection: lessons learned from a multicenter review of 2861 cases. *Ann Surg* 2018; **268:** 1051-57. doi: 10.1097/sla.0000000000002332

31. Azagra JS, Goergen M, Gilbart E, Jacobs D. Laparoscopic anatomical (hepatic) left lateral segmentectomy-technical aspects. *Surg Endosc* 1996; **10:** 758-61. doi: 10.1007/bf00193052

32. Ban D, Tanabe M, Ito H, Otsuka Y, Nitta H, Abe Y, et al. A novel difficulty scoring system for laparoscopic liver resection. *J Hepatobiliary Pancreat Sci* 2014; **21:** 745-53. doi: 10.1002/jhbp.166

33. Goh BKP, Prieto M, Syn N, Koh YX, Lim KI. Critical appraisal of the learning curve of minimally invasive hepatectomy: experience with the first 200 cases of a Southeast Asian early adopter. *ANZ J Surg* 2020; **90:** 1092-98. doi: 10.1111/ans.15683

research article

In vitro maturation of immature oocytes for fertility preservation in cancer patients compared to control patients with fertility problems in an *in vitro* fertilization program

Irma Virant-Klun[1], Jure Bedenk[2], Nina Jancar[2]

[1] Clinical Research Centre, University Medical Centre Ljubljana, Ljubljana, Slovenia
[2] Division of Obstetrics and Gynecology, University Medical Centre Ljubljana, Ljubljana, Slovenia

Radiol Oncol 2022; 56(1): 119-128.

Received 5 August 2021
Accepted 25 November 2021

Correspondence to: Prof. Irma Virant-Klun, Ph.D., Clinical Research Centre, University Medical Centre Ljubljana, Zaloška cesta 2, SI 1000 Ljubljana, Slovenia. E-mail: irma.virant@kclj.si

Disclosure: No potential conflicts of interest were disclosed.

Background. The aim of this study was to determine whether *in vitro* maturation (IVM) of immature oocytes after controlled hormonal stimulation of the ovaries could be important in cancer patients to improve their chances of conception in the future.

Patients and methods. After ovarian stimulation in cancer patients, the number of oocytes and their quality and maturity were compared to control patients with fertility problems in the *in vitro* fertilization (IVF) program. In both groups of patients, immature oocytes at the developmental stage of germinal vesicle were matured *in vitro* and the proportion of oocytes that matured *in vitro* was compared between groups. In a subset of women with fertility problems, intracytoplasmic sperm injection (ICSI) was performed on IVM oocytes to assess their ability to be fertilized and develop into an embryo compared to *vivo* matured oocytes in the same cycles and consider the procedure in cancer patients.

Results. In patients with different cancers, the disease did not affect the number and quality of retrieved oocytes. In cancer patients, there was even a significantly lower proportion of immature oocytes than in patients with fertility problems (30.0% *vs.* 43.6%; $P < 0.05$). However, in patients with cancer, fewer oocytes per patient matured *in vitro* than in patients with fertility problems (1.39 ± 1.04 *vs.* 2.48 ± 1.83; $P < 0.05$). After ICSI, the proportions of fertilized oocytes and fertilized oocytes developing into an embryo did not differ between oocytes matured *in vitro* and *in vivo* in the same cycles.

Conclusions. Oocyte IVM is proving to be a reliable procedure for resolving immature oocytes after controlled ovarian stimulation in cancer patients.

Key words: cancer; fertility preservation; oocyte; *in vitro* maturation; vitrification

Introduction

Many young women in the reproductive period of life who do not yet have children or would like to have another child suffer from cancer. Today, cancer therapies are successful, but unfortunately, they can negatively affect the ovarian function (including oocyte quality) and fertility. At a median of 5.0 years from initial breast cancer diagnosis, 49% patients after adjuvant chemotherapy with anthracyclines and taxanes and 11% after therapy with tamoxifen had become post- and peri-menopausal.[1] Decreased ovarian follicle reserve occurs in more than one-third of patients after breast can-

cer treatment resulting in permanent infertility.[2] In long-term female survivors of pediatric hematologic malignancies 26.7% experienced premature ovarian insufficiency and face infertility after cancer treatment.[3] The situation is similar with other cancers; cancer therapy is the cause of premature ovarian failure in 25% of women with this diagnosis.[4] Therefore, it is very important to consider the preservation of female fertility before oncotherapy. An improvement in the survival rates of cancer patients and recent advances in assisted reproductive technologies have led to significant progress in fertility preservation treatments.

One option is vitrification and long-term storage of the patient's oocytes for later *in vitro* fertilization (IVF) with partner's sperm and transfer of embryos into the uterus. This program is established in many health care institutions around the world for a variety of cancers, including breast cancer.[5-12] Oocyte cryopreservation is an effective approach[13-15], but it is still thought that further studies are needed in cancer patients to ensure the excellent outcomes obtained in women without cancer.[16] After controlled hormonal stimulation of the ovaries, *in vitro* maturation (IVM) of immature oocytes before vitrification is recommended and not after vitrification/devitrification procedure.[17] Even if there are no differences in survival rates between oocytes vitrified before or after IVM procedure, decreased maturation rates of immature oocytes vitrified before IVM may be explained by underlying ultrastructural and biomolecular alterations.[17]

Human oocyte cryopreservation may offer some advantages compared to embryo freezing in cancer patients and also eliminates some ethical, legal, and moral concerns of embryo freezing[17], and is an option in young cancer patients who are single.[9,18] However, the chance of success depends primarily on the number of oocytes that have been vitrified in the patient[15] and some breast cancer patients may have contraindications to exogenous gonadotropin administration for controlled ovarian stimulation.[19] Some recent data show that ovarian stimulation for oocyte vitrification does not modify disease-free survival and overall survival rates in patients with early breast cancer[20] and the safety of pregnancy after an established diagnosis of breast cancer has been confirmed in numerous studies.[21]

In the case of vitrification and storage of oocytes, controlled hormonal stimulation of the ovaries is required to obtain oocytes. Despite careful hormonal stimulation of the ovaries, the significant proportion of oocytes obtained by ultrasound-guided aspiration of ovarian follicles is immature as metaphase I (MI) oocytes or prophase I oocytes with germinal vesicle (GV). Immature MI oocytes mostly mature spontaneously *in vitro* and are vitrified, while immature GV oocytes do not mature spontaneously and are incapable of fertilization. Therefore, GV oocytes are not vitrified and stored in liquid nitrogen in clinical practice and are discarded and lost to the patient. The important question is whether the maturation of these oocytes *in vitro* makes sense. There is a lack of data regarding the outcome of *in vitro* matured oocytes cryopreserved in cancer patients.[22] Recently, the first birth achieved after fertility preservation using vitrification of *in vitro* matured oocytes in a patient with breast cancer has been reported.[23]

The purpose of this study was to investigate the effectiveness of maturation of immature GV oocytes of cancer patients in laboratory conditions (in maturation medium and co-culture with cumulus cells from mature oocytes of the same patients) compared to control women involved in the IVF program due to fertility problems. Because all oocytes of cancer patients are still frozen, we tried to elucidate the success of IVF procedure, actually intracytoplasmic sperm injection (ICSI), on the *in vitro* matured oocytes of patients with fertility problems as a model for cancer patients.

Patients and methods

This research was approved by the Slovenian National Medical Ethical Committee (No. 0120-222/2016-2; KME 115/04/16). In this prospective research the immature (germinal vesicle-GV, prophase I) oocytes of two groups of patients were included: i) 45 oocytes of 18 cancer patients with predominating breast cancer (Figure 1) and ii) 74 oocytes of 21 healthy (non-cancer) patients (control) with fertility problems (partners of infertile men with impaired semen quality: oligozoospermia with less than 15 million spermatozoa/ml or teratozoospermia with less than 4% morphologically normal spermatozoa according to the World Health Organization (WHO) Criteria 2010[24] who were included in the IVF program. All patients were in the reproductive period of life, aged 18 to 43 years.

Oocytes after controlled hormonal stimulation of the ovaries

In both groups of patients, both immature and mature oocytes were together retrieved after controlled hormonal stimulation of the ovaries using

the same, antagonist protocol and ultrasound-guided aspiration of ovarian follicles. In patients with fertility problems, the stimulation was started on day 2 of the menstrual cycle with 150 to 300 I.U. of recombinant follicle-stimulating hormone (rFSH) daily. In cancer patients, the stimulation was initiated immediately after they have been sent to our department, no matter of the cycle phase. The ovarian stimulation was started with 225 to 300 I.U. of rFSH. In breast cancer patients, an aromatase inhibitor – letrozole (2.5 mg every 12 hours) was added to prevent estradiol rise and its possible detrimental effect on breast cancer. In all patients, the gonadotropin-releasing hormone (GnRH) antagonist was added, when dominant follicle measured 14 mm in a diameter. In patients with fertility problems, the oocyte maturation was triggered with choriogonadotropin alfa – Ovitrelle, when follicles measured 18 mm or more. If there were more than 15 follicles in both ovaries, the maturation triggering was performed with GnRH agonist. In majority of cancer patients, GnRH agonist was used for oocyte maturation to prevent ovarian hyperstimulation (ovarian hyperstimulation syndrome; OHSS), but some of them, if there were less than 10 follicles in both ovaries, were also treated by Ovitrelle. All follicles with a diameter of 16 mm or more were aspirated in all patients. A constant aspiration pressure of 180 mm Hg was used to aspirate the oocytes from the follicles.

Mature oocytes with expressed polar body were immediately vitrified by soaking in a mixture of cryoprotectants, direct plunging into liquid nitrogen (-196°C), and stored in it, as described elsewhere.[25]

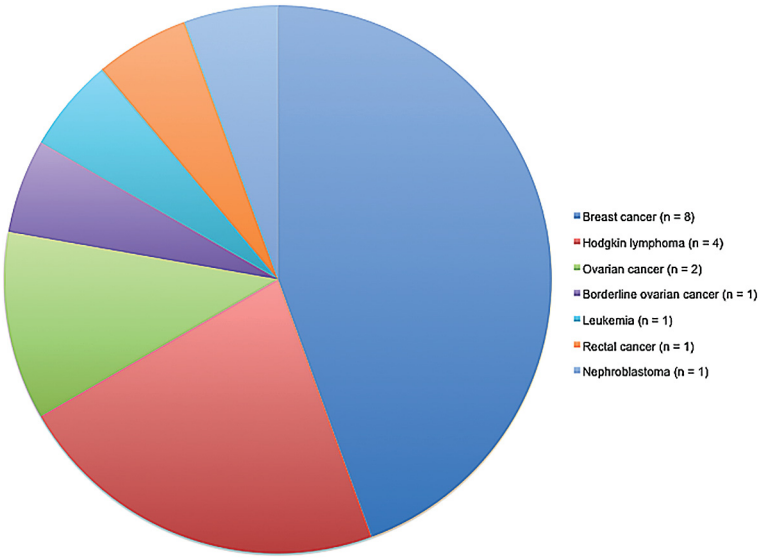

FIGURE 1. Types of disease in cancer patients included in this study. Breast cancer patients predominated.

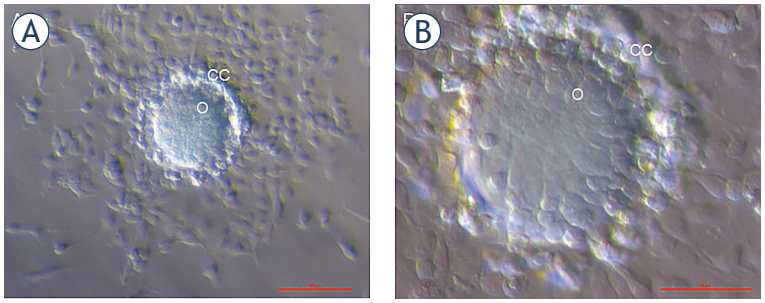

FIGURE 2. *In vitro* maturation of the oocyte in the maturation medium and in coculture with the cumulus cells of mature oocytes in the same patient at magnification 40 X **(A)** and magnification 100 X **(B)**.

CC = cumulus (granulosa) cells; O = oocyte; Red bar = A) 100 µm in B) 50 µm

In vitro maturation of immature oocytes

Immature GV oocytes were exposed to the procedure of IVM in a seria of media of the IVM Maturation System (MediCult IVM®System, Origio/CooperSurgical, Denmark).

For IVM, each GV oocyte was first exposed for two hours in the LAG Medium for conditioning and then for 24 to 28 hours to the maturation medium of this system containing the reproductive hormones: follicle stimulating hormone (FSH; 75 mIU/ml) and human chorionic gonadotropin (HCG; 100 mIU/ml) and in a co-culture with cumulus cells denuded from mature oocytes of the same patient, as described elsewhere (Figure 2).[26] During incubation in these media, oocytes were cultured in a CO_2-incubator at 37°C and 6% CO_2 in air. Oocytes were supposed to be mature (in a metaphase II) when they extruded a polar body. All oocytes of cancer patients and the majority of oocytes of women with fertility problems that matured *in vitro* were vitrified and stored in liquid nitrogen for later clinical use (IVF). Patients with ≥ 31% GV oocytes had increased oocyte immaturity. A subset of *in vitro* matured oocytes of women with fertility problems was fertilized *in vitro*.

In vitro fertilization by ICSI

In a subgroup of 17 *in vitro* matured oocytes from 17 patients (1 oocyte per patient) with fertility problems (female partners of infertile men with oligozoospermia or teratozospermia) ICSI was performed with partner's sperm one day later after oocyte and sperm retrieval from a couple. Oocytes were denuded by hyaluronidase to remove the cumulus cells and microinjection of one spermatozoon per oocyte was performed, as described elsewhere.[27] Only motile spermatozoa were used for ICSI. The next day, fertilization (presence of two pronuclei and extruded second polar body) was checked and embryo cleavage one day later. Good quality embryos were vitrified and stored in liquid nitrogen (-196°C) for later clinical use (transfer to the uterus). The rates of fertilization and embryo cleavage were compared between oocytes that matured *in vitro* and *in vivo* (in the ovaries; aspirated as mature) in the same patients after controlled ovarian hormonal stimulation.

Statistics

Both groups of patients, cancer and infertile patients, were compared in terms of the number of oocytes obtained after controlled hormonal stimulation of their ovaries, the proportion of immature and degenerated oocytes, and the proportion of immature (GV) oocytes that matured *in vitro*. Due to the relatively small number of patients/oocytes included and the abnormal distribution of data, tested by Shapiro-Wilk normality test, non-parametric tests (Fisher's exact and Mann-Whitney U tests) were performed; statistical significance was set at $P < 0.05$. After ICSI, the fertilization and embryo cleavage rates of oocytes that matured *in vitro* were compared with oocytes of the same patients that matured *in vivo* and were aspirated from the ovaries as mature oocytes in the same cycle of controlled ovarian hormonal stimulation using Fisher's exact and Wilcoxon tests; statistical significance was set at $P < 0.05$.

Results

Cancer patients had different types of cancer, but breast cancer was predominant (Figure 1). The average age of cancer patients was 30.3 ± 6.3 years and of women with fertility problems 33.4 ± 5.0 years. The two groups of women did not differ significantly in their age. There was also no significant difference in the age of patients with breast cancer and patients with other cancers (32.0 ± 6.2 *vs*. 29.0 ± 6.0 years).

Numbers, quality and immaturity of oocytes after controlled hormonal stimulation of the ovaries

After controlled hormonal stimulation of the ovaries, 198 oocytes were retrieved in cancer patients and 259 oocytes in infertile women. Cancer patients and patients with fertility problems did not differ significantly in the number of retrieved oocytes (11.0 ± 9.0 oocytes/patient *vs*. 12.3 ± 9.2 oocytes/patient), as revealed by Mann-Whitney U test. In cancer patients, the proportion of immature GV and MI oocytes was significantly lower than in patients with fertility problems (30.0% *vs*. 43.6%; $P < 0.05$), as revealed by Fisher's exact test (Table 1). The groups did not differ significantly in the proportion of GV oocytes (23.0% *vs*. 28.6%) (Table 1); among patients with immature oocytes, 50% of cancer patients and 48.0% of patients with fertility problems had increased proportion (≥ 31%) of GV oocytes with a germinal vesicle, which did not differ significantly. There was also no difference in the proportion of degenerated oocytes between cancer patients and patients with fertility problems (8.6 *vs*. 6.5%) (Table 1).

If we considered the type of cancer, we found that there was no significant difference in the number of all immature (MI and GV) oocytes in patients with breast cancer compared to patients with fertility problems or patients with other cancers (4.17 ± 3.25 *vs*. 5.29 ± 3.76 and 2.92 ± 2.47 immature oocytes/patient, respectively), as revealed by Mann-Whitney U test. There was also no statistically significant difference in the proportion of all immature (GV and MI) oocytes in breast cancer patients compared to patients with other cancers or patients with fertility problems (36.0% *vs*. 27.0% and 43.6%), as found using the Fisher's exact test. Nevertheless, there was a tendency for a significantly higher proportion of immature, GV oocytes in breast cancer patients compared to patients with other cancers (31.43% *vs*. 18.75%; $P = 0.0531$, Fisher's exact test).

In vitro matured oocytes

Forty-five GV oocytes in cancer patients and 74 GV oocytes in patients with fertility problems underwent IVM procedure (Table 2); the proportion of oocytes (15.5% in cancer patients and 12.2% in

women with fertility problems) degenerated just before or during conditioning in LAG medium. We found that a lower proportion of oocytes matured *in vitro* in cancer patients compared to patients with fertility problems (66.0 *vs*. 80.0%), however, the difference was not statistically significant, as revealed by Fisher's exact test. In spite of that, number of oocytes that matured *in vitro* per patient was significantly lower in cancer patients than in patients with fertility problems (1.39 ± 1.04 *vs*. 2.48 ± 1.83 oocytes/patient; P < 0.05, Mann-Whitney U test), as shown in Table 2.

In cancer patients, there was also a lower proportion of oocytes that matured *in vitro* in patients with breast cancer than in patients with other cancers and patients with fertility problems (54.5% *vs*. 81.2% and 80.0%) (Table 2). The difference between patients with breast cancer and women with fertility problems tended to be statistically significant (P = 0.0862; Fisher's exact test) and was probably not significant due to the relatively low number of oocytes included.

Overall, 198 oocytes were retrieved in cancer patients, of which 139 were mature. Following IVM, the number of total mature oocytes increased to 164 (13.0% increase in mature oocyte yield). In patients with fertility problems, 259 oocytes were retrieved, of which 146 were mature. After IVM, the number of total mature oocytes increased to 198, which means 20.1% increase in mature oocyte yield. Thus, there was no significant difference in the yield of mature oocytes after IVM between cancer patients and patients with fertility problems. 15.5% (7/45) GV oocytes in cancer patients and 12.2% (9/74) GV oocytes in patients with fertility problems degenerated before *in vitro* maturation procedure.

TABLE 1. Differences in the number, quality and immaturity of oocytes after controlled hormonal stimulation of the ovaries in cancer patients compared to patients with fertility problems

	Cancer patients (n = 18)	Patients with fertility problems (n = 21)
Age (years)	30.3 ± 6.3	33.4 ± 5.0
Number of retrieved oocytes	198	259
Oocytes per patient	11.0 ± 9.0	12.3 ± 9.2
Number of degenerated oocytes	17 (8.6%)	17 (6.5%)
Number of immature (MI + GV) oocytes	59 (30.0%)*	113 (43.6%) *
Number of immature GV oocytes	45 (23.0%)	74 (28.6%)

* = statistically significant difference (P = 0.0064) revealed by Fisher's exact test; significance was set at P < 0.05; GV = germinal vesicle; MI = metaphase I (oocyte meiosis)

TABLE 2. Numbers and percentages of oocytes that matured *in vitro* in patients with different cancers compared to patients with fertility problems

	Number of oocytes that underwent in vitro maturation	Number of oocytes that matured in vitro
All cancer patients (n = 18)	38 / 45	25 (1.39 ± 1.04 per patient)* (66.0%)
Patients with breast cancer (n = 8)	22	12 (54.5%)
Patients with other cancers (n = 10)	16	13 (81.2%)
Patients with fertility problems (n = 21)	65 / 74	52 (2.48 ± 1.83 per patient)* (80.0%)

* = statistically significant difference (P < 0.05; Mann-Whitney U test)

Results of ICSI of *in vitro* matured oocytes in patients with fertility problems

In vitro fertilization of 49 oocytes in 17 patients with fertility problems (average age 34.3 ± 4.4 years) was performed by ICSI with partner's semen (in 2 men oligozoospermia and 15 men teratozoospermia). After performing this method, 27 (55.1%) oocytes were fertilized (expressing two pronuclei and two polar bodies) and 23 (85.2%) fertilized oocytes (zygotes) further developed into an embryo, as shown in Table 3; four zygotes did not cleave further. Good quality embryos were vitrified and stored in liquid nitrogen for future clinical use in patients (transfer into the uterus).

After ICSI, the fertilization and cleavage rates of 49 oocytes that matured *in vitro* were compared with 121 oocytes of the same patients that matured *in vivo* and were aspirated from their ovaries as mature oocytes (metaphase II [MII] oocyte meiosis) in the same cycle of controlled ovarian hormonal stimulation. Of the 121 oocytes obtained as mature oocytes, 69 oocytes were fertilized, representing a fertilization rate of 57.0%. Sixty-one fertilized oocytes further developed into an embryo (Table 3). Fisher's exact test revealed no statistical differences in the proportions of fertilized oocytes, non-cleaved zygotes, and embryos obtained by ICSI on *in vitro* and *in vivo* matured oocytes (Table 3).

TABLE 3. Non-significant differences in fertilized oocytes, non-cleaved zygotes, and cleavage embryos obtained by intracytoplasmic sperm injection (ICSI) on *in vitro* matured and *in vivo* matured oocytes of patients with fertility problems (in the same cycles)

ICSI cycles (n = 17)	*In vitro* matured oocytes	*In vivo* matured oocytes*
Number of microinjected oocytes	49	121
Fertilized oocytes	27 (55.1%)	69 (57.0%)
Non-cleaved zygotes	4 (15.0%)	8 (11.6%)
Cleavage embryos	23 (85.2%)	61 (88.4%)

* = non-significant differences, as revealed by Fisher's exact test

TABLE 4. Non-significant differences in results of intracytoplasmic sperm injection (ICSI) cycles (fertilized oocytes, non-cleaved zygotes, cleavage embryos) on *in vitro* matured oocytes of patients with fertility problems regarding the number of immature (germinal vesicle [GV]) oocytes

ICSI cycles (n = 17)	≤ 30% GV oocytes	≥ 31% GV oocytes
Female age (years)	34.4 ± 3.0	34.3 ± 5.6
Number of microinjected oocytes	16	33
Fertilized oocytes	11 (69.0%)	16 (48.5%)
Non-cleaved zygotes	0 (0%)	4 (25.0%)
Cleavage embryos	11 (100%)	12 (75%)

Non-significant differences, as revealed by Fisher's exact test

In patients with an increased proportion of immature (GV) oocytes (≥ 31%), there was a tendency for a lower proportion of fertilized oocytes and a higher proportion of non-cleaved zygotes, but the differences were not statistically significant (Table 4).

Discussion

The results of this research show that cancer and control healthy patients with fertility problems did not differ in the number and quality of oocytes after controlled hormonal stimulation of their ovaries, which is positive. In cancer patients, there was even a significantly lower proportion of immature oocytes than in patients with fertility problems. However, in patients with cancer, fewer oocytes per patient matured *in vitro* than in patients with fertility problems (1.39 ± 1.04 *vs*. 2.48 ± 1.83, $P < 0.05$). Following ICSI of oocytes in patients with fertility problems, the fertilization and embryo cleavage rates were approximately the same in oocytes that matured *in vitro* and *in vivo* in the same patients, in the same cycles of controlled hormonal stimulation of the ovaries. This is also to be expected in cancer patients.

The proportion of mature, MII oocytes in the patients with fertility problems included in this research was relatively low (56.4%) compared to the internationally accepted reference value of 70-80%[28], because we included mainly patients with a higher proportion of immature oocytes which did not reflect the average condition; in cancer patients, the proportion of mature oocytes was higher (70%) and within the reference value.[28] The number and quality of oocytes in cancer patients did not differ between different cancers and from control patients with fertility problems. The same has been found in other studies for different types of cancer such as breast cancer, lymphoma, gliomas and other cancers.[29,30] For breast cancer, the results of various studies are otherwise contradictory. In a study by Malacarne *et al*., as in our study, the average number of oocytes obtained per breast cancer patient after ovarian stimulation did not differ significantly from healthy control women including oocyte donors, women with fertility preservation for non-medical reasons, and female partners of infertile men in an IVF program[31]; it was concluded that patients with breast cancer undergoing controlled ovarian hormonal stimulation for fertility preservation can expect the ovarian response predicted for their age. The results obtained by different studies do not support the notion of a negative impact of the breast cancer gene 1/2 (*BRCA1/2)* mutation on the ovarian response of women with breast cancer.[31-33] Nevertheless, the results of some other studies suggest the reduced number and maturity of oocytes obtained for cryostorage in patients with breast cancer[34],which may be attributed to the higher grade of cancer[35] or different expression of hormonal receptors.[36]

There is little data in the literature on how different cancers affect the oocyte IVM in cancer patients. The oocyte IVM rate in breast cancer patients was found to be approximately 53.2 to 64.2% in the

study of Shalom Paz *et al.*[37], which is very similar to our study (54.5%), or slightly higher – 62.0%, 66.0% or 66.7% in some other studies.[22,32] In this study, the proportion of immature oocytes matured *in vitro* tended to be lower in breast cancer patients (54.5%) than in patients with fertility problems (80.0%), while this was not observed in patients with other cancers (81.2%). Although, the difference was not significant, possibly due to relatively low number of patients and oocytes included. In a study conducted by *Liu et al.*, 811 genes were identified that were expressed differently in malignant breast tissue compared to healthy breast tissue[38]; among the up-regulated genes was also a group of genes involved in the cell cycle and progesterone-mediated oocyte maturation. For cancer patients, Cohen *et al.* found that the mean oocyte maturation rate in stimulated IVF cycles was 38%[39], which is significantly lower than in our study (66.0%; 54.5% in breast cancer and 81.0% in other cancers). In our study, IVM of oocytes in coculture with cumulus cells from mature oocytes in the same patients may have been beneficial, at least in part providing an ovarian niche.[26] Also Chatroudi *et al.* found that cumulus cell supplementation in IVM culture media enhances the viability of human embryos (blastocysts) after IVF.[40] The rates of *in vitro* matured oocytes in cancer patients and patients with fertility problems in our study were very similar to the published rates of IVM of immature oocytes in the usual IVF program, where 65.0%, 68.7%, 68.9% and 69.7% maturation rates were obtained in different maturation media.[41-43] Oktay *et al.* reported the 45% increase in mature oocyte yield after IVM of immature oocytes after controlled hormonal stimulation of the ovaries in breast cancer patients and a high fertilization rate of these oocytes.[44] Moreover, an IVM of oocytes retrieved without hormonal stimulation of the ovaries was considered for fertility preservation in breast cancer patients to avoid the ovarian stimulation, shorten the time to oocyte retrieval, and not to increase both the serum estradiol level and delay in cancer treatment.[45-47]

It should be noted that our study was limited to a relatively small number of patients involved and a small number of oocytes. In cancer patients and patients with fertility problems, we tried to perform as comparable controlled hormonal stimulation of the ovaries as possible using a GnRH antagonist. Nevertheless, we also had to take certain safety precautions in cancer patients. In these patients, the ovarian hormonal stimulation was initiated immediately after they have been sent to our department, no matter of the cycle phase to be fast and prevent further progression of disease. The oocyte maturation in cancer patients was initiated by GnRH analogue to prevent hyperstimulation, but more patients with less than 10 follicles were also treated with Ovitrelle similar to patients with fertility problems. Thus, in most patients, oocyte maturation was triggered by Ovitrelle. If we used exactly the same method of hormonal ovarian stimulation and triggering oocyte maturation in cancer patients and patients with fertility problems, there might be more immature oocytes in cancer patients, but this was not possible for cancer-related safety reasons.

In addition, for safety reasons, breast cancer patients were also treated with an aromatase inhibitor, letrozole, to prevent an increase in estradiol and worsening of the disease. Thus, based on our own experience and literature[48,49], we believe that both random start of hormonal stimulation in cancer patients and use of aromatase inhibitor in patients with breast cancer do not affect the number, maturity and *in vitro* maturation of oocytes obtained in these patients.

Letrozole treatment may also increase the intraovarian androgen levels, which have a negative impact on granulosa cells (apoptosis) in the late antral and pre-ovulatory follicles.[50] In this research, granulosa (cumulus) cells were used in co-culture for oocyte maturation, which may lower the maturation rate. However, we performed *in vitro* maturation of oocytes with cumulus cells of mature oocytes because our previous work showed that coculture with cumulus cells does not affect the proportion of *in vitro* matured oocytes, but improves the molecular status of oocytes (gene expression profile) compared to oocytes matured *in vivo*.[26]

In patients with fertility problems, we determined the FSH, LH and AMH levels in early follicular phase of the cycle as well as the number of antral follicles. For cancer patients, we have no such data. Only informative ovarian scan with antral follicle estimation was performed at the beginning of ovarian stimulation.

In our study, approximately the same proportion of oocytes were fertilized and further cleaved into an embryo after ICSI of *in vitro* and *in vivo* matured oocytes. Some studies have shown poorer embryo development and live birth rates with *in vitro* matured oocytes[51,52], which could be linked to structural and morphologic differences in human oocytes after IVM[53] due to suboptimal maturation medium and lack of ovarian niche. It needs to be point out that in our study, oocyte IVM was performed in coculture with cumulus cells from ma-

ture oocytes of the same patients thus providing a degree of ovarian niche. In spite of a lower rate of good-quality embryos and different developmental dynamics of embryos, pregnancy rates as well as live births did not necessarily differ after oocyte IVM, as found by Roesner *et al*.[54] Moreover, in a matched setting between IVM and IVF babies born from women with polycystic ovaries, no significant increased risk associated with IVM has been identified in 2-year-old singletons born after IVM and after a mean follow-up up to 7.5 years.[55,56] In general, more studies are urgently required to improve IVM –vitrification method to successfully preserve oocytes collected from cancer patients.[57,58]

Conclusions

We may conclude that 'rescue' of immature oocytes with IVM is a useful strategy to improve the mature oocyte yield of fertility preservation cycles in cancer patients. Immature oocytes retrieved during oocyte and also embryo cryopreservation cycles in cancer patients should not be discarded in order to improve the future potential of pregnancy in these patients. Their immature oocytes can mature *in vitro* comparable to healthy controls. After ICSI, approximately the same proportion of *in vitro* matured oocytes could be fertilized and developed into an embryo as in oocytes matured *in vivo*.

Acknowledgments

We would like to thank all colleagues, gynecologists, embryologists, and nurses at the Department of Gynecology and Obstetrics, Reproductive Unit (IVF), who in any way helped in this work. We also thank all the patients who kindly donated immature oocytes for this research. Last but not least, we would also like to thank our institution, University Medical Centre Ljubljana, which funded this research as part of a tertiary research project.

References

1. Yeo W, Pang E, Liem GS, Suen JJS, Ng RYW, Yip CCH, et al. Menopausal symptoms in relationship to breast cancer-specific quality of life after adjuvant cytotoxic treatment in young breast cancer survivors. *Health Qual Life Outcomes* 2020; **18:** 24. doi: 10.1186/s12955-020-1283-x
2. Silvestris E, Dellino M, Cafforio P, Paradiso AV, Cormio G, D'Oronzo S. Breast cancer: an update on treatment-related infertility. *J Cancer Res Clin Oncol* 2020; **146:** 647-57. doi: 10.1007/s00432-020-03136-7
3. Felicetti F, Castiglione A, Biasin E, Fortunati N, Dionisi-Vici M, Matarazzo P, et al. Effects of treatments on gonadal function in long-term survivors of pediatric hematologic malignancies: a cohort study. *Pediatr Blood Cancer* 2020; **67:** e28709. doi: 10.1002/pbc.28709
4. Yeganeh L, Boyle JA, Gibson-Helm M, Teede H, Vincent AJ. Women's perspectives of early menopause: development of a word cloud. *Climacteric* 2020; **23:** 417-20. doi: 10.1080/13697137.2020.1730318
5. Delattre S, Segers I, Van Moer E, Drakopoulos P, Mateizel I, Enghels L, et al. Combining fertility preservation procedures to spread the eggs across different baskets: a feasibility study. *Hum Reprod* 2020; **35:** 2524-36. doi: 10.1093/humrep/deaa193.
6. Dinas KD. Fertility counseling and preservation for breast cancer patients. *Adv Exp Med Biol* 2020; **1252:** 181-87. doi: 10.1007/978-3-030-41596-9_25
7. Bénard J, Duros S, El Hachem H, Sonigo C, Sifer C, Grynberg M. Freezing oocytes or embryos after controlled ovarian hyperstimulation in cancer patients: the state of the art. *Future Oncol* 2016; **12:** 1731-41. doi: 10.2217/fon-2016-0095
8. de Pedro M, Otero B, Martín B. Fertility preservation and breast cancer: a review. *Ecancer* 2015; **9:** 503. doi: 10.3332/ecancer.2015.503
9. Kasum M, Beketić-Orešković L, Peddi PF, Orešković S, Johnson RH. Fertility after breast cancer treatment. *Eur J Obstet Gynecol Reprod Biol* 2014; **173:** 13-8. doi: 10.1016/j.ejogrb.2013.11.009
10. Peccatori FA, Pup LD, Salvagno F, Guido M, Sarno MA, Revelli A, et al. Fertility preservation methods in breast cancer. *Breast Care* 2012; **7:** 197-202. doi: 10.1159/000339671
11. Redig AJ, Brannigan R, Stryker SJ, Woodruff TK, Jeruss JS. Incorporating fertility preservation into the care of young oncology patients. *Cancer* 2011; **117:** 4-10. doi: 10.1002/cncr.25398
12. Meirow D. Reproduction post-chemotherapy in young cancer patients. *Mol Cell Endocrinol* 2000; **169:** 123-31. doi: 10.1016/s0303-7207(00)00365-8
13. Specchia C, Baggiani A, Immediata V, Ronchetti C, Cesana A, Smeraldi A, et al. Oocyte cryopreservation in oncological patients: eighteen years' experience of a tertiary care referral center. *Front Endocrinol* 2019; **10:** 600. doi: 10.3389/fendo.2019.00600
14. Gook DA, Edgar DH. Cryopreservation of female reproductive potential. *Best Pract Res Clin Obstet Gynaecol* 2019; **55:** 23-36. doi: 10.1016/j.bpobgyn.2018.08.005
15. Cobo A, García-Velasco J, Domingo J, Pellicer A, Remohí J. Elective and onco-fertility preservation: factors related to IVF outcomes. *Hum Reprod* 2018; **33:** 2222-31. doi: 10.1093/humrep/dey321
16. Dolmans MM, Donnez J. Fertility preservation in women for medical and social reasons: oocytes vs ovarian tissue. *Best Pract Res Clin Obstet Gynaecol* 2020; **21:** S1521-6934(20)30122-X. doi: 10.1016/j.bpobgyn.2020.06.011
17. Khalili MA, Shahedi A, Ashourzadeh S, Nottola SA, Macchiarelli G, Palmerini MG. Vitrification of human immature oocytes before and after in vitro maturation: a review. *J Assist Reprod Genet* 2017; **34:** 1413-26. doi: 10.1007/s10815-017-1005-4
18. Ata B, Chian RC, Tan SL. Cryopreservation of oocytes and embryos for fertility preservation for female cancer patients. *Best Pract Res Clin Obstet Gynaecol* 2010; **24:** 101-12. doi: 10.1016/j.bpobgyn.2009.11.007
19. El Hachem H, Atallah D, Grynberg M. Fertility preservation in breast cancer patients. *Future Oncol* 2014; **10:** 1767-77. doi: 10.2217/fon.14.55
20. Muñoz E, Domingo J, De Castro G, Lorenzo I, García-Velasco JA, Bellver J, et al. Ovarian stimulation for oocyte vitrification does not modify disease-free survival and overall survival rates in patients with early breast cancer. *Reprod Biomed Online* 2019; **39:** 860-67. doi: 10.1016/j.rbmo.2019.07.003
21. Rodgers RJ. Fertility preservation in breast cancer patients. *Minerva Ginecol* 2019; **71:** 196-206. doi: 10.23736/S0026-4784.19.04409-5
22. Grynberg M, Poulain M, le Parco S, Sifer C, Fanchin R, Frydman N. Similar in vitro maturation rates of oocytes retrieved during the follicular or luteal phase offer flexible options for urgent fertility preservation in breast cancer patients. *Hum Reprod* 2016; **31:** 623-9. doi: 10.1093/humrep/dev325
23. Grynberg M, Mayeur Le Bras A, Hesters L, Gallot V, Frydman N. First birth achieved after fertility preservation using vitrification of in vitro matured oocytes in a woman with breast cancer. *Ann Oncol* 2020; **31:** 541-42. doi: 10.1016/j.annonc.2020.01.005

24. World Health Organisation. *WHO laboratory manual for the examination and processing of human semen.* Geneva: WHO Press; 2010.

25. Stimpfel M, Vrtacnik-Bokal E, Virant-Klun I. No difference in mitochondrial distribution is observed in human oocytes after cryopreservation. *Arch Gynecol Obstet* 2017; **296:** 373-81. doi: 10.1007/s00404-017-4428-3

26. Virant-Klun I, Bauer C, Ståhlberg A, Kubista M, Skutella T. Human oocyte maturation in vitro is improved by co-culture with cumulus cells from mature oocytes. *Reprod Biomed Online* 2018; **36:** 508-23. doi: 10.1016/j.rbmo.2018.01.011

27. Stimpfel M, Verdenik I, Zorn B, Virant-Klun I. Magnetic-activated cell sorting of non-apoptotic spermatozoa improves the quality of embryos according to female age: a prospective sibling oocyte study. *J Assist Reprod Genet* 2018; **35:** 1665-74. doi:10.1007/s10815-018-1242-1

28. ESHRE Special Interest Group of Embryology and Alpha Scientists in Reproductive Medicine. The Vienna consensus: report of an expert meeting on the development of art laboratory performance indicators. *Hum Reprod Open* 2017; **2017:** 1-17. doi: 10.1093/hropen/hox011

29. Lefebvre T, Mirallié S, Leperlier F, Reignier A, Barrière P, Fréour T. Ovarian reserve and response to stimulation in women undergoing fertility preservation according to malignancy type. *Reprod Biomed Online* 2018; **37:** 201-7. doi: 10.1016/j.rbmo.2018.04.047

30. Nordan T, Thomas AM, Ginsburg ES, Wen PY, Dolinko AV, Bortoletto P. Fertility preservation outcomes in women with gliomas: a retrospective case-control study. *J Neurooncol* 2020; **147:** 371-76. doi: 10.1007/s11060-020-03429-4

31. Malacarne E, Devesa M, Martinez F, Rodriguez I, Coroleu B. COH outcomes in breast cancer patients for fertility preservation: a comparison with the expected response by age. *J Assist Reprod Genet* 2020; **37:** 3069-76. doi: 10.1007/s10815-020-01944-x

32. Grynberg M, Dagher Hayeck B, Papanikolaou EG, Sifer C, Sermondade N, Sonigo C. BRCA1/2 gene mutations do not affect the capacity of oocytes from breast cancer candidates for fertility preservation to mature in vitro. *Hum Reprod* 2019; **34:** 374-79. doi: 10.1093/humrep/dey358

33. Gunnala V, Fields J, Irani M, D'Angelo D, Xu K, Schattman G, et al. BRCA carriers have similar reproductive potential at baseline to noncarriers: comparisons in cancer and cancer-free cohorts undergoing fertility preservation. *Fertil Steril* 2019; **111:** 363-71. doi: 10.1016/j.fertnstert.2018.10.014

34. Moria A, Das M, Shehata F, Holzer H, Son WY, Tulandi T. Ovarian reserve and oocyte maturity in women with malignancy undergoing in vitro maturation treatment. *Fertil Steril* 2011; **95:** 1621-3. doi: 10.1016/j.fertnstert.2010.12.041

35. Volodarsky-Perel A, Cai E, Tulandi T, Son WY, Suarthana E, Buckett W. Influence of stage and grade of breast cancer on fertility preservation outcome in reproductive-aged women. *Reprod Biomed Online* 2020; **40:** 215-22. doi: 10.1016/j.rbmo.2019.11.006

36. Balayla J, Tulandi T, Buckett W, Holzer H, Steiner N, Shrem G, et al. Outcomes of ovarian stimulation and fertility preservation in breast cancer patients with different hormonal receptor profiles. *J Assist Reprod Genet* 2020; **37:** 913-21. doi: 10.1007/s10815-020-01730-9

37. Shalom-Paz E, Almog B, Shehata F, Huang J, Holzer H, Chian RC, et al. Fertility preservation for breast-cancer patients using IVM followed by oocyte or embryo vitrification. *Reprod Biomed Online* 2010; **21:** 566-71. doi: 10.1016/j.rbmo.2010.05.003

38. Liu Z, Liang G, Tan L, Su AN, Jiang W, Gong C. High-efficient screening method for identification of key genes in breast cancer through microarray and bioinformatics. *Anticancer Res* 2017; **37:** 4329-35. doi: 10.21873/anticanres.11826

39. Cohen Y, Tannus S, Volodarsky-Perel A, Son WY, Tulandi T, Buckett W. Added benefit of immature oocyte maturation for fertility preservation in women with malignancy. *Reprod Sci* 2020; **27:** 2257-64. doi: 10.1007/s43032-020-00245-z

40. Chatroudi MH, Khalili MA, Ashourzadeh S, Anbari F, Shahedi A, Safari S. Growth differentiation factor 9 and cumulus cell supplementation in in vitro maturation culture media enhances the viability of human blastocysts. *Clin Exp Reprod Med* 2019; **46:** 166-72. doi: 10.5653/cerm.2019.00402

41. Sacha CR, Kaser DJ, Farland LV, Srouji S, Missmer SA, Racowsky C. The effect of short-term exposure of cumulus-oocyte complexes to in vitro maturation medium on yield of mature oocytes and usable embryos in stimulated cycles. *J Assist Reprod Genet* 2018; **35:** 841-49. doi: 10.1007/s10815-018-1155-z

42. Pongsuthirak P, Songveeratham S, Vutyavanich T. Comparison of blastocyst and Sage media for in vitro maturation of human immature oocytes. *Reprod Sci* 2015; **22:** 343-6. doi: 10.1177/1933719114542027

43. Junk SM, Yeap D. Improved implantation and ongoing pregnancy rates after single-embryo transfer with an optimized protocol for in vitro oocyte maturation in women with polycystic ovaries and polycystic ovary syndrome. *Fertil Steril* 2012; **98:** 888-92. doi: 10.1016/j.fertnstert.2012.06.055

44. Oktay K, Buyuk E, Rodriguez-Wallberg KA, Sahin G. In vitro maturation improves oocyte or embryo cryopreservation outcome in breast cancer patients undergoing ovarian stimulation for fertility preservation. *Reprod Biomed Online* 2010; **20:** 634-8. doi: 10.1016/j.rbmo.2010.01.012

45. D'Hondt C, Vanhoeij M, Van Moer E, Segers I, Fontaine C, Tournaye H, et al. Fertility preservation does not delay the initiation of chemotherapy in breast cancer patients treated with adjuvant or neo-adjuvant chemotherapy. *Breast Cancer Res Treat* 2020; **184:** 433-44. doi: 10.1007/s10549-020-05858-1

46. Huang JY, Chian RC, Gilbert L, Fleiszer D, Holzer H, Dermitas E, et al. Retrieval of immature oocytes from unstimulated ovaries followed by in vitro maturation and vitrification: A novel strategy of fertility preservation for breast cancer patients. *Am J Surg* 2010; **200:** 177-83. doi: 10.1016/j.amjsurg.2009.04.004

47. Oktay K, Demirtas E, Son WY, Lostritto K, Chian RC, Tan SL. In vitro maturation of germinal vesicle oocytes recovered after premature luteinizing hormone surge: description of a novel approach to fertility preservation. *Fertil Steril* 2008; **89:** 228.e19-22. doi: 10.1016/j.fertnstert.2007.02.028

48. Marklund A, Eloranta S, Wikander I, Kitlinski ML, Lood M, Nedstrand E, et al. Efficacy and safety of controlled ovarian stimulation using GnRH antagonist protocols for emergency fertility preservation in young women with breast cancer-a prospective nationwide Swedish multicenter study. *Hum Reprod* 2020; **35:** 929-38. doi: 10.1093/humrep/deaa029

49. American Society for Reproductive Medicine. Fertility preservation in patients undergoing gonadotoxic therapy or gonadectomy: a committee opinion. Practice Committee of the American Society for Reproductive Medicine. *Fertil Steril* 2019; **112:** 1022-33. doi: 10.1016/j.fertnstert.2019.09.013

50. Rose BI, Brown SE. A review of the physiology behind letrozole applications in infertility: are current protocols optimal? *J Assist Reprod Genet* 2020; **37:** 2093-104. doi: 10.1007/s10815-020-01892-6

51. Santiquet NW, Greene AF, Becker J, Barfield JP, Schoolcraft WB, Krisher RL. A pre-in vitro maturation medium containing cumulus oocyte complex ligand-receptor signaling molecules maintains meiotic arrest, supports the cumulus oocyte complex and improves oocyte developmental competence. *Mol Hum Reprod* 2017; **23:** 594-606. doi: 10.1093/molehr/gax032

52. Walls ML, Hunter T, Ryan JP, Keelan JA, Nathan E, Hart RJ. In vitro maturation as an alternative to standard in vitro fertilization for patients diagnosed with polycystic ovaries: a comparative analysis of fresh, frozen and cumulative cycle outcomes. *Hum Reprod* 2015; **30:** 88-96. doi: 10.1093/humrep/deu248

53. Walls ML, Hart R, Keelan JA, Ryan JP. Structural and morphologic differences in human oocytes after in vitro maturation compared with standard in vitro fertilization. *Fertil Steril* 2016; **106:** 1392-98. doi: 10.1016/j.fertnstert.2016.08.014

54. Roesner S, Dietrich JE, Weigert J, Montag M, Toth B, Strowitzki T. Time-lapse imaging reveals differences in growth dynamics of embryos after in vitro maturation compared with conventional stimulation. *Fertil Steril* 2017; **107:** 606-12. doi: 10.1016/j.fertnstert.2016.12.026

55. Belva F, Roelants M, Vermaning S, Desmyttere S, De Schepper J, Bonduelle M, et al. Growth and other health outcomes of 2-year-old singletons born after IVM versus controlled ovarian stimulation in mothers with polycystic ovary syndrome. *Hum Reprod Open* 2020; **2020:** hoz043. doi: 10.1093/hropen/hoz043

56. Yu EJ, Yoon TK, Lee WS, Park EA, Heo JY, Ko YK, et al. Obstetrical, neonatal, and long-term outcomes of children conceived from in vitro matured oocytes. *Fertil Steril* 2019; **112:** 691-99. doi: 10.1016/j.fertnstert.2019.05.034

57. Son WY, Henderson S, Cohen Y, Dahan M, Buckett W. Immature Oocyte for Fertility Preservation. *Front Endocrinol* 2019; **10:** 464. doi: 10.3389/fendo.2019.00464

58. Shirasawa H, Terada Y. In vitro maturation of human immature oocytes for fertility preservation and research material. *Reprod Med Biol* 2017; **16:** 258-67. doi: 10.1002/rmb2.12042

Radiol Oncol 2022; 56(1): 1-13.
doi: 10.2478/raon-2022-0002

Genska terapija raka postane viralna. Vzpon platform virusnih vektorjev

Bezeljak U

Izhodišča. Zdravljenje raka z virusnimi vektorji je obetalo revolucijo v onkologiji vse od vzpona vektorske genske terapije v 90. letih prejšnjega stoletja. Vektorji, ki temeljijo na virusnih delcih, ponujajo edinstveno kombinacijo učinkovite transdukcije tumorja in stimulacijo imunskega sistema za zdravljenje raka. Kljub začetni obetavnosti se zdravljenje z virusnimi vektorji šele sedaj prebija v ospredje. Virusne vektorje uporabljamo kot gensko orodje za pripravo celičnih terapevtikov CAR-T, kot cepiva za raka in kot ciljana onkolitična zdravila. Da bi dosegli tako širok nabor področij uporabe smo premagali vrsto preprek – od razumevanja temeljne biologije raka do procesov priprave in načrtovanja vektorjev. Objavljamo pregled najnovejših dognanj in uporabe virusnih vektorjev pri zdravljenju raka. Izpostavljamo platforme za proizvodnjo virusnih delcev, ki omogočajo splošno uporabo virusnih vektorjev pri genski terapiji raka.

Zaključki. Virusni vektorji ponujajo številne priložnosti pri zdravljenju raka. Nedavni napredek v proizvodnih platformah vektorjev odpira nove možnosti za varno in učinkovito zdravljenje ter poenostavlja prenos tehnologije iz laboratorija v kliniko. Tehnologija virusnih vektorjev je v zadnjih letih napredovala do stopnje, da lahko postane standardno orodje pri zdravljenju raka.

Radiol Oncol 2022; 56(1): 14-22.
doi: 10.2478/raon-2022-0004

Ultrazvočno vodeno injiciranje v karpalni kanal

Tumpaj T, Potočnik Tumpaj V, Albano D, Snoj Ž

Izhodišča. Sindrom karpalnega kanala je ena izmed najpogostejših utesnitvenih mononevropatij, ki predstavlja velik socialno-ekonomski problem zaradi nezmožnosti dela, invalidnosti in podaljšane rehabilitacije. Ultrazvok je slikovna metoda izbora za potrditev diagnoze ter sledenje bolnikov s sindromom karpalnega kanala. V zadnjih letih se je za zdravljenje blage do zmerne oblike sindroma karpalnega kanala uveljavilo ultrazvočno vodeno injiciranje v karpalni kanal. S pregledom literature smo strnili zabeležene razlike pri naslednjih korakih: priprava bolnika, pristop vboda, položaj igle, vrsta in količina injiciranih učinkovin. V literaturi opisujejo tri pristope: ulnarni, radialni in longitudinalni. Vse tri pristope lahko izvedemo z enkratnim ali večkratnim injiciranjem z različnimi količinami učinkovin. Učinkovine, ki jih uporabljamo za izvedbo postopka so kortikosteroidi, lokalni anestetiki, dekstroza, fiziološka raztopina, plazma obogatena s trombociti in progesteron.

Zaključki. Soglasja glede optimalnega protokola še ni. Pri pregledu literature se za najbolj najbolj primeren pristop kaže ulnarni pristop z enkratnim vbrizganjem, najboljši rezultati pa so bili doseženi pri uporabi dekstroze v večjih količinah. Zaradi terminoloških razlik v literaturi je primerjava protokolov težavna, zato lahko predstavljeni koraki ultrazvočno vodenih injekcij služijo kot vodilo nadaljnjim raziskavam.

Radiol Oncol 2022; 56(1): 23-31.
doi: 10.2478/raon-2021-0051

Kopičenje amiloida beta ni povezano z lokalnim metabolizmom glukoze pri bolnikih z zgodnjim stadijem Alzheimerjeve bolezni

Ehrlich D, Dunzinger A, Malsiner-Walli G, Grün B, Topakian R, Hodolic M, Kainz E, Pichler R

Izhodišča. Pri bolnikih z Alzheimerjevo boleznijo so ugotovili nabiranje amiloida beta, kar povzroča disfunkcijo sinaps in nato odmiranje nevronov. Ni še znano, ali količina kopičenja amiloida beta korelira s stopnjo kognitivne prizadetosti. Slikovna diagnostika bi lahko vodila k boljšemu razumevanju vloge amiloida beta pri razvoju kognitivne prizadetosti. Namen pričujoče raziskave je bil preučiti, ali nabiranje amiloida beta v posameznih predelih možganov pri bolnikih z zgodnjo Alzheimerjevo boleznijo sovpada z disfunkcijo nevronov in kognitivno prizadetostjo, kar bi lahko videli z znižanim metabolizmom glukoze.

Bolniki in metode. Pri 30 bolnikih z Alzheimerjevo boleznijo in dokazanim nabiranjem amiloida smo izvedli 2-(18F)Fluoro-2-deoksi-d-glukozni (FDG) PET/CT. Izračunali smo povprečno kopičenje (18F)flutemetamola (Vizamyal) za 16 področij v vsaki možganski hemisferi in izračunali razmerje vrednosti standardiziranega privzema (*angl. standardised uptake value ratio*; SUVR), tako da smo delili intenziteto nabiranja (18F)flutemetamola z srednjim kopičenjem pozitivnih in negativnih kontrolnih področij. Podatke smo analizirali z okoljem R za statistični in grafični izračun.

Rezultati. Nismo ugotovili nobene negativne korelacije med kopičenjem amiloida beta in metabolizmom glukoze pri 32 področjih možganov ob obravnavi bolnikov z Alzheimerjevo boleznijo in demenco. Noben koeficient korelacije ni bil statistično značilno višji od 0, izračunano s pomočjo dvostranske p vrednosti.

Zaključki. Regionalno kopičenje amiloida beta ni koreliralo z lokalnim metabolizmom glukoze pri bolnikih z zgodnjim stadijem Alzheimerjeve bolezni. Rezultati raziskave podpirajo vlogo amiloida beta kot pomembnega biološkega označevalca, vendar ne moremo zaključiti, da je amiloid beta vzrok spremenjenega metabolizma glukoze in nevronske disfunkcije.

Radiol Oncol 2022; 56(1): 32-36.
doi: 10.2478/raon-2021-0056

Zanesljivost novih rentgenskih meritvenih tehnik pri kostni utesnitvi komolca

Meglič U, Zupanc O

Izhodišča. Ugotavljanje lokacije in obsega rentgenskih sprememb pri kostni utesnitvi komolca je ključnega pomena pri oblikovanju ustrezne diagnoze in načrta zdravljenja za tovrstne bolnike. Namen pričujoče raziskave je bil oceniti zanesljivost novih rentgenskih parametrov, sprednjega utesnitvenega kota in zadnjega utesnitvenega kota, pri kostni utesnitvi komolca in ugotoviti ali obstaja povezava med rentgenskimi parametri in klinično oceno.

Bolniki in metode. Rentgenske posnetke 60 bolnikov (30 v skupini s kostno utesnitvijo komolca in 30 v skupini brez bolezni) so z 2-tedenskim razmakom dvakrat ocenjevali trije ocenjevalci različnih stopenj usposobljenosti. Zanesljivost med ocenjevalci je bila izračunana s koeficienti korelacije (ICC) s 95-odstotnim intervalom zaupanja. Korelacijo med rentgenskimi parametri in klinično oceno smo izračunali s Pearsonovim korelacijskim koeficientom.

Rezultati. V obeh skupinah je bila zanesljivost merjenja med ocenjevalci dobra. Za obe meritvi ni bilo pomembnih razlik v zanesljivosti meritve med kirurgi specialisti in specializanti. Ugotovljena je bila dobra korelacija med rentgenskimi meritvami in obsegom giba.

Zaključki. Meritve sprednjega utesnitvenega kota in zadnjega utesnitvenega kota so pokazale dobro zanesljivost merjenja med ocenjevalci, tako pri slikah bolnikov s kostno utesnitvijo komolca kot pri normalnih rentgenskih slikah. Dobra zanesljivost ocenjevanja, ki smo jo ugotovili pri specialistih kirurgih in tudi pri specializantih na usposabljanju ter dobra korelacija med rentgenskimi meritvami in kliničnim testiranjem, kaže, da se nove rentgenske meritvene tehnike lahko enostavno in zanesljivo uporabljajo v vsakodnevni praksi.

Radiol Oncol 2022; 56(1): 37-45.
doi: 10.2478/raon-2022-0005

Učinkovitost transvaginalnega ultrazvoka v primerjavi z magnetno resonančnim slikanjem za predoperativno oceno invazije miometrija pri bolnicah z endometrioidnim rakom endometrija. Prospektivna primerjalna raziskava

Cerovac A, Ljuca D, Arnautalić L, Habek D, Bogdanović G, Mustedanagić-Mujanović J, Grgić G

Izhodišča. Primerjali smo natančnost predoperativnega transvaginalnega ultrazvoka (TVUS) in slikanja z magnetno resonanco (MRI) za oceno invazije miometrija pri bolnicah z rakom endometrija. Dokončna histopatološka diagnoza je služila kot referenčna metoda.

Bolniki in metode. Raziskavo smo izvedli v terciarnem centru v obdobju 2019 do 2021 in vanjo vključili bolnice s histopatološko dokazanim rakom endometrija, ki smo jih hospitalizirali zaradi načrtovane operacije. Invazijo miometrija smo ocenili s TVUS in MRI pred kirurško določitvijo stadija. Uporabili smo dve objektivni metodi TVUS (Gordonovo in Karlssonovo metodo) in MRI. Bolnike smo po operaciji in histopatološki oceni invazije miometrija razdelili v dve skupini: površinsko (≤ 50 % invazije) in globoko (> 50 % invazije).

Rezultati. Za študijsko obravnavo je bilo primernih 60 bolnic. Histopatološko je bilo v raziskavi 34 (56,7 %) bolnic z invazije miometrija ≤ 50 % in 26 (43,3 %) bolnic z invazije miometrija > 50 %. Obe slikovni metodi, TVUS in MRI, nista pokazali statistično pomembnih razlik pri predoperativni oceni invazije miometrija. Koeficient skladnosti med metodami TVUS in MRI ter histopatološko je bil statistično pomemben ($p < 0,001$). Gordonova metoda za izračun invazije miometrija je dosegla pozitivno napovedno vrednost (PNV) 83 %, negativno napovedno vrednost (NNV) 83 %, občutljivost 77 %, specifičnost 88 % in splošno natančnost 83 %; Karlssonova metoda je dosegla PNV 82 %, NNV 79 %, občutljivost 69 %, specifičnost 88 % in splošno natančnost 80 %. MRI pa je dosegla PNV 83 %, NNV 97 %, občutljivost 97 %, specifičnost 85 % in splošno natančnost 90 %.

Zaključki. V raziskavi je bila ocena invazije miometrija izvedena s TVUS primerljiva z natančnostjo MRI pri bolnicah z rakom endometrija.

Radiol Oncol 2022; 56(1): 46-53.
doi: 10.2478/raon-2021-0055

Paragangliom sečnega mehurja. Značilnosti računalniškotomografskega in magnetnoresonančnega slikanja pri 16 bolnikih

Zhang J, Bai X, Yuan J, Zhang X, Xu W, Ye H, Wang H

Izhodišča. Paragangliom sečnega mehurja je redek feokromociton izven adrenalne žleze. Pogosto povzroča različne simptome, ki jih lahko napačno interpretiramo in zato neustrezno zdravimo. Namen raziskave je bil, opredeliti radiološke značilnosti paraganglioma z uporabo računalniškotomografskega (CT) in magnetnoresonančnega (MR) slikanja.

Bolniki in metode. Retrospektivno smo proučevali bolnike, ki smo jim diagnosticirali paragangliom sečnega mehurja v obdobju od oktobra 2009 do oktobra 2017 in smo jim pred kirurškim posegom naredili CT ali MR slikanje. Analizirali smo klinične značilnosti, ter značilnosti njihove CT in MR diagnostike.

Rezultati. V raziskavo smo vključili 16 bolnikov s 16 tumorji sečnega mehurja (srednja starost 51 let, 9 žensk). Pri 13 bolnikih smo naredili slikanje s CT in pri 8 z MR. Velikost tumorjev je bila 1,6–5,4 cm. Večina tumorjev je vraščala v mehur (n = 11) z ovalno obliko (n = 10) in dobro omejenim robom (n = 14). Pri dveh bolnikih smo opazili intratumorsko cistično degeneracijo ali nekrozo in tudi periferno tkivno invazijo, kar je nakazovalo na maligni paragangliom. Vseh 13 lezij, diagnosticiranih s CT slikanjem, je kazalo rahlo hipoatenuacijo signala in srednjo do izrazito ojačenje signala. V primerjavi z *m. gluteus maximus*, so vse lezije imele rahlo ojačitev T2 poudarjenega slikanja, hiperintenzivnost difuzijsko poudarjenega slikanja in hipointenzivnost na različnih slikah difuzijske konstante, hiperintenzivnost na T1 poudarjenih slikah in ‚'hitro in upočasnjeno'' (*angl.* ‚'*fast and slow out*'') ojačenega signala na MR slikah.

Zaključki. Paragangliomi so največkrat ovalne oblike, široko razraščeni in dobro ožiljeni tumorji z hipoatenuacijo na slikah CT-ja brez kontrasta, s hiperintenzivnostjo na T2 poudarjenih slikah, rahlo hiperintenzivni na T1 poudarjenih slikah in v primerjavi z mišičnim tkivom izrazito omejen difuziji poudarek slikanja. Periferna tkivna invazija tumorja je zelo sumljiva za maligni paragangliom. Vse te karakteristike lahko pomagajo pri predoperativnem odločanju in načrtovanju operacije.

Radiol Oncol 2022; 56(1): 54-59.
doi: 10.2478/raon-2021-0052

Diagnostična učinkovitost vrednosti dejanskega difuzijskega koeficienta za diferenciacijo med intrahepatičnim holangiokarcinomom in jetrnimi metastazami adenokarcinoma prebavil

Yilmaz TF, Gultekin MA, Turk HM, Besiroglu M, Cesme DH, Simsek M, Alkan A, Toprak H

Izhodišča. Želeli smo raziskati, ali obstaja razlika med intrahepatičnim holangiokarcinomom in jetrnimi metastazami adenokarcinoma prebavil glede na vrednosti dejanskega difuzijskega koeficienta (*angl. apparent diffusion coefficient*, ADC).

Bolniki in metode. Med januarjem 2018 in januarjem 2020 smo retrospektivno pregledali zdravstveno dokumentacijo 13 bolnikov z intrahepatičnim holangiokarcinomom in 64 bolnikov z metastazami v jetrih zaradi adenokarcinoma prebavil. Po upoštevanju izključitvenih kriterijev smo v raziskavo vključili 10 bolnikov z intrahepatičnim holangiokarcinomom in 53 bolnikov z metastazami adenokarcinoma prebavil (53 metastaz) ter na ta način hkrati bolnike razdelili v dve skupini. Za povprečno vrednost dejanskega difuzijskega koeficienta (*angl.* ADC_{mean}) smo področje zanimanja (*angl. region of interes*, ROI) postavili v solidni del lezij. Primerjali smo povprečne vrednosti ADC obeh skupin.

Rezultati. Povprečna starost skupine z intrahepatičnim holangiokarcinomom je bila 62,50 ± 13,49 let, skupine z metastazami pa 61,15 ± 9,18 let. Povprečne vrednosti ADC so bile v skupini z intrahepatičnim holangiokarcinomom značilno višje v primerjavi z skupino z metastazami ($p < 0,001$). Metoda s krivuljami ROC je pokazala visoko diagnostično natančnost (območje pod krivuljo [AUC] = 0,879), z mejno vrednostjo < 1178 x 10–6 mm^2/s za povprečno vrednost ADC (senzitivnost = 90,57; specifičnost = 70,0; pozitivna napovedna vrednost [PPV] = 94,1; negativna napovedna vrednost [NPV] = 58,3) pri razlikovanju intrahepatičnega holangiokarcinoma od metastaz adenokarcinoma prebavil.

Zaključki. Rezultati pričujoče raziskave kažejo, da imajo vrednosti ADC potencialno vlogo pri diferenciaciji med intrahepatičnim holangiokarcinomom in jetrnimi metastazami adenokarcinoma prebavil, kar je lahko pomembno pri nadaljnji obravnavi bolnikov.

Radiol Oncol 2022; 56(1): 60-68.
doi: 10.2478/raon-2022-0001

Ocena učinkovitosti zdravljenja žlez slinavk z beleženjem T_2 pri bolnikih, ki so bili zdravljeni s hiperbarično oksigenacijo in so bili predhodno obsevani zaradi tumorjev glave in vratu

Vidmar J, Cankar K, Grošelj M, Finderle Ž, Serša I

Izhodišča. V raziskavi smo analizirali vpliv terapevtske hiperbarične oksigenacije (HBO) na funkcijo žlez slinavk po zaključeni radioterapiji pri bolnikih s tumorji glave in vratu.

Bolniki in metode. Učinek terapije HBO smo vrednotili s pomočjo slikanja z magnetno resonanco (MRI) žlez slinavk z uporabo metode kartiranja karakterističnega časa transverzalne relaksacije (relaksacijskega časa) T_2 na kliničnem sistemu jakosti 3T. V raziskavo smo vključili 18 bolnikov s prejeto dozo sevanja od 50 do 80 Gy ter 18 kontrolnih oseb, uravnoteženih po spolu in starosti. Izhodiščne meritve so bile opravljene pred prvo terapijo HBO (40,2 ± 20 mesecev po radioterapiji), nato pa po prejetih 20 dnevnih terapijah HBO pri 2,5 absolutne atmosfere (ATA), pri katerih so bolniki vsak dan 90 minut vdihovali 100% kisik. Poleg meritev MRI smo zabeležili tudi pretok, kapaciteto pufra in pH sline.

Rezultati. Povprečne vrednosti T_2 na obsevani strani so se ob koncu zdravljenja s HBO zmanjšale s 121 ± 20 ms na 113 ± 16 msec (p = 0,002), medtem ko na kontralateralni strani ni bilo opaziti statistično značilnih sprememb. Analiza je dodatno pokazala negativen Pearsonov korelacijski koeficient med povprečno vrednostjo izmerjenih T_2 vrednosti v parotidni žlezi na obsevani strani in nestimuliranim pH sline (R = -0,647, p = 0,004) ter stimuliranim pretokom sline (R = -0,592, p = 0,01).

Zaključki. Z raziskavo smo potrdili hipotezo, da je s kartiranjem relaksacijskega časa T_2 žlez slinavk mogoče precej zanesljivo kvantitativno in indirektno opredeliti odziv žlez slinavk na zdravljenje s HBO ter je zato takšna metoda lahko komplementarno diagnostično orodje za oceno funkcije žlez slinavk pri po-obsevanih bolnikih s hiposalivacijo.

Radiol Oncol 2022; 56(1): 69-75.
doi: 10.2478/raon-2021-0047

Primerjava lokalnih recidivov jeternoceličnega raka zdravljenega s kemoembolizacijo in kopičenja jodiranega olja v koronskem delu tumorja v kratkotrajnem opazovanem obdobju

Watanabe Y, Ogawa M, Kaneko M, Kumagawa M, Hirayama M, Matsumoto N, Nakagawara H, Yamamoto Y, Moriyama M

Izhodišča. Lokalne ponovitve jeternoceličnega raka so pogoste v žilnem povirju jeter. Sij okoli tumorja (koronski del tumorja) vidimo pri računalniški tomografiji med arteriografijo in naj bi predstavljal področje drenaže tumorja. Namen raziskave je bil raziskati povezavo med embolizacijo tega sija okoli tumorja in ponovitvami bolezni jetnoceličnega raka, ki smo ga zdravili z transkatetersko arterijsko kemoembolizacijo (TACE).

Bolniki in metode. V retrospektivno raziskavo smo vključili 52 bolnikov s 60 lezijami jeternoceličnega raka, ki so kazali koronski sij okoli tumorja v pozni fazi računalniško tomografske arteriografije in so homogeno kopičili jodirano olje. Opazovane lezije so bile vidne na slikah računalniške tomografije brez kontrasta takoj po TACE. Razdelili smo jih v dve skupini: (A) tiste, kjer se je jodirano olje kopičilo in (B) tiste, kjer se jodirano olje ni kopičilo po celotnem predelu koronskega sija. Ocenjevali smo število lokalnih ponovitev bolezni.

Rezultati. Stopnja ponovitev bolezni je bila v skupini A (n = 36) 2,8 %, 2,8 % in 8,3 % po 3, 6 in 12 mesecih po posegu, medtem ko je bila v skupini B 20,8 %, 45,8 % in 75 % po 3, 6, in 12 mesecih po posegu. Stopnja ponovitev bolezni je tako bila v skupini A statistično značilno nižja kot v skupini B (razmerje obetov [HR] 0,079; 95 % interval zaupanja [CI] 0,026–0,24; $p < 0.001$).

Zaključki. Rezultati nakazujejo, da je koronski sij natančen varnostni rob pri TACE ter ga je potrebno upoštevati in embolizirati celotno njegovo površino.

Radiol Oncol 2022; 56(1): 76-82.
doi: 10.2478/raon-2021-0036

Ocena tveganja za ponovitev bolezni pri bolnicah z rakom endometrija. Razlike v izidih molekularnih in kliničnih klasifikacij pri slovenski skupini bolnic

Knez J, Sobočan M, Belak U, Kavalar R, Zupin M, Büdefeld T, Potočnik U, Takač I

Izhodišča. Cilj raziskave je bil primerjati klinično oceno tveganja za ponovitev raka endometrija z integriranim profiliranjem molekularnega tveganja.

Bolniki in metode. V prospektivno raziskavo smo k sodelovanju povabili bolnice s histološko dokazanim rakom endometrija, ki so bile zdravljene v UKC Maribor med januarjem 2020 in februarjem 2021. Klinične podatke smo ocenili in razvrstili v skladu s trenutno veljavnimi smernicami o zdravljenju raka endometrija Evropskega združenja za ginekološko onkologijo, Evropskega združenja za radioterapijo in onkologijo ter Evropskega združenja za patologijo (ESGO/ESTRO/ESP). Molekularna karakterizacija tumorjev je vključevala določitev statusa mutacij DNA polimeraze epsilon *(POLE)* s sekvenciranjem po Sangerju ter imunohistokemično oceno prisotnosti pomanjkljivosti neujemanja proteinov popravljanja DNA (MMRd) in p53 izraženosti (p53abn).

Rezultati. V raziskavo smo vključili 45 bolnic z rakom endometrija. V skupino z nespecifičnim mutacijskim profilom (NSMP) smo uvrstili 22 bolnic (56,4 %), v skupino z visoko verjetnostjo MMRd pa 13 (33,3 %), v skupino p53abn smo uvrstili tri (7,7 %) in v skupino z mutacijo POLE eno bolnico (2,6 %). Več molekularnih označevalcev je imelo šest bolnic (15,4 %). To skupino bolnic smo proučevali ločeno in niso bile vključene v primarno oceno tveganja. Glede na klinično ocena smo med nizko tvegane uvrstili 21 bolnic (53,8 %), v skupino z zmernim tveganjem pa pet (12,8 %), v skupino z zmerno-visokim tveganjem 2 (5,1 %), visoko tveganih smo opredelili 10 (25,6 %) in v skupino napredovalih metastatskih bolezni smo uvrstili eno bolnico (2,6 %). Integrirana molekularna klasifikacija je spremenila tveganje pri 4 bolnicah (10,3 %).

Zaključki. Integrirana molekularna ocena tveganja za ponovitev bolezni izboljša invidualizirano oceno tveganja pri raku endometrija in bi lahko izboljšala terapevtsko natančnost. Večjo pozornost je potrebno dodatno nameniti skupini NSMP pri prepoznavi dodatnih molekularnih bioloških označevalcev za boljšo individualizacijo zdravljenja.

Radiol Oncol 2022; 56(1): 83-91.
doi: 10.2478/raon-2021-0049

Cistatin C in cistatin SN kot možna tumorska označevalca za uvealni maligni melanom

Dikovskaya MA, Russkikh GS, Loktev, Johnston TP, Gevorgyan MM, Voronina NP, Chernykh VV, Trunov AN, Korolenko TA

Izhodišča. Namen raziskave je bil opredeliti endogene koncentracije cistatinov C in SN kot potencialne tumorske označevalce v serumu in bioloških tekočinah očesa pri bolnikih z uvealnim melanomom in pri zdravih ljudeh.

Bolniki in metode. Koncentracije obeh statinov smo določali v intraokularni tekočini, solzah in serumu bolnikov z uvealnim melanomom ter jih primerjali s kontrolnimi vrednostmi v intraokularni tekočini, solzah, serumu, cerebralni tekočini, slini in urinu zdravih ljudi.

Results. Koncentracije cistatina C so bile veliko višje kot cistatina SN pri zdravih ljudeh ter so bile neodvisne od spola bolnikov. Prav tako so bile koncentracije cistatina C statistično značilno povišane v solzah prizadetega očesa, kot tudi kontralateralnega očesa pri bolnikih v primerjavi z zdravimi ljudmi ter neodvisne od velikosti tumorja. Koncentracije cistatina SN pa so bile znižane v intraokularni tekočini bolnikov z uvealnim melanomom v primerjavi z zdravimi ljudmi.

Zaključki. Rezultati nakazujejo, da razmerje med cistatinoma (CysC : CysSN), tako v serumu, kot v solzah ter tudi koncentracija cistatina SN v intraokularni tekočini kažejo na prisotnost uvelanega melanoma. To nakazuje na potrebo po večplastni diagnostiki bolnikov s sumom na uvelani melanom, kot so določevanje cistatina C in cistatina SN v serumu, solzah, intraokularni tekočini, bazi očesa kot tudi opredelitev sprememb z ultrazvokom in histopatološko.

Radiol Oncol 2022; 56(1): 92-101.
doi: 10.2478/raon-2021-0050

Kliničen pomen sprememb v številu kopij genov, povezanih z diferenciacijo celic B in uravnavanjem celičnega cikla, pri pediatrični B-celični akutni limfoblastni levkemiji. Izkušnje terciarnega centra

Črepinšek K, Marinšek G, Kavčič M, Prelog T, Kitanovski L, Jazbec J, Debeljak M

Izhodišča. Delecije v genu *IKZF1* predstavljajo slab napovedni dejavnik pri pediatričnih bolnikih z B-celično akutno limfoblastno levkemijo (B-ALL), zlasti ob prisotnosti dodatnih delecij v drugih genih (profil *IKZF1*^{plus}). Namen raziskave je bil določiti pri slovenskih pediatričnih bolnikih z B-ALL pogostost delecij v genu *IKZF1* ter delecij v drugih genih, povezanih z diferenciacijo celic B in z nadzorovanjem celičnega cikla. Zato smo raziskovali tudi gene *PAX5, ETV6, RB1, BTG1, EBF1, CDKN2A/2B* in pet genov v regiji PAR1. Želeli smo ugotoviti njihov napovedni vpliv na potek bolezni.

Bolniki in metode. Preučili smo kohorto 99 bolnikov, ki smo jim ugotovili B-ALL med januarjem 2012 in decembrom 2020, ter jih zdravili po protokolu ALL IC-BFM 2009. Analizirali smo 88 vzorcev kostnega mozga ali periferne krvi in ugotavljali prisotnosti sprememb števila kopij genov z uporabo reagenčnega kompleta SALSA MLPA P335 ALL-IKZF1.

Rezultati. Pri več kot 65 % analiziranih vzorcev smo odkrili vsaj eno spremembo v številu kopij genov. Najpogostejše so bile spremembe v genih *PAX5* in *CDKN2A/2B* (30,7 %, 26,1 % in 25,0 %). Delecije v genu *IKZF1* so bile prisotne pri 18,2 % analiziranih vzorcev in so bile povezane s slabšim petletnim preživetjem brez dogodka (54,8 % proti 85,9 %, p = 0,016). Profil *IKZF1*^{plus} smo prepoznali pri 12,5 % analiziranih vzorcev, ti bolniki pa so imeli slabše petletno preživetje brez dogodka kakor tisti, ki so imeli prisotne delecije le v genu *IKZF1*, in tisti brez delecij (50,8 % proti 75,0 % proti 85,9 %, p = 0,049). Celokupno preživetje je bilo prav tako slabše pri bolnikih s profilom *IKZF1*^{plus}, kakor pri bolnikih, ki so imeli prisotne delecije le v genu *IKZF1*, in tistih brez delecij (petletno celokupno preživetje 76,2 % proti 100 % proti 93,0 %), vendar razlike med skupinami niso bile statistično značilne.

Zaključki. Rezultati pričujoče raziskave so v skladu z rezultati, pridobljenimi v obsežnejših kliničnih raziskavah, v katerih je sodelovalo več inštitucij. Analiza sprememb v številu kopij genov z reagenčnim kompletom SALSA MLPA je zanesljivo orodje za začetno diagnostiko pri otrocih z B-ALL, tudi v manjših ustanovah v državah z nizkim in srednjim dohodkom.

Radiol Oncol 2022; 56(1): 102-110.
doi: 10.2478/raon-2022-0003

Perkutana elektrokemoterapija primarnih in sekundarnih jetrnih tumorjev. Lokalna kontrola in vpliv na preživetje bolnikov

Spallek H, Bischoff P, Zhou W, de Terlizzi F, Jakob F, Kovàcs A

Izhodišča. Lokalne ablativne tehnike so terapija izbora za zdravljenje bolnikov z jetrnimi tumorji ali jetrnimi metastazami. Ena novejših ablativnih tehnik je elektrokemoterapija. Retrospektivno smo pregledali lokalno učinkovitost in varnost zdravljenja ter vpliv na preživetje elektrokemoterapije pri bolnikih z jetrnimi tumorji ali metastazami.

Bolniki in metode. V raziskavo smo vključili 18 bolnikov, ki smo jih zdravili z elektrokemoterapijo in so imeli izmerljive jetrne lezije tumorjev različnega izvora, predvsem kolorektalnega raka, raka dojke in jetrnoceličnega raka. Elktrokemoterapijo smo izvedli s perkutanim pristopom, po standardiziranih postopkih, v splošni anesteziji z miorelaksacijo. Plan zdravljenja smo naredili na osnovi predoperativnih slik magnetne resonance (MR). Učinek zdravljenja smo sledili s slikanjem MR, narejenim s kontrastnim sredstvom 1–3 mesece po končanem zdravljenju in za tem 5., 7., 9., 12., 18. mesec, vse do napredovanja bolezni ali smrti bolnika.

Rezultati. Po elektrokemoterapiji smo zaznali le blage ali zmerne stranske učinke. Zabeležili smo 85,7 % objektivnih odgovorov tumorjev na elektrokemoterapijo (popolnih odgovorov 61,9 %; delnih odgovorov 23,8 %). Srednji čas preživetja brez napredovanja bolezni je bil 9,0 ± 8,2 mesecev, celokupno preživetje pa 11,3 ± 8,6 mesecev. Najboljši odgovor na zdravljenje je bil pri tumorjih velikosti 3 in 6 cm v premeru ($p = 0,0242$, $p = 0,0297$). Učinek elektrokemoterapije je bil neodvisen od lege tumorjev, ali so bili oddaljeni ali blizu vitalnih jetrnih struktur, ali pa so jih obraščali. Preživetje brez napredovanja bolezni in celokupno preživetje sta bila neodvisni od primarne histološke diagnoze tumorjev.

Zaključki. Elektrokemoterapija je pomembna pri zdravljenje neresektabilnih jetrnih tumorjev in jetrnih metastaz, ki niso primerni za druge ablativne tehnike.

Radiol Oncol 2022; 56(1): 111-118.
doi: 10.2478/raon-2021-0035

Učna krivulja laparoskopske resekcije jeter, ki upošteva točkovni sistem težavnosti

Ivanecz A, Plahuta I, Mencinger M, Peruš I, Magdalenić T, Turk Š, Potrč S

Izhodišče. Namen raziskave je bil kvantitativno oceniti kirurgovo učno krivuljo laparoskopske resekcije jeter.

Bolniki in metode. Opravili smo retrospektivni pregled prospektivno vodene podatkovne baze laparoskopskih resekcij jeter. Med aprilom 2008 in aprilom 2021 smo s to metodo operirali 171 bolnikov. Za teoretično napoved medoperativnega zapleta smo uporabili točkovni sistem težavnosti, ki so ga vpeljali Halls in sodelavci. Medoperativni zaplet nastopi, če bolnik izgubi kot več kot 775 mL krvi, če so nenamerno poškodovani okolni organi ali če je potrebno nadaljevati operacijo z odprto metodo. Teoretično zvezo med Hallsovim točkovnim sistemom težavnosti in napovedano verjetnostjo medoperativnega zapleta smo uporabili kot objektivno oceno učnega izida z namenom pridobitve učne krivulje.

Rezultati. Pridobljena učna krivulja je bila rezultat trinajstletnega prizadevanja kirurga (AI). V matematičnem modelu je bila privzeta aditivna funkcija, sestavljena iz absolutnega in relativnega prispevka (kompleksnosti) k učni krivulji. Absolutni prispevek predstavlja logaritemska funkcija, relativnega pa regresijski polinom pete stopnje. Pridobljena učna krivulja predstavlja funkcijsko odvisnost učnega izida v odvisnosti od časa. Lokalni ekstremi predstavljajo vrhove in doline v učnem procesu kirurga, dokler (končno) ne doseže odličnosti.

Zaključki. Učna krivulja prikazuje dolgotrajen učni proces laparoskopske resekcije jeter. Predlagani matematični model je mogoče uporabiti za katerikoli (kirurški) postopek, ki premore točkovni sistem tveganja in teoretično napovedan odnos med njim in objektivnim učnim izidom (npr. medoperativnim zapletom).

Radiol Oncol 2022; 56(1): 119-128.
doi: 10.2478/raon-2021-0053

Zorenje nezrelih jajčnih celic *in vitro* za ohranjanje plodnosti pri bolnicah z rakom v primerjavi s kontrolnimi bolnicami, ki so imele težave s plodnostjo v programu zunajtelesne oploditve

Virant-Klun I, Jure Bedenk J, Jančar N

Izhodišča. Namen raziskave je bil ugotoviti, ali je lahko *in vitro* zorenje nezrelih jajčnih celic, ki smo ga izvedli po nadzorovanem hormonskem spodbujanju jajčnikov, pomembno za izboljšanje možnosti zanositve pri bolnicah, ki so zbolele za rakom.

Bolniki in metode. Obravnavali smo bolnice, ki so zbolele za rakom in so želele v prihodnosti zanositi. Po spodbujanju jajčnikov smo primerjali število jajčnih celic, njihovo kakovost in zrelost s kontrolnimi bolnicami, ki so imele težave s plodnostjo in so bile vključene v program zunajtelesne oploditve. V obeh skupinah bolnic smo *in vitro* dozorevali njihove nezrele jajčne celice v razvojni fazi germinalnega vezikla in primerjali delež jajčnih celic, ki so *in vitro* dozorele. Pri podskupini bolnic s težavami s plodnostjo smo neposredno vnesli semenčice v citoplazmo jajčne celice (*angl. intracytoplasmic sperm injection,* ICSI) na *in vitro* dozorelih jajčnih celicah, da bi ocenili njihovo sposobnost oploditve in razvoja v zarodek v primerjavi z *in vivo* dozorelimi jajčnimi celicami v istih postopkih in ocenili primernost postopka pri bolnicah z rakom.

Rezultati. Pri bolnicah z različnimi raki onkološka bolezen ni vplivala na število in kakovost pridobljenih jajčnih celic. Pri bolnicah z rakom je bil delež nezrelih jajčnih celic celo značilno manjši kot pri bolnicah s težavami s plodnostjo (30,0 % proti 43,6 %; $P < 0,05$). Vendar pa je pri bolnicah z rakom *in vitro* dozorelo značilno manj jajčnih celic na bolnico kot pri bolnicah s težavami s plodnostjo (1,39 ± 1,04 vs. 2,48 ± 1,83; $P < 0,05$). Po ICSI se deleži oplojenih jajčnih celic in oplojenih jajčnih celic, ki so se razvile v zarodek, niso razlikovali med jajčnimi celicami, ki so dozorele *in vitro* ali *in vivo* v istih postopkih.

Zaključki. Metoda *in vitro* zorenja nezrelih jajčnih celic je zanesljiv postopek za dozorevanje jajčnih celic, ki smo jih pridobili z nadzorovanim spodbujanjem jajčnikov pri bolnicah z rakom.

Fundacija "Docent dr. J. Cholewa"
je neprofitno, neinstitucionalno in nestrankarsko
združenje posameznikov, ustanov in organizacij, ki želijo
materialno spodbujati in poglabljati raziskovalno
dejavnost v onkologiji.

Dunajska 106
1000 Ljubljana
IBAN: SI56 0203 3001 7879 431

TANTUM VERDE®

benzidaminijev klorid

Za lajšanje bolečine in oteklin v ustni votlini in žrelu, ki so posledica radiomukozitisa

Bistvene informacije iz Povzetka glavnih značilnosti zdravila

Tantum Verde 1,5 mg/ml oralno pršilo, raztopina
Tantum Verde 3 mg/ml oralno pršilo, raztopina
Sestava 1,5 mg/ml: 1 ml raztopine vsebuje 1,5 mg benzidaminijevega klorida, kar ustreza 1,34 mg benzidamina. V enem razpršku je 0,17 ml raztopine. En razpršek vsebuje 0,255 mg benzidaminijevega klorida, kar ustreza 0,2278 mg benzidamina. **Sestava 3 mg/ml:** 1 ml raztopine vsebuje 3 mg benzidaminijevega klorida, kar ustreza 2,68 mg benzidamina. V enem razpršku je 0,17 ml raztopine. En razpršek vsebuje 0,51 mg benzidaminijevega klorida, kar ustreza 0,4556 mg benzidamina. **Terapevtske indikacije:** Samozdravljenje: Lajšanje bolečine in oteklin pri vnetju v ustni votlini in žrelu, ki so lahko posledica okužb in stanj po operaciji. Po nasvetu in navodilu zdravnika: Lajšanje bolečine in oteklin v ustni votlini in žrelu, ki so posledica radiomukozitisa. **Odmerjanje in način uporabe:** Odmerjanje 1,5 mg/ml: Odrasli: 4 do 8 razprškov 2- do 6-krat na dan (vsake 1,5 do 3 ure). Pediatrična populacija: Mladostniki, stari od 12 do 18 let: 4-8 razprškov 2- do 6-krat na dan. Otroci od 6 do 12 let: 4 razprški 2- do 6-krat na dan. Otroci, mlajši od 6 let: 1 razpršek na 4 kg telesne mase; do največ 4 razprške 2- do 6-krat na dan. Odmerjanje 3 mg/ml: Uporaba 2- do 6-krat na dan (vsake 1,5 do 3 ure). Odrasli: 2 do 4 razprški 2- do 6-krat na dan. Pediatrična populacija: Mladostniki, stari od 12 do 18 let: 2 do 4 razprški 2- do 6-krat na dan. Otroci od 6 do 12 let: 2 razprška 2- do 6-krat na dan. Otroci, mlajši od 6 let: 1 razpršek na 8 kg telesne mase; do največ 2 razprška 2- do 6-krat na dan. Starejši bolniki, bolniki z jetrno okvaro in bolniki z ledvično okvaro: Uporabo oralnega pršila z benzidaminijevim kloridom se svetuje pod nadzorom zdravnika. Način uporabe: Za orofaringealno uporabo. Zdravilo se razprši v usta in žrelo. **Kontraindikacije:** Preobčutljivost na učinkovino ali katero koli pomožno snov. **Posebna opozorila in previdnostni ukrepi:** Če se simptomi v treh dneh ne izboljšajo, se mora bolnik posvetovati z zdravnikom ali zobozdravnikom, kot je primerno. Benzidamin ni priporočljiv za bolnike s preobčutljivostjo nasalicilno kislino ali druga nesteroidna protivnetna zdravila. Pri bolnikih, ki imajo ali so imeli bronhialno astmo, lahko pride do bronhospazma, zato je potrebna previdnost. To zdravilo vsebuje majhne količine etanola (alkohola), in sicer manj kot 100 mg na odmerek. To zdravilo vsebuje metilparahidroksibenzoat (E218). Lahko povzroči alergijske reakcije (lahko zapoznele). Zdravilo z jakostjo 3 mg/ml vsebuje makrogolglicerol hidroksistearat 40. Lahko povzroči želodčne težave in drisko. **Medsebojno delovanje z drugimi zdravili in druge oblike interakcij:** Študij medsebojnega delovanja niso izvedli. **Nosečnost in dojenje:** O uporabi benzidamina pri nosečnicah in doječih ženskah ni zadostnih podatkov. Uporaba zdravila med nosečnostjo in dojenjem ni priporočljiva. **Vpliv na sposobnost vožnje in upravljanja strojev:** Zdravilo v priporočenem odmerku nima vpliva na sposobnost vožnje in upravljanja strojev. **Neželeni učinki:** Neznana pogostnost (ni mogoče oceniti iz razpoložljivih podatkov): anafilaktične reakcije, preobčutljivostne reakcije, odrevenelost, laringospazem, suha usta, navzea in bruhanje, angioedem, fotosenzitivnost, pekoč občutek v ustih. Neposredno po uporabi se lahko pojavi občutek odrevenelosti v ustih in v žrelu. Ta učinek se pojavi zaradi načina delovanja zdravila in po kratkem času izgine. **Način in režim izdaje zdravila:** BRp-Izdaja zdravila je brez recepta v lekarnah in specializiranih prodajalnah.

Imetnik dovoljenja za promet: Aziende Chimiche Riunite Angelini Francesco – A.C.R.A.F. S.p.A., Viale Amelia 70, 00181 Rim, Italija **Datum zadnje revizije besedila:** 14. 10. 2019

Pred svetovanjem ali izdajo preberite celoten Povzetek glavnih značilnosti zdravila.

Samo za strokovno javnost.

Datum priprave informacije: oktober 2021

Odgovoren za trženje: Bonifar d.o.o.

ANGELINI

PR/BSI/BEN/2022/013

Podaljšajmo, kar lahko.

Dokazano podaljša celokupno preživetje (OS) na več kot 1 leto (12,6 mesecev VARGATEF® + docetaksel v primerjavi z 10,3 mesecev placebo + docetaksel; HR: 0,83 [95% CI 0,70 – 0,99]; P = 0,0359) pri bolnikih, ki ga prejemajo v kombinaciji z docetakselom, z lokalno napredovalim, metastatskim ali lokalno ponovljivim nedrobnoceličnim pljučnim rakom (non-small cell lung cancer – NSCLC) s histologijo adenokarcinoma po kemoterapiji prve izbire.[1,2]

Vargatef 100 mg mehke kapsule, Vargatef 150 mg mehke kapsule

Sestava: ena mehka kapsula vsebuje 100 mg nintedaniba oz. 150 mg nintedaniba (v obliki esilata). Vsebuje 1,2 mg oz. 1,8 mg sojinega lecitina .**Terapevtske indikacije:** indicirano v kombinaciji z docetakselom za zdravljenje odraslih bolnikov z lokalno napredovalim, metastatskim ali lokalno ponovljivim nedrobnoceličnim pljučnim rakom (*NSCLC*) s histologijo adenokarcinoma po kemoterapiji prve izbire. **Odmerjanje in način uporabe:** zdravljenje mora uvesti in nadzirati zdravnik, ki ima izkušnje z uporabo onkoloških zdravil. Priporočeni odmerek nintedaniba je 200 mg 2x/dan, ki ga je treba jemati v približno 12-urnem razmiku, od 2. do 21. dne standardnega 21-dnevnega cikla zdravljenja z docetakselom. Bolnik ne sme vzeti Vargatefa istega dne, ko prejme kemoterapijo z docetakselom (to je 1. dne). Če bolnik pozabi vzeti priporočeni odmerek nintedaniba, naj ga začne ponovno jemati ob naslednjem načrtovanem času. Posameznih dnevnih priporočenih odmerkov nintedaniba ni dovoljeno povečati, zato da bi nadomestili pozabljene odmerke. Ne smete prekoračiti niti največjega priporočenega dnevnega odmerka 400 mg. Bolniki lahko z zdravljenjem z nintedanibom nadaljujejo po prekinitvi docetaksela, dokler so vidne klinične koristi ali do pojava nesprejemljive toksičnosti. ***Prilagajanje odmerka:*** začetni ukrep za obravnavo neželenih učinkov je začasna prekinitev zdravljenja z nintedanibom, dokler specifični neželeni učinek ne bo izzvenel do ravni, ki omogoča nadaljevanje zdravljenja (do 1. stopnje ali izhodiščnega stanja). Zdravljenje lahko nadaljujete z zmanjšanim odmerkom; priporočljivo je postopno prilagajanje odmerka po 100 mg na dan (to je zmanjšanje za 50 mg na odmerek) na podlagi individualne varnosti in prenašanja. Kadar neželeni učinki ne izginejo, tj. če bolnik ne prenaša odmerka po 100 mg 2x/dan, je treba zdravljenje trajno ukiniti. V primeru specifičnih povišanih vrednosti AST/ALT na > 3 x ULN v povezavi s povečanjem celokupnega bilirubina na ≥ 2 x ULN in ALKP < 2 x ULN je treba zdravljenje prekiniti. Če ni ugotovljen drug razlog, je treba zdravljenje trajno ukiniti. ***Posebne skupine bolnikov:*** varnost in učinkovitost pri otrocih, starih 0 do 18 let, še nista dokazani. Pri starejših bolnikih (≥ 65 let) pa na splošno niso opazili razlike. Začetnega odmerka ni treba prilagajati bolnikovi starosti. Podatki o varnosti za črnce in Afroameričane so omejeni. Bolnikom z blago do zmerno ledvično okvaro ali z blago jetrno okvaro začetnega odmerka ni treba prilagajati. Začetnega odmerka pri bolnikih z blago jetrno okvaro (Child Pugh A) na podlagi kliničnih podatkov ni treba prilagajati. Zdravljenje bolnikov z zmerno (Child Pugh B) in hudo (Child Pugh C) jetrno okvaro z Vargatefom ni priporočeno. Kapsule Vargatefa je treba zaužiti cele z vodo, najbolje s hrano; ne sme se jih žvečiti. Kapsule se ne sme odpreti ali drobiti. V primeru stika z vsebino kapsule, je potrebno takoj umiti roke z veliko vode. **Kontraindikacije:** preobčutljivost za nintedanib, arašide ali sojo ali katerokoli pomožno snov. **Previdnostni ukrepi in opozorila:** bolezni prebavil (driska, ki tesno sovpada z dajanjem docetaksela; resni primeri driske s posledično dehidracijo in elektrolistkimi motnjami, navzea in bruhanje; zdravljenje je zato včasih treba prekiniti, zmanjšati odmerek ali trajno ukiniti), nevtropenija in sepsa (tudi smrtni primeri; zato je zlasti v kombinaciji s docetakselom potrebno spremljati krvno sliko), delovanje jeter (večja izpostavljenost pri Child Pugh A, zdravljenje pri Child Pugh B ali C pa ni priporočeno, opažene poškodbe jeter (vključno s hudo poškodbo jeter s smrtnim izidom), tveganje za povečanje ravni jetrnih encimov), delovanje ledvic (pozornost ob ledvični okvari/odpovedi), krvavitev (blaga do zmerna epistaksa, večina usodnih krvavitev je bila povezanih s tumorjem. Poročali so o resnih in neresnih krvavitvah (tudi smrtni izid), ki vključujejo prebavila, dihala in organe osrednjega živčnega sistema, najbolj pogoste pa so krvavitve v dihalih. V primeru krvavitve je treba razmisliti o prilagoditvi odmerka, prekinitvi ali trajni ukinitvi zdravljenja na podlagi klinične ocene), terapevtska antikoagulacija, metastaza v možganih (stabilne in aktivne metastaze v možganih), venska trombembolija (povečano tveganje za vensko trombembolijo, vključno s pljučno embolijo in globoko vensko trombozo), arterijski trombembolični dogodki (pri bolnikih z IPF, z večjim srčnožilnim tveganjem, vključno z znano koronarno arterijsko boleznijo), anevrizme in disekcije arterij (pred uvedbo Vargatefa je treba tveganje spodbude nastanka anevrizme in/ali disekcij arterij skrbno preučiti pri bolnikih z hipertenzijo ali anamnezo anevrizme), predrtje prebavil, zelo redko so poročali o primerih nefrotske proteinurije, zapleti s celjenjem ran, vpliv na interval QT, alergijska reakcija (alergija na sojo in arašidove beljakovine), posebne populacije (izpostavljenost se veča z bolnikovo starostjo in obratno korelira s telesno maso, večja pri bolnikih azijske rase). Nosečnice nintedaniba ne smejo uporabljati, razen če je zdravljenje potrebno zaradi njihovega kliničnega stanja. Ženskam je treba svetovati, naj obvestijo zdravnika ali farmacevta, če med zdravljenjem z Vargatefom zanosijo. **Interakcije:** močni zaviralci P-gp (ketokonazol, eritromicin), močni induktorji P-gp (rifampicin, karbamazepin, fenitoin in šentjanževka), encimi citokroma (CYP). Sočasno dajanje nintedaniba z docetakselom ni spremenilo farmakokinetike nobenega od zdravil v pomembnem obsegu. Sočasno dajanje nintedaniba s peroralnimi hormonskimi kontraceptivi ni pomembno spremenilo farmakokinetike peroralnih hormonskih kontraceptivov. **Neželeni učinki:** ***Zelo pogosti:*** nevtropenija (vključno s febrilno nevtropenijo), zmanjšan apetit, neravnovesje elektrolitov, periferna nevropatija, krvavitev, driska, bruhanje, navzea, trebušna bolečina, povečana vrednost ALT, AST in ALKP, mukozitis (vključno s stomatitisom), izpuščaj in alopecija. ***Pogosti:*** febrilna nevtropenija, abscesi, sepsa, trombocitopenija, dehidracija, zmanjšanje telesne mase, glavobol, venska trombembolija, hipertenzija, hiperbilirubinemija, povečana vrednost GGT, pruritus in proteinurija. ***Občasni:*** miokardni infarkt, perforacija, pankreatitis, z zdravilom povzročena poškodba jeter in ledvična odpoved. ***Neznana pogostnost***: anevrizme in disekcije arterij, kolitis. **Imetnik dovoljenja za promet:** Boehringer Ingelheim International GmbH, Binger Str. 173, D-55216 Ingelheim am Rhein, Nemčija. **Način in režim izdaje:** Rp. **Za podrobnejše informacije glejte SPC, z dne 10/2021.**

Literatura: 1. VARGATEF® Povzetek glavnih značilnosti zdravila 2021 **2.** Reck M et al. Lancet Oncol. 2014;15:143-55.

V kolikor imate medicinsko vprašanje v povezavi z zdravilom podjetja Boehringer Ingelheim, Podružnica Ljubljana,
Vas prosimo, da pokličete na telefonsko številko 01/5864-000 ali pošljete vaše vprašanje na elektronski naslov: medinfo@boehringer-ingelheim.com.

Boehringer Ingelheim

Boehringer Ingelheim RCV
podružnica Ljubljana
Šlandrova 4b, 1231 Ljubljana Črnuče

PC-SL-100772
Samo za strokovno javnost.
Datum priprave informacije: februar 2022

VARGATEF® NINTEDANIB

KLJUČ ZA VEČ PRILOŽNOSTI PRI ZDRAVLJENJU VAŠIH BOLNIKOV

KEYTRUDA®
(pembrolizumab, MSD)

KEYTRUDA je odobrena za zdravljenje 18 indikacij rakavih obolenj[1]

Referenca: 1. Keytruda EU SmPC

Ime zdravila: KEYTRUDA 25 mg/ml koncentrat za raztopino za infundiranje vsebuje pembrolizumab. **Terapevtske indikacije:** Zdravilo KEYTRUDA je kot samostojno zdravljenje indicirano za zdravljenje: napredovalega (neoperabilnega ali metastatskega) melanoma pri odraslih; za adjuvantno zdravljenje odraslih z melanomom v stadiju III, ki se je razširil na bezgavke, po popolni kirurški odstranitvi; metastatskega nedrobnoceličnega pljučnega raka (NSCLC) v prvi liniji zdravljenja pri odraslih, ki imajo tumorje z ≥ 50 % izraženostjo PD-L1 (TPS) in brez pozitivnih tumorskih mutacij EGFR ali ALK; lokalno napredovalega ali metastatskega NSCLC pri odraslih, ki imajo tumorje z ≥ 1 % izraženostjo PD-L1 (TPS) in so bili predhodno zdravljeni z vsaj eno shemo kemoterapije, bolniki s pozitivnimi tumorskimi mutacijami EGFR ali ALK so pred prejemom zdravila KEYTRUDA morali prejeti tudi tarčno zdravljenje; odraslih in pediatričnih bolnikov, starih 3 leta ali več, s ponovljenim ali neodzivnim klasičnim Hodgkinovim limfomom (cHL), pri katerih avtologna presaditev matičnih celic (ASCT) ni bila uspešna, ali po najmanj dveh predhodnih zdravljenjih kadar ASCT ne pride v poštev kot možnost zdravljenja; lokalno napredovalega ali metastatskega urotelijskega raka pri odraslih, predhodno zdravljenih s kemoterapijo, ki je vključevala platino; lokalno napredovalega ali metastatskega urotelijskega raka pri odraslih, ki niso primerni za zdravljenje s kemoterapijo, ki vsebuje cisplatin in imajo tumorje z izraženostjo PD-L1 ≥ 10, ocenjeno s kombinirano pozitivno oceno (CPS); ponovljenega ali metastatskega ploščatoceličnega raka glave in vratu (HNSCC) pri odraslih, ki imajo tumorje z ≥ 50 % izraženostjo PD-L1 (TPS), in pri katerih je bolezen napredovala med zdravljenjem ali po zdravljenju s kemoterapijo, ki je vključevala platino; za adjuvantno zdravljenje odraslih z rakom ledvičnih celic s povišanim tveganjem za ponovitev bolezni po nefrektomiji, ali po nefrektomiji in kirurški odstranitvi metastatskih lezij in za prvo linijo zdravljenja metastatskega kolorektalnega raka z visoko mikrosatelitsko nestabilnostjo (MSI-H – microsatellite instability-high) ali s pomanjkljivim popravljanjem neujemanja pri podvojevanju DNA (dMMR - mismatch repair deficient) pri odraslih. Zdravilo KEYTRUDA je kot samostojno zdravljenje ali v kombinaciji s kemoterapijo s platino in 5-fluorouracilom (5-FU) indicirano za prvo linijo zdravljenja metastatskega ali neoperabilnega ponovljenega ploščatoceličnega raka glave in vratu pri odraslih, ki imajo tumorje z izraženostjo PD-L1 s CPS ≥ 1. Zdravilo KEYTRUDA je v kombinaciji s pemetreksedom in kemoterapijo na osnovi platine indicirano za prvo linijo zdravljenja metastatskega neploščatoceličnega NSCLC pri odraslih, pri katerih tumorji nimajo pozitivnih mutacij EGFR ali ALK; v kombinaciji s karboplatinom in bodisi paklitakselom bodisi nab-paklitakselom je indicirano za prvo linijo zdravljenja metastatskega ploščatoceličnega NSCLC pri odraslih; v kombinaciji z aksitinibom ali v kombinaciji z lenvatinibom je indicirano za prvo linijo zdravljenja napredovalega raka ledvičnih celic (RCC) pri odraslih; v kombinaciji s kemoterapijo s platino in fluoropirimidinom je indicirano za prvo linijo zdravljenja lokalno napredovalega neoperabilnega ali metastatskega raka požiralnika ali HER-2 negativnega adenokarcinoma gastroezofagealnega prehoda pri odraslih, ki imajo tumorje z izraženostjo PD-L1 s CPS ≥ 10; v kombinaciji s kemoterapijo je indicirano za zdravljenje lokalno ponovljenega neoperabilnega ali metastatskega trojno negativnega raka dojk pri odraslih, ki imajo tumorje z izraženostjo PD-L1 s CPS ≥ 10 in predhodno niso prejeli kemoterapije za metastatsko bolezen; v kombinaciji z lenvatinibom je indicirano za zdravljenje napredovalega ali ponovljenega raka endometrija (EC) pri odraslih z napredovalo boleznijo med ali po predhodnem zdravljenju s kemoterapijo, ki je vključevala platino, v katerih koli terapevtskih okoliščinah, in ki niso kandidati za kurativno operacijo ali obsevanje. **Odmerjanje in način uporabe:** Testiranje PD-L1: Če je navedeno v indikaciji, je treba izbiro bolnika za zdravljenje z zdravilom KEYTRUDA na podlagi izraženosti PD-L1 tumorja potrditi z validirano preiskavo. Testiranje MSI-H/dMMR pri bolnikih s CRC: Za samostojno zdravljenje z zdravilom KEYTRUDA je priporočljivo opraviti testiranje MSI-H/dMMR statusa tumorja z validirano preiskavo, da se izbere bolnike s CRC. Odmerjanje: Priporočeni odmerek zdravila KEYTRUDA pri odraslih je bodisi 200 mg na 3 tedne ali 400 mg na 6 tednov, apliciran z intravensko infuzijo v 30 minutah. Priporočeni odmerek zdravila KEYTRUDA za samostojno zdravljenje pri pediatričnih bolnikih s cHL, starih 3 leta ali več, je 2 mg/kg telesne mase (do največ 200 mg) na 3 tedne, apliciran z intravensko infuzijo v 30 minutah. Za uporabo v kombinaciji glejte povzetke glavnih značilnosti zdravil sočasno uporabljenih zdravil. Če se uporablja kot del kombiniranega zdravljenja skupaj z intravensko kemoterapijo, je treba zdravilo KEYTRUDA aplicirati prvo. Bolnike je treba zdraviti do napredovanja bolezni ali nesprejemljivih toksičnih učinkov (in do maksimalnega trajanja zdravljenja, če je le to določeno za indikacijo). Pri adjuvantnem zdravljenju melanoma ali RCC je treba zdravilo uporabljati do ponovitve bolezni, pojava nesprejemljivih toksičnih učinkov oziroma mora zdravljenje trajati do enega leta. Če je aksitinib uporabljen v kombinaciji s pembrolizumabom, se lahko razmisli o povečanju odmerka aksitiniba nad začetnih 5 mg v presledkih šest tednov ali več. V primeru uporabe v kombinaciji z lenvatinibom je treba zdravljenje z enim ali obema zdraviloma prekiniti, kot je primerno. Uporabo lenvatiniba je treba zadržati, odmerek zmanjšati ali prenehati z uporabo, v skladu z navodili v povzetku glavnih značilnosti zdravila za lenvatinib, in sicer za kombinacijo s pembrolizumabom. Pri bolnikih starih ≥ 65 let, bolnikih z blago do zmerno okvaro ledvic, bolnikih z blago okvaro jeter prilagoditev odmerka ni potrebna. Odložitev odmerka ali ukinitev zdravljenja: Zmanjšanje odmerka zdravila KEYTRUDA ni priporočljivo. Za obvladovanje neželenih učinkov je treba uporabo zdravila KEYTRUDA zadržati ali ukiniti, prosimo, glejte celoten Povzetek glavnih značilnosti zdravila. **Kontraindikacije:** Preobčutljivost na učinkovino ali katero koli pomožno snov. **Povzetek posebnih opozoril, previdnostnih ukrepov, interakcij in neželenih učinkov:** Imunsko pogojeni neželeni učinki (pnevmonitis, kolitis, hepatitis, nefritis, endokrinopatije, neželeni učinki na kožo in drugi): Pri bolnikih, ki so prejemali pembrolizumab, so se pojavili imunsko pogojeni neželeni učinki, vključno s hudimi in smrtnimi primeri. Večina imunsko pogojenih neželenih učinkov, ki so se pojavili med zdravljenjem s pembrolizumabom, je bila reverzibilnih in so jih obvladali s prekinitvami uporabe pembrolizumaba, uporabo kortikosteroidov in/ali podporno oskrbo. Pojavijo se lahko tudi po zadnjem odmerku pembrolizumaba in hkrati prizadanejo več organskih sistemov. V primeru suma na imunsko pogojene neželene učinke je treba poskrbeti za ustrezno oceno za potrditev etiologije oziroma izključitev drugih vzrokov. Glede na izrazitost neželenega učinka je treba zadržati uporabo pembrolizumaba in uporabiti kortikosteroide – za natančna navodila, prosimo, glejte Povzetek glavnih značilnosti zdravila Keytruda. Zdravljenje s pembrolizumabom lahko poveča tveganje za zavrnitev pri prejemnikih presadkov čvrstih organov. Pri bolnikih, ki so prejemali pembrolizumab, so poročali o hudih z infuzijo povezanih reakcijah, vključno s preobčutljivostjo in anafilaksijo. Pembrolizumab se iz obtoka odstrani s katabolizmom, zato presnovnih medsebojnih delovanj zdravil ni pričakovati. Uporabi sistemskih kortikosteroidov ali imunosupresivov pred uvedbo pembrolizumaba se je treba izogibati, ker lahko vplivajo na farmakodinamično aktivnost in učinkovitost pembrolizumaba. Vendar pa je kortikosteroide ali druge imunosupresive mogoče uporabiti za zdravljenje imunsko pogojenih neželenih učinkov. Kortikosteroide je mogoče uporabiti tudi kot premedikacijo, če je pembrolizumab uporabljen v kombinaciji s kemoterapijo, kot antiemetično profilakso in/ali za ublažitev neželenih učinkov, povezanih s kemoterapijo. Ženske v rodni dobi morajo med zdravljenjem s pembrolizumabom in vsaj še 4 mesece po zadnjem odmerku pembrolizumaba uporabljati učinkovito kontracepcijo, med nosečnostjo in dojenjem se ga ne sme uporabljati. Varnost pembrolizumaba pri samostojnem zdravljenju so v kliničnih študijah ocenili pri 7.148 bolnikih z napredovalim melanomom, kirurško odstranjenim melanomom v stadiju III (adjuvantno zdravljenje), NSCLC, cHL, urotelijskim rakom, HNSCC, CRC, rakom endometrija, želodca, tankega črevesa, žolčnika, trebušne slinavke ali adjuvantnim zdravljenjem RCC s štirimi odmerki (2 mg/kg telesne mase na 3 tedne, 200 mg na 3 tedne in 10 mg/kg telesne mase na 2 ali 3 tedne). V tej populaciji bolnikov je mediani čas opazovanja znašal 7,9 meseca (v razponu od 1 dneva do 39 mesecev), najpogostejši neželeni učinki zdravljenja s pembrolizumabom pa so bili utrujenost (31 %), diareja (22 %) in navzea (21 %). Večina poročanih neželenih učinkov pri samostojnem zdravljenju je bila po izrazitosti 1. ali 2. stopnje. Najresnejši neželeni učinki so bili imunsko pogojeni neželeni učinki in hude z infuzijo povezane reakcije. Pojavnost imunsko pogojenih neželenih učinkov pri uporabi pembrolizumaba samega za adjuvantno zdravljenje (n = 1.480) je znašala 36,1 % za vse stopnje in 8,9 % od 3. do 5. stopnje, pri metastatski bolezni (n = 5.375) pa 24,2 % za vse stopnje in 6,4 % od 3. do 5. stopnje. Pri adjuvantnem zdravljenju niso zaznali nobenih novih imunsko pogojenih neželenih učinkov. Varnost pembrolizumaba pri kombiniranem zdravljenju s kemoterapijo so ocenili pri 2.033 bolnikih z NSCLC, HNSCC, rakom požiralnika ali TNBC, ki so v kliničnih študijah prejemali pembrolizumab v odmerkih 200 mg, 2 mg/kg telesne mase ali 10 mg/kg telesne mase na vsake 3 tedne. V tej populaciji bolnikov so bili najpogostejši neželeni učinki naslednji: anemija (52 %), navzea (52 %), utrujenost (37 %), zaprtost (34 %), nevtropenija (33 %), diareja (32 %), zmanjšanje apetita (30 %) in bruhanje (28 %). Pojavnost neželenih učinkov 3. do 5. stopnje je pri bolnikih z NSCLC pri kombiniranem zdravljenju s pembrolizumabom znašala 67 % in pri zdravljenju samo s kemoterapijo 66 %, pri bolnikih s HNSCC pri kombiniranem zdravljenju s pembrolizumabom 85 % in pri zdravljenju s kemoterapijo v kombinaciji s cetuksimabom 84 %, pri bolnikih z rakom požiralnika pri kombiniranem zdravljenju s pembrolizumabom 86 % in pri zdravljenju samo s kemoterapijo 83 % ter pri bolnikih s TNBC pri kombiniranem zdravljenju s pembrolizumabom 78 % in pri zdravljenju samo s kemoterapijo 74 %. Varnost pembrolizumaba v kombinaciji z aksitinibom ali lenvatinibom pri napredovalem RCC in v kombinaciji z lenvatinibom pri napredovalem EC so ocenili pri skupno 1.456 bolnikih z napredovalim RCC ali napredovalim EC, ki so v kliničnih študijah prejemali 200 mg pembrolizumaba na 3 tedne skupaj s 5 mg aksitiniba dvakrat na dan ali z 20 mg lenvatiniba enkrat na dan, kot je bilo ustrezno. V teh populacijah bolnikov so bili najpogostejši neželeni učinki diareja (58 %), hipertenzija (54 %), hipotiroidizem (46 %), utrujenost (41 %), zmanjšan apetit (40 %), navzea (40 %), artralgija (30 %), bruhanje (28 %), zmanjšanje telesne mase (28 %), disfonija (28 %), bolečine v trebuhu (28 %), proteinurija (27 %), sindrom palmarno-plantarne eritrodizestezije (26 %), izpuščaj (26 %), stomatitis (25 %), zaprtost (25 %), mišično-skeletna bolečina (23 %), glavobol (23 %) in kašelj (21 %). Neželenih učinkov od 3. do 5. stopnje je bilo pri bolnikih z RCC med uporabo pembrolizumaba v kombinaciji z aksitinibom ali lenvatinibom 80 % in med uporabo sunitiniba samega 71 %. Pri bolnicah z EC je bilo neželenih učinkov od 3. do 5. stopnje med uporabo pembrolizumaba v kombinaciji z lenvatinibom 89 % in med uporabo kemoterapije same 73 %. Za celoten seznam neželenih učinkov, prosimo, glejte celoten Povzetek glavnih značilnosti zdravila. Za dodatne informacije o varnosti v primeru uporabe pembrolizumaba v kombinaciji glejte povzetke glavnih značilnosti zdravila za posamezne komponente kombiniranega zdravljenja. **Način in režim izdaje zdravila:** H – Predpisovanje in izdaja zdravila je le na recept, zdravilo se uporablja samo v bolnišnicah. **Imetnik dovoljenja za promet z zdravilom:** Merck Sharp & Dohme B.V. , Waarderweg 39, 2031 BN Haarlem, Nizozemska.

MSD
Merck Sharp & Dohme inovativna zdravila d.o.o.,
Ameriška ulica 2, 1000 Ljubljana,
tel: +386 1/ 520 42 01, fax: +386 1/ 520 43 50;
Pripravljeno v Sloveniji, 01/2022; SI-KEY-00404 EXP: 01/2024
Samo za strokovno javnost.
H - Predpisovanje in izdaja zdravila je le na recept, zdravilo pa se uporablja samo v bolnišnicah. Pred predpisovanjem, prosimo, preberite celoten Povzetek glavnih značilnosti zdravila Keytruda, ki je na voljo pri naših strokovnih sodelavcih ali na lokalnem sedežu družbe.

IMFINZI™
durvalumab
50 mg/ml koncentrat za raztopino za infundiranje

AKTIVIRA IMUNSKI SISTEM. PREPOZNA. **REAGIRA.**

SKRAJŠAN POVZETEK GLAVNIH ZNAČILNOSTI ZDRAVILA

▼ Za to zdravilo se izvaja dodatno spremljanje varnosti. Tako bodo hitreje na voljo nove informacije o njegovi varnosti. Zdravstvene delavce naprošamo, da poročajo o katerem koli domnevnem neželenem učinku zdravila.

Imfinzi 50 mg/ml koncentrat za raztopino za infundiranje

SESTAVA: 1 ml koncentrata za raztopino za infundiranje vsebuje 50 mg durvalumaba. Ena viala z 2,4 ml koncentrata vsebuje 120 mg durvalumaba. Ena viala z 10 ml koncentrata vsebuje 500 mg durvalumaba. **INDIKACIJE:** Zdravilo Imfinzi je kot samostojno zdravljenje indicirano za zdravljenje lokalno napredovalega, neoperabilnega nedrobnoceličnega raka pljuč (NSCLC – "non small cell lung cancer") pri odraslih, ki imajo tumorje z ≥ 1 % izraženostjo PD-L1 na tumorskih celicah in pri katerih bolezen ni napredovala po kemoradioterapiji na osnovi platine. Zdravilo Imfinzi je v kombinaciji z etopozidom in bodisi karboplatinom bodisi cisplatinom indicirano za prvo linijo zdravljenja odraslih z razsejanim drobnoceličnim rakom pljuč (ES SCLC – "extensive stage small cell lung cancer"). **ODMERJANJE IN NAČIN UPORABE:** Zdravljenje mora uvesti in nadzorovati zdravnik, ki ima izkušnje na področju zdravljenja raka. Bolnike z lokalno napredovalim nedrobnoceličnim rakom pljuč je treba za zdravljenje izbrati na podlagi izraženosti PD-L1, ugotovljene z validirano testno metodo. Odmerjanje: Priporočeni odmerek zdravila Imfinzi pri samostojnem zdravljenju je 10 mg/kg na 2 tedna ali 1500 mg na 4 tedne do napredovanja bolezni, nesprejemljivih toksičnih učinkov ali največ 12 mesecev . Bolniki s telesno maso 30 kg ali manj morajo prejemati odmerke na podlagi telesne mase, in sicer 10 mg/kg na 2 tedna ali 20 mg/kg na 4 tedne kot samostojno zdravljenje, dokler se telesna masa ne poveča na več kot 30 kg. V kombinaciji s kemoterapijo je priporočeni odmerek zdravila Imfinzi 1500 mg v kombinaciji s kemoterapijo na 3 tedne (21 dni) 4 cikluse in nato 1500 mg na 4 tedne kot samostojno zdravljenje. Zdravilo Imfinzi se uporablja v intravenski infuziji, ki traja 1 uro. Povečevanje ali zmanjševanje odmerka ni priporočljivo. Glede na individualno varnost in prenašanje je lahko potrebna odložitev odmerka ali prenehanje uporabe zdravila. V primeru domnevnih imunsko pogojenih neželenih učinkov je treba opraviti ustrezno ovrednotenje za potrditev etiologije oziroma izključitev druge etiologije. Glede na resnost neželenega učinka je treba prenehati uporabljati zdravilo IMFINZI in pričeti z dajanjem kortikosteroidov. Če se stanje ne izboljša ali se poslabša, pride v poštev povečanje odmerka kortikosteroidov in/ali dodatna uporaba sistemskih imunosupresivov. Po izboljšanju na ≤ 1. stopnjo je treba začeti s postopnim zmanjševanjem kortikosteroida in ga zmanjševati v obdobju vsaj 1 meseca. Po odložitvi uporabe je mogoče zdravilo Imfinzi znova začeti uporabljati v času 12 tednov, če se neželeni učinki izboljšajo na ≤ 1. stopnjo in je odmerek kortikosteroida zmanjšan na ≤ 10 mg prednizona ali ekvivalenta na dan. Zdravilo IMFINZI je treba dokončno ukiniti, če se imunsko pogojeni neželeni učinki 3. stopnje (močno izraženi) ponavljajo in pri katerih koli imunsko pogojenih neželenih učinkih 4. stopnje (življenjsko nevarni), razen pri endokrinopatijah, ki jih nadziramo z nadomestnimi hormoni. Pri ne imunsko pogojenih neželenih učinkih, v primeru 2. ali 3. stopnje izraženosti, odložite uporabo zdravila IMFINZI do izboljšanja neželenih učinkov na ≤ 1. stopnjo ali na izhodiščno raven. Z uporabo zdravila Imfinzi je treba prenehati v primeru neželenih učinkov 4. stopnje (razen v primeru laboratorijskih nepravilnosti 4. stopnje, pri katerih naj odločitev o prekinitvi uporabe zdravila temelji na spremljajočih kliničnih znakih oziroma simptomih in na klinični presoji zdravnika). Zdravilo Imfinzi je namenjeno za intravensko uporabo. Dati ga je treba kot raztopino za intravensko infundiranje v obdobju 1 ure. **KONTRAINDIKACIJE:** Preobčutljivost na učinkovino (učinkovine) ali katero koli pomožno snov. **OPOZORILA IN PREVIDNOSTNI UKREPI:** Za izboljšanje sledljivosti bioloških zdravil je treba jasno zabeležiti lastniško ime in številko serije uporabljenega zdravila. Imunsko pogojeni pnevmonitis: Pri bolnikih, ki so prejemali zdravilo Imfinzi, sta se pojavila imunsko pogojeni pnevmonitis ali intersticijska bolezen pljuč, opredeljeno kot potreba po uporabi sistemskih kortikosteroidov in brez jasne druge etiologije. Pri bolnikih, zdravljenih z radioterapijo pljuč, je pogost radiacijski pnevmonitis in klinična slika pnevmonitisa in radiacijskega pnevmonitisa je zelo podobna. V študiji PACIFIC sta se pri bolnikih, ki so opravili zdravljenje z najmanj 2 cikloma sočasne kemoradioterapije od 1 do 42 dni pred začetkom preizkušanja, pnevmonitis ali radiacijski pnevmonitis pojavila pri 161 (33,9 %) bolnikih v skupini z zdravilom Imfinzi in pri 58 (24,8 %) bolnikih v skupini s placebom, vključno s 3. stopnjo (3,4 % in 3,0 %) in 5. stopnjo (1,1 % in 1,7 %). Bolnike je treba spremljati glede znakov in simptomov pnevmonitisa ali radiacijskega pnevmonitisa. Imunsko pogojeni hepatitis: Pri bolnikih, ki so prejemali zdravilo Imfinzi, se je pojavil imunsko pogojeni hepatitis, opredeljen kot potreba po sistemskih kortikosteroidih in brez jasne druge etiologije. Imunsko pogojeni kolitis: Pri bolnikih, ki so prejemali zdravilo Imfinzi, sta se pojavila imunsko pogojeni kolitis ali driska, opredeljeno kot potreba po sistemskih kortikosteroidih in brez jasne druge etiologije. Imunsko pogojene endokrinopatije: Imunsko pogojeni hipotiroidizem, hipertiroidizem in tiroiditis: Pri bolnikih, ki so prejemali zdravilo Imfinzi, so se pojavili imunsko pogojeni hipotiroidizem, hipertiroidizem in tiroiditis; hipertiroidizmu lahko sledi hipotiroidizem. Bolnike je treba spremljati glede nenormalnih izvidov delovanje ščitnice pred zdravljenjem in redno med zdravljenjem ter kot je potrebno glede na klinično oceno. Imunsko pogojeni hipotiroidizem, hipertiroidizem in tiroiditis je treba obravnavati in ukrepati, kot je priporočeno v povzetku glavnih značilnosti zdravila. Imunsko pogojena adrenalna insuficienca: Pri bolnikih, ki so prejemali zdravilo Imfinzi, se je pojavila imunsko pogojena adrenalna insuficienca. Bolnike je treba spremljati glede kliničnih znakov in simptomov adrenalne insuficience. Imunsko pogojena sladkorna bolezen tipa 1: Pri bolnikih, ki so prejemali zdravilo Imfinzi, se je pojavila imunsko pogojena sladkorna bolezen tipa 1, ki se lahko najprej kaže kot diabetična ketoacidoza, ki je lahko smrtno nevarna, če je dovolj zgodaj ne odkrijemo. Bolnike je treba spremljati glede kliničnih znakov in simptomov sladkorne bolezni tipa 1. Imunsko pogojeni hipofizitis/hipopituitarizem: Pri bolnikih, ki so prejemali zdravilo Imfinzi, sta se pojavila imunsko pogojena hipofizitis ali hipopituitarizem. Bolnike je treba spremljati glede kliničnih znakov in simptomov hipofizitisa ali hipopituitarizma. Imunsko pogojeni nefritis: Pri bolnikih, ki so prejemali zdravilo Imfinzi, se je pojavil imunsko pogojeni nefritis, opredeljen kot potreba po sistemskih kortikosteroidih in brez jasne druge etiologije. Imunsko pogojeni izpuščaj: Pri bolnikih, ki so prejemali zdravilo Imfinzi, se je pojavil imunsko pogojeni izpuščaj ali dermatitis (vključno s pemfigoidom), opredeljen kot potreba po sistemskih kortikosteroidih in brez jasne druge etiologije. Pri bolnikih, ki so bili zdravljeni z zaviralci PD-1, so poročali o pojavljanju Stevens-Johnsonovega sindroma ali toksične epidermalne nekrolize. Drugi imunsko pogojeni neželeni učinki: Glede na mehanizem delovanja zdravila Imfinzi se lahko pojavijo še drugi potencialno imunsko pogojeni učinki. Naslednji imunsko pogojeni neželeni učinki so bili opaženi pri bolnikih, ki so prejemali samostojno zdravljenje z zdravilom Imfinzi: miastenija gravis, miokarditis, miozitis, polimiozitis, meningitis, encefalitis, Guillain Barréjev sindrom, imunska trombocitopenija in neinfektivni cistitis. V programu kliničnih študij so pri bolnikih poročali o primerih pankreatitisa. Bolnike je treba spremljati glede znakov in simptomov in ukrepati, kot je priporočeno za druge imunsko pogojene neželene učinke. Z infundiranjem povezane reakcije: Bolnike je treba spremljati glede znakov in simptomov z infundiranjem povezanih reakcij. Pri bolnikih, ki so prejemali zdravilo Imfinzi, so bile opisane hude z infundiranjem povezane reakcije. Bolniki, ki niso bili vključeni v klinična preizkušanja: V klinična preskušanja niso bili vključeni bolniki z naslednjimi značilnostmi: izhodiščno oceno zmogljivosti ECOG ≥ 2; aktivno ali predhodno dokumentirano avtoimunsko boleznijo v 2 letih pred začetkom študije; anamnezo imunske pomanjkljivosti; anamnezo hudih imunsko pogojenih neželenih učinkov; boleznimi, ki so zahtevale sistemsko imunosupresijo, razen fiziološkega odmerka sistemskih kortikosteroidov (≤ 10 mg na dan prednizona ali ekvivalenta); neobvladanimi sočasnimi boleznimi; aktivno tuberkulozo ali okužbo s hepatitisom B ali C ali HIV; bolniki, ki so prejeli živo oslabljeno cepivo v 30 dneh pred začetkom zdravljenja z zdravilom Imfinzi ali v 30 dneh po začetku. Dokler takšnih podatkov ni, je treba durvalumab v teh skupinah bolnikov uporabljati previdno ter po skrbnem individualnem pretehtanju možnih koristi in tveganj za posameznega bolnika. Varnost sočasnega profilaktičnega kranialnega obsevanja obenem z zdravilom Imfinzi pri bolnikih z ES SCLC ni znana. **MEDSEBOJNO DELOVANJE Z DRUGIMI ZDRAVILI:** Razen fizioloških odmerkov sistemskih kortikosteroidov (≤ 10 mg na dan prednizona ali ekvivalenta) pred uvedbo durvalumaba ni priporočljivo uporabljati sistemskih kortikosteroidov ali imunosupresivov, ker lahko vplivajo na farmakodinamično aktivnost in učinkovitost durvalumaba. Vendar pa je mogoče kortikosteroide ali druge imunosupresive uporabiti po začetku zdravljenja z durvalumabom za zdravljenje imunsko pogojenih neželenih učinkov. Z durvalumabom niso izvedli formalnih farmakokinetičnih (PK) študij medsebojnega delovanja zdravil. Primarni poti odstranjevanja durvalumaba sta katabolizem beljakovin preko retikuloendotelijskega sistema oziroma tarčno posredovano odstranjevanje, zato ni pričakovati presnovnih medsebojnih delovanj med zdravili. Farmakokinetična medsebojna delovanja med durvalumabom in kemoterapijo so ocenjevali v študiji CASPIAN; izkazalo se je, da sočasno zdravljenje z durvalumabom ne vpliva na farmakokinetiko etopozida, karboplatina ali cisplatina. Poleg tega populacijska farmakokinetična analiza kaže, da sočasno zdravljenje s kemoterapijo ne vpliva pomembno na farmakokinetiko durvalumaba. **PLODNOST, NOSEČNOST IN DOJENJE:** Ženske v rodni dobi morajo med zdravljenjem z durvalumabom in vsaj še 3 mesece po zadnjem odmerku durvalumaba uporabljati učinkovito kontracepcijo. Podatkov o uporabi durvalumaba pri nosečnicah ni. Glede na mehanizem delovanja durvalumab lahko vpliva na vzdrževanje nosečnosti; v alogenskem modelu nosečnosti pri miših je bilo ugotovljeno, da moteno signaliziranje PD-L1 poveča izgubo plodov. Pri nosečnici uporabljeni durvalumab lahko škoduje plodu in ga ni priporočljivo uporabljati med nosečnostjo in pri ženskah v rodni dobi, ki ne uporabljajo učinkovite kontracepcije med zdravljenjem in vsaj še 3 mesece po zadnjem odmerku. Ni znano, ali se durvalumab pri človeku izloča v materinem mleku. Pri človeku protitelesa lahko prehajajo v materino mleko, a možnost absorpcije in škode za novorojenčka ni znana. Toda možnega tveganja za dojenega otroka ni mogoče izključiti. Odločiti se je treba, ali naj ženska prekine z dojenjem ali naj prekine zdravljenje z durvalumabom oziroma sploh ne začne zdravljenja z njim, pri čemer je treba upoštevati koristi dojenja za otroka in koristi zdravljenja za žensko. Podatkov o možnih vplivih durvalumaba na plodnost pri človeku ali živalih ni. **NEŽELENI UČINKI:** Ugotovitve o varnosti zdravila Imfinzi pri samostojnem zdravljenju temeljijo na kumulativnih podatkih 3006 bolnikov z več vrstami tumorjev. Zdravilo Imfinzi so uporabljali v odmerku 10 mg/kg na 2 tedna ali v odmerku 20 mg/kg na 4 tedne. Najpogostejši neželeni učinki (> 10 %) so bili kašelj/produktiven kašelj (21,5 %), driska (16,3 %), izpuščaj (16,0 %), zvišana telesna temperatura (13,8 %), okužbe zgornjih dihal (13,5 %), bolečine v trebuhu (12,7 %), srbenje (10,8 %) in hipotiroidizem (10,1 %). Ugotovitve o varnosti zdravila Imfinzi v kombinaciji s kemoterapijo temeljijo na podatkih 265 bolnikov z SCLC. Zdravilo Imfinzi so uporabljali v odmerku 1500 mg na 3 tedne v kombinaciji s kemoterapijo in nato pri samostojnem zdravljenju na 4 tedne. Najpogostejši neželeni učinki (> 20 %) so bili nevtropenija (48,7 %), anemija (38,5 %), navzea (33,6 %), utrujenost (32,1 %), alopecija (31,3 %), trombocitopenija (21,1 %) in levkopenija (20,0 %). Zdravilo Imfinzi pri samostojnem zdravljenju: Zelo pogosti neželeni učinki: okužbe zgornjih dihal, hipotiroidizem, kašelj/produktiven kašelj, driska, bolečine v trebuhu, izpuščaj, srbenje, zvišana telesna temperatura. Pogosti neželeni učinki: pljučnica, zobne okužbe in okužbe ustnih mehkih tkiv, oralna kandidoza, gripa, hipertiroidizem, pnevmonitis, disfonija, zvišanje vrednosti aspartat aminotransferaze ali zvišanje vrednosti alanin aminotransferaze, nočno znojenje, dermatitis, mialgija, zvišanje vrednosti kreatinina v krvi, disurija, periferni edemi, z infundiranjem povezane reakcije. Občasni neželeni učinki: tiroiditis, adrenalna insuficienca, intersticijska bolezen pljuč, kolitis, hepatitis, dermatitis, miozitis, nefritis. Redki neželeni učinki: sladkorna bolezen tipa 1, hipofizitis / hipopituitarizem, diabetes insipidus, miastenija gravis, meningitis, miokarditis, pemfigois, polimiozitis, imunska trombocitopenija. Zdravilo Imfinzi v kombinaciji s kemoterapijo: Zelo pogosti neželeni učinki: nevtropenija, anemija, trombocitopenija, levkopenija, zmanjšan apetit, kašelj/produktiven kašelj, navzea, zaprtost, bruhanje, izpadanje las, utrujenost. Pogosti neželeni učinki: okužbe zgornjih dihal, pljučnica, zobne okužbe in okužbe ustnih mehkih tkiv, febrilna nevtropenija, pancitopenija, hipotiroidizem, hipertiroidizem, tiroiditis, adrenalna insuficienca, pnevmonitis, driska, bolečine v trebuhu, stomatitis, zvišanje vrednosti aspartat aminotransferaze ali zvišanje vrednosti alanin aminotransferaze, hepatitis, izpuščaj, srbenje, dermatitis, mialgija, zvišanje vrednosti kreatinina v krvi, disurija, zvišana telesna temperatura. Občasni neželeni učinki: gripa, sladkorna bolezen tipa 1, disfonija, intersticijska bolezen pljuč. **VRSTA IN VSEBINA OVOJNINE:** 2,4 ml koncentrata v stekleni viali iz stekla tipa 1 z elastomernim zamaškom in sivo snemno aluminijsko zaporo; viala vsebuje 120 mg durvalumaba. Pakiranje vsebuje 1 vialo. 10 ml koncentrata v stekleni viali iz stekla tipa 1 z elastomernim zamaškom in belo snemno aluminijsko zaporo; viala vsebuje 500 mg durvalumaba. Pakiranje vsebuje 1 vialo. **NAČIN IZDAJANJA ZDRAVILA:** H - Predpisovanje in izdaja zdravila je le na recept. **DATUM REVIZIJA BESEDILA:** oktober 2021 (SI-1834) **IMETNIK DOVOLJENJA ZA PROMET:** AstraZeneca AB, S-151 85, Sodertalje, Švedska

Pred predpisovanjem, prosimo, preberite celoten povzetek glavnih značilnosti zdravila. Datum priprave informacije: november 2021.
Dodatne informacije so na voljo pri družbi AstraZeneca UK Limited, Podružnica v Sloveniji, Verovškova 55, Ljubljana.

AstraZeneca

SI-1880

GAVRETO® ▼

Monoterapija za zdravljenje odraslih bolnikov z napredovalim nedrobnoceličnim rakom pljuč (NDRP) s preureditvijo gena RET (*rearranged during transfection*), ki predhodno še niso bili zdravljeni z zaviralcem RET.[1]

Vir: 1. Povzetek glavnih značilnosti zdravila Gavreto je dosegljiv na povezavi: https://www.ema.europa.eu/en/documents/product-information/gavreto-epar-product-information_sl.pdf

▼Za to zdravilo se izvaja dodatno spremljanje varnosti. Tako bodo hitreje na voljo nove informacije o njegovi varnosti. Zdravstvene delavce naprošamo, da poročajo o katerem koli domnevnem neželenem učinku zdravila. Kako poročati o neželenih učinkih, si poglejte skrajšani povzetek glavnih značilnosti zdravila pod "Poročanje o domnevnih neželenih učinkih".

GAVRETO® ▼
pralsetinib 100 mg kapsule

Skrajšan povzetek glavnih značilnosti zdravila Gavreto

Ime zdravila: Gavreto 100 mg trde kapsule. **Kakovostna in količinska sestava:** Ena trda kapsula vsebuje 100 mg pralsetiniba. **Terapevtske indikacije:** Zdravilo Gavreto je indicirano kot monoterapija za zdravljenje odraslih bolnikov z napredovalim nedrobnoceličnim rakom pljuč (NDRP) s preureditvijo gena RET (*rearranged during transfection*), ki predhodno še niso bili zdravljeni z zaviralcem RET. **Odmerjanje in način uporabe:** Izbira bolnikov za zdravljenje napredovalega NDRP s preureditvijo gena RET mora temeljiti na validirani testni metodi. Odmerjanje: Priporočeni odmerek pralsetiniba je 400 mg enkrat na dan na prazen želodec. Zdravljenje je treba nadaljevati do napredovanja bolezni ali nesprejemljivih neželenih učinkov. *Prilagoditve odmerka v primeru neželenih učinkov:* Za obvladanje neželenih učinkov pride v poštev prekinitev zdravljenja z zmanjšanjem odmerka ali brez njega. Bolnikom je mogoče odmerek zmanjševati po 100 mg do najmanjšega odmerka 100 mg enkrat na dan. Način uporabe: Zdravilo Gavreto je namenjeno za peroralno uporabo. Trde kapsule morajo bolniki pogoltniti cele s kozarcem vode na prazen želodec. Bolniki ne smejo jesti vsaj dve uri pred jemanjem pralsetiniba in vsaj eno uro po njem. **Kontraindikacije:** Preobčutljivost na učinkovino ali katero koli pomožno snov. **Posebna opozorila in previdnostni ukrepi:** Pnevmonitis/intersticijska bolezen pljuč: Pri bolnikih, ki so v kliničnih preskušanjih prejemali pralsetinib, so poročali o hudih, življenje ogrožajočih ali smrtnih primerih pnevmonitisa/intersticijske bolezni pljuč. Bolnikom je treba naročiti, da morajo zdravnika nemudoma obvestiti o novonastalih dihalnih simptomih ali poslabšanju takšnih simptomov. Pri bolnikih z akutnimi dihalnimi simptomi ali poslabšanjem dihalnih simptomov s sumom na pnevmonitis/intersticijsko bolezen pljuč je treba opraviti ustrezno diagnostiko, da se izključijo drugi možni vzroki. Če je ocenjeno, da je pnevmonitis/intersticijska bolezen pljuč povezana s pralsetinibom, je treba glede na izrazitost potrjenega pnevmonitisa/intersticijske bolezni pljuč odmerjanje zdravila Gavreto prekiniti, zmanjšati ali dokončno ukiniti. Hipertenzija: V kliničnih preskušanjih so pri bolnikih, zdravljenih s pralsetinibom, opažali hipertenzijo. Z zdravljenjem povezano hipertenzijo so najpogosteje obvladovali z antihipertenzivnimi zdravili. Bolnikom z neurejeno hipertenzijo se ne sme uvesti zdravljenja z zdravilom Gavreto. Že obstoječo hipertenzijo je treba pred začetkom zdravljenja z zdravilom Gavreto ustrezno urediti. Krvni tlak je priporočljivo preverjati po 1 tednu, nato pa vsaj enkrat na mesec in kot je klinično indicirano. Uvesti je treba antihipertenzivno zdravljenje oziroma ga prilagoditi, kot je primerno. Glede na to, kako izrazita je hipertenzija, opažena med zdravljenjem z zdravilom Gavreto, je treba odmerjanje zdravila prekiniti, zmanjšati ali dokončno ukiniti. Zvišanja transaminaz: Pri bolnikih, ki so v kliničnih preskušanjih prejemali pralsetinib, so poročali o hudih primerih zvišanja transaminaz. Vrednosti ALT in AST je treba preveriti pred uvedbo zdravila Gavreto, nato na 2 tedna prve 3 mesece, potem pa enkrat na mesec in kot je klinično indicirano. Glede na to, kako izrazito je zvišanje transaminaz, opaženo med zdravljenjem z zdravilom Gavreto, je treba odmerjenje zdravila prekiniti, zmanjšati ali dokončno ukiniti. Krvavitve: Pri zdravljenju z zdravilom Gavreto se lahko pojavijo hude krvavitve, vključno s smrtnimi. Pri bolnikih z življenje ogrožajočimi ali ponovljenimi hudimi krvavitvami je treba zdravljenje z zdravilom Gavreto dokončno ukiniti. Podaljšanje intervala QT: Pri bolnikih, ki so prejemali zdravilo Gavreto v kliničnih preskušanjih, so opažali podaljšanje intervala QT. Zato morajo imeti bolniki pred začetkom zdravljenja z zdravilom Gavreto interval QTc ≤ 470 ms in serumske elektrolite v normalnem območju. Hipokaliemijo, hipomagneziemijo in hipokalciemijo je treba korigirati tako pred zdravljenjem z zdravilom Gavreto kot med zdravljenjem z njim. Elektrokardiogram in elektrolite v serumu je treba kontrolirati ob koncu prvega tedna in prvega meseca zdravljenja z zdravilom Gavreto, nato pa občasno, kot je klinično indicirano, odvisno tudi od prisotnosti drugih dejavnikov tveganja. Pralsetinib je treba previdno uporabljati pri bolnikih z anamnezo motenj srčnega ritma ali podaljšanja intervala QT, prav tako tudi pri bolnikih, ki prejemajo močne zaviralce CYP3A4 ali zdravila, za katera je znano, da podaljšajo interval QT/QTc. Morda bo treba prekiniti zdravljenje z zdravilom Gavreto, prilagoditi odmerek ali zdravljenje ukiniti. Plodnost in nosečnost: Moški, ki imajo partnerke v rodni dobi, morajo med zdravljenjem z zdravilom Gavreto in vsaj še 1 teden po njegovem zadnjem odmerku uporabljati učinkovito kontracepcijo. Ženskam v rodni dobi je treba povedati, da med zdravljenjem z zdravilom Gavreto ne smejo zanositi. Ženske morajo med zdravljenjem s pralsetinibom uporabljati visoko učinkovito nehormonsko kontracepcijo, kajti pralsetinib lahko povzroči neučinkovitost hormonske kontracepcije. Uporabo učinkovite kontracepcije je treba nadaljevati vsaj 2 tedna po zadnjem odmerku zdravila. **Medsebojno delovanje z drugimi zdravili in druge oblike interakcij:** Farmakokinetično medsebojno delovanje: Podatki *in vitro* kažejo, da se pralsetinib presnovi predvsem s CYP3A4 in prenaša s P-gp. Zato lahko spodbujevalci in zaviralci CYP3A4 in P-gp spremenijo koncentracijo pralsetiniba v plazmi. Učinkovine, ki lahko vplivajo na pralsetinib: *Močni zaviralci CYP3A4 ali kombinacija zaviralcev P-gp in močnih zaviralcev CYP3A4:* Sočasna uporaba pralsetiniba z močnim zaviralcem CYP3A4 ali kombinacijo zaviralca P-gp in močnega zaviralca CYP3A4 lahko poveča koncentracijo pralsetiniba v plazmi, to pa lahko poveča pojavnost in izrazitost neželenih učinkov pralsetiniba. Zato se je treba izogibati sočasni uporabi pralsetiniba z močnimi zaviralci CYP3A4 ali kombinaciji zaviralcev P-gp in močnih zaviralcev CYP3A4. Če se sočasni uporabi z močnim zaviralcem CYP3A4 ali kombinaciji z zaviralci P-gp in močnimi zaviralci CYP3A4 ni mogoče izogniti, zmanjšajte trenutni odmerek pralsetiniba. *Močni spodbujevalci CYP3A4:* Sočasna uporaba pralsetiniba z močnim spodbujevalcem CYP3A4 lahko zmanjša koncentracijo pralsetiniba v plazmi, to pa lahko zmanjša učinkovitost pralsetiniba. Zato se je treba izogibati sočasni uporabi pralsetiniba z močnimi spodbujevalci CYP3A4. Če se sočasni uporabi ni mogoče izogniti, povečajte odmerek pralsetiniba. *Občutljivi substrati CYP3A4, CYP2C8, CYP2C9, P-gp, BCRP, OATP1B1, OATP1B3, OAT1, MATE1 in MATE2-K z ozkim terapevtskim indeksom:* Sočasno dajanje pralsetiniba lahko spremeni izpostavljenost občutljivim substratom encimov CYP in zgoraj naštetim prenašalcem. Zdravilom, ki so substrati omenjenih encimov CYP in prenašalci z ozkim terapevtskim indeksom, se je treba izogibati. **Neželeni učinki:** Najpogostejši neželeni učinki so bili anemija, zvišana aspartataminotransferaza, nevtropenija, zaprtje, mišično-skeletna bolečina, utrujenost, levkopenija, zvišana alanin-aminotransferaza in hipertenzija. Najpogostejši resni neželeni učinki so bili pljučnica, pnevmonitis in anemija. Poročanje o domnevnih neželenih učinkih: Poročanje o domnevnih neželenih učinkih zdravila po izdaji dovoljenja za promet je pomembno. Omogoča namreč stalno spremljanje razmerja med koristmi in tveganji zdravila. Od zdravstvenih delavcev se zahteva, da poročajo o katerem koli domnevnem neželenem učinku zdravila na: Javna agencija Republike Slovenije za zdravila in medicinske pripomočke, Sektor za farmakovigilanco, Nacionalni center za farmakovigilanco, Slovenčeva ulica 22, SI-1000 Ljubljana, Tel: +386 (0)8 2000 500, Faks: +386 (0)8 2000 510, e-pošta: h-farmakovigilanca@jazmp.si, spletna stran: www.jazmp.si. **Režim izdaje zdravila:** Rp/Spec. **Imetnik dovoljenja za promet:** Roche Registration GmbH, Emil-Barell-Strasse 1, 79639 Grenzach-Wyhlen, Nemčija. Verzija: 1.0/22.

DODATNE INFORMACIJE SO NA VOLJO PRI: Roche farmacevtska družba d.o.o., Stegne 13G, 1000 Ljubljana

Samo za strokovno javnost.

M-SI-00000413(v1.0) Datum priprave informacije: februar 2022.

ONIVYDE: IZDELAN POSEBEJ ZA BOJ PROTI RAKU TREBUŠNE SLINAVKE

ONIVYDE pegylated liposomal je odobren za zdravljenje metastatskega adenokarcinoma trebušne slinavke v kombinaciji s 5-fluorouracilom (5-FU) in levkovorinom (LV) pri odraslih bolnikih, pri katerih je bolezen po zdravljenju na osnovi gemcitabina napredovala.[1]

ONIVYDE VSEBUJE PEGILIRANE LIPOSOME Z IRINOTEKANOM IN JE IZDELAN POSEBEJ ZA UČINKOVITO ZDRAVLJENJE METASTATSKEGA RAKA TREBUŠNE SLINAVKE[2–5]

KLINIČNI PODATKI ŠTUDIJE 3. FAZE POTRJUJEJO EDINSTVENO KLINIČNO VREDNOST ZDRAVILA ONIVYDE V KOMBINACIJI S 5-FU/LV:

- skladni podatki o učinkovitosti pri vseh opazovanih dogodkih: pomembno podaljšanje preživetja in povečana stopnja odziva[6–8]
- ohranjena kakovost življenja[6,9]
- dobro poznan varnostni profil[1,6,7]

POMEMBNA UČINKOVITOST ONIVYDE + 5-FU/LV JE POTRJENA V KLINIČNI PRAKSI[10–12]

ONIVYDE + 5-FU/LV PRIPOROČAJO VSE GLAVNE MEDNARODNE SMERNICE[13–16]

LITERATURA: 1. Povzetek glavnih značilnosti zdravila ONIVYDE pegylated liposomal. **2.** Lamb YN, Scott LJ. *Drugs*. 2017;77:785–792. **3.** Drummond DC et al. *Cancer Res*. 2006;66:3271–3277. **4.** Kalra AV et al. *Cancer Res*. 2014;74:7003–7013. **5.** Carnevale J, Ko AH. *Future Oncol*. 2016;12:453–464. **6.** Wang-Gillam A et al. *Lancet*. 2016;387:545–557. **7.** Wang-Gillam A et al. *Eur J Cancer*. 2019;108:78–87. **8.** Chen LT et al. *Eur J Cancer*. 2018;105:71–78. **9.** Hubner RA et al. *Eur J Cancer*. 2019;106:24–33. **10.** Kieler M et al. *Ther Adv Med Oncol*. 2019;11:1–13. **11.** Yoo C et al. *Ther Adv Med Oncol*. 2019;11:1–9. **12.** Pellino A et al. *ESMO*. 2019;P660. **13.** Ducreux M et al. *Ann Oncol*. 2015;25(suppl 5):v56–v68. **14.** eUpdate Cancer of the Pancreas Treatment Recommendations. Objavljeno 20. junija, 2019. ESMO Guidelines Committee. **15.** Okusaka T et al. *Pancreas*. 2020;49(3):326–335. **16.** NCCN Guidelines Version 2, 2021. Pancreatic Adenocarcinoma. Objavljeno 25. februarja, 2021.

SERVIER

onivyde®
pegylated liposomal irinotecan

SKRAJŠAN POVZETEK GLAVNIH ZNAČILNOSTI ZDRAVILA Onivyde pegylated liposomal 4,3 mg/ml SESTAVA*: Onivyde pegylated liposomal 4,3 mg/ml koncentrat za disperzijo za infundiranje: ena viala z 10 ml koncentrata vsebuje 43 mg brezvodnega irinotekana (v obliki irinotekanijeve soli saharoznega oktasulfata v pegilirani liposomski formulaciji). **TERAPEVTSKE INDIKACIJE*:** Zdravljenje metastatskega adenokarcinoma trebušne slinavke v kombinaciji s 5fluorouracilom (5-FU) in levkovorinom (LV) pri odraslih bolnikih, pri katerih je bolezen po zdravljenju na osnovi gemcitabina napredovala. **ODMERJANJE IN NAČIN UPORABE*:** Onivyde pegylated liposomalsmejo bolnikom predpisati in dajati samo zdravstveni delavci, ki imajo izkušnje pri uporabi zdravil za zdravljenje raka. Zdravilo Onivyde pegylated liposomal ni enakovredno drugim neliposomskim formulacijam irinotekana, zato jih ne smemo zamenjevati. Priporočeni odmerek in režim odmerjanja zdravila Onivyde pegylated liposomal je 70 mg/m^2 intravensko 90 minut, čemur sledi LV 400 mg/m^2 intravensko 30 minut in nato 5FU 2400 mg/m^2 intravensko 46 ur, vsaka 2 tedna. Zdravilo Onivyde pegylated liposomal se ne daje kot samostojno zdravilo. Pri bolnikih z znano homozigotnostjo za alel UGT1A1*28 je treba razmisliti o manjšem začetnem odmerku zdravila Onivyde pegylated liposomal 50 mg/m^2. Če zdravilo bolniki dobro prenašajo, lahko v naslednjih ciklih razmislimo o odmerku zdravila Onivyde pegylated liposomal 70 mg/m^2. Prilagajanje odmerka se priporoča za obvladovanje toksičnosti 3. ali 4. stopnje, povezane z zdravilom Onivyde pegylated liposomal. **KONTRAINDIKACIJE*:** Anamneza hude preobčutljivosti na irinotekan ali katero koli pomožno snov. Dojenje. **OPOZORILA*:** Zdravilo Onivyde pegylated liposomal ni enakovredno drugim neliposomskim formulacijam irinotekana, zato jih ne smemo zamenjevati. *Mielosupresija/nevtropenija:* Med zdravljenjem z zdravilom Onivyde pegylated liposomal se priporoča nadziranje celotne krvne slike. Bolniki se morajo zavedati tveganja za nevtropenijo in pomena povišane telesne temperature. Febrilno nevtropenijo je treba nujno zdraviti v bolnišnici s širokospektralnimi intravenskimi antibiotiki. Pri bolnikih, ki doživijo hude hematološke neželene učinke, se priporoča zmanjšanje odmerka ali prekinitev zdravljenja. Bolnikov s hudo odpovedjo kostnega mozga ne smemo zdraviti z zdravilom Onivyde pegylated liposomal. Anamneza predhodnega obsevanja trebuha poveča tveganje za hudo nevtropenijo in febrilno nevtropenijo po zdravljenju z zdravilom Onivyde pegylated liposomal. Pri bolnikih, ki hkrati prejemajo zdravilo Onivyde pegylated liposomal in so obsevani, je potrebna previdnost. Bolniki s pomanjkljivo glukuronidacijo bilirubina, kot so bolniki z Gilbertovim sindromom, imajo med zdravljenjem z zdravilom Onivyde pegylated liposomal lahko večje tveganje za mielosupresijo. Bolniki azijskega porekla imajo večje tveganje za hudo in febrilno nevtropenijo. Posamezniki s homozigotnostjo 7/7 za alel UGT1A1*28 imajo povečano tveganje za nevtropenijo. *Imunosupresivni učinki in cepiva:* Dajanje živih ali atenuiranih cepiv bolnikom z oslabljenim imunskim sistemom lahko povzroči resne ali smrtne okužbe. *Interakcije z močnimi induktorji encima CYP3A4, močnimi zaviralci encima CYP3A4 in močnimi zaviralci encima UGT1A1:* Zdravila Onivyde pegylated liposomal ne smemo dajati skupaj z močnimi induktorji encima CYP3A4, močnimi zaviralci encima CYP3A4 ali z močnimi zaviralci encima UGT1A1, razen če ni drugih terapevtskih možnosti. Zdravljenje z močnimi zaviralci encima CYP3A4 moramo prekiniti vsaj 1 teden pred začetkom zdravljenja z zdravilom Onivyde pegylated liposomal. *Driska:* Driska se lahko pojavi zgodaj (v ≤ 24 urah po začetku zdravljenja z zdravilom Onivyde pegylated liposomal) ali pozno (> 24 ur). Pri bolnikih, ki doživijo zgodnji pojav driske (v ≤ 24 urah po začetku zdravljenja z zdravilom Onivyde pegylated liposomal), je treba razmisliti o terapevtskem in profilaktičnem zdravljenju z atropinom, razen če je kontraindicirano. Bolnike je treba opozoriti na tveganje za zapoznelo drisko (> 24 ur), ki je izčrpavajoča in v redkih primerih tudi življenjsko nevarna. Loperamid je treba uvesti ob prvem pojavu neoblikovanega ali mehkega blata ali takoj, ko odvajanje blata postane pogostejše kot običajno. Loperamid je treba dajati, dokler bolnik ni brez driske vsaj 12 ur. Če driska traja tudi, ko bolnik prejema loperamid več kot 24 ur, je treba razmisliti o dodatni peroralni antibiotični podpori. Loperamida zaradi tveganja za paralitični ileus ne smemo uporabljati več kot 48 ur zaporedoma. Zdravljenje z zdravilom Onivyde pegylated liposomal je treba odložiti, dokler se driska ne umiri do ≤ 1. stopnje (2–3 odvajanja/dan več kot pred zdravljenjem). Zdravila Onivyde pegylated liposomal ne smemo dajati bolnikom z zaporo črevesja ali kronično vnetno črevesno boleznijo, dokler se ta ne pozdravi. *Holinergične reakcije:* Zgodnjo drisko lahko spremljajo rinitis, povečano slinjenje, zardevanje, diaforeza, bradikardija, mioza in hiperperistaltika. Uporabiti je treba atropin. *Akutne infuzijske in povezane reakcije:* V primeru hudih preobčutljivostnih reakcij je treba zdravljenje z zdravilom Onivyde pegylated liposomal prekiniti. *Predhodna Whipplova operacija:* Večje tveganje za resne okužbe. Bolnike je treba spremljati glede znakov okužbe. *Žilne bolezni:* Zdravilo Onivyde pegylated liposomal je bilo povezano s trombemboličnimi dogodki, kot so pljučna embolija, venska tromboza in arterijska trombembolija. Treba je pridobiti podrobno zdravstveno anamnezo, da bi prepoznali bolnike z več dejavniki tveganja poleg osnovne neoplazme. Bolnike je treba obvestiti o znakih in simptomih trombembolije in jim svetovati, da se v primeru katerega od teh znakov ali simptomov takoj obrnejo na svojega zdravnika ali medicinsko sestro. *Pljučna toksičnost:* Pri bolnikih, ki so prejemali neliposomski irinotekan, so se pojavili dogodki, podobni intersticijski pljučni bolezni (IPB), ki so vodili do smrtnih primerov. Pri bolnikih z dejavniki tveganja (obstoječo pljučno boleznijo, uporabo pnevmotoksičnih zdravil, kolonije stimulirajočimi dejavniki ali predhodnim zdravljenjem z obsevanjem) je treba pred zdravljenjem z zdravilom Onivyde pegylated liposomal in po njem skrbno nadzirati respiratorne simptome. Dokler ni opravljena diagnostična ocena, je treba ob pojavu nove ali napredovale dispneje, kašlja in povišane telesne temperature zdravljenje z zdravilom Onivyde pegylated liposomal začasno prekiniti. Pri bolnikih s potrjeno diagnozo IPB moramo zdravljenje z zdravilom Onivyde pegylated liposomal dokončno prekiniti. *Jetrna okvara:* Bolniki s hiperbilirubinemijo so imeli povišane koncentracije skupnega SN-38, zato je tveganje za nevtropenijo povečano. Pri bolnikih z vrednostjo skupnega bilirubina 1,0–2,0 mg/dl je treba redno nadzirati celotno krvno sliko. Previdnost je potrebna pri bolnikih z jetrno okvaro (bilirubin > 2-kratna zgornja meja normalnih vrednosti [ULN]; aminotransferaze > 5-kratna ULN). Previdnost je potrebna, če zdravilo Onivyde pegylated liposomal dajemo v kombinaciji z drugimi hepatotoksičnimi zdravili. *Ledvična okvara:* Uporaba zdravila Onivyde pegylated liposomal pri bolnikih s pomembno ledvično okvaro ni bila ocenjena. *Bolniki s premajhno telesno maso (indeks telesne mase < 18,5 kg/m^2):* Potrebna je previdnost. *Pomožne snovi:* To zdravilo vsebuje 33,1 mg natrija na vialo, kar je enako 1,65 % največjega dnevnega vnosa natrija za odrasle osebe, ki ga priporoča SZO in znaša 2 g. En mililiter zdravila Onivyde pegylated liposomal vsebuje 0,144 mmol (3,31 mg) natrija. **INTERAKCIJE*:** *Previdnostni ukrepi:* Sočasno dajanje z induktorji encima CYP3A4 (npr. antikonvulzivi, rifampicin, rifabutin in šentjanževka) lahko zmanjša sistemsko izpostavljenost zdravilu Onivyde pegylated liposomal. Sočasno dajanje z zaviralci encima CYP3A4 (npr. grenivkinim sokom, klaritromicinom, indinavirjem, itrakonazolom, lopinavirjem, nefazodonom, nelfinavirjem, ritonavirjem, sakvinavirjem, telaprevirjem, vorikonazolom) ali encima UGT1A1 (npr. atazanavirja, gemfibrozila, indinavirja, regorafeniba) lahko poveča sistemsko izpostavljenost zdravilu Onivyde pegylated liposomal. **PLODNOST*. NOSEČNOST*:** Uporaba ni priporočljiva. **DOJENJE*:** Zdravilo je kontraindicirano. **KONTRACEPCIJA*:** Ženske v rodni dobi morajo med zdravljenjem in še 1 mesec po zdravljenju z zdravilom Onivyde pegylated liposomal uporabljati učinkovito kontracepcijo. Moški morajo med zdravljenjem z zdravilom Onivyde pegylated liposomal in 4 mesece po zdravljenju uporabljati kondome. **VPLIV NA SPOSOBNOST VOŽNJE IN UPRAVLJANJA STROJEV*:** Bolniki morajo biti med zdravljenjem pri vožnji in upravljanju strojev previdni. **NEŽELENI UČINKI*:** *Zelo pogosti:* nevtropenija, levkopenija, anemija, trombocitopenija, hipokaliemija, hipomagneziemija, dehidracija, zmanjšan apetit, omotica, driska, bruhanje, navzea, bolečine v trebuhu, stomatitis, alopecija, pireksija, periferni edem, vnetje sluznic, utrujenost, astenija, zmanjšana telesna masa. *Pogosti:* septični šok, sepsa, pljučnica, febrilna nevtropenija, gastroenteritis, oralna kandidoza, limfopenija, hipoglikemija, hiponatriemija, hipofosfatemija, nespečnost, holinergični sindrom, dizgevzija, hipotenzija, pljučna embolija, embolija, globoka venska tromboza, dispneja, disfonija, kolitis, hemoroidi, hipoalbuminemija, akutna ledvična odpoved, z infuzijo povezana reakcija, edem, zvišana raven bilirubina, zvišana raven alanin-aminotransferaze, zvišana raven aspartat-aminotransferaze, zvišano mednarodno umerjeno razmerje. *Občasni:* biliarna sepsa, preobčutljivost, tromboza, hipoksija, ezofagitis, proktitis, makulopapulozni izpuščaj, obarvanje nohtov. **PREVELIKO ODMERJANJE*:** Za preveliko odmerjanje zdravila ni znanega antidota. Treba je uvesti maksimalno podporno nego, s katero preprečimo dehidracijo zaradi driske in zdravimo zaplete zaradi okužb. **FARMAKODINAMIČNE LASTNOSTI*:** Irinotekan (zaviralec topoizomeraze I), inkapsuliran v vezikel z lipidnim dvoslojem oziroma liposom. Irinotekan je derivat kamptotecina. Kamptotecini delujejo kot specifični zaviralci encima DNA-topoizomeraza I. Irinotekan in njegov aktivni presnovek SN-38 se reverzibilno vežeta na kompleks topoizomeraze I in DNA ter sprožita poškodbe v enoverižni DNA, kar zaustavi replikacijske vilice pri podvajanju DNA in povzroča citotoksičnost. Irinotekan se presnavlja s karboksilesterazo do SN-38. SN-38 je približno 1.000-krat močnejši kot irinotekan kot zaviralec topoizomeraze I, očiščene iz tumorskih celičnih linij človeka in glodavcev. **PAKIRANJE*:** Pakiranje vsebuje eno vialo z 10 ml koncentrata. **NAČIN PREDPISOVANJA IN IZDAJE ZDRAVILA: H - Predpisovanje in izdaja zdravila je le na recept, zdravilo pa se uporablja samo v bolnišnicah. DATUM ZADNJE REVIZIJE BESEDILA: september 2021. Imetnik dovoljenja za promet:** Les Laboratoires Servier, 50, rue Carnot, 92284 Suresnes cedex, Francija. ***Pred predpisovanjem preberite celoten povzetek glavnih značilnosti zdravila. Celoten povzetek glavnih značilnosti zdravila in podrobnejše informacije so na voljo pri: Servier Pharma d.o.o., Podmilščakova ulica 24, 1000 Ljubljana, www.servier.si.**

Zdravilo je na slovenskem trgu na voljo v tuji ovojnini. Za uporabnika so informacije v slovenskem jeziku dostopne na uradni spletni strani www.cbz.si. Navodila za uporabo v slovenskem jeziku so na voljo tudi na www.servier.si.

Samo za strokovno javnost. Datum priprave informacije: september 2021. ONI AD1 C1 2021-22.

Instructions for authors

The editorial policy

Radiology and Oncology is a multidisciplinary journal devoted to the publishing original and high quality scientific papers and review articles, pertinent to diagnostic and interventional radiology, computerized tomography, magnetic resonance, ultrasound, nuclear medicine, radiotherapy, clinical and experimental oncology, radiobiology, medical physics and radiation protection. Therefore, the scope of the journal is to cover beside radiology the diagnostic and therapeutic aspects in oncology, which distinguishes it from other journals in the field.

The Editorial Board requires that the paper has not been published or submitted for publication elsewhere; the authors are responsible for all statements in their papers. Accepted articles become the property of the journal and, therefore cannot be published elsewhere without the written permission of the editors.

Submission of the manuscript

The manuscript written in English should be submitted to the journal via online submission system Editorial Manager available for this journal at: **www.radioloncol.com**.

In case of problems, please contact Sašo Trupej at **saso.trupej@computing.si** or the Editor of this journal at **gsersa@onko-i.si**

All articles are subjected to the editorial review and when the articles are appropriated they are reviewed by independent referees. In the cover letter, which must accompany the article, the authors are requested to suggest 3-4 researchers, competent to review their manuscript. However, please note that this will be treated only as a suggestion; the final selection of reviewers is exclusively the Editor's decision. The authors' names are revealed to the referees, but not vice versa.

Manuscripts which do not comply with the technical requirements stated herein will be returned to the authors for the correction before peer-review. The editorial board reserves the right to ask authors to make appropriate changes of the contents as well as grammatical and stylistic corrections when necessary. Page charges will be charged for manuscripts exceeding the recommended length, as well as additional editorial work and requests for printed reprints.

Articles are published printed and on-line as the open access (**https://content.sciendo.com/raon**).

All articles are subject to 1200 EUR + VAT publication fee. Exceptionally, waiver of payment may be negotiated with editorial office, upon lack of funds.

Manuscripts submitted under multiple authorship are reviewed on the assumption that all listed authors concur in the submission and are responsible for its content; they must have agreed to its publication and have given the corresponding author the authority to act on their behalf in all matters pertaining to publication. The corresponding author is responsible for informing the coauthors of the manuscript status throughout the submission, review, and production process.

Preparation of manuscripts

Radiology and Oncology will consider manuscripts prepared according to the Uniform Requirements for Manuscripts Submitted to Biomedical Journals by International Committee of Medical Journal Editors (www.icmje.org). The manuscript should be written in grammatically and stylistically correct language. Abbreviations should be avoided. If their use is necessary, they should be explained at the first time mentioned. The technical data should conform to the SI system. The manuscript, excluding the references, tables, figures and figure legends, must not exceed 5000 words, and the number of figures and tables is limited to 8. Organize the text so that it includes: Introduction, Materials and methods, Results and Discussion. Exceptionally, the results and discussion can be combined in a single section. Start each section on a new page, and number each page consecutively with Arabic numerals. For ease of review, manuscripts should be submitted as a single column, double-spaced text.and must have continuous line numbering.

The Title page should include a concise and informative title, followed by the full name(s) of the author(s); the institutional affiliation of each author; the name and address of the corresponding author (including telephone, fax and E-mail), and an abbreviated title (not exceeding 60 characters). This should be followed by the abstract page, summarizing in less than 250 words the reasons for the study, experimental approach, the major findings (with specific data if possible), and the principal conclusions, and providing 3-6 key words for indexing purposes. Structured abstracts are required. Slovene authors are requested to provide title and the abstract in Slovene language in a separate file. The text of the research article should then proceed as follows:

Introduction should summarize the rationale for the study or observation, citing only the essential references and stating the aim of the study.

Materials and methods should provide enough information to enable experiments to be repeated. New methods should be described in details.

Results should be presented clearly and concisely without repeating the data in the figures and tables. Emphasis should be on clear and precise presentation of results and their significance in relation to the aim of the investigation.

Discussion should explain the results rather than simply repeating them and interpret their significance and draw conclusions. It should discuss the results of the study in the light of previously published work.

Charts, Illustrations, Images and Tables

Charts, Illustrations, Images and Tables must be numbered and referred to in the text, with the appropriate location indicated. Charts, Illustrations and Images, provided electronically, should be of appropriate quality for good reproduction. Illustrations and charts must be vector image, created in CMYK color space, preferred font "Century Gothic", and saved as .AI, .EPS or .PDF format. Color charts, illustrations and Images are encouraged, and are published without additional charge. Image size must be 2.000 pixels on the longer side and saved as .JPG (maximum quality) format. In Images, mask the identities of the patients. Tables should be typed double-spaced, with a descriptive title and, if appropriate, units of numerical measurements included in the column heading. The files with the figures and tables can be uploaded as separate files.

References

References must be numbered in the order in which they appear in the text and their corresponding numbers quoted in the text. Authors are responsible for the accuracy of their references. References to the Abstracts and Letters to the Editor must be identified as such. Citation of papers in preparation or submitted for publication, unpublished observations, and personal communications should not be included in the reference list. If essential, such material may be incorporated in the appropriate place in the text. References follow the style of Index Medicus, DOI number (if exists) should be included.

All authors should be listed when their number does not exceed six; when there are seven or more authors, the first six listed are followed by "et al.". The following are some examples of references from articles, books and book chapters:

Dent RAG, Cole P. In vitro maturation of monocytes in squamous carcinoma of the lung. *Br J Cancer* 1981; **43:** 486-95. doi: 10.1038/bjc.1981.71

Chapman S, Nakielny R. *A guide to radiological procedures*. London: Bailliere Tindall; 1986.

Evans R, Alexander P. Mechanisms of extracellular killing of nucleated mammalian cells by macrophages. In: Nelson DS, editor. *Immunobiology of macrophage.* New York: Academic Press; 1976. p. 45-74.

Authorization for the use of human subjects or experimental animals

When reporting experiments on human subjects, authors should state whether the procedures followed the Helsinki Declaration. Patients have the right to privacy; therefore the identifying information (patient's names, hospital unit numbers) should not be published unless it is essential. In such cases the patient's informed consent for publication is needed, and should appear as an appropriate statement in the article. Institutional approval and Clinical Trial registration number is required. Retrospective clinical studies must be approved by the accredited Institutional Review Board/Committee for Medical Ethics or other equivalent body. These statements should appear in the Materials and methods section.

The research using animal subjects should be conducted according to the EU Directive 2010/63/EU and following the Guidelines for the welfare and use of animals in cancer research (Br J Cancer 2010; 102: 1555 – 77). Authors must state the committee approving the experiments, and must confirm that all experiments were performed in accordance with relevant regulations.

These statements should appear in the Materials and methods section (or for contributions without this section, within the main text or in the captions of relevant figures or tables).

Transfer of copyright agreement

For the publication of accepted articles, authors are required to send the License to Publish to the publisher on the address of the editorial office. A properly completed License to Publish, signed by the Corresponding Author on behalf of all the authors, must be provided for each submitted manuscript.

The non-commercial use of each article will be governed by the Creative Commons Attribution-NonCommercial-NoDerivs license.

Conflict of interest

When the manuscript is submitted for publication, the authors are expected to disclose any relationship that might pose real, apparent or potential conflict of interest with respect to the results reported in that manuscript. Potential conflicts of interest include not only financial relationships but also other, non-financial relationships. In the Acknowledgement section the source of funding support should be mentioned. The Editors will make effort to ensure that conflicts of interest will not compromise the evaluation process of the submitted manuscripts; potential editors and reviewers will exempt themselves from review process when such conflict of interest exists. The statement of disclosure must be in the Cover letter accompanying the manuscript or submitted on the form available on **www.icmje.org/coi_disclosure.pdf**

Page proofs

Page proofs will be sent by E-mail to the corresponding author. It is their responsibility to check the proofs carefully and return a list of essential corrections to the editorial office within three days of receipt. Only grammatical corrections are acceptable at that time.

Open access

Papers are published electronically as open access on **https://content.sciendo.com/raon**, also papers accepted for publication as E-ahead of print.

Inlyta®
aksitinib

Zagotovite svojim bolnikom z metastatskim karcinomom ledvičnih celic v drugi liniji zdravljenja vsakodnevne zmage z **zdravilom Inlyta®.**[1–3]

Zdravilo Inlyta je indicirano za zdravljenje napredovalega karcinoma ledvičnih celic pri odraslih bolnikih, pri katerih predhodno zdravljenje s sunitinibom ali citokinom ni bilo uspešno.[4]

BISTVENI PODATKI IZ POVZETKA GLAVNIH ZNAČILNOSTI ZDRAVILA

Inlyta 1 mg/3 mg/5 mg/7 mg filmsko obložene tablete
Sestava in oblika zdravila: Ena tableta vsebuje 1 mg, 3 mg, 5 mg oz. 7 mg aksitiniba. **Indikacije:** Zdravljenje napredovalega karcinoma ledvičnih celic (RCC) pri odraslih bolnikih, pri katerih predhodno zdravljenje s sunitinibom ali citokinom ni bilo uspešno. **Odmerjanje in način uporabe:** Zdravljenje mora izvajati zdravnik, ki ima izkušnje z uporabo zdravil za zdravljenje rakavih bolezni. Priporočeni odmerek je 5 mg dvakrat na dan. Zdravljenje naj traja, dokler je mogoče opaziti klinično korist oz. do pojava nesprejemljive toksičnosti, ki je ni mogoče obvladovati s sočasno uporabljanimi zdravili ali prilagajanjem odmerka. Če bolnik bruha ali izpusti odmerek, ne sme vzeti dodatnega odmerka; naslednji predpisan odmerek je treba vzeti ob običajnem času. *Prilagajanja odmerka*: Pri bolnikih, ki aksitinib v začetnem odmerku 5 mg dvakrat na dan prenašajo brez neželenih učinkov > 2. stopnje dva tedna zapored, je odmerek mogoče zvečati na 7 mg dvakrat na dan, razen če je krvni tlak pri bolniku > 150/90 mmHg ali če jemlje antihipertenzive. Kasneje je z uporabo enakih meril pri bolnikih, ki prenašajo 7 mg dvakrat na dan, odmerek mogoče zvečati na največ 10 mg dvakrat na dan. Za obvladovanje nekaterih neželenih učinkov bo morda treba začasno ali trajno prekiniti zdravljenje in/ali zmanjšati odmerek na 3 mg dvakrat na dan in nato na 2 mg dvakrat na dan. Prilagajanje odmerka glede na bolnikovo starost, raso, spol ali telesno maso ni potrebno. *Sočasno zdravljenje z močnimi zaviralci CYP3A4/5:* Lahko zveča plazemske koncentracije aksitiniba. V primeru sočasne uporabe močnega zaviralca CYP3A4/5, je odmerek aksitiniba priporočljivo zmanjšati na približno polovico odmerka; morda bo potrebna začasna ali trajna prekinitev zdravljenja z aksitinibom. Če prekinemo sočasno uporabo močnega zaviralca, je treba razmisliti o vrnitvi na odmerek aksitiniba, ki je bil uporabljen pred uvedbo močnega zaviralca CYP3A4/5. *Sočasno zdravljenje z močnimi induktorji CYP3A4/5:* Lahko zmanjša plazemske koncentracije aksitiniba. V primeru sočasne uporabe močnega induktorja CYP3A4/5 je odmerek aksitiniba priporočljivo postopoma zvečati in bolnika skrbno nadzorovati glede pojava toksičnosti. Morda bo treba začasno ali trajno prekiniti zdravljenje in/ali zmanjšati odmerek aksitiniba. Če prekinemo sočasno uporabo močnega induktorja, je treba takoj začeti uporabljati odmerek aksitiniba, ki je bil uporabljen pred uvedbo močnega induktorja CYP3A4/5. *Okvara ledvic:* Prilagajanje odmerka ni potrebno; o uporabi pri bolnikih z očistkom kreatinina < 15 ml/min ni podatkov. *Okvara jeter:* Prilagajanje odmerka ni potrebno pri bolnikih z blago okvaro jeter (razred A po Child-Pughu). Zmanjšanje odmerka je priporočljivo pri bolnikih z zmerno okvaro jeter (razred B). Zdravila se ne sme uporabljati pri bolnikih s hudo okvaro jeter (razred C). *Pediatrična populacija*: Varnost in učinkovitost pri otrocih < 18 let nista bili dokazani; podatkov ni na voljo. *Način uporabe*: Peroralna uporaba. Tablete je treba pogoltniti cele, s kozarcem vode, dvakrat na dan, v približno 12-urnih časovnih presledkih, s hrano ali brez nje. **Kontraindikacije:** Preobčutljivost na aksitinib ali katerokoli pomožno snov. **Posebna opozorila in previdnostni ukrepi:** *Dogodki srčnega popuščanja*: Poročali so o dogodkih srčnega popuščanja. Med zdravljenjem je treba redno spremljati znake ali simptome srčnega popuščanja. Obravnava dogodkov srčnega popuščanja lahko zahteva začasno ali stalno prekinitev zdravljenja z aksitinibom in/ali zmanjšanje odmerka. *Hipertenzija*: O hipertenziji so poročali zelo pogosto. Pred začetkom zdravljenja mora biti krvni tlak ustrezno urejen; bolnike je treba spremljati in po potrebi uporabiti standardno antihipertenzivno zdravljenje. V primeru trdovratne hipertenzije (kljub uporabi antihipertenzivov) je treba odmerek aksitiniba zmanjšati, pri hudi hipertenziji pa zdravljenje začasno prekiniti in ga ponovno uvesti z manjšim odmerkom, ko se krvni tlak normalizira. Pri hudi ali trdovratni arterijski hipertenziji in simptomih sindroma posteriorne reverzibilne encefalopatije je treba razmisliti o diagnostičnem slikanju možganov z uporabo magnetne resonance. *Motnje delovanja ščitnice*: Poročali so o primerih hipotiroidizma in, v manjšem obsegu, hipertiroidizma. Delovanje ščitnice je treba spremljati pred začetkom zdravljenja in v rednih časovnih presledkih med zdravljenjem. *Venski in arterijski embolični in trombotični dogodki*: Poročali so o venskih in arterijskih emboličnih in trombotičnih dogodkih. Previdna uporaba pri bolnikih s tveganjem za pojav teh dogodkov ali anamnezo teh dogodkov. *Zvišanje ravni hemoglobina ali hematokrita*: Med zdravljenjem lahko pride do zvišanj ravni hemoglobina ali hematokrita, njuno raven je treba spremljati pred začetkom zdravljenja in v rednih časovnih presledkih med zdravljenjem. *Krvavitve*: Poročali so o pojavu krvavitev. Pri bolnikih z znaki nezdravljenih možganskih metastaz ali nedavne aktivne krvavitve v prebavilih se zdravila ne sme uporabljati. Če je pri krvavitvi potreben zdravniški poseg, je treba z odmerjanjem aksitiniba začasno prekiniti. *Anevrizme in arterijske disekcije*: Uporaba zaviralcev poti VEGF pri bolnikih s hipertenzijo ali brez nje lahko spodbudi nastanek anevrizem in/ali disekcij arterij. Pred uvedbo aksitiniba je treba to tveganje skrbno preučiti pri bolnikih z dejavniki tveganja, kot sta hipertenzija ali anamneza anevrizme. *Perforacija prebavil in nastanek fistule:* Poročali so o pojavu perforacij prebavil in fistul. Med zdravljenjem je potrebno redno spremljanje glede morebitnega pojava simptomov perforacije prebavil ali nastanka fistule. *Zapleti pri celjenju ran*: Zdravljenje z aksitinibom je treba prekiniti najmanj 24 ur pred načrtovanim kirurškim posegom; odločitev glede ponovne uvedbe zdravljenja po posegu mora temeljiti na klinični presoji ustreznosti celjenja rane. *Sindrom posteriorne reverzibilne encefalopatije (PRES)*: Poročali so o primerih PRES. Pri bolnikih z znaki ali simptomi PRES je treba zdravljenje začasno ali trajno prekiniti. Varnost ponovne uvedbe zdravljenja pri bolnikih, pri katerih je v preteklosti prišlo do PRES, ni znana. *Proteinurija:* Poročali so o proteinuriji, vključno s proteinurijo 3. in 4. stopnje izraženosti. Pred začetkom zdravljenja in v rednih časovnih presledkih med zdravljenjem je priporočljivo spremljanje glede pojava proteinurije; ob pojavu zmerne do hude proteinurije je treba zmanjšati odmerek ali začasno prekiniti zdravljenje. Zdravljenje je treba trajno prekiniti, če se pri bolniku pojavi nefrotski sindrom. *Neželeni učinki na jetra*: Zvišanja ravni ALT, AST in bilirubina v krvi. Pred začetkom zdravljenja in v rednih časovnih presledkih med njim je treba spremljati rezultate preiskav delovanja jeter. *Zdravilo vsebuje laktozo*: Bolniki z redko dedno intoleranco za galaktozo, odsotnostjo encima laktaze ali malabsorpcijo glukoze/galaktoze ne smejo jemati tega zdravila. **Medsebojno delovanje z drugimi zdravili in druge oblike interakcij:** *Zaviralci CYP3A4/5:* Sočasna uporaba z močnimi zaviralci (npr. ketokonazol, itrakonazol, klaritromicin, eritromicin, atazanavir, indinavir, nefazodon, nelfinavir, ritonavir, sakvinavir in telitromicin) ter uživanje grenivk lahko zveča plazemske koncentracije aksitiniba. Priporočljiva je izbira sočasno uporabljanih zdravil, ki ne zavirajo ali minimalno zavirajo CYP3A4/5. Če je treba sočasno uporabljati močan zaviralec CYP3A4/5, je odmerek aksitiniba priporočljivo prilagoditi. *Zaviralci CYP1A2 in CYP2C19*: Zaradi tveganja, da se plazemske koncentracije aksitiniba povečajo, je potrebna previdnost. *Induktorji CYP3A4/5*: Sočasna uporaba aksitiniba z močnimi induktorji (npr. rifampicin, deksametazon, fenitoin, karbamazepin, rifabutin, rifapentin, fenobarbital in šentjanževka) lahko zmanjša plazemske koncentracije aksitiniba. Priporočljiva je izbira sočasno uporabljanih zdravil, ki ne inducirajo ali minimalno inducirajo CYP3A4/5. Če je treba sočasno uporabljati močan induktor CYP3A4/5, je odmerek aksitiniba priporočljivo prilagoditi. **Plodnost, nosečnost in dojenje:** Ne sme se uporabljati med nosečnostjo, razen če klinično stanje ženske zahteva zdravljenje s tem zdravilom. Ženske v rodni dobi morajo uporabljati kontracepcijo med zdravljenjem in še en teden po njem. V obdobju dojenja se ne sme uporabljati. Lahko neugodno vpliva na sposobnost razmnoževanja in plodnost pri ljudeh. **Vpliv na sposobnost vožnje in upravljanja strojev:** Ima blag vpliv na sposobnost vožnje in upravljanja strojev. Med zdravljenjem se lahko pojavijo učinki, kot je npr. omotica in/ali utrujenost. **Neželeni učinki:** Najpogostejši (≥ 20 %) neželeni učinki so bili driska, hipertenzija, utrujenost, zmanjšan apetit, navzea, zmanjšana telesna masa, hripavost, sindrom palmarno-plantarne eritrodisestezije (sindrom dlani-podplati), krvavitev, hipotiroidizem, bruhanje, proteinurija, kašelj in zaprtje. Ostali zelo pogosti (≥ 1/10 bolnikov) neželeni učinki so: glavobol, disgevzija, dispneja, bolečine v trebuhu, stomatitis, dispepsija, izpuščaj, suha koža, artralgija, bolečine v okončinah, astenija, vnetje sluznice. **Način in režim izdaje:** Predpisovanje in izdaja zdravila je le na recept, zdravilo pa se uporablja samo v bolnišnicah. Izjemoma se lahko uporablja pri nadaljevanju zdravljenja na domu ob odpustu iz bolnišnice in nadaljnjem zdravljenju. **Imetnik dovoljenja za promet:** Pfizer Europe MA EEIG, Boulevard de la Plaine 17, 1050 Bruxelles, Belgija. **Datum zadnje revizije besedila:** 29.07.2021

Pred predpisovanjem se seznanite s celotnim povzetkom glavnih značilnosti zdravila.

Literatura: 1. Melichar B, Poprach A, Kubackova K, et al. Efficacy and tolerability of axitinib in metastatic renal cell carcinoma (mRCC): Comparison of Czech clinical registry and AXIS trial data. ECC. 25–29 September 2015. Vienna, Austria. Poster: 2615. **2.** Matias M, Le Teuff G, Albiges L, et al. Real world prospective experience of axitinib in metastatic renal cell carcinoma in a large comprehensive cancer centre. Eur J Cancer. 2017;79:185–192. **3.** Rossetti S, Romano FJ, D'Aniello C, et al. Activity of second line axitinib in metastatic renal cell carcinom (mRCC) patients treated with sunitinib: Results from SAX Italian real world trial. J Clin Oncol. 2017;35(15_suppl):e16054. **4.** Povzetek glavnih značilnosti zdravila Inlyta, 29.7.2021.

Pfizer Luxembourg SARL, GRAND DUCHY OF LUXEMBOURG, 51, Avenue J.F. Kennedy, L – 1855,
Pfizer, podružnica Ljubljana, Letališka cesta 29a, 1000 Ljubljana

Samo za strokovno javnost. • Datum priprave: januar 2022 • PP-INL-EEP-0040

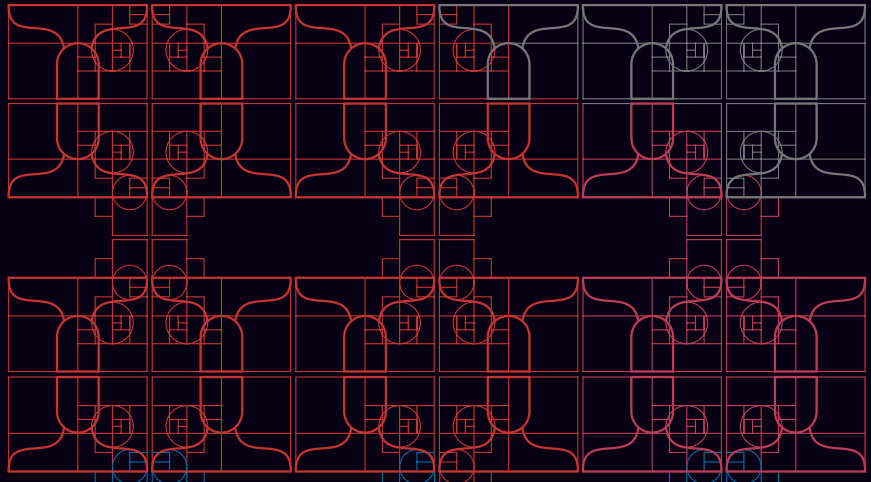

Radiology and Oncology | Ljubljana | Slovenia | https://content.sciendo.com/raon

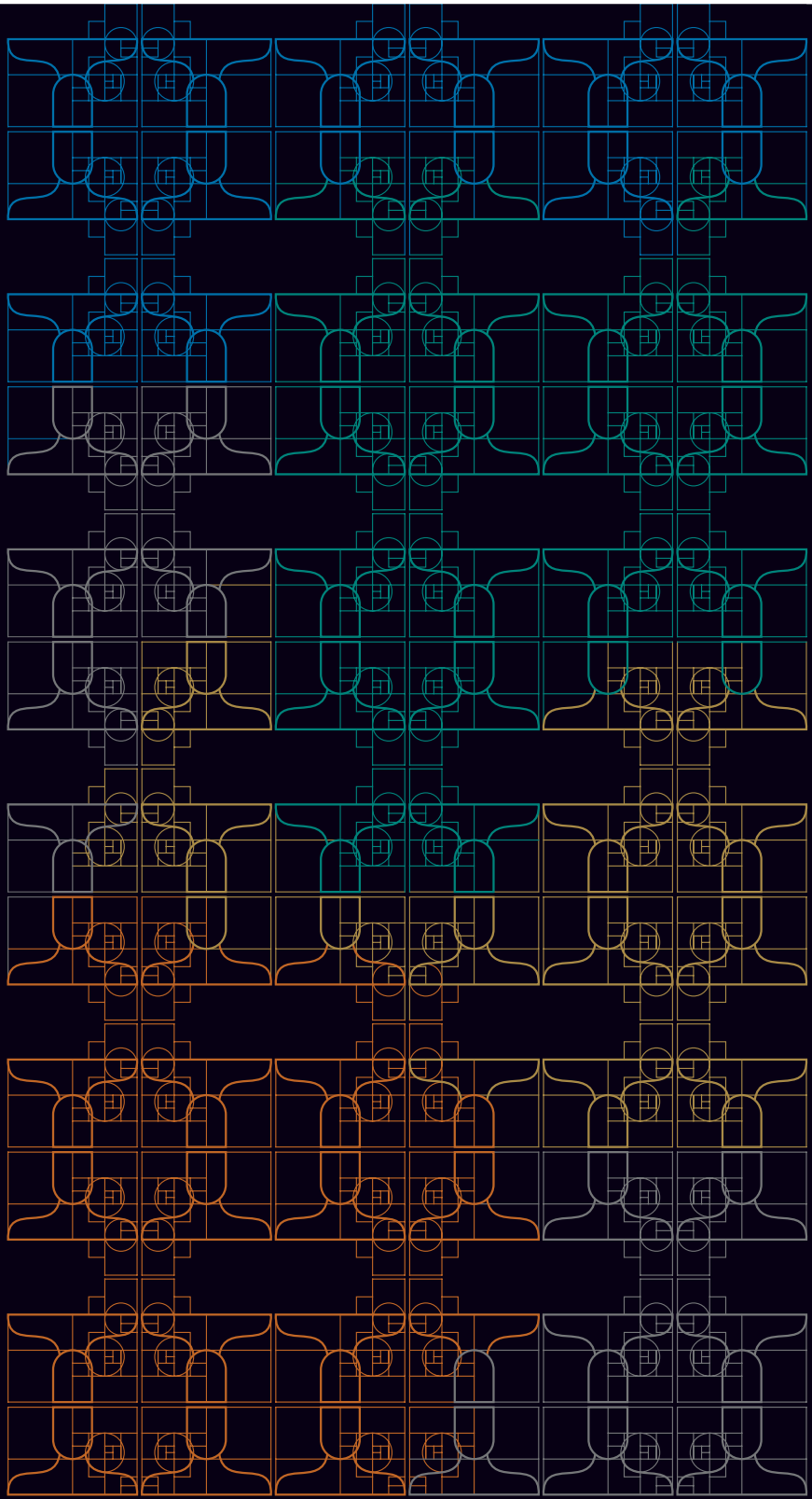

ISSN 1318 - 2099